

Université du Québec
Institut National de la Recherche Scientifique
Énergie, Matériaux & Télécommunications

Decision Making for Smart Grids with Renewable Energy



Hieu Trung Nguyen

A dissertation submitted to INRS-EMT
In partial fulfillment of the requirements for the degree of
Doctor of Philosophy in Telecommunications

Thesis Committee

Chair of Committee and Internal Committee Examiner	André Girard Professor, INRS-EMT
External Committee Examiner	Lyne Woodward Professor, École de Technologie Supérieure (ETS)
External Committee Examiner	Xiaozhe Wang Assistant Professor, McGill University
Supervisor:	Long Bao Le Associate Professor, INRS-EMT

Montréal, Québec, Canada, April 2017
©All rights reserved to Hieu Trung Nguyen, 2017.

This thesis is dedicated to my parents, who raised me up to the person I am today.

Declaration

I certify that the work in this thesis has not been previously submitted for a degree nor has it been submitted as a part of the requirements for other degree except as fully acknowledged within the text. I also certify that this thesis has been written by me. Any help that I have received in my research and in the preparation of the thesis itself has been fully acknowledged. In addition, I certify that all information sources and literature used are quoted in the thesis.

Hieu Trung Nguyen

Acknowledgments

First of all, I would like to express my sincerely thanks to my PhD supervisor, Professor Long Bao Le, for providing me a great opportunity to pursue my PhD study at INRS-ÉMT, University of Quéc. From the very first day, he has always instructed me in research directions, broadened my visions, and inspired me to pursue my research career. I am extremely grateful for his patience with my inexperience and for the long hours he spent discussing technical details with me. His guidance and encouragement in the course of my doctoral works have absolutely helped me to finish this thesis.

I would also like to send my gratefulness to other members of my PhD committee – Professor André Girard, from INRS-ÉMT, University of Québec, who has reviewed this thesis as an internal examiner; Professor Lyne Woodward, from École de Technologie Supérieure (ETS), and Professor Xiaozhe Wang, from McGill University, for reviewing this thesis as external examiners. It is my honor to have them peer review this work. Their constructive comments and suggestions have helped me improve this work significantly.

INRS has an extremely professional research environment and I thank the support staff for taking excellent care of every administrative detail so that I could focus on my study. I would like to thank the NSERC/PERSWADE program and the Wpred team for providing me an internship. I thank them for their valuable industry experiences. I would like to thank the INRS Student Association and the INRS football group for organizing many interesting activities so I could enjoy my student time.

My gratitude is also delivered to all lab-mates for the magnificent and unforgettable time at the Networks and Cyber Physical Systems Lab (NECPHY-Lab). Their concerns and supports for over four years have helped me overcome many obstacles to focus on my research. Special thanks to Duong Tung Nguyen, who shared with me your invaluable knowledge and experiences, which is extremely helpful to my research. I believe you will certainly achieve your career goals. Thank Tuong Duc Hoang for your helpful advices and discussions, I believe in your future success. Outside of academia, I thank you both for being great friends over the years.

Most importantly, my thesis could not have been completed without the encouragement and support from my family. I would like to dedicate my thesis to my passed-away father, Nguyen Tuan Hai, my mother, Cao Thi Hoai, my brother, Nguyen Thanh Long, my grandparents, Nguyen Van Phai and Nguyen Thi Dac, who are the source of care, love, support and strength during my graduate study. My study would not be fulfilled without the consistent and immeasurable support from you. Words cannot describe how thankful I am and my hope is that you will be proud of me.

Abstract

We are at the dawn of the smart grid era where there is significant increase in the demand-side participation in the grid's operations. One important smart grid research topic concerns active demand-side management which can potentially result in great benefits for different involved grid entities (e.g., electricity customers, utility, resource aggregators) and enable to support increasing penetration of distributed renewable energy resources. However, efficient design for different decision making problems must be conducted to realize the potential impacts of the active demand-side management, which is the focus of this dissertation. Specifically, we study three decision making problems of the corresponding demand-side smart grid entities considering integration of renewable energy sources, which are smart home energy management, smart load serving entity (LSE) pricing design, and cost allocation for cooperative demand-side resource aggregators (DRAs) under the virtual power plant (VPP) framework. Our research has resulted in three major contributions, which are presented in three main chapters of this dissertation.

The first contribution is related to the efficient energy scheduling design for smart homes equipped with solar assisted thermal load. This design is conducted under the time-varying dynamic pricing scheme which can potentially bring great demand response benefits for home electric consumers. Specifically, we develop a rolling two-stage stochastic programming based algorithm, which aims to minimize the electricity cost, guarantee user comfort, and efficiently utilize renewable energy resources. We also propose to exploit the solar assisted thermal load for the energy management and analyze the impacts of different parameters on the smart home economic improvements.

The second contribution concerns the development of a dynamic pricing scheme for a load serving entity (LSE) that can incentivize electric customers to provide demand response services. The design can effectively encourage participation of electric customers with flexibilities in energy consumption while not negatively affecting other electric customers lacking flexibilities in changing their energy consumption. Moreover, the proposed pricing scheme is compatible with the current market structure. Toward this end, we consider the pricing design as a bilevel optimization problem where the grid operator is the leader, who determines the demand response price, and the flexible customers are followers, whose energy consumption is adjusted in response to that price signal. We describe how to transform the proposed bilevel optimization problem, which is difficult to be solved directly, into an equivalent single objective mixed integer linear program (MILP), which can be solved efficiently by a branch and cut algorithm. Numerical results show that our proposed pricing design can be beneficial to both grid operator and electric customers.

The third contribution aims to develop an efficient cost allocation scheme for cooperative demand-side resource aggregators (DRA), which are coordinated under an emerging smart grid concept, namely,

the virtual power plant (VPP). We address this problem by using the core based cooperative game theoretic approach. Since the core of the underlying game can contain many cost allocation solutions, our design enables us to choose an appropriate cost allocation solution inside the core that optimizes both stability and fairness metrics. This core based cost allocation problem is formulated as a large-scale bi-objective optimization problem with an exponential number of implicit constraints related to the core definition. In particular, the parameters of these constraints are the function values of coalitions of DRAs, which are the outcomes of the optimal bidding strategies of the corresponding coalitions of DRAs. To tackle this highly complex bi-objective optimization problem, we propose to employ the ε -constraint and row constraint generation methods, which exploit the fact that the number of optimization variables can be much smaller than the number of optimization constraints. Numerical studies show that the proposed algorithm allows to construct the Pareto front with a large number of Pareto points for a VPP consisting of a large number of DRAs. Moreover, the proposed framework enables the VPP to determine a suitable cost allocation for its members considering the trade-off between stability and fairness.

Contents

List of Figures	xv
List of Tables	xix
List of Abbreviations	1
A Summary	3
A.1 Research Motivation	3
A.2 Research Objectives and Contributions	4
A.3 Energy Management of Smart Home with Solar Assisted Thermal Load Considering Price and Renewable Energy Uncertainties	6
A.4 Dynamic Pricing Design for Demand Response Integration in Distribution Networks	12
A.5 Cost Allocation for Cooperative Demand-Side Resource Aggregators	17
B Résumé	25
B.1 Motivation de la recherche	25
B.2 Objectifs et contributions de la recherche	26
B.3 Gestion de l'énergie d'une maison intelligente avec une charge thermique et solaire assistée avec considération des incertitudes des prix et des énergies renouvelables	28
B.4 Conception dynamique des prix pour l'Intégration de la réponse à la demande dans les réseaux de distribution	34
B.5 Répartition des coûts pour les agrégats coopératifs de ressources à la demande	40
1 Introduction	49
1.1 Research Motivation	49
1.2 Challenges in Active Demand-Side Management	50
1.2.1 Challenges in Smart Home Energy Management	50
1.2.2 Challenges in Demand Response Design for Distribution Networks	52
1.2.3 Challenges in Electricity Market's Decision Makings	53
1.3 Literature Review	54
1.3.1 Home Energy Management Under Smart Grid	54
1.3.2 Demand Response Designs in Distribution Network	55
1.3.3 Market Bidding and Cost Sharing Design	56

1.4	Research Objectives and Contributions	58
1.5	Thesis Outline	59
2	Mathematical Background	61
2.1	Mathematical Optimization	61
2.1.1	Basic Concepts	61
2.1.2	Linear Programming and Mixed Integer Linear Programming	61
2.1.3	Stochastic Programming	62
2.1.4	Bilevel Programming	65
2.1.5	Multi-Objective Programming	66
2.2	Cooperative Game Theory	67
2.2.1	Basic Concepts	67
2.2.2	Solution Concepts and The Core	68
2.2.3	Linear Programming (LP) Game	68
2.3	Computation Setup and Numerical Study	69
2.4	Summary	69
3	Energy Management of Smart Home with Solar Assisted Thermal Load Considering Price and Renewable Energy Uncertainties	71
3.1	Abstract	71
3.2	Introduction	72
3.3	Notations	74
3.4	System Model	75
3.5	Energy Management Design	76
3.5.1	Design Objective and Solution Approach	76
3.5.2	Solar Assisted HVAC and Water Heating System	78
3.5.3	System Constraints	81
3.5.4	Constraints for Different Controllable Loads	81
3.5.5	Uncertainty Modeling	83
3.5.6	Energy Scheduling Optimization Problem	84
3.5.7	Grid Stability under RTP	84
3.6	Numerical Results	85
3.6.1	Simulation Data	85
3.6.2	Energy Management Performance	85
3.6.3	Parameter Sensitivities Analysis	88
3.7	Conclusion and Future Works	93
4	Dynamic Pricing Design for Demand Response Integration in Distribution Networks	97
4.1	Abstract	97
4.2	Introduction	97
4.3	Notations	100

4.4	System Model	101
4.5	Problem Formulation	104
4.5.1	Objective Function of the LSE	104
4.5.2	Power Balance Constraints	104
4.5.3	Power Trading with Main Grid	105
4.5.4	Renewable Energy Constraints	105
4.5.5	Involuntary Load Curtailment	105
4.5.6	DR Price	105
4.5.7	Operation Constraints of DGs	105
4.5.8	Battery Constraints	106
4.5.9	Follower Problems	106
4.5.10	Extension with Power Flow Constraints	108
4.6	Solution Approach	109
4.7	Numerical Results	112
4.7.1	Simulation Data	112
4.7.2	Sensitivity Analysis	115
4.7.3	Complexity of Proposed Approach	119
4.7.4	Constraints of Distribution Network, Batteries, and DGs	122
4.8	Conclusion and Future Directions	124
5	Cost Allocation for Cooperative Demand-Side Resource Aggregators	127
5.1	Abstract	127
5.2	Introduction	127
5.2.1	Background and Motivation	127
5.2.2	Aims and Approach	128
5.2.3	Literature Review, Contributions, and Chapter Organization	128
5.3	Notations	129
5.4	System Model	130
5.4.1	Cooperative Demand-Side Resource Aggregator under Virtual Power Plant	130
5.4.2	Market Framework	131
5.4.3	Cost Allocation Procedure	131
5.4.4	Uncertainties Modeling	132
5.5	Problem Formulation	133
5.5.1	Cost Function	133
5.5.2	Bi-objective Optimization Based Core Cost Allocation	135
5.6	Solution Approach	137
5.6.1	The ϵ -Constraint Approach	137
5.6.2	The Row Constraint Generation Approach	138
5.7	Numerical Results	143
5.7.1	Simulation Data	143
5.7.2	Numerical Performance Analysis	144

5.7.3	Computation Analysis	149
5.8	Extensions and Future Work	152
5.8.1	Verifying The Existence of The Core	152
5.8.2	Computation Improvement	153
5.9	Conclusion	154
6	Conclusions and Future Works	155
6.1	Major Contributions	155
6.2	Future Research Directions	156
6.2.1	Multi-Agent System Approach for Smart Grid Energy Management	156
6.2.2	Machine Learning for Decision Making Problems in Smart Grids	156
6.3	Publications	157
	References	159

List of Figures

A.1	NIST Smart grid conceptual model 3.0 [1]	5
A.2	Problems addressed in this thesis	6
A.3	Solar assisted HVAC-water heating system	7
A.4	Rolling stochastic scheduling for Home Energy Management system	9
A.5	Effects of system parameters on electricity cost	10
A.6	Energy cost versus solar collector size and tank temperature limit	11
A.7	System Model and Solution Approach	13
A.8	DR utility function	15
A.9	DR price	16
A.10	Schematic of cooperative DRAs under the VPP's coordination	18
A.11	Pareto fronts under different parameter settings	24
B.1	Modèle Conceptuel NIST Smart Grid 3.0 [1]	27
B.2	Problèmes traités dans cette thèse	28
B.3	Le système de chauffage assisté par eau solaire HVAC	29
B.4	Planification Stochastique Roulant pour la Gestion de L'Énergie Domestique	31
B.5	Effets des paramètres du système sur le coût de l'électricité	33
B.6	Coût de l'énergie par rapport à la taille du collecteur solaire et de la température de la cuve	34
B.7	Modèle de Système et Approche de Solution	36
B.8	Fonction d'utilité DR	37
B.9	Prix DR	39
B.10	Schéma des DRA coopératives sous la coordination du VPP	41
B.11	Fronts de Pareto sous différents paramètres	47
1.1	NIST Smart grid conceptual model 3.0 [1]	51
1.2	Demand-side customer centrality in the smart grid [1]	51
1.3	Problems addressed in this thesis and their relations	59
3.1	Solar assisted HVAC-water heating system	76
3.2	Rolling stochastic scheduling for Home Energy Management system	77
3.3	Computation time of proposed scheduling algorithm	86
3.4	Simulation data for numerical results	87

3.5	Energy management with solar assisted HVAC-water heating	89
3.6	Energy management with conventional HVAC and water heating	90
3.7	Water tank temperature in conventional HVAC and solar water heating system	91
3.8	Energy consumptions of other controllable loads	91
3.9	Total energy consumption of scheduled loads.	92
3.10	Energy management with solar assisted HVAC-water heating (Noncontinously Modulated Power)	93
3.11	Energy management conventional HVAC and water heating (Noncontinously Modulated Power)	94
3.12	Energy cost comparison between power continuously and noncontinuously modulated thermal system	95
3.13	Effects of system parameters on electricity cost	95
3.14	Energy cost versus solar collector size and tank temperature limit	96
3.15	Pareto-optimal constant-cost curves vs solar collector size, room temperature tolerance, tank temperature limit	96
3.16	Energy costs in different months	96
4.1	System Model	102
4.2	DR utility function	107
4.3	Summary of the proposed solution algorithm	113
4.4	Forecast data	114
4.5	DR price	116
4.6	DR load	117
4.7	Involuntary load curtailment	118
4.8	Power exchange with the main grid ($c_t^R = 60$ \$/MWh)	118
4.9	Impact of min DR on the optimal revenue	119
4.10	Renewable energy curtailment	120
4.11	DR load	120
4.12	DR price	121
4.13	Comparison between Scheme 1 (S1) and Scheme 2 (S2)	121
4.14	IEEE 6-bus system	122
4.15	Dispatch of DGs	123
4.16	Power exchange with the main grid	124
5.1	Schematic of cooperative DRAs under the VPP's coordination	131
5.2	Simulation data	145
5.3	Pareto fronts under different parameter settings	147
5.4	Illustration of Fairness core and Nucleolus allocation	148
5.5	Cost saving due to cooperation	149
5.6	Pareto front with $\lambda^P = 150$ \$/MWh, $\beta = 0.1$ and varying NK	150
5.7	The gap of individual bidding cost between bidirectional and unidirectional market	150

5.8	The difference of Pareto fronts obtained in two markets	151
-----	---	-----

List of Tables

A.1	Comparison between Scheme 1 and Scheme 2	16
B.1	Comparaison entre le Schéma 1 et le Schéma 2	38
3.2	Parameters for Different Loads	86
3.3	Solar assisted HVAC-water heating for based case	86
3.4	House Thermal Parameters	88
4.1	Summary of discussed DR methodologies	99
4.3	System Parameters in Base Case	113
4.4	Data for DR aggregators	114
4.5	Comparison between Scheme 1 and Scheme 2	115
4.6	Impact of number of DR aggregators on computation time	122
5.2	Flexible Load Data	144
5.3	Computation Report	152
5.4	Impact of number of Pareto points and complexity of $v(S)$	152

List of Abbreviations

BES	Battery Energy Storage
COP	Coefficient of performance
DA	Day ahead
DR	Demand Response
DRA	Demand-side resource aggregator
DSM	Demand-side Management
DG	Distributed generator
ESP	Energy service provider
EV	Electric vehicle
FERC	Federal Energy Regulatory Commission
HVAC	Heating, ventilation and air conditioning
LP	Linear programming
LSE	Load serving entity
LSF	Load scaling factor
MIP	Mixed integer programming
MILP	Mixed integer linear programming
MG	Microgrid
NIST	National Institute of Standards and Technology
PV	Solar units
RT	Real time
RTP	Real-time pricing
RES	Renewable energy sources
RESF	Renewable energy scaling factor
SOC	State of Charge
VPP	Virtual Power Plant

Chapter A

Summary

A.1 Research Motivation

The electricity industry has seen the significant transformation from centralized power systems dominated by big utilities and highly dependent on fossil energy resources, to smart grids with high penetration of eco-friendly distributed renewable energy and active participation of energy consumers under market deregulation[2]. One of the most important changes is probably the widespread adoption of active demand side management in the smart grids [3]. In fact, it was defined in Title XIII of the Energy Independence and Security Act (EISA) in 2007 that the smart grid is an electrical grid which integrates a variety of operational and energy measures including smart meters, smart appliances, renewable energy resources, and energy efficient resources to motivate the active demand side management [3]. The framework for smart grid interoperability standards defined by the National Institute of Standards and Technology (NIST) is illustrated in Figure A.1 [1].

Research and realization of various smart grid concepts and technologies have received tremendous investment from governments worldwide. In particular, advanced information and communication technology (ICT) infrastructure has been significantly upgraded in many countries [4–6] where a massive number of smart meters has been installed, e.g., over 45 million smart meters have been deployed by the Department of Energy (DoE) smart grid investment grant [7]. Moreover, the deployed communications networks and data management systems form the advanced metering infrastructure (AMI), which enables two-way communication between utilities and customers [8]. The upgraded ICT infrastructure has paved the way to the realization of active demand side management [9–15]. Smart decision making taken by demand-side entities can bring about many benefits to the smart grid [2]. For example, home energy consumers can exploit dynamic pricing schemes to schedule their energy consumption so as to minimize their electricity consumption costs [16–23]. Hence, the main decision making is to schedule the energy consumption wisely to reduce the energy payment while still maintaining certain operations, user comfort, privacy requirements.

Thanks to the deployment of the grid's ICT infrastructure, home energy consumers and grid operator are connected and demand response (DR) services can be offered to the grid operator through changing the energy consumption as [13, 14, 24–27], which can enable the grid to operate more efficiently. The grid operator, however, may be interested in motivating their energy customers to actively

participate in the DR program through for example a suitable pricing policy. A well-known approach to enable the grid operator to manage DR services from its customers is to deploy the so-called Load Serving Entity (LSE) [28]. Finally, small-scale demand-side entities can cooperate to act as a single entity under the coordination of a demand-side resource aggregator [29, 30] or a virtual power plant [31], to purchase energy in the wholesale market since the wholesale energy prices tend to be cheaper than the retail prices [32]. In order to participate in the wholesale market, the demand-side entities have to make several decisions such as coordination decisions to form a large cooperation coalition, energy bidding in the market, and sharing the cooperation benefits with each other.

In general, design of smart decision making frameworks for demand-side entities can be quite challenging in the smart grid environment with increasing penetration of renewable energy in the distribution network [6, 33]. Although being friendly to the environment, renewable energy resources such as solar and wind power can be quite unpredictable, which can lead to great difficulties to ensure efficient and reliable operations for the involved distribution network [2]. In particular, adoption of a poor energy management strategy can result in low utilization of renewable energy [19, 34]. In addition, poor pricing design cannot tackle the fluctuation of renewable energy sources, which eventually results in unstable grid operations [35]. Finally, appropriate design of a bidding strategy can have positive impacts on the achieved profit/cost of demand-side entities participating in the electricity market. This is an important issue because market participants must be responsible for managing uncertainties of their renewable energy sources [29, 36].

In summary, successful exploitation of active demand side management requires addressing several decision-making problems for the involved smart grid entities in the distribution network. This dissertation aims to address some of these problems.

A.2 Research Objectives and Contributions

This thesis aims to address three important challenges described above, whose contributions can be illustrated in Figure A.2 and summarized as follows.

In Chapter 3, we study the home energy scheduling problem in the real-time pricing environment. Specifically, we propose a comprehensive model considering the integration of renewable energy in the home energy system, i.e., the eco-friendly solar assisted HVAC-water heating system. Then, we propose a real-time Model Predictive Control (MPC) based design for a smart home equipped with solar assisted HVAC-water heating system and other controllable loads in response to the real-time pricing signal. We devise a rolling algorithm based on two-stage stochastic programming for home energy management so that it can minimize the energy payment cost, guarantee system constraints while exploiting the energy coupling relation of the solar thermal storage and HVAC system to improve the system energy efficiency.

In Chapter 4, we consider the pricing design problem in the distribution network to motivate the demand response participation from energy consumers. In particular, we propose a dynamic pricing scheme implementable in the distribution network under the model of Load Serving Entity (LSE), which is easy to implement and compatible with the current market structure. Our design creates an in-

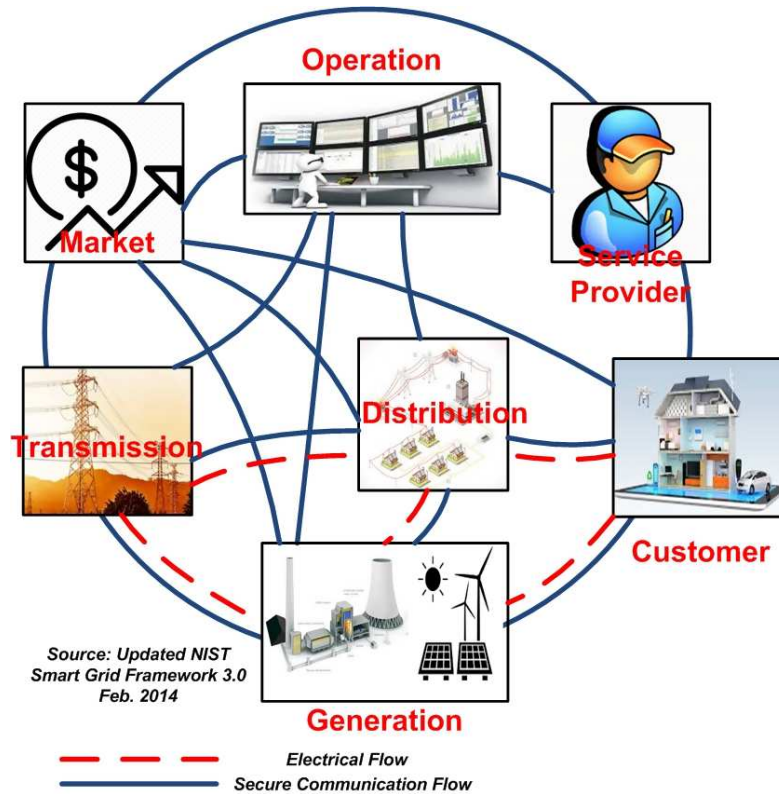


Figure A.1 – NIST Smart grid conceptual model 3.0 [1]

centive for the flexible load to perform demand response that can help the LSE address the fluctuations of electricity prices, conventional nonflexible load, and distributed renewable energy. Specifically, we present the formulation of the proposed pricing design by using the bilevel programming framework. Given the lower-level sub-problem is linear, we employ the optimal KKT conditions to convert the bilevel problem into the single objective mathematics with equilibrium constraints (MPEC), which is then transformed into an equivalent single objective mixed integer linear program (MILP) by using the Fortuny-Amat formula and strong duality theorem of linear programming. The obtained MILP can be solved efficiently by using available commercial solvers. Numerical results are then presented to illustrate the effectiveness of our design in motivating demand response integration in the distribution network.

Chapter 5 studies how to share the cost for the cooperative Demand-Side Resource Aggregators (DRAs), which are based on generic models of active demand-side agents. Specifically, these DRAs are coordinated under the Virtual Power Plant framework to jointly bid in the electricity market and the corresponding attained cost must be split among members. Toward this end, we first present the comprehensive cost allocation model, which is applicable to the current market structure. Then, the cost allocation problem is modeled as the solution of a cooperative game where all DRAs act as players and the value function of coalitions of players are the outcomes of their optimal market bidding strategies which are obtained by solving the corresponding two-stage stochastic programs. We show that the core of the studied game, which defines all budget-balanced and stable cost allocation vectors, is nonempty. Then, we propose to determine the cost allocation vector inside the core considering the trade-off between different criteria through solving a bi-objective optimization. This bi-objective opti-

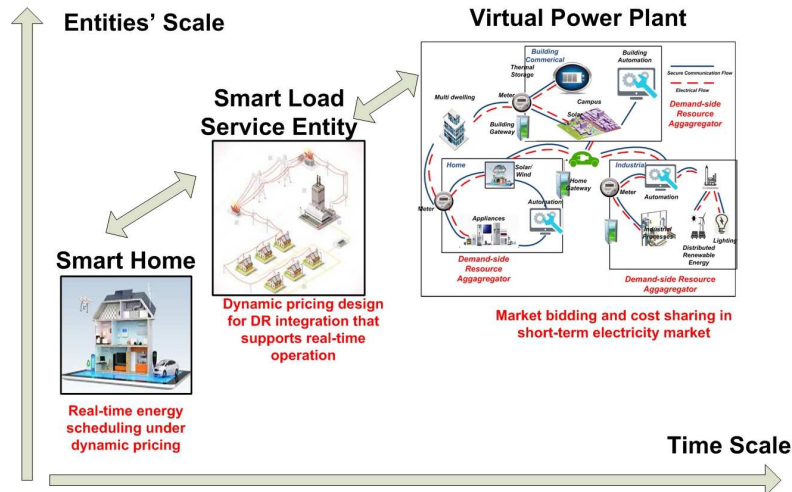


Figure A.2 – Problems addressed in this thesis

mization has an exponential number of constraints with implicit parameters which are the coalitions' function values. Since the number of cost shares are only equal to the number of DRAs, which is much smaller than the number of constraints, we propose an algorithm based on the combination of ϵ -constraint and row constraint generation methods to construct the Pareto front within manageable computation effort.

A.3 Energy Management of Smart Home with Solar Assisted Thermal Load Considering Price and Renewable Energy Uncertainties

The contributions of this study was published in the paper [19]. In particular, we investigate how a single smart home equipped with renewable energy based appliances can respond to time-varying price signals in the best economic way.

System Model

We consider a typical household in the RTP environment where energy scheduling is performed for the 24-hour scheduling period. The household is equipped with a solar assisted HVAC-water heating system and other loads of different types such as electric vehicle (EV), washing machine, washing dryer, television, and water supply pump. The household loads excluding the joint HVAC-water heating system is classified into controllable and non-controllable types [37]. Non-controllable loads are those whose operations are dependent on the will of users such as computer, lighting, and television. The operations of non-controllable loads are not considered in our optimization. In contrast, the operation schedule of controllable loads can be optimized without disturbing the user life style. We divide the considered scheduling period into N scheduling time slots of equal length τ where the electricity price in each time slot is assumed to be constant.

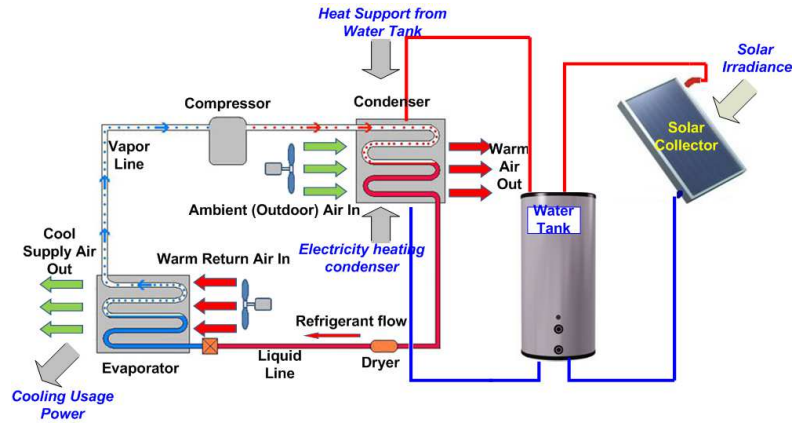


Figure A.3 – Solar assisted HVAC-water heating system

Denote A as the set of all controllable appliances and A_1 represents the HVAC, A_2 for interruptible and deferrable loads, A_3 for noninterruptible and deferrable loads, and A_4 for noninterruptible and nondeferrable loads. Then, we have $A = A_1 \cup A_2 \cup A_3 \cup A_4$.

The solar assisted HVAC-water heating system represents an important load of the household, which is described in the following. The typical components and design of this system is illustrated in Figure A.3 [38]. It consists of a solar collector, a water storage tank, and the HVAC system. Solar energy is collected and transformed into thermal energy which is stored in the water tank by the solar collector. Hot water from the tank then supports the domestic hot water demand and heating/cooling demand of the HVAC system. The operation of HVAC is based on the principle that energy which is used to move heat around is often smaller than the energy used to generate heat. Hence, extra heat from the water tank can be used to support the necessary energy which is used to control the heat cycle in heating/cooling mode of HVAC. To cover the remaining heat demand for the cloudy day or during night time, the water tank is also equipped with an auxiliary heater. In this paper, we use t and s to denote time slot and scenario indices, respectively.

In the solar assisted HVAC and water heating system, solar energy is collected and transformed into thermal energy which is stored in the water tank by solar collector. In addition, HVAC transfers heat by circulating a refrigerant through a cycle of evaporation and condensation. The refrigerant is pumped between two heat exchanger coils named evaporator and condenser by the compressor pump. In the evaporator coil, the refrigerant is evaporated at the low pressure and absorbs heat from its surroundings. The refrigerant is compressed at high pressure and then transferred to the condenser coil where it is condensed at the high pressure and releases the heat it absorbed earlier in the evaporator. The cycle is fully reversible; hence, the HVAC can provide cooling and heating mode. For cooling, the heat is extracted from home and released to outside area. For heating, the heat extracted from outside is used to heat the indoor area.

Energy consumption of HVAC lies mostly in the compressor pump and condenser, especially to maintain temperature at the condenser [39]. By adding support heat to the condenser, less energy consumption is needed for the HVAC to operate the heat cycle, hence the coefficient of operation (COP) is increased. For solar assisted HVAC-water heating, the heat captured in the water tank is used to support heat for the HVAC. For the conventional models, the heat from water tank is not utilized

to support the heat requirement of the HVAC's condenser. For modeling, we impose the following constraints for the solar assisted HVAC and water heating system.

Energy Management Strategy

We employ the two-stage stochastic programming to formulate the scheduling problem where the Monte Carlo simulation technique is used to generate random scenarios. In addition, the formulated problem is solved by using the rolling procedure [16]. Toward this end, we repeatedly solve the underlying stochastic optimization problem in each time slot given the realization of the random variables (i.e., electricity price and renewable energy) in the current time slot t_0 . In particular, we minimize the sum of the electricity cost due to energy consumption at the current time t_0 (as electricity price, solar irradiance, and outdoor temperature at the current time slot are known) and the expected electricity cost from time slot $t_0 + 1$ to the last time slot N . Known information about system uncertainties such as price, solar irradiance, outdoor temperature, non-controllable load power consumption are updated during this rolling process. Therefore, we consider the following optimization objective at each time t_0

$$\min_{p_{i,t}^s} \sum_{i \in A} \left\{ p_{i,t_0} c_{t_0} \tau + \sum_{s=1}^{NS} \rho^s \sum_{t=t_0+1}^N p_{i,t}^s c_t^s \tau \right\} \quad (\text{A.1})$$

where ρ^s denotes the probability of scenario s , which is used to calculate the expected cost toward the end of the scheduling period, c_t is the price, and $p_{i,t}^s$ is the power consumption of load i at time t in scenario s .

This rolling two-stage stochastic programming technique for home energy management follows the tree reduction method where multiple scenarios are generated to capture the uncertainty in electricity price and weather factors [16]. This optimization problem is subject to operation constraints of each type of appliances and the total energy consumption constraints, which can be summarized as follows:

$$\min_{p_{i,t}^s} \sum_{i \in A} \left\{ p_{i,t_0} c_{t_0} \tau + \sum_{s=1}^{NS} \rho^s \sum_{t=t_0+1}^N p_{i,t}^s c_t^s \tau \right\} \quad (\text{A.2})$$

- s. t. System constraints,
 Constraints of solar assisted HVAC-water heating system, A1,
 Constraints of interruptible and deferrable loads, A2,
 Constraints of noninterruptible and deferrable loads, A3,
 Constraints of noninterruptible and nondeferrable loads, A4. (A.3)

The computation procedure is illustrated in Figure A.4. This problem is a mixed integer linear program, which is solved by using the CPLEX solver. We employ the Monte Carlo simulation method to generate scenarios to represent various uncertain factors including price forecast error, solar irradiance, outdoor temperature, and power consumption of non-controllable load. In general, the number

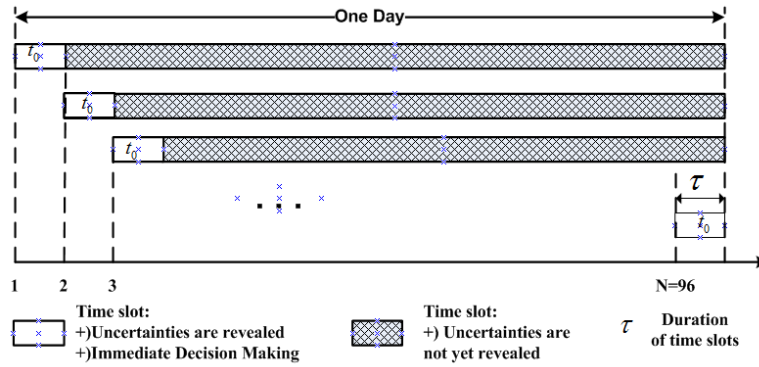


Figure A.4 – Rolling stochastic scheduling for Home Energy Management system

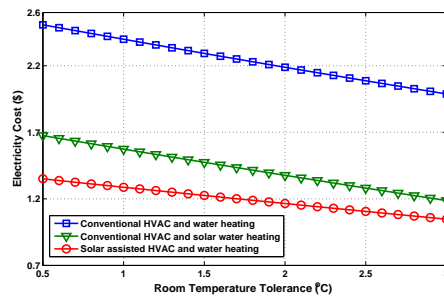
of generated scenarios needs to be sufficiently large to guarantee the energy scheduling efficiency. However, a large number of scenarios may lead to large computation complexity. For a large-scale problem, a scenario reduction method can be used to eliminate the scenario with very low probability, aggregate scenarios of close distances based on certain probability metric, reduce the number of scenarios, and consequently relax the computation burden. We use GAMS/SCENRED software [40] to generate/reduce the set of scenarios in this paper.

Numerical Results

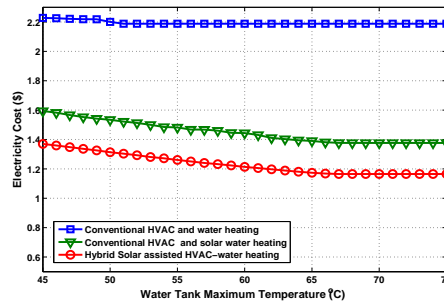
We consider a typical household with solar assisted HVAC-water heating and 3 different controllable loads. The power limit of all controllable loads is assumed 20 KW for simplicity and the threshold for energy consumption in one hour is 15 KWh. Water demand data is taken from [25]. The parameters for solar assisted HVAC and water heating system are described as follows. The solar collector has aperture area about $5 m^2$, the peak power of auxiliary heater is 5 KW, and the initial energy conversion efficiency $\eta_{s1}^0 = 0.7$. The thermal storage tank has volume of 84 gal, which is equivalent to $0.32 m^3$. The tank can receive energy from the heater and solar collector. COP of hybrid and stand alone system are 5 and 3, respectively [39]. Other parameters of the solar system are taken from [41]. Tank temperature is required to be in the range of $[40^\circ C, 70^\circ C]$. The temperature comfort range is chosen as $[20 - \Delta T, 20 + \Delta T]$ where ΔT represents the thermal tolerance, which is set equal 1 unless stated otherwise.

The operations and corresponding costs of the household are influenced by different system parameters including the thermal comfort tolerance, water tank temperature constraint, and solar collector size. We study the variations of energy cost for three different cases, namely conventional HVAC-water heating, conventional HVAC-solar water heating, and solar assisted HVAC-water heating. First, the effect of room temperature tolerance on the energy cost is shown in Figure A.5(a). This figure shows that increasing the room temperature tolerance result in reduction of electricity cost as expected.

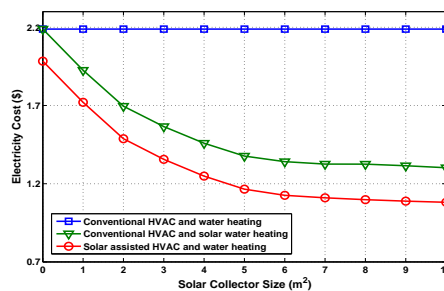
Figure A.5(b) illustrates the influence of maximum water tank temperature on energy cost. By increasing the maximum temperature of water tank, more energy can be stored, which allow more flexibility in scheduling energy consumption to reduce the electricity cost. It is interesting to notice that the electricity cost decreases before saturating at the minimum value. This implies that for a given



(a) Effect of room temperature tolerance



(b) Effect of water tank temperature limit

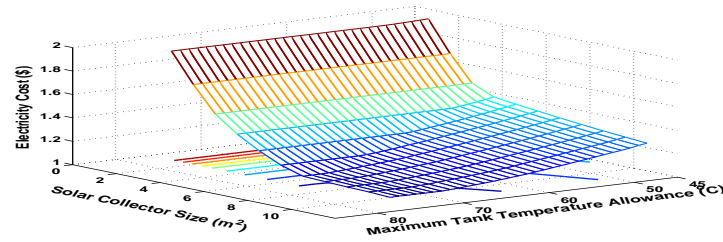


(c) Effect of solar collector size

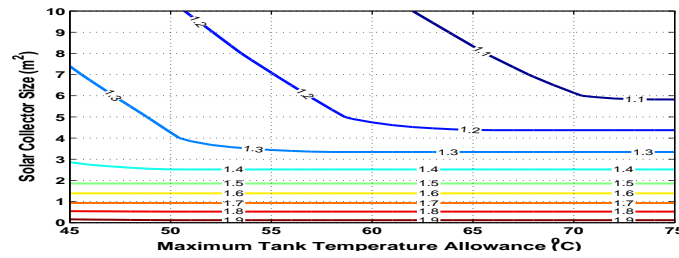
Figure A.5 – Effects of system parameters on electricity cost

solar collector size and auxiliary heater, the amount of captured solar energy and the heater power are limited; hence, the energy stored in tank is also limited. Note also that increasing the maximum water tank temperature can result in better cost-saving, which, however, may effect the equipment life time.

Figure A.5(c) describes the variation of electricity cost with the solar collector size. For the conventional HVAC and water heating system, solar energy is not utilized so the electricity cost remained unchanged. For systems integrating solar energy, as we increase the solar collector size, which means more solar energy can be captured, the electricity cost reduces before setting down at the minimum value. The minimum value corresponds to the thermal capacity limit of the water tank. From the results in Figures A.5(a), A.5(b), and A.5(c), it can be seen that the solar assisted HVAC-water heating achieves the largest cost saving. This is indeed thanks to the utilization of solar energy and the flexible operation of the water tank, which serves as energy storage facility to support both HVAC and water heating loads.



(a) Electricity cost as a function of solar collector size and tank temperature limit



(b) Pareto-optimal constant-cost curves for solar collector size and tank temperature limit

Figure A.6 – Energy cost versus solar collector size and tank temperature limit

Figures A.6(a) and A.6(b) illustrate the impacts of the solar collector size and maximum water tank temperature allowance, which is proportional to the tank thermal capacity, on the energy cost. These figures show that increasing the maximum water tank temperature allowance, which would reduce the life time of the water tank, and increasing solar collector size result in the reduction of energy cost. However, the energy cost converges asymptotically to its minimum values. Thus, above a certain value of solar collector size and maximum temperature allowance, the working cycle of the auxiliary heater reaches its minimum to maintain the water tank temperature when the solar is not available. This minimum value corresponds to the water tank capacity (m^3) and the heat loss. When the solar collector size is small, apparently the cost is not effected by the auxiliary heater. This is because the captured solar energy is insufficient to support the heat loss and the thermal load. Hence, the tank operates mainly by relying on its auxiliary heater. The impact of the maximum water tank temperature limit is only significant when the solar collector size is large enough (above $3m^2$) when the amount of solar energy captured is considerable.

Conclusion

We have proposed unified HEM design to minimize the electricity cost that considers users’ comfort preference and solar assisted thermal load. The developed mathematical model captures the joint operation of the solar assisted HVAC and hot water system accounting for detailed operations of various types of home appliances and the uncertainty in the solar energy and electricity price. We have proposed to solve the energy problem by using the rolling two-stage stochastic optimization approach. Finally, numerical results have been presented to show the significant energy saving for the system with solar assisted thermal load in comparison with other conventional systems.

A.4 Dynamic Pricing Design for Demand Response Integration in Distribution Networks

System Model

We consider a LSE which can procure energy from various sources including the main grid, DR resources, batteries, and local DERs including RESs (e.g., wind and solar energy) and dispatchable DGs (e.g., diesel generators, microturbines, and fuel cells) to serve its customers, which is shown in Figure A.7(a). The energy scheduling problem is considered in a one-day period which is divided into 24 equal time slots. For simplicity, we assume that the LSE possesses several conventional DGs such as diesel generators and fuel cells, and it does not buy energy from privately owned conventional DGs. Additionally, the LSE does not own any renewable energy sources. We assume that the LSE has *take-or-pay* contracts [42], which are also called Power Purchase Agreements (PPA) in some markets [42, 43], with local wind farms and/or solar farms to buy renewable energy from them. In the *take-or-pay* contracts, the LSE buys all available renewable energy generated from these wind/solar farms at a fixed price which is typically lower than the average price from the main grid [42]. Without loss of generality, we assume that the prices paid to all renewable energy sources are the same (c_t^{RES}). Finally, the LSE may own some battery storage units.

System loads are assumed to belong to one of the two categories, namely flexible and inflexible loads. Inflexible loads or critical loads are those that the LSE has to serve. If the LSE cannot fully serve the inflexible loads, a portion of the inflexible loads has to be shed, which is called involuntary load curtailment (ILC). A very high penalty cost (c^{LC}) is imposed on the LSE for ILC since the main goal of the LSE is to guarantee electricity supply to its customers [43]. Inflexible loads are charged under the regular retail price (c_t^{R}). In contrast, flexible loads are assumed to be aggregated by one or several DR aggregators which enjoy a dynamic pricing tariff that should be designed to bring advantages to the DR aggregators. One practical strategy to encourage DR aggregators participating in our proposed operation model is to ensure cost saving for them.

In practice, a flexible load customer might be hesitant to participate in a real-time pricing scheme since electricity prices in this scheme may be greater than the regular retail price for several hours of a day. The loads of a flexible load customer include critical load which should not be shed or shifted and flexible load that can be shed or shifted. Therefore, if the flexible load customer has a large portion of critical load during high price hours, we might not be able to guarantee cost saving for the customer compared to the case where the customer is charged at the fixed retail price. Hence, one of the most practical approaches that the LSE may use to attract flexible load customers to participate in the proposed pricing model is to offer DR price (i.e., the retail price that the LSE charges flexible loads or DR aggregators), which is always lower or equal to the retail price in each hour. In the worst case when the DR price is equal to the regular retail price, the cost imposed on participating entities is the same with the one when they are charged under the regular retail price.

This design allows us to prevent individual small flexible energy customers from interacting directly with the wholesale market, which would complicate the operation of the wholesale market. Moreover, our design ensures that the number of participating parties in our model as well as the number of

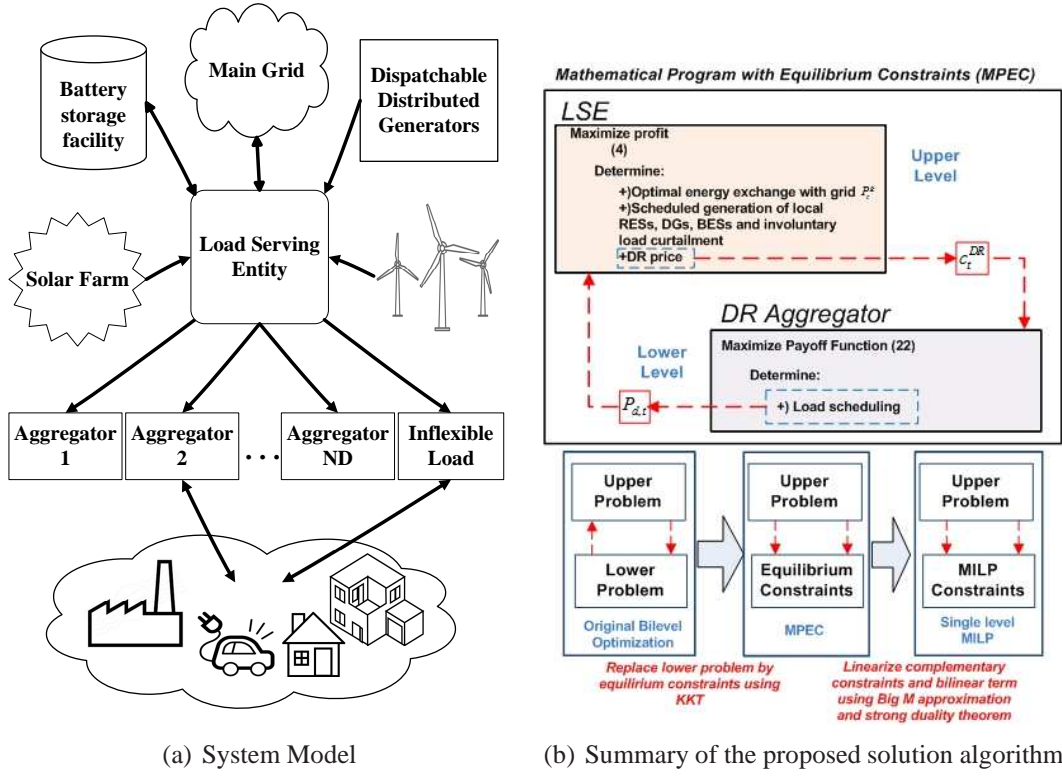


Figure A.7 – System Model and Solution Approach

variables in our formulated optimization problem be reduced significantly. In addition, we assume that DR aggregators have DR contracts with flexible load customers so that these customers can declare the characteristics of their loads (e.g., utility function [14, 42, 44–46] or discomfort function in the case of load reduction or load shifting [10, 43, 44]) to the DR aggregators. Based on the load information provided by their customers, each DR aggregator can construct a suitable aggregated utility function, which is then sent to the LSE.

The underlying optimization problem is formulated as a bilevel program where the LSE is the leader and each DR aggregator is a follower. The outcome of this problem contains optimal dynamic DR price series (c_t^{DR}) over the scheduling horizon. Additionally, the outputs of the proposed problem include the hourly energy trading between the LSE and the main grid (P_t^{G}), the scheduled generation of local RESs (P_t^{RES}) and local DGs ($P_{i,t}$), charging/discharging power of batteries ($P_{k,t}^{\text{c}}, P_{k,t}^{\text{d}}$), amount of ILC (D_t^{LC}), and hourly energy consumption of DR aggregators ($P_{d,t}$).

Problem Formulation

The objective of LSE is to maximize its profit $Profit = Rev - Cost$ where Rev is the retail revenue obtained by serving inflexible loads (at price c_t^{R}) and flexible loads (at price c_t^{DR}), i.e.,

$$Rev = \sum_{t=1}^{NT} \Delta T \left[c_t^{\text{R}} (D_t - D_t^{\text{LC}}) + \sum_{d=1}^{ND} c_t^{\text{DR}} P_{d,t} \right] \quad (\text{A.4})$$

where $D_t - D_t^{\text{LC}}$ is the amount of inflexible load that the LSE serves at time t . The operating cost of the LSE includes the cost of buying/selling electricity power P_t^{g} from/to the main grid with price c_t^{g} , buying renewable energy $P_t^{\text{RES,a}}$ with price c_t^{RES} , operation costs of DGs including start-up cost $SU_{i,t}$ and dispatch cost $C_i(P_{i,t})$ [43], and the penalty cost for involuntary load curtailment $c^{\text{LC}}D_t^{\text{LC}}$. Hence, we have

$$\text{Cost} = \sum_{t=1}^{NT} \Delta T \left[P_t^{\text{g}} c_t^{\text{g}} + c_t^{\text{RES}} P_t^{\text{RES,a}} + \sum_{i=1}^{NG} (SU_{i,t} + C_i(P_{i,t})) + c^{\text{LC}} D_t^{\text{LC}} \right]. \quad (\text{A.5})$$

This objective of LSE is subject to several constraints including power balance constraints, power trading with main grid constraints, renewable energy constraints, involuntary load curtailment constraints, thermal generator constraints, battery constraints, which are MILP constraints, and DR flexible load constraints, which is modeled as a lower optimization problem. In particular, the energy consumption $P_{d,t}$ of DR aggregator d depends on the DR price c_t^{DR} set by LSE, ($c_t^{\text{DR}} \leq c_t^{\text{R}}, \forall t$) as follows:

$$\max_{P_{d,t}} \sum_{t=1}^{NT} \left[U_{d,t}(P_{d,t}) - \Delta T c_t^{\text{DR}} P_{d,t} \right] \quad (\text{A.6})$$

where $U_{d,t}(P_{d,t})$ is utility of DR aggregator d when consuming $P_{d,t}$ and $\Delta T c_t^{\text{DR}} P_{d,t}$ is the cost DR aggregator d pays for LSE.

In this paper, the utility functions of $U_{d,t}(P_{d,t})$ are modeled by multi-block utility functions, which are commonly used in the literature [42, 44–46]. The marginal utility of a demand block decreases as the index of demand blocks increases. Figure A.8 shows the utility function of DR aggregator d at time t . As we can observe, this function has four demand blocks (i.e., $NM_d = 4$). The values at point A, C, D, E are $P_{d,1,t}^{\text{max}}$, $P_{d,1,t}^{\text{max}} + P_{d,2,t}^{\text{max}}$, $P_{d,1,t}^{\text{max}} + P_{d,2,t}^{\text{max}} + P_{d,3,t}^{\text{max}}$, and $P_{d,1,t}^{\text{max}} + P_{d,2,t}^{\text{max}} + P_{d,3,t}^{\text{max}} + P_{d,4,t}^{\text{max}}$, respectively. If the scheduled demand of DR aggregator d at time t is OB (i.e., $P_{d,t} = \text{OB}$), then the utility value for load consumption of aggregator d at time t is equal to the shaded area. Generally, we have

$$U_{d,t}(P_{d,t}) = \Delta T \sum_{m=1}^{NM_d} u_{d,m,t} P_{d,m,t} \quad (\text{A.7})$$

$$P_{d,t} = \sum_{m=1}^{NM_d} P_{d,m,t}. \quad (\text{A.8})$$

Modeling this utility function will result in a linear program that describes the follower (lower) optimization problem of DR aggregator d . Since the lower problem is a linear program, we first replace it by its optimal KKT conditions. The obtained problem is a single objective optimization problem with complementary constraints (MPEC). We then remove the nonlinear terms in the MPEC by using the Fortuny-Amat approximation [47] and the strong duality theorem of linear programming problem. The

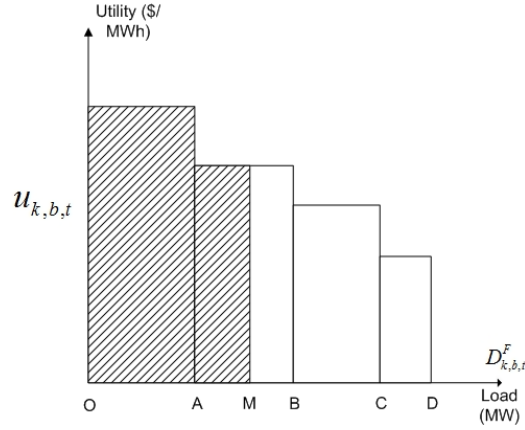


Figure A.8 – DR utility function

final equivalent optimization problem is MILP, which can be solved easily with GAMS/CPLEX. These steps are summarized in Figure A.7(b)

Numerical Results

We assume that the LSE can predict electricity price, inflexible load, and renewable energy generation with high accuracy. For simplicity, we use historical data of the corresponding system parameters as their forecast values. Specifically, the penalty cost for involuntary load curtailment is set equal to 1000 \$/MWh [48]. The renewable energy price that the LSE pays for local wind/solar farms is assumed to be 40 \$/MWh. For simplicity, we assume that $P_t^{g,\max} = P^{\text{grid}}$ and $c_t^R = c^R, \forall t$. The regular retail price in the base case is \$60/MWh and we assume the LSE does not possess any battery storage unit in the base case. Further data can be found in Chapter 5.

We consider the two following schemes.

- **Scheme 1 (S1):** The LSE solves the proposed optimization model. The DR aggregators enjoy a dynamic retail price tariff.
- **Scheme 2 (S2):** The LSE solves the same optimization problem. However, the regular retail price is applied to DR aggregators (i.e., $c_t^{\text{DR}} = c_t^R, \forall t$). In this scheme, DR aggregators have no incentives to modify their loads.

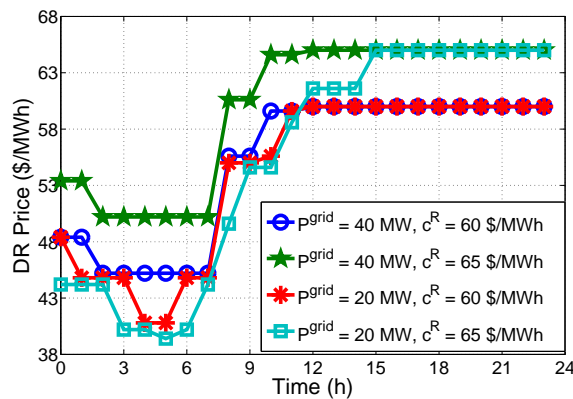
Table A.1 presents the performance comparison between Scheme 1 and Scheme 2 for different values of the regular retail price. Payoff 1, Payoff 2 represent total payoffs of DR aggregators; Profit 1, Profit 2 indicate the optimal profit values of the LSE; and DR1 and DR2 represent the total energy consumption of DR aggregators over the scheduling horizon for Scheme 1 and Scheme 2, respectively. Table A.1 shows that the minimum energy consumption level of all DR aggregators is 201.6 MWh and the total payoff of DR aggregators as well as the optimal profit of the LSE in Scheme 1 are significantly larger than those in Scheme 2. Therefore, we can conclude that Scheme 1 outperforms Scheme 2 in terms of DR aggregators' payoffs and LSE's profit.

Figure A.9 shows the optimal hourly DR prices over the scheduling horizon for different values of c^R and P^{grid} . We can observe that DR price is very low during time slots 1-8, quite low for some period during time slots 9-16, and very high during time slots 17-24. Intuitively, the LSE would set a low DR

Table A.1 – Comparison between Scheme 1 and Scheme 2

c_t^R \$/MWh	Payoff 1 \$	Payoff 2 \$	Profit 1 \$	Profit 2 \$	DR1 MWh	DR 2 MWh
47	2607.2	2403.2	695.7	146.8	272.0	213.6
50	2061.2	1786.6	2103.9	1476.9	270.0	201.6
55	1250.2	778.6	4599.9	3942.8	240.0	201.6
60	251.0	-229.4	7191.3	6408.7	201.6	201.6
65	-756.9	-1237.4	9657.2	8874.6	201.6	201.6

price during some time slots to encourage DR aggregators to consume more energy. In addition, it can set a high DR price (i.e., close or equal to the regular retail price) to discourage DR aggregators from consuming energy.

**Figure A.9** – DR price

There are several reasons for the LSE to set low DR price. First, when the *grid price* is low, the LSE would be interested in buying more energy from the main grid to serve its customers at a DR price between the grid price and the regular retail price. Second, the grid price can vary significantly over the scheduling horizon, which offers opportunities for the LSE to arbitrate between low and high price periods. Therefore, the LSE sets low DR prices at some time slots and high at some other time slots to encourage load shifting from DR aggregators in order to reduce the importing cost of energy from the main grid. Also, DR aggregators can reduce their bills by shifting their loads to low DR price hours. Finally, if renewable energy generation is high, the LSE faces the power limit at the PCC (i.e., P^{grid}); hence, it would sell as much energy as possible to its customers at low DR prices rather than curtailing the renewable energy surplus.

Conclusion

In this paper, we have proposed a novel operation framework for a LSE, which serves both flexible and inflexible loads. The proposed pricing scheme can be readily implemented since it is compatible with the existing pricing structure in the retail market. Extensive numerical results have shown that the proposed scheme helps increase the profit of the LSE, increase payoff for DR aggregators, reduce involuntary load curtailment, and renewable energy curtailment.

A.5 Cost Allocation for Cooperative Demand-Side Resource Aggregators

In Smart Grid, demand-side resources can be aggregated to participate in the electricity market [24, 29, 30], which can be considered as a short-term decision making problem [2]. We will investigate how the aggregated demand-side resources bid energy in the market and allocate the cost to each member. The contribution of this chapter was published in the paper [49]

System Model

We consider a set of cooperative DRAs [29] coordinated by a commercial *virtual power plant* (VPP) [31] as shown in Figure A.10. The commercial VPP [50] manages the output of on-site distributed renewable energy generators, energy consumption of flexible loads, deploys load reduction services, and satisfies nonflexible load demands of multiple cooperative DRAs [29]. Each DRA can be considered as a cluster of several types of load, namely nonflexible load, flexible load, reducible load, and distributed renewable energy sources such as rooftop solar panels and wind turbines [29]. Nonflexible load is the one whose energy consumption cannot be deferred [16, 29]. The flexible load is modeled by a multi-block utility function widely adopted in the literature [14, 28, 42, 44–46]¹. The DRA can employ various load reduction services including load curtailment, back-up generator, and battery which are captured via “reducible load” [10]. Detailed load reduction modeling is not considered for simplicity [10]. All DRAs are coordinated via a commercial VPP [50], which participates in the short-term two-settlement electricity market including the wholesale day-ahead (DA) and the real-time (RT) markets [24, 29] as a single entity [31]. The VPP is assumed to act as a price taker [31] and the bids do not affect the DA/RT clearing prices [24, 29, 31]. Unidirectional interaction with the grid is adopted [24], i.e., we can bid to purchase but cannot sell surplus energy to the grid [24, 29, 30]. The uniform pricing rule and two-settlement system are used to model the financial settlement of DA and RT energy deliveries [24]. In addition, the total cost of VPP or coalitions of DRAs must include the penalty cost of energy bidding deviation [24], the load reduction services’ cost [10], and the flexible load utility [42]. Detailed description of the considered market framework is presented in [24].

¹Other flexible load models such as energy aggregation [29], EV aggregator [24], HVAC aggregator [16], load elastic model [51–53] and their uncertainties can be integrated into the model, which will be considered in our future work.

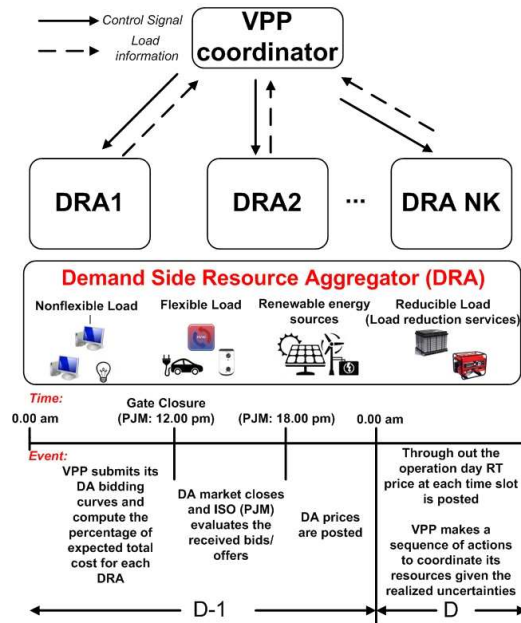


Figure A.10 – Schematic of cooperative DRAs under the VPP's coordination

Cost Allocation Under Cooperative Game Model

The VPP makes decisions on the joint bidding strategy, i.e., the DA bidding decisions before the stochastic scenario materializes [29, 31]², and determines the cost share of each DRA. The resulting bidding cost $v(\mathcal{K})$ must be split among the participants, i.e., the VPP needs to allocate each DRA's percentage quota $x_k(\%)$ of total expected bidding cost $v(\mathcal{K})$ before the planning horizon begins:

$$\sum_{k=1}^{NK} x_k = 1 \text{ (100\%)}, x_k \geq 0.$$

The cost allocation problem, i.e., the determination of x_k , is addressed by using the cooperative game theory [54]. In this study, the bidding strategy is modeled as risk averse two-stage stochastic program [2] where Conditional Value at Risk (CVaR) is used as a risk measure. The cost function v is modeled as the optimal cost value achieved by a risk averse bidding optimization in the electricity market and the percentage quota $x_k(\%)$ of the total VPP's bidding cost $v(\mathcal{K})$ is considered as the solution of the studied cooperative game $\mathcal{G}(\mathcal{K}, v)$.

²PJM time line: <http://pjm.com//media/training/nerc-certifications/EM3-twosettlement.ashx>

Cost function

The cost function $v(S)$ of a coalition S of DRAs can be defined as follows:

$$\begin{aligned}
v(S) = v(e^S) = & \min_{P_t^{\text{DA}}, P_{t,s}^{\text{RT}}, D_{k,t,s}^{\text{F}}, D_{k,b,t,s}^{\text{F}}, U_{k,t,s}, P_{k,t,s}^{\text{G}}, D_{k,t,s}^{\text{R}}, \xi, \eta_s} \\
& (1-\beta) \sum_{s=1}^{\text{NS}} \pi_s \sum_{t=1}^{\text{NT}} \left\{ \lambda_{t,s}^{\text{DA}} P_t^{\text{DA}} \Delta T + \lambda_{t,s}^{\text{RT}} (P_{t,s}^{\text{RT}} - P_t^{\text{DA}}) \Delta T \right. \\
& \left. + \lambda^p |P_{t,s}^{\text{RT}} - P_t^{\text{DA}}| \Delta T + \sum_{k=1}^{\text{NK}} \left(\lambda_k^r D_{k,t,s}^{\text{R}} \Delta T - U_{k,t,s} \right) \right\} \\
& + \beta \left(\xi + \frac{1}{1-\alpha} \sum_{s=1}^{\text{NS}} \pi_s \eta_s \right). \tag{A.9}
\end{aligned}$$

s.t. Constraints of Flexible Load

Constraint of Reducible Load

Constraint of Distributed Generator

Power Balance Constraints

CVaR Constraints

(A.10)

The cost function value obtained from (A.9) results from the risk averse expected cost minimization of a coalition S consisting of individual DRAs $k \in S$ participating in the two-settlement electricity market. It is the weighted sum of the expected cost of market bidding and the CVaR (the last term) which are multiplied with $1 - \beta$ and β , respectively. The expected market bidding's cost includes the energy trading costs in DA market $\lambda_{t,s}^{\text{DA}} P_t^{\text{DA}} \Delta T$, RT market $\lambda_{t,s}^{\text{RT}} (P_{t,s}^{\text{RT}} - P_t^{\text{DA}}) \Delta T$, plus penalty cost due to mismatch between DA bidding and RT dispatch $\lambda^p |P_{t,s}^{\text{RT}} - P_t^{\text{DA}}| \Delta T$ [24, 29], plus the cost of using load reduction minus flexible load's utility $\sum_{k=1}^{\text{NK}} (\lambda_k^r D_{k,t,s}^{\text{R}} \Delta T - U_{k,t,s})$ [10, 42]. These cost components are calculated over NT time slots and NS generated scenarios where π_s is the probability of scenario s .

Based on the modelings of the constraints (A.10), the optimization defining $v(S)$ is a linear programming problem. In addition, the right-hand side of constraints is a linear transformation of coalition indication vector e^S where $e_k^S = 1$ if $k \in S$ and 0 otherwise. The cooperative game that has this special cost function form is called a Linear Programming game, which is totally balance [55] and has a nonempty core $\mathcal{C}(v)$ which contain all budget balanced and stable cost allocation vector x :

$$\mathcal{C}(v) = \left\{ x \in \mathcal{R}^{\text{NK}} : \sum_{k=1}^{\text{NK}} x_k = 1, \sum_{k \in S} x_k v(\mathcal{K} \leq v(S), \forall S \in 2^{\text{NK}} \setminus \{\emptyset\} \right\}. \tag{A.11}$$

Bi-objective Based Cost Allocation

The nonempty core by definition (A.11) is a polyhedron with $NK-1$ dimensions, which can contain many potential cost allocation vectors x . An arbitrary allocation x in the core can correspond to a *weak stable* solution since some coalitions attain very small or zero cost saving value and they might not receive significant benefits to stay in the cooperation [54]. It might also be *unfair* since some DRAs have larger percentage cost reduction than others [54]. Therefore, an efficient design must address two main issues mentioned above, namely stability and fairness. In particular, the stability and fairness metrics employed to design an efficient cost allocation strategy are described as follows:

- *Stability metric*: captures the minimal satisfaction, i.e., the worst-case cost saving $\delta(\$)$ among all coalitions S .
- *Fairness metric*: captures the maximum deviation of the percentage cost saving among individual DRAs which is the difference in percentage cost saving $\gamma(\%)$ between the DRA that achieves the highest percentage cost saving and the DRA that achieves smallest percentage cost saving for a given allocation vector $x \in \mathcal{C}(v)$ [54].

The core cost allocation design aims to find a cost allocation vector $x \in \mathcal{C}(v)$ that achieves efficient tradeoff between the fairness and stability metrics, which can be modeled as a bi-objective optimization problem as follows: (P0)

$$\min_{\bar{\Phi}, \underline{\Phi}, \delta, x_k, \gamma} \gamma \quad (\text{A.12})$$

$$\min_{\delta, x_k} -\delta \quad (\text{A.13})$$

$$\text{s.t: } \sum_{k=1}^{NK} x_k = 1, x_k \geq 0, \quad (\text{A.14})$$

$$\delta \leq v(S) - \sum_{k \in S} x_k v(\mathcal{K}), \forall S \in 2^{NK} \setminus \{\emptyset, \mathcal{K}\} \quad (\text{A.15})$$

$$\delta \geq 0 \quad (\text{A.16})$$

$$\underline{\Phi} \leq x_k \frac{v(\mathcal{K})}{v(\{k\})} \leq \bar{\Phi}, \forall k \in \mathcal{K} \quad (\text{A.17})$$

$$\gamma = \bar{\Phi} - \underline{\Phi}, \quad (\text{A.18})$$

where the optimization of the objective functions (A.12)-(A.13), which minimizes the valued vector $[\gamma, -\delta]$, aims to achieve the fairness and stability, respectively. Moreover, constraint (A.14) means that the total cost (in fraction) is distributed among all DRAs while the auxiliary variable δ in (A.15) provides the lower bound of the cost saving of all coalitions S under cost allocation solution x . The minimal satisfaction, i.e., the worst-case cost saving $\delta(\$)$ among all coalitions S is maximized in (A.13). The constraint (A.16) forces the allocation to be in the core $x \in \mathcal{C}(v)$ while constraint (A.17) provides the lower bound $\underline{\Phi}$ and upper bound $\bar{\Phi}$ for the ratio between allocated cost under grand coalition and cost due to the non-cooperative scenario for all DRAs k (i.e., the cost percentage saving).

The maximum deviation γ of the percentage cost saving of individual DRAs, which is the difference of $\underline{\Phi}$ and $\overline{\Phi}$ as in (A.18), is minimized in (A.12).

To obtain Pareto optimal points, we convert problem (P0) into a single-objective optimization problem (P3) using the ε -constraint method [56] since problem (P0) is linear. The stability objective function (A.13) is chosen to be optimized while the fairness objective (A.12) is converted into a constraint. Let $M + 1$ be the number of grid points of the Pareto front and $m \in \{0, 1, \dots, M\}$. Two extremes points, $m = 0$, and $m = M + 1$, are determined by solving two following optimization problems respectively:

$$(P1) \quad \min_{\overline{\Phi}, \underline{\Phi}, \delta, x_k, \gamma} \gamma$$

s.t: constraints (A.14) - (A.18).

$$(P2) \quad \max_{\delta, x_k} \delta$$

s.t: constraints (A.14)- (A.15).

Then, the m^{th} point on the Pareto front can be obtained by solving the following single-objective optimization problem:

$$(P3) \quad \max_{\overline{\Phi}, \underline{\Phi}, \delta, x_k, \gamma} \delta$$

s.t: constraints (A.14)-(A.15), (A.17)-(A.18)

$$\gamma \leq \gamma^m, \tag{A.19}$$

where γ^m is a parameter defining the m^{th} point on the Pareto front. In particular, γ^m is chosen as $\gamma^{\min} \leq \gamma^m \leq \gamma^{\max}$. γ^{\min} and γ^{\max} can be obtained from the payoff table when we solve (P1), which minimizes the maximum deviation of the percentage cost saving γ^{\min} , and (P2), which finds the nucleolus allocation solution with δ^{\max} , respectively. In this study, the parameter γ^m identifying m^{th} is chosen as follows:

$$\gamma^m = \gamma^{\min} + m \frac{\gamma^{\max} - \gamma^{\min}}{M}. \tag{A.20}$$

Pareto Front Construction

We solve (P1), (P2), and (P3) to have $M + 1$ points that define the Pareto front. All of them are large scale optimization problem subject to $2^{\text{NK}} - 2$ constraints (A.15) with only NK optimization variables

x_k . Hence, row constraint generation is a natural approach. In particular, we solve (P1) by solving iteratively the master problem (MP1), which is a relaxed version of (P1) that only considers condition (A.15) for a subset $\mathcal{O}(S) \in 2^{\text{NK}} - 2$, and the sub problem (SP1) that find the most violated constraint with x^* obtained from solving (MP1). The sub-problem (SP1) identifying a unexplored coalition S^* that achieves the least cost reduction as follows:

(SP1)

$$\begin{aligned} \underline{\delta} = \min & \left[v(S) - \sum_{k=1}^{\text{NK}} e_k^S x_k^* v(\mathcal{K}) \right] = \min_{e_k^S, P_t^{\text{DA}}, P_t^{\text{RT}}, D_{k,t,s}^F, D_{k,b,t,s}^F, U_{k,t,s}, P_{k,t,s}^G, D_{k,t,s}^R, \xi, \eta_s} \\ & (1-\beta) \sum_{s=1}^{\text{NS}} \pi_s \sum_{t=1}^{\text{NT}} \left\{ \lambda_{t,s}^{\text{DA}} P_t^{\text{DA}} \Delta T + \lambda_{t,s}^{\text{RT}} (P_{t,s}^{\text{RT}} - P_t^{\text{DA}}) \Delta T \right. \\ & \left. + \lambda^p |P_{t,s}^{\text{RT}} - P_t^{\text{DA}}| \Delta T + \sum_{k=1}^{\text{NK}} \left(\lambda_k^r D_{k,t,s}^R \Delta T - U_{k,t,s} \right) \right\} \\ & + \beta \left(\xi + \frac{1}{1-\alpha} \sum_{s=1}^{\text{NS}} \pi_s \eta_s \right) - \sum_{k=1}^{\text{NK}} e_k^S x_k^* v(\mathcal{K}) \end{aligned} \quad (\text{A.21})$$

$$\text{s.t: } 1 \leq \sum_{k=1}^{\text{NK}} e_k^S \leq \text{NK} - 1, e_k^S \in \{0, 1\} \quad (\text{A.22})$$

$$\sum_{k \in S} (1 - e_k^S) + \sum_{k \notin S} (e_k^S) \geq 1, \forall S \in \mathcal{O}(S) \quad (\text{A.23})$$

$$\text{Constraints (A.10) defining } v(S). \quad (\text{A.24})$$

The sub-problem (SP1) is a mixed integer linear program (MILP) with extra binary variables e_k^S acting as first-stage variables. Solving (SP1) enables us to obtain e^{S^*} , which give S^* and $v(S^*)$ simultaneously. Constraint (A.22), which means $S \in 2^{\text{NK}} \setminus \{\emptyset, \mathcal{K}, \mathcal{O}(S)\}$, and constraint (A.23), which means $S \notin \mathcal{O}(S)$, ensures only unexplored coalitions S are considered in this optimization problem. All original constraints required in computing $v(S)$ are given in (A.24). If we solve (MP1) and (SP1) iteratively as summarized in Algorithm 1, we finally reach x^* such that $\underline{\delta} \geq 0$ since the core is nonempty. Then, γ is minimized and the obtained $x^* \in \mathcal{C}(v)$ is the final cost allocation solution for (P1). Similarly, we can solve (P2) and (P3) optimally using the row constraint generation approach since the number of constraints are much greater than the number of optimization variables. Solving (P1) (P2) and m (P3) with different γ^m let us have $M + 1$ Pareto points that form the Pareto front.

Numerical Results

We consider a VPP that coordinates the cooperation of NK DRAs. The scheduling horizon is one day, which is divided into $\text{NT} = 24$ equal time slots, each lasting $\Delta T = 1$ hour. We assume that in each time slot t , each DRA k can aggregate 10% of total nonflexible load, which can be reduced by using the load reduction (LR) services with price $\lambda^r = 100\$/\text{MWh}$. The power capacity transferred via main

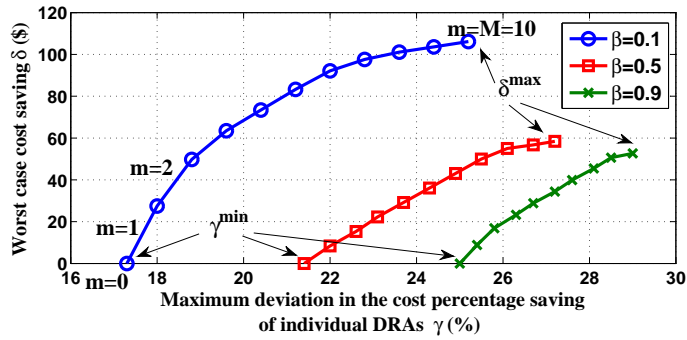
grid is $P_k^{\max} = 15\text{MW}$. Finally, $v(S)$ is assumed to be well-defined, i.e., the market bidding optimization problem due to coalition S is feasible. Other data can be found in Chapter 5.

Figure A.11(a), A.11(b), A.11(c) show the Pareto fronts for the cost allocation problem when we vary the risk parameter β , flexible load scale E_{scale}^F , and penalty price λ^p , respectively. Each obtained Pareto front describes the tradeoffs between the stability represented by the worst-case cost saving value δ and the fairness captured by the maximum deviation of the percentage cost saving γ . For all cases, when $\gamma = \gamma^{\min}$ then we have $\delta = 0$ meaning that we reach the minimum value of δ while still guaranteeing to operate in the core whose definition is given in (A.11). On the other hand, as δ reaches its maximum value δ^{\max} , which corresponds to the nucleolus as the minimum deviation of the percentage cost saving among players, we achieves its maximum value $\gamma = \gamma^{\max}$.

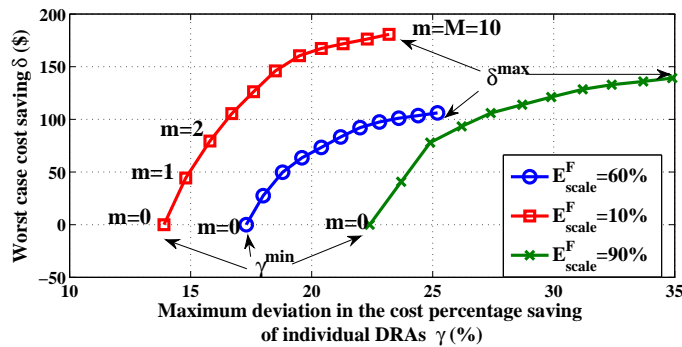
These two extreme points in the Pareto front correspond to the cases where the cost allocation solution x is either at the fairness core point, γ^{\min} , or the lexicographically optimal point, the nucleolus δ^{\max} , in the polyhedron $\mathcal{C}(v)$. These figures show that the proposed design enables us to determine multiple different Pareto-efficient solutions in the core of the underlying cooperative game. Moreover, one can choose an operation point on the Pareto front with desirable stability-fairness tradeoff. Specifically, for a certain desired value of the maximum deviation of the cost percentage saving γ , one can determine the corresponding cost allocation vector with the achievable value of the worst-case cost saving δ being maximized. This demonstrates the flexibility and efficiency of our proposed cost allocation design compared to other existing designs such as the nucleolus-based cost allocation.

Conclusion

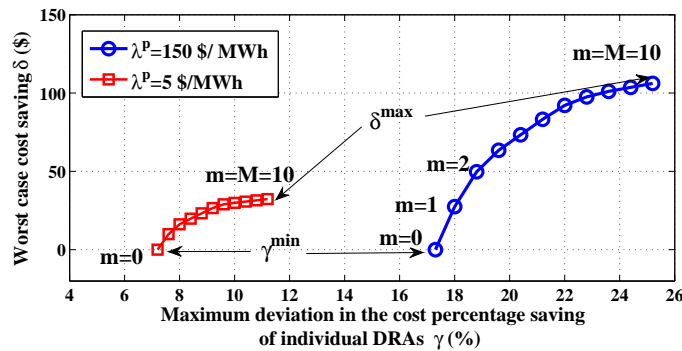
This study presents a computationally efficient cost allocation design for cooperative DRAs based on the cooperative game core concept. We have proposed to exploit the nonempty core property of the underlying balanced game and develop a bi-objective optimization framework that strikes the balance between the allocation stability and fairness. We have employed the ε -constraint and row constraint generation methods to successfully construct the Pareto front of the cost allocation solutions with manageable computation complexity. The proposed design can efficiently allocate percentage quota of total bidding cost to individual DRAs while achieving desirable stability-fairness trade-off.



(a) Pareto front with $\lambda^p = 150\$/MWh$, $E_{scale}^F = 60\%$, and varying β



(b) Pareto front with $\lambda^p = 150\$/MWh$, $\beta = 0.1$ and varying E_{scale}^F



(c) Pareto front with $E_{scale}^F = 60\%$, $\beta = 0.1$, and varying λ^p

Figure A.11 – Pareto fronts under different parameter settings

Chapitre B

Résumé

B.1 Motivation de la recherche

L'industrie électrique a connu une transformation importante en passant des systèmes d'énergie centralisés dominés par les grandes entreprises de services publics et très dépendants des ressources énergétiques fossiles, aux réseaux intelligents avec une forte pénétration en terme d'énergies renouvelables distribuées qui respectent l'environnement et impliquent activement des consommateurs d'énergie sur le marché déréglementation [2]. L'un des changements les plus importants est probablement l'adoption généralisée de la gestion active de la demande dans les réseaux intelligents [3]. En fait, il a été défini dans le titre XIII de la Loi sur l'acte d'indépendance et de sécurité énergétique (AISE) en 2007 que le réseau intelligent est un réseau électrique qui intègre une variété de mesures opérationnelles et énergétiques, y compris les compteurs intelligents, les appareils intelligents, les ressources énergétiques renouvelables, et des ressources énergétiques pour motiver la gestion de la demande active [3]. Le cadre des normes d'interopérabilité pour les réseaux intelligents définie par l'Institut national des normes et de la technologie (INNT) est illustrée dans la figure B.1 [1].

La recherche et la réalisation de divers concepts et technologies de réseaux intelligents ont reçu des investissements énormes provenant des gouvernements dans le monde entier. En particulier, l'infrastructure avancée des technologies de l'information et de la communication (TIC) a été considérablement améliorée dans de nombreux pays où un nombre massif de compteurs intelligents ont été installés, par exemple, plus de 45 millions de compteurs intelligents ont été déployés par Le ministère de l'énergie dans le cadre des subventions d'investissement du réseau intelligent [7]. De plus, les réseaux de communication déployés et les systèmes de gestion des données forment l'infrastructure de mesure avancée (IMA), qui permet une communication bidirectionnelle entre les services publics et les clients [8]. La mise à niveau de l'infrastructure des TIC a ouvert la voie à la réalisation d'une gestion active de la demande [9–15]. La décision intelligente prise par les entités 'côté demande' peut apporter de nombreux avantages au réseau intelligent [2]. Par exemple, les consommateurs d'énergie résidentielle peuvent exploiter des systèmes de tarification dynamiques pour planifier leur consommation d'énergie afin de minimiser leurs coûts[16–23].

Grâce au déploiement de l'infrastructure TIC du réseau, les consommateurs d'énergie résidentielle et l'opérateur de réseau sont connectés et des services de 'réponse à la demande' (RD) peuvent être

offerts à l'opérateur du réseau en modifiant la consommation d'énergie, ce qui peut permettre au réseau de fonctionner plus efficacement [13, 14, 24–27]. L'opérateur du réseau peut cependant être intéressé à motiver ses clients (consommateurs d'énergie) à participer activement au programme RD par le biais, par exemple, d'une politique de tarification appropriée. Une approche bien connue pour permettre à l'opérateur de réseau de gérer les services RD de ses clients consiste à déployer l'entité LSE (Load Serving Entity) [28]. Enfin, les petites entités du côté de la demande peuvent coopérer pour agir en tant qu'entité unique sous la coordination d'un agrégat de ressources de la demande [29, 30] ou d'une centrale électrique virtuelle [31], pour acheter de l'énergie sur le marché de gros puisque les prix de l'énergie en gros tendent à être moins chers que les prix de détail [32]. Afin de participer au marché de gros, les entités de la demande doivent prendre plusieurs décisions telles que les décisions de coordination pour former une grande coalition de coopération, enchère d'énergie dans le marché, et partager les avantages de la coopération entre eux.

En général, la conception des structures intelligentes de prise de décision pour les entités de la demande peut être très difficile dans l'environnement du réseau intelligent avec une pénétration croissante des énergies renouvelables dans le réseau de distribution [6, 33]. Bien que respectueux de l'environnement, les ressources énergétiques renouvelables telles que l'énergie solaire et éolienne peuvent être très imprévisibles, ce qui peut conduire à de grandes difficultés pour assurer des opérations efficaces et fiables du réseau de distribution impliqué [2]. En particulier, l'adoption d'une mauvaise stratégie de gestion de l'énergie peut entraîner une faible utilisation des énergies renouvelables [19, 34]. En outre, la mauvaise paramétrage des prix ne peut pas s'attaquer à la fluctuation des sources d'énergie renouvelables, ce qui entraîne éventuellement des opérations instables du réseau [35]. Enfin, la conception appropriée d'une stratégie d'appel d'offres peut avoir des effets positifs sur le résultat ainsi que le coût des entités participant au marché de l'électricité côté demande. C'est une question importante parce que les participants au marché doivent être responsables de la gestion des incertitudes de leurs sources d'énergie renouvelable [29, 36].

En résumé, l'exploitation réussie de la gestion active de la demande exige la résolution de plusieurs problèmes de prise de décision pour les entités de réseaux intelligents impliqués dans le réseau de distribution. Cette thèse vise à résoudre certains de ces problèmes.

B.2 Objectifs et contributions de la recherche

Cette thèse vise à répondre à trois défis importants décrits ci-dessus, dont les contributions peuvent être illustrées à la figure B.2 et résumées comme suit.

Au chapitre 3, nous étudions le problème d'ordonnancement de l'énergie domestique dans l'environnement de tarification en temps réel. Plus précisément, nous proposons un modèle complet tenant compte de l'intégration des énergies renouvelables dans le système énergétique domestique, c'est-à-dire le système de chauffage solaire assisté par l'eau (HVAC). Ensuite, nous proposons une conception d'un modèle de contrôle prédictif (MCP) en temps réel pour une maison intelligente équipée d'un système de chauffage solaire assisté par l'eau (HVAC) et d'autres charges contrôlables en réponse à la tarification en temps réel du signal. Nous concevons un algorithme à horizon glissant pour la gestion

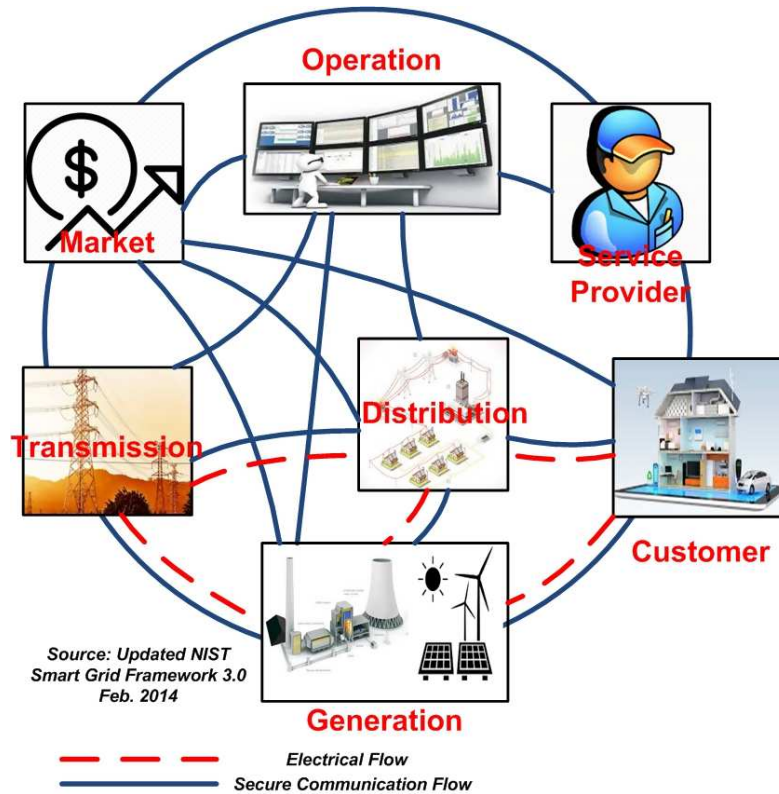


FIGURE B.1 – Modèle Conceptuel NIST Smart Grid 3.0 [1]

de l'énergie domestique afin de minimiser son coût, de garantir les contraintes du système tout en exploitant la relation de couplage énergétique du système de chauffage solaire thermique et le système HVAC pour améliorer leur efficacité énergétique.

Au chapitre 4, nous considérons le problème du paramétrage des prix dans le réseau de distribution pour motiver la participation des consommateurs d'énergie au service de la 'réponse à la demande'. En particulier, nous proposons un système de tarification dynamique pouvant être mis en œuvre dans le réseau de distribution sous le modèle d'entité de service de Charge (LSE), qui est facile à implémenter et compatible avec la structure de marché actuelle. Notre conception crée une incitation pour la charge flexible de répondre à la demande qui peut aider le LSE à s'adapter aux fluctuations des prix de l'électricité, de la charge conventionnelle non flexible et des énergies renouvelables distribuées. Plus précisément, nous présentons la formulation de la conception des prix proposée en utilisant la structure de programmation à deux niveaux. Étant donné que le sous-problème de niveau inférieur est linéaire, nous utilisons les conditions optimales KKT pour convertir le problème de deux niveaux en un seul objectif mathématique avec des contraintes d'équilibre (MPEC), qui est ensuite transformé en un programme linéaire de nombre entier mixé avec un seul objectif équivalent (MILP) en utilisant la formule de Fortuny-Amat et le théorème de la forte dualité de la programmation linéaire. Le MILP obtenu peut être résolu efficacement en utilisant des solutions commerciales disponibles. Des résultats numériques sont ensuite présentés pour illustrer l'efficacité de notre conception dans la motivation de l'intégration de la réponse à la demande dans le réseau de distribution.

Le chapitre 5 étudie comment partager le coût des agrégats coopératifs de ressources à côté la demande (DRA), qui sont basés sur des modèles génériques d'agents actifs de la demande. Plus préci-

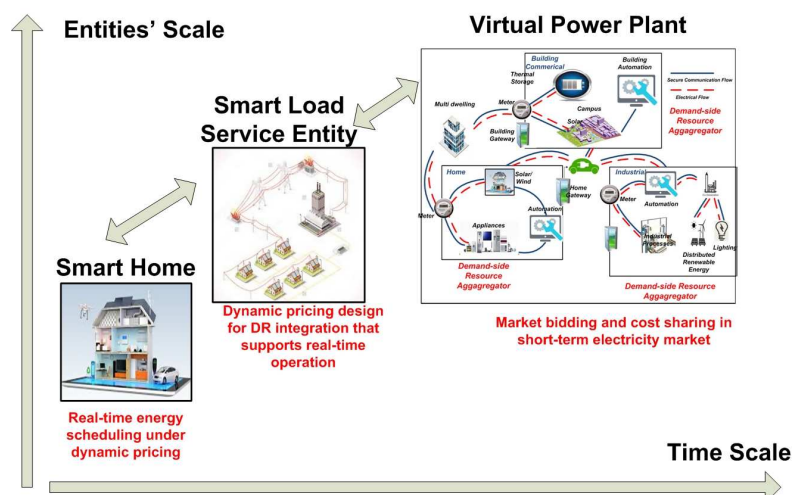


FIGURE B.2 – Problèmes traités dans cette thèse

sément, ces DRA sont coordonnés dans le cadre de la centrale virtuelle d'énergie pour soumissionner conjointement sur le marché de l'électricité et le coût correspondant doit être réparti entre les membres. À cette fin, nous présentons pour la première fois le modèle global d'allocation des coûts, applicable à la structure actuelle du marché. Ensuite, le problème de la répartition des coûts est modélisé comme la solution d'un jeu coopératif dans lequel toutes les DRAs agissent en tant que joueurs et la valeur de la fonction des coalitions des joueurs est le résultat de leurs stratégies optimales du marché de l'enchère qui sont obtenues en résolvant les programmes stochastiques correspondants en deux étapes. Nous montrons que le noyau du jeu étudié, qui définit tous les vecteurs de répartition budgétaire équilibrés et stables, est non vide. Ensuite, nous proposons de déterminer le vecteur de répartition des coûts à l'intérieur du noyau, en considérant le compromis entre différents critères en résolvant une optimisation bi-objectif. Cette dernière a un nombre exponentiel de contraintes avec des paramètres implicites qui sont les valeurs de la fonction des coalitions. Étant donné que le nombre de partage des coûts est seulement égal au nombre de DRAs, qui est beaucoup plus petit que le nombre de contraintes, nous proposons un algorithme basé sur la combinaison des méthodes ϵ -constraint et de génération des contraintes ligne pour construire le front de Pareto dans un effort de calcul facile à gérer.

B.3 Gestion de l'énergie d'une maison intelligente avec une charge thermique et solaire assistée avec considération des incertitudes des prix et des énergies renouvelables

Les contributions de cette étude ont été publiées dans l'article [19]. En particulier, nous étudions comment une seule maison intelligente équipée d'appareils à base d'énergie renouvelable peut répondre aux signaux de prix variant dans le temps de la meilleure façon économique.

Modèle de système

Nous considérons un ménage typique dans l'environnement RTP où l'ordonnancement énergétique est effectuée pour une période de 24 heures. Le ménage est équipé d'un système de chauffage à eau HVAC

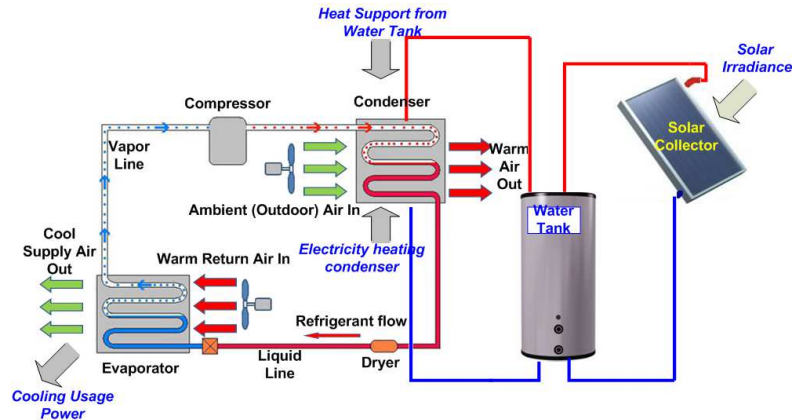


FIGURE B.3 – Le système de chauffage assisté par eau solaire HVAC

assisté par l'énergie solaire et d'autres charges de différents types telles qu'un véhicule électrique (EV), machine à laver, un sèche-linge, une télévision et une pompe d'alimentation en eau. Les charges, à l'exclusion du système de chauffage combiné HVAC-eau, sont classées selon les types contrôlables et non contrôlables [37]. Les charges non contrôlables sont celles dont les opérations dépendent de la volonté des utilisateurs tels que l'ordinateur, l'éclairage et la télévision. Les opérations de charges non contrôlables ne sont pas prises en compte dans notre optimisation. En revanche, le programme d'exploitation des charges contrôlables peut être optimisé sans perturber le style de vie de l'utilisateur. Nous divisons la période d'ordonnancement considérée en N intervalles de temps d'ordonnancement de longueur égale à τ où le prix de l'électricité dans chaque intervalle de temps est supposé être constant.

Notons A comme l'ensemble de tous les appareils contrôlables et A_1 représentant le HVAC, A_2 pour les charges interruptibles et reportables, A_3 pour les charges non interruptibles et reportables, et A_4 pour les charges non interruptibles et non reportables. Alors, nous avons $A = A_1 \cup A_2 \cup A_3 \cup A_4$.

Le système de chauffage solaire assisté par l'eau HVAC représente une charge importante du ménage, qui est décrite dans ce qui suit. Les composants typiques et la conception de ce système sont illustrés à Figure B.3 [38]. Il se compose d'un capteur solaire, d'un réservoir d'eau et d'un système HVAC. L'énergie solaire est collectée et transformée en énergie thermique qui est stockée dans le réservoir d'eau par le capteur solaire. L'eau chaude du réservoir supporte alors la demande d'eau chaude sanitaire et la demande de chauffage/refroidissement du système HVAC. Le fonctionnement du HVAC est basé sur le principe que l'énergie utilisée pour déplacer la chaleur autour est souvent plus petite que l'énergie utilisée pour générer de la chaleur. Par conséquent, la chaleur supplémentaire du réservoir d'eau peut être utilisée pour supporter l'énergie nécessaire utilisée pour commander le cycle thermique en mode chauffage/refroidissement du HVAC. Pour couvrir la demande de chaleur restante en temps nuageux ou pendant la nuit, le réservoir d'eau est également équipé d'un chauffage auxiliaire. Dans cet article, nous utilisons t et s pour désigner les indices de créneaux horaires et de scénarios, respectivement.

Dans le système de chauffage solaire assisté HVAC et le système de chauffage par l'eau, l'énergie solaire est collectée et est transformée en énergie thermique qui est stockée dans le réservoir d'eau par le biais du collecteur solaire. De plus, le HVAC transfère de la chaleur d'appoint au condenseur. Le fluide frigorigène est pompé entre deux serpentins échangeurs de chaleur appelés évaporateur et

condenseur par la pompe du compresseur. Dans l'évaporateur, le réfrigérant est évaporé à basse pression et absorbe la chaleur de son environnement. Le fluide frigorigène est comprimé sous haute pression puis transféré dans la bobine du condenseur où il est condensé à haute pression et libère la chaleur absorbée plus tôt dans l'évaporateur. Le cycle est entièrement réversible ; Par conséquent, le HVAC peut fournir le mode de refroidissement et de chauffage. Pour le refroidissement, la chaleur est extraite de la maison et libérée à l'extérieur. Pour le chauffage, la chaleur extraite de l'extérieur est utilisée pour chauffer la zone intérieure.

La consommation d'énergie du système HVAC réside principalement dans la pompe du compresseur et le condenseur pour maintenir la température du condenseur [39]. En ajoutant de la chaleur de support au condenseur, moins de consommation d'énergie est nécessaire pour faire fonctionner le cycle de la chaleur du HVAC. Le coefficient de fonctionnement (COP) est donc augmenté. Pour le chauffage assisté par l'énergie solaire, la chaleur captée dans le réservoir d'eau est utilisée comme chaleur d'appoint pour le HVAC. Pour la modélisation, nous imposons les contraintes pour le système de chauffage et de HVAC assisté par l'énergie solaire.

Stratégie de gestion de l'énergie

Nous utilisons la programmation stochastique en deux étapes pour formuler le problème d'ordonnancement où la technique de simulation Monte Carlo est utilisée pour générer des scénarios aléatoires. En outre, le problème formulé est résolu en utilisant la procédure à horizon glissant [16]. À cette fin, nous résolvons à plusieurs reprises le problème d'optimisation stochastique sous-jacent dans chaque intervalle de temps compte tenu de la réalisation des variables aléatoires (c'est-à-dire le prix de l'électricité et l'énergie renouvelable) dans l'intervalle de temps actuel t_0 . En particulier, nous minimisons la somme du coût de l'électricité due à la consommation d'énergie à l'heure actuelle t_0 (étant donné que le prix de l'électricité, l'éclairement solaire et la température extérieure à l'heure actuelle t_0 actuel sont connus) et le coût prévu de l'électricité entre le créneau horaire $t_0 + 1$ et la dernière tranche horaire N . Les informations connues sur les incertitudes du système telles que le prix, l'éclairement solaire, la température extérieure, la consommation d'énergie de charge non contrôlable sont mises à jour au cours de ce processus à horizon glissant.

Par conséquent, nous considérons l'objectif d'optimisation suivant à chaque instant t_0

$$\min_{p_{i,t}^s} \sum_{i \in A} \left\{ p_{i,t_0} c_{t_0} \tau + \sum_{s=1}^{NS} \rho^s \sum_{t=t_0+1}^N p_{i,t}^s c_t^s \tau \right\} \quad (\text{B.1})$$

où ρ^s indique la probabilité du scénario s , qui est utilisée pour calculer le coût attendu vers la fin de la période d'ordonnancement, et $p_{i,t}^s$ est la consommation d'énergie de la charge i à l'instant t dans le scénario s .

Cette technique de programmation stochastique en deux étapes pour la gestion de l'énergie domestique suit la méthode de réduction des arbres, où de multiples scénarios sont générés pour saisir l'incertitude des facteurs de prix et de conditions climatiques [16]. Ce problème d'optimisation est soumis aux contraintes d'exploitation de chaque type d'appareils et aux contraintes de consommation totale d'énergie, qui peuvent être résumées comme suit :

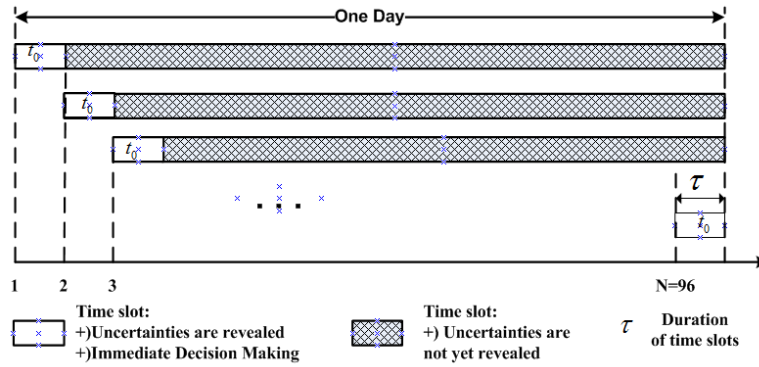


FIGURE B.4 – Planification Stochastique Roulant pour la Gestion de L'Énergie Domestique

$$\min_{p_{i,t}^s} \sum_{i \in A} \left\{ p_{i,t_0} c_{t_0} \tau + \sum_{s=1}^{NS} \rho^s \sum_{t=t_0+1}^N p_{i,t}^s c_t^s \tau \right\} \quad (B.2)$$

- s. c. Contraintes du système,
 Contraintes du système de chauffage solaire assisté par l'eau HVAC, A1,
 Contraintes de charges interruptibles et reportables, A2,
 Contraintes des charges non interruptibles et reportables, A3,
 Contraintes de charges non interruptibles et non reportables, A4. (B.3)

La procédure de calcul est illustrée à la Figure B.4. Ce problème est un programme linéaire à variables mixtes (MILP), qui est résolu en utilisant le solveur CPLEX. Nous utilisons la méthode de simulation Monte Carlo pour générer des scénarios afin de représenter divers facteurs incertains, y compris l'erreur de prévision de prix, l'éclairage solaire, la température extérieure et la consommation d'énergie de la charge non contrôlable. En général, le nombre de scénarios générés doit être suffisamment grand pour garantir l'efficacité de l'ordonnancement énergétique. Cependant, un grand nombre de scénarios peut conduire à une grande complexité de calcul. Pour un problème de grande envergure, on peut utiliser une méthode de réduction de scénarios pour éliminer le scénario ayant une probabilité très faible, agréger des scénarios de distances rapprochées basés sur une certaine métrique de probabilité, et réduire le nombre de scénarios et donc minimiser la charge de calcul. Nous utilisons le logiciel GAMS/SCENRED [40] pour générer/réduire l'ensemble des scénarios de ce travail.

Résultats numériques

Nous considérons un ménage typique avec chauffage à eau HVAC assisté par l'énergie solaire et 3 différentes charges contrôlables. La limite de la puissance de toutes les charges contrôlables est supposée égales à 20 KW pour la simplicité et le seuil pour la consommation d'énergie pour une heure est 15 KWh. Les données sur la demande d'eau sont extraites de [25]. Les paramètres pour le chauffage solaire assisté HVAC et le système de chauffage par l'eau sont décrits comme suit. Le réservoir de stockage thermique a un volume de 84 gal, ce qui équivaut à 0.32 m³. Le réservoir peut recevoir

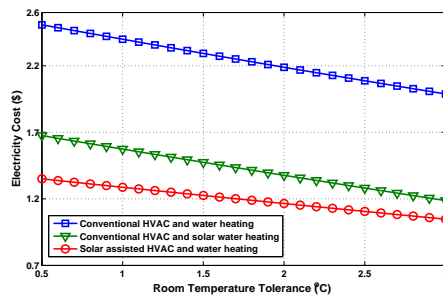
l'énergie du chauffage et du collecteur solaire. Le *COP* des systèmes hybride et autonome sont 5 et 3, respectivement [39]. D'autres paramètres du système solaire sont extraits de [41]. La température du réservoir doit être comprise entre $[40^{\circ}\text{C}, 70^{\circ}\text{C}]$. L'intervalle de confort de température est choisie $[20 - \Delta T, 20 + \Delta T]$ où ΔT représente la tolérance thermique, qui est égale à 1 sauf indication contraire.

Le fonctionnement et les coûts correspondants à la maison intelligente sont influencés par différents paramètres du système, y compris la tolérance du confort thermique, la contrainte de température du réservoir d'eau, et la taille du collecteur solaire. Nous étudions les variations du coût de l'énergie pour trois cas différents. Tout d'abord, l'effet de la tolérance de la température ambiante sur le coût de l'énergie est montré à la Figure B.5(a). Cette figure montre que l'augmentation de la tolérance à la température interne entraîne une diminution du coût de l'électricité comme prévu.

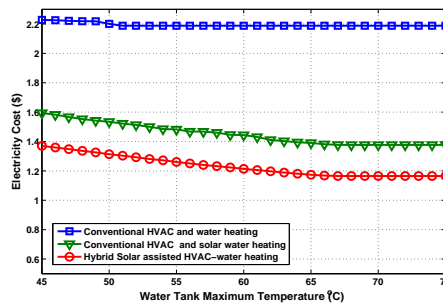
La figure B.5(b) illustre l'influence de la température maximale du réservoir d'eau sur le coût énergétique. En augmentant la température maximale du réservoir d'eau, plus d'énergie peut être stockée, ce qui permet une plus grande souplesse dans la consommation d'énergie d'ordonnancement pour réduire le coût de l'électricité. Il est intéressant de noter que le coût de l'électricité diminue avant de saturer à la valeur minimale. Cela implique que pour une taille de collecteur solaire donnée et un dispositif de chauffage auxiliaire, la quantité d'énergie solaire captée et la puissance de chauffage sont limitées ; par conséquent, l'énergie stockée dans le réservoir est également limitée. Notez également que l'augmentation de la température maximale du réservoir d'eau peut entraîner une meilleure économie, ce qui peut toutefois affecter la durée de vie de l'équipement.

La Figure B.5(c) décrit la variation du coût de l'électricité avec la taille du collecteur solaire. Pour le chauffage conventionnel HVAC et le chauffage par l'eau, l'énergie solaire n'est pas utilisée de sorte que le coût de l'électricité reste inchangé. Pour les systèmes intégrant l'énergie solaire, à mesure que nous augmentons la taille du capteur solaire, ce qui signifie qu'une plus grande quantité d'énergie solaire peut être captée, le coût de l'électricité diminue avant de s'établir à la valeur minimale. Cette dernière correspond à la limite de la capacité thermique du réservoir d'eau. A partir des résultats des Figures B.5(a), B.5(b) et B.5(c), on constate que le chauffage à eau HVAC assisté par l'énergie solaire permet d'obtenir la plus grande économie des coûts. C'est en effet grâce à l'utilisation de l'énergie solaire et la souplesse de fonctionnement du réservoir d'eau, qui sert au stockage de l'énergie pour supporter à la fois les charges du HVAC et celles du chauffage par l'eau.

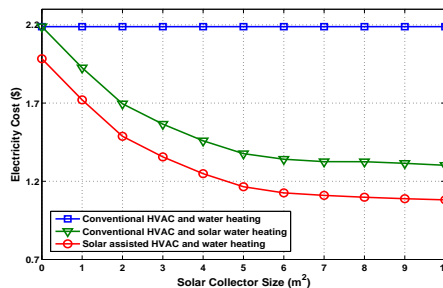
Les Figures B.6(a) et B.6(b) illustrent les impacts de la taille de certaine dimension du capteur solaire et de la température maximale du réservoir d'eau, proportionnelle à la capacité thermique du réservoir, sur le coût énergétique. Ces chiffres montrent que l'augmentation de la température maximale admissible du réservoir d'eau, qui réduirait la durée de vie du réservoir d'eau, et l'augmentation de la taille du capteur solaire entraîneraient une réduction du coût énergétique. Cependant, le coût énergétique converge asymptotiquement vers ses valeurs minimales. Ainsi, au-delà d'une certaine valeur de capteur solaire et de température maximale, le cycle de travail du chauffage auxiliaire atteint son minimum pour maintenir la température du réservoir d'eau lorsque le soleil n'est pas disponible. Cette valeur minimale correspond à la capacité du réservoir d'eau (m^3) et à la perte de chaleur. Lorsque la taille du collecteur solaire est faible, apparemment le coût n'est pas affecté par le chauffage auxiliaire. En effet, l'énergie solaire captée est insuffisante pour supporter la perte de chaleur et la charge



(a) Effet de la tolérance à la température intérieure



(b) Effet de la limite de température du réservoir d'eau



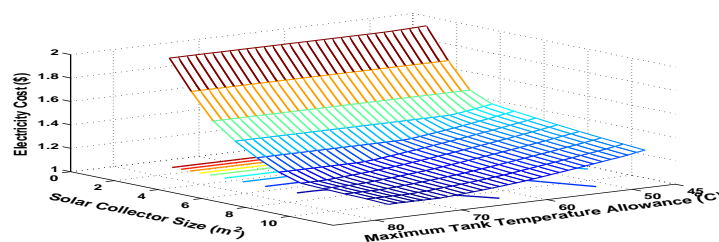
(c) Effet de la taille du capteur solaire

FIGURE B.5 – Effets des paramètres du système sur le coût de l'électricité

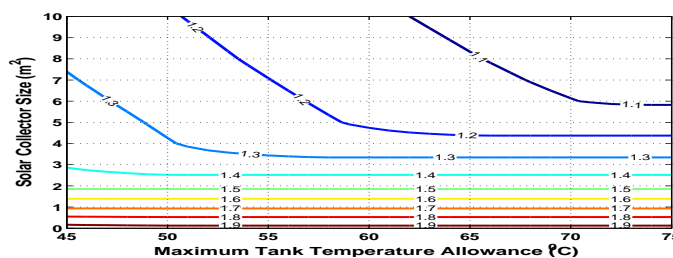
thermique. Par conséquent, le réservoir opère principalement en se basant sur son appareil de chauffage auxiliaire. L'impact de la limite maximale de température du réservoir d'eau n'est significatif que lorsque la taille du collecteur solaire est suffisamment grande (au-dessus de $3m^2$) et lorsque la quantité d'énergie solaire captée est considérable.

Conclusion

Nous avons proposé une conception de gestion de la maison enrgy (HEM) unifiée pour minimiser le coût de l'électricité qui tient compte des préférences de confort des utilisateurs et de la charge thermique assistée par le soleil. Le modèle mathématique développé capture l'opération conjointe de la HVAC assisté par le soleil et le système à eau chaude tout en tenant compte des opérations détaillées de divers types d'appareils ménagers et de l'incertitude dans le prix de l'énergie solaire et d'électricité.



(a) Le coût de l'électricité en fonction de la taille du capteur solaire et de la limite de température du réservoir



(b) Courbes constante coûts optimaux Pareto pour la taille du capteur solaire et de la limite de température du réservoir

FIGURE B.6 – Coût de l'énergie par rapport à la taille du collecteur solaire et de la température de la cuve

Nous avons proposé de résoudre le problème énergétique en utilisant l'approche stochastique en deux étapes. Enfin, des résultats numériques ont été présentés pour montrer l'économie d'énergie significative pour le système avec la charge thermique solaire assistée en comparaison avec d'autres systèmes classiques.

B.4 Conception dynamique des prix pour l'Intégration de la réponse à la demande dans les réseaux de distribution

Modèle de système

Nous considérons un LSE qui peut prendre l'énergie à partir de diverses sources, y compris le réseau principale, les ressources DR, les batteries et les DER locales y compris les RES (par exemple l'énergie éolienne et solaire) et les DG d'appoint (par exemple, les générateurs diesel, les microturbines et les piles à combustible) pour servir ses clients, ce qui est illustré à la Figure B.7. Le problème d'ordonnancement énergétique est considéré dans une période d'une journée qui est divisée en 24 tranches de temps égales. Par souci de simplicité, nous supposons que le LSE a plusieurs DG conventionnelles telles que les générateurs diesel et les piles à combustible, et n'achète pas d'énergie des DG traditionnelles privées. En outre, la LSE n'a pas d'énergies renouvelables. Nous supposons que le LSE a des contrats de *take-or-pay* [42], également connus sous le nom de Power Purchase Agreements (PPA) dans certains marchés, avec des fermes éoliennes locales et/ou d'énergie renouvelable. Dans les contrats *take-or-pay*, la LSE achète toute l'énergie renouvelable disponible générée par ces fermes éoliennes/solaires à un prix fixe qui est généralement inférieur au prix moyen du réseau principal. Sans

perte de généralité, nous supposons que les prix payés à toutes les sources d'énergie renouvelables sont les mêmes (c_t^{RES}). Enfin, le LSE peut avoir quelques batteries de stockage.

On suppose que les charges du système appartiennent à l'une des deux catégories, à savoir les charges flexibles et inflexibles. Les charges inflexibles ou les charges critiques sont celles que le LSE doit servir. Si le LSE ne peut pas servir pleinement les charges inflexibles, certaines des charges inflexibles doivent être réduites, ce qui est appelé réduction de charge involontaire (ILC). Un coût de pénalité très élevé (c^{LC}) est imposé à la LSE pour la ILC puisque l'objectif principal de la LSE est d'assurer la fourniture d'électricité à ses clients [43]. Des frais inflexibles sont facturés sur la base du prix de vente régulier (c_t^{R}). En revanche, on suppose que les charges flexibles sont agrégées par un ou plusieurs agrégats de DR qui bénéficient d'une tarification dynamique qui devrait être conçu pour offrir des avantages aux agrégats de DR. Une stratégie pratique pour encourager les agrégats DR à participer à notre modèle d'exploitation proposé consiste à leur permettre d'économiser des coûts.

Dans la pratique, un client de charge souple peut hésiter à participer à un système de tarification en temps réel puisque les prix de l'électricité dans ce régime peuvent être supérieurs au prix de détail régulier pour plusieurs heures de la journée. Les charges d'un client de charge flexible incluent la charge critique qui ne doit pas être perdue ou déplacée et la charge flexible qui peut être versé ou déplacé. Par conséquent, si le client de charge flexible a une grande partie de la charge critique pendant les heures de prix élevés, nous ne pourrions pas être en mesure de garantir des économies pour le client par rapport au cas où le client est facturé au prix fixe. Par conséquent, l'une des approches les plus pratiques que le LSE peut utiliser pour attirer des clients de charge flexible à participer au modèle de tarification proposé est d'offrir le prix DR (c'est-à-dire le prix de détail que le LSE facture aux charges flexibles ou aux agrégats DR) inférieur ou égal au prix de détail à chaque heure. Dans le pire des cas où le prix DR est égal au prix régulier de vente au détail, le coût imposé aux entités participantes est le même que celui auquel ils sont facturés au prix de détail régulier.

Cette conception nous permet d'empêcher les petits consommateurs individuels d'énergie flexibles d'interagir directement avec le marché de gros, ce qui compliquerait le fonctionnement du marché de gros. En outre, notre conception assure que le nombre de parties prenantes dans notre modèle ainsi que le nombre de variables dans le problème d'optimisation formulé soit réduit de manière significative. De plus, nous supposons que les agrégats DR ont des contrats DR avec des clients de charge flexibles pour que ces clients puissent déclarer les caractéristiques de leurs charges ou fonction inconfort dans le cas de la réduction de la charge ou le transfert de charge aux agrégats DR. Sur la base des informations de charge fournies par leurs clients, chaque agrégat DR peut construire une fonction d'utilité agrégée appropriée, qui est ensuite envoyée au LSE.

Le problème d'optimisation sous-jacent est formulé comme un programme à deux niveaux où le LSE est le leader et chaque agrégat DR est un suiveur. Le résultat de ce problème contient les séries de prix DR dynamiques optimales (c_t^{DR}) sur l'horizon d'ordonnancement. De plus, les sorties du problème proposé inclut les commerces horaires de l'énergie entre le LSE et le réseau principal (P_t^{E}), la génération prévue des ressources locales RES et DG (P_t^{RES}) ($P_{i,t}$), respectivement, la charge/décharge des batteries ($P_{k,t}^{\text{C}}, P_{k,t}$ LC) et la consommation horaire d'énergie des agrégats DR ($P_{d,t}$).

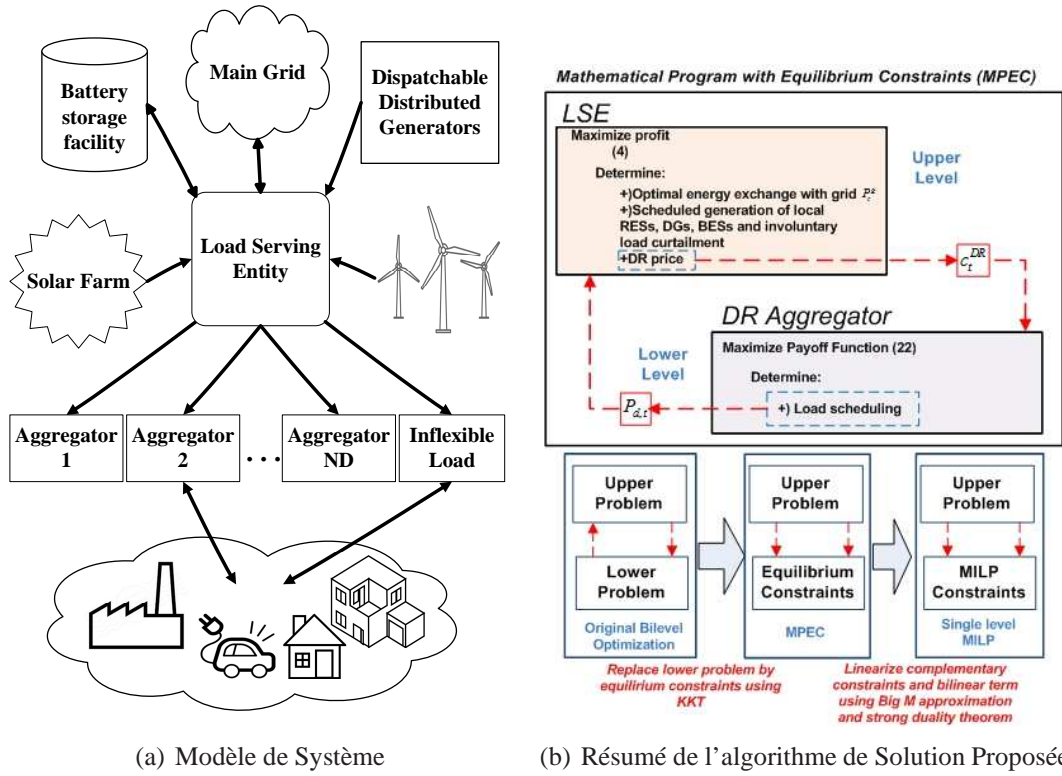


FIGURE B.7 – Modèle de Système et Approche de Solution

Formulation du problème

L'objectif de LSE est de maximiser son profit $Profit = Rev - Cost$ où Rev est le revenu de détail obtenu en servant des charges inflexibles (au prix c_t^{sfR}) et des charges flexibles (au prix c_t^{sfDR}) :

$$Rev = \sum_{t=1}^{NT} \Delta T \left[c_t^R (D_t - D_t^{LC}) + \sum_{d=1}^{ND} c_t^{DR} P_{d,t} \right] \quad (B.4)$$

où $D_t - D_t^{LC}$ est la quantité de charge inflexible que le LSE sert au temps t . Le coût d'exploitation de la LSE inclut le coût d'achat / vente de l'électricité du réseau principal avec le prix c_t^g , l'achat d'énergie renouvelable $P_t^{RES,a}$ à prix c_t^{RES} . Les coûts d'exploitation de la DG, y compris le coût de démarrage $SU_{i,t}$, le coût d'expédition $C_i(P_{i,t})$ [43], et le coût de pénalité pour la réduction involontaire de la charge $c^{LC} D_t^{LC}$. Par conséquent, nous avons

$$Cost = \sum_{t=1}^{NT} \Delta T \left[P_t^g c_t^g + c_t^{RES} P_t^{RES,a} + \sum_{i=1}^{NG} (SU_{i,t} + C_i(P_{i,t})) + c^{LC} D_t^{LC} \right]. \quad (B.5)$$

Cet objectif du LSE est soumis à plusieurs contraintes, notamment les contraintes de balance de puissance, les contraintes d'échange d'énergie avec le réseau principale, les contraintes d'énergie renouvelable, les contraintes involontaires de restriction de charge, les contraintes de générateur thermique, les contraintes de batterie, qui sont MILP, et les contraintes de charge flexible DR, qui sont modélisées comme un problème d'optimisation plus faible sous-jacent.

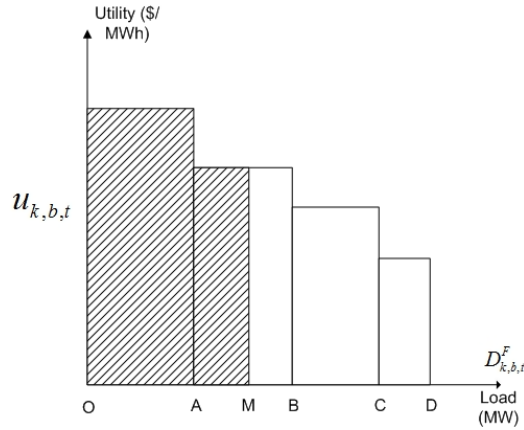


FIGURE B.8 – Fonction d'utilité DR

En particulier, la consommation d'énergie $P_{d,t}$ de l'agrégat DR d dépend du prix DR c_t^{DR} fixé par le LSE, ($c_t^{\text{DR}} \leq c_t^{\text{R}}, \quad \forall t$) comme suit :

$$\max_{P_{d,t}} \sum_{t=1}^{NT} \left[U_{d,t}(P_{d,t}) - \Delta T c_t^{\text{DR}} P_{d,t} \right]. \quad (\text{B.6})$$

où $U_{d,t}(P_{d,t})$ est l'utilité de l'agrégat DR d en consommant $P_{d,t}$ et $\Delta T c_t^{\text{DR}} P_{d,t}$ est le coût que l'agrégat DR d paie pour le LSE.

Dans cet article, les fonctions d'utilité de $U_{d,t}(P_{d,t})$ sont modélisées par des fonctions utilitaires multi-bloc, qui sont couramment utilisées dans la littérature [42, 44–46]. L'utilité marginale d'un bloc de demande diminue dans la mesure que l'indice des blocs de demande augmente. Figure B.8 montre la fonction d'utilité de l'agrégat DR d à l'instant t . Comme nous pouvons l'observer, cette fonction a quatre blocs de demande (c'est-à-dire, $NM_d = 4$). Les valeurs au point A, C, D, E sont $P_{d,1,t}^{\text{max}}$, $P_{d,1,t}^{\text{max}} + P_{d,2,t}^{\text{max}}$, $P_{d,1,t}^{\text{max}} + P_{d,2,t}^{\text{max}} + P_{d,3,t}^{\text{max}}$, et $P_{d,1,t}^{\text{max}} + P_{d,2,t}^{\text{max}} + P_{d,3,t}^{\text{max}} + P_{d,4,t}^{\text{max}}$, respectivement. Si la demande planifiée de l'agrégat DR d à l'instant t est OB (c'est-à-dire, $P_{d,t} = \text{OB}$), alors la valeur d'utilité pour la consommation de charge de l'agrégat d à l'instant t est égale à la zone ombrée. Généralement, nous avons

$$U_{d,t}(P_{d,t}) = \Delta T \sum_{m=1}^{NM_d} u_{d,m,t} P_{d,m,t} \quad (\text{B.7})$$

$$P_{d,t} = \sum_{m=1}^{NM_d} P_{d,m,t}. \quad (\text{B.8})$$

La modélisation de cette fonction d'utilité se traduira par un programme linéaire qui décrit le problème d'optimisation du suiveur (inférieur) de l'agrégat DR d . Puisque le problème inférieur est un programme linéaire, nous le remplaçons en premier par ses conditions optimales KKT. Le problème obtenu est un problème d'optimisation uni-objectif avec des contraintes complémentaires (MPEC). Nous supprimons ensuite les termes non linéaires dans le MPEC en utilisant l'approximation Fortuny-Amat [47] et le théorème de la dualité forte du problème de programmation linéaire. Le problème final

d'optimisation équivalente est MILP, qui peut être facilement résolu avec GAMS/CPLEX. Ces étapes sont résumées dans la Figure B.7(b).

Résultats numériques

Nous supposons que le LSE peut prédire le prix de l'électricité, la charge inflexible, et la production d'énergie renouvelable avec une grande précision. Pour simplifier, nous utilisons les données historiques des paramètres du système correspondant comme leurs valeurs de prévision. Plus précisément, le coût de pénalité pour une réduction involontaire de charge est égale à 1000\$/MWh [48]. Le prix de l'énergie renouvelable que le LSE paie pour les fermes vent/solaires locales est supposé être 40 \$/MWh. Pour simplifier, nous supposons que $P_t^{g,max} = P^{grid}$ et $c_t^R = c^R, \forall t$. Le prix de détail courant dans le cas de base est 60 \$/MWh et nous supposons que le LSE ne possède pas de batterie de stockage dans le cas de base. On trouvera d'autres données au chapitre 5.

Les deux schémas suivants sont considérés :

- **Schéma 1 (S1)** : Le LSE résout le modèle d'optimisation proposé. Les agrégats DR bénéficient d'un tarif de détail dynamique.
- **Schéma 2 (S2)** : Le LSE résout le même problème d'optimisation. Cependant, le prix de détail régulier est appliqué aux agrégats DR (c'est-à-dire $c_t^{DR} = c_t^R, \forall t$). Dans ce schéma, les agrégats DR n'ont aucune incitation à modifier leurs charges.

TABLE B.1 – Comparaison entre le Schéma 1 et le Schéma 2

c_t^R \$/MWh	Paiement 1 \$	Paiement 2 \$	Profit 1 \$	Profit 2 \$	DR1 MWh	DR 2 MWh
47	2607.2	2403.2	695.7	146.8	272.0	213.6
50	2061.2	1786.6	2103.9	1476.9	270.0	201.6
55	1250.2	778.6	4599.9	3942.8	240.0	201.6
60	251.0	-229.4	7191.3	6408.7	201.6	201.6
65	-756.9	-1237.4	9657.2	8874.6	201.6	201.6

Le tableau B.1 montre la comparaison des performances entre le Schéma 1 et le Schéma 2 pour différentes valeurs du prix de détail régulier. Paiement 1, Paiement 2 représentent les gains totaux des agrégats DR; Profit 1, Profit 2 indiquent les valeurs du profit optimales du LSE; DR1 et DR2 représentent la consommation d'énergie totale des agrégats DR sur l'horizon de planification pour le Schéma 1 et le Schéma 2, respectivement. Le tableau B.1 montre que le niveau minimal de consommation d'énergie de tous les agrégats DR est de 201.6 MWh et que les avantages totaux des agrégats DR et le bénéfice optimal de la LSE sur la Figure 1 sont nettement plus importants que ceux du Schéma 2. Par conséquent, nous pouvons conclure que le Schéma 1 surpasse le Schéma 2 en termes d'amélioration des paiements des agrégats DR et du bénéfice de LSE.

La Figure B.9 montre les prix horaires optimaux du DR sur l'horizon de planification pour différentes valeurs de c^R et P^{grid} . On peut observer que le prix de DR est très faible pendant les tranches de temps 1-8, assez bas pendant l'intervalle de temps 9-16 et très élevé pendant les créneaux de temps 17-24. Intuitivement, le LSE fixerait un prix de DR faible pendant certains créneaux horaires pour encourager les agrégats DR à consommer plus d'énergie. En outre, il peut fixer un prix de DR élevé (c'est-à-dire, proche ou égal au prix de détail régulier) pour décourager les agrégats DR à consommer de l'énergie.

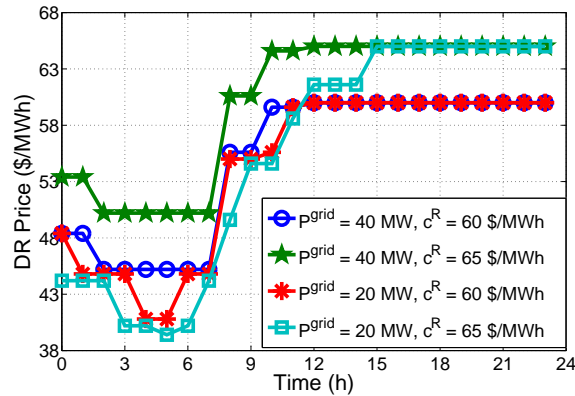


FIGURE B.9 – Prix DR

Il y a plusieurs raisons pour que le LSE fixe un prix de DR bas. Tout d'abord, lorsque le *prix de réseau* est faible, le LSE serait intéressé à acheter plus d'énergie à partir du réseau principal au service de ses clients à un prix de DR entre le prix de du réseau et le prix de détail régulier. Deuxièmement, le prix du réseau peut varier de manière significative sur l'horizon de la planification, ce qui offre des possibilités aux le LSE pour arbitrer entre les périodes hautes et basses prix. Par conséquent, le LSE établit des prix de DR bas pour encourager le transfert de charge des agrégats DR afin de réduire le coût d'importation de l'énergie du réseau principal. En outre, les agrégats DR peuvent réduire leurs factures en déplaçant leurs charges aux heures de faible prix de DR. Enfin, si la production d'énergie renouvelable est élevée, le LSE fait face à la limite de puissance au PCC (à savoir, P^{grid}); par conséquent, il se vendrait autant d'énergie que possible à ses clients à des prix DR bas plutôt que de restreindre l'excédent d'énergie renouvelable.

Conclusion

Dans cette étude, nous avons proposé un nouveau cadre opérationnel pour un LSE, qui sert à la fois aux charges souples et inflexibles. Le système de tarification proposé peut être facilement mis en œuvre puisqu'il est compatible avec la structure de prix existante sur le marché de détail. De nombreux résultats numériques ont montré que le régime proposé contribue à accroître le bénéfice de la LSE et les retombées pour les agrégats de DR, à réduire la réduction de la charge involontaire et l'énergie renouvelable.

B.5 Répartition des coûts pour les agrégats coopératifs de ressources à la demande

Dans le réseau intelligent, les ressources à la demande peuvent être agrégées pour participer au marché de l'électricité [24, 29, 30], qui peut être considéré comme un problème de décision à court terme [2]. Nous examinerons comment ils achètent de l'énergie sur le marché et attribuent le coût à chacun de leur membre. La contribution de ceux-ci chapitre a été publiée dans l'article [49]

Modèle de système

Nous considérons un ensemble de DRA coopératifs [29] coordonné par une *Centrale électrique virtuelle* commerciale (VPP) [31] comme le montre la Figure B.10. Le VPP [50] gère la production des générateurs d'énergie renouvelable distribués sur place, la consommation d'énergie des charges flexibles, déploie des services de réduction de charge et satisfait aux exigences de charge non flexibles de multiples DRA coopératifs. Chaque DRA peut être considéré comme une grappe de plusieurs types de charge, à savoir la charge non flexible, la charge flexible, la charge réductible, et les sources d'énergie renouvelables distribuées telles que les panneaux solaires et les éoliennes [29]. La charge non flexible est celle dont la consommation d'énergie ne peut être différée [16, 29]. La charge flexible est modélisée par une fonction de multi-bloc d'utilité largement adoptée dans la littérature [14, 28, 42, 44–46]¹. Le DRA peut employer divers services de réduction de charge, y compris la raccourcissement de charge, le générateur de secours et la batterie qui sont capturés via la charge réductible [10]. La modélisation détaillée de la réduction de charge n'est pas considérée sa simplification [10]. Toutes les DRAs sont coordonnées par l'intermédiaire d'un VPP [50] commercial, qui participe au marché d'électricité à court terme à deux règlements, y compris le commerce de gros du jour-avant (DA) et les marchés en temps réel (RT) [24, 29] comme une entité unique [31]. Le VPP est supposé agir comme preneur de prix [31] et les enchères n'affectent pas les prix DA/RT [24, 29, 31]. L'interaction unidirectionnelle avec le réseau est adoptée [24], c'est-à-dire que, nous pouvons enchérir pour acheter, mais nous ne pouvons pas vendre de l'énergie excédentaire au réseau [24, 29, 30]. La règle de tarification uniforme et le système à deux règlements sont utilisés pour modéliser le règlement financier des livraisons des énergies de DA et RT [24]. En outre, le coût total de VPP ou de coalitions de DRA doit inclure le coût de pénalité de l'écart d'enchères d'énergie, le coût de services de réduction de charge et l'utilitaire de charge flexible [42]. Une description détaillée du cadre de marché considéré est présentée dans [24].

Allocation de coûts dans le modèle de jeu coopératif

Le VPP prend des décisions sur la stratégie conjointe d'appel d'offres, c'est-à-dire les décisions d'appel d'offres de la DA avant que le scénario stochastique ne se matérialise [29, 31]², et détermine la part de coût de chaque DRA. Le coût d'enchères résultant $v(\mathcal{K})$ doit être réparti entre les participants,

¹Autres modèles de charge flexibles tels que l'agrégation d'énergie [29], agrégat EV [24] et leur incertitude peuvent être intégrées dans le modèle, ce qui sera considéré dans notre futur travail

²PJM time line : <http://pjm.com/media/training/nerc-certifications/EM3-twosettlement.ashx>

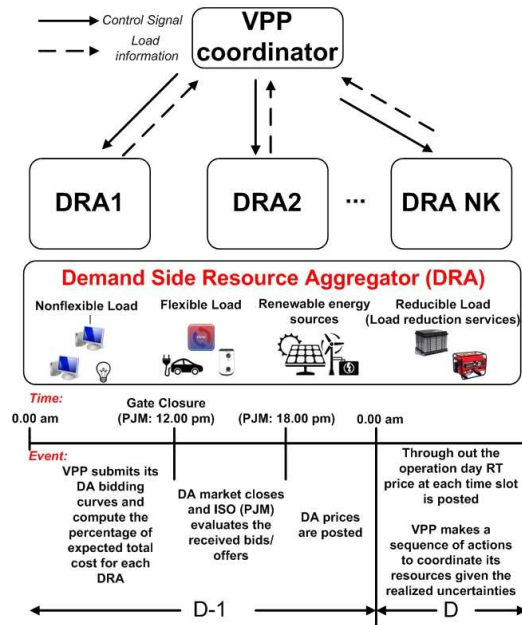


FIGURE B.10 – Schéma des DRA coopératives sous la coordination du VPP

c'est-à-dire que le VPP doit allouer le quota de chaque DRA $x_k(\%)$ du coût d'enchères attendu $v(\mathcal{H})$ avant que l'horizon de planification commence :

$$\sum_{k=1}^{NK} x_k = 1 \text{ (100\%)}, x_k \geq 0.$$

Le problème d'allocation des coûts, c'est-à-dire, la détermination de x_k , est résolu en utilisant la théorie des jeux coopératifs [54]. Dans cette étude, la stratégie d'appel d'offres est modélisée comme un programme stochastique en deux étapes à risque avéré [2] où la valeur conditionnelle à risque (CVaR) est utilisée comme mesure de risque. La fonction de coût v est modélisée comme la valeur optimale de coût obtenue par une enchère d'optimisation à risque avéré dans le marché de l'électricité et le pourcentage $x_k(\%)$ du coût total d'enchères de VPP $v(\mathcal{H})$ est considéré comme la solution étudié du jeu coopératif $\mathcal{G}(\mathcal{H}, v)$.

Fonction coût

La fonction de coût $v(S)$ d'une coalition S de DRA peut être définie comme suit :

$$\begin{aligned}
v(S) = v(e^S) = & \min_{P_t^{DA}, P_{t,s}^{RT}, D_{k,t,s}^F, D_{k,b,t,s}^F, U_{k,t,s}, P_{k,t,s}^G, D_{k,t,s}^R, \xi, \eta_s} \\
(1-\beta) \sum_{s=1}^{NS} \pi_s \sum_{t=1}^{NT} & \left\{ \lambda_{t,s}^{DA} P_t^{DA} \Delta T + \lambda_{t,s}^{RT} (P_{t,s}^{RT} - P_t^{DA}) \Delta T \right. \\
& \left. + \lambda^p |P_{t,s}^{RT} - P_t^{DA}| \Delta T + \sum_{k=1}^{NK} \left(\lambda_k^r D_{k,t,s}^R \Delta T - U_{k,t,s} \right) \right\} \\
& + \beta \left(\xi + \frac{1}{1-\alpha} \sum_{s=1}^{NS} \pi_s \eta_s \right). \tag{B.9}
\end{aligned}$$

$$\begin{aligned}
\text{s.t.} \quad & \text{Contraintes de charge flexible} \\
& \text{Contraintes de la charge reduite} \\
& \text{Contraintes du générateur Distributed} \\
& \text{Contraintes d'équilibre de puissance} \\
& \text{Contraintes CVaR} \tag{B.10}
\end{aligned}$$

La valeur de la fonction de coût obtenue de (B.9) résulte de la minimisation des coûts prévus d'une coalition S composée de $k \in S$ DR participant au marché de l'électricité à deux règlements. Il s'agit de la somme pondérée du coût attendu des enchères de marché et CVaR (le dernier terme), qui sont multipliées par $1 - \beta$ et β respectivement. Le coût de l'offre de marché attendue comprend les coûts de négociation d'énergie sur le marché DA $\lambda_{t,s}^{DA} P_t^{DA} \Delta T$, le marché DA $\lambda_{t,s}^{RT} (P_{t,s}^{RT} - P_t^{DA}) \Delta T$, plus pénalité $\lambda^p |P_{t,s}^{RT} - P_t^{DA}| \Delta T$ [24, 29], plus le coût d'utilisation de la réduction de charge moins l'utilité de la charge flexible $\sum_{k=1}^{NK} (\lambda_k^r D_{k,t,s}^R \Delta T - U_{k,t,s})$ [10, 42]. Ces composantes de coût sont calculées sur NT créneaux horaires et NS scénarios où π_s est la probabilité du scénario s .

L'optimisation définissant $v(S)$ est un problème de programmation linéaire. En outre, le côté droit des contraintes est une transformation linéaire de l'indication de vecteur de coalition e^S où $e_k^S = 1$ si $k \in S$ et 0 sinon. Le jeu coopératif qui a cette forme de fonction de coût spécial est appelé ensemble de programmation linéaire, qui est totalement équilibré [55] et a un noyau non vide $\mathcal{C}(v)$ qui contiennent tout le budget-équilibré et stable allocation des coûts vecteur x :

$$\mathcal{C}(v) = \left\{ x \in \mathcal{R}^{NK} : \sum_{k=1}^{NK} x_k = 1, \sum_{k \in S} x_k v(\mathcal{K}) \leq v(S), \forall S \in 2^{NK} \setminus \{\emptyset\} \right\}. \tag{B.11}$$

Répartition des coûts basé bi-objectif

Le noyau non vide par définition (B.11) est un polyèdre avec $NK-1$ dimensions, qui peut contenir de nombreux vecteurs d'allocation potentiels x . Une allocation x arbitraire dans le noyau peut correspondre à une solution *faible stable* puisque certaines coalitions atteignent une valeur d'épargne très faible ou nulle et peuvent ne pas recevoir d'avantages significatifs pour rester dans la coopération [54]. Il pourrait également être *injuste* puisque certains DRA ont une réduction de coût plus élevée que les autres [54]. Par conséquent, une conception efficace doit aborder deux questions principales mentionnées ci-dessus, à savoir la stabilité et l'équité. En particulier, les indicateurs de stabilité et d'équité sont utilisés pour concevoir une stratégie efficace d'allocation des coûts :

- *Métrique de stabilité* : capture la satisfaction minimale, à savoir, la pire économie de coûts $\delta(\$)$ parmi toutes les coalitions S .
- *Métrique d'équité* : capture l'écart maximal du pourcentage de réduction des coûts entre les DRA individuels, à savoir, la différence en pourcentage d'économies de coût $\gamma(\%)$ entre le DRA qui réalise le plus grand pourcentage de réduction de coûts et le DRA qui réalise le plus faible pourcentage d'économies pour un le vecteur d'allocation donné $x \in \mathcal{C}(v)$ [54].

La conception de la répartition des coûts vise à trouver un vecteur de répartition des coûts $x \in \mathcal{C}(v)$ qui permette un compromis efficace entre les mesures d'équité et de stabilité, qui peut être modélisé comme un problème d'optimisation bi-objectif comme suit : (P0)

$$\min_{\overline{\Phi}, \underline{\Phi}, \delta, x_k, \gamma} \gamma \quad (\text{B.12})$$

$$\min_{\delta, x_k} -\delta \quad (\text{B.13})$$

$$\text{s.c : } \sum_{k=1}^{NK} x_k = 1, x_k \geq 0, \quad (\text{B.14})$$

$$\delta \leq v(S) - \sum_{k \in S} x_k v(\mathcal{K}), \forall S \in 2^{NK} \setminus \{\emptyset, \mathcal{K}\} \quad (\text{B.15})$$

$$\delta \geq 0 \quad (\text{B.16})$$

$$\underline{\Phi} \leq x_k \frac{v(\mathcal{K})}{v(\{k\})} \leq \overline{\Phi}, \forall k \in \mathcal{K} \quad (\text{B.17})$$

$$\gamma = \overline{\Phi} - \underline{\Phi}, \quad (\text{B.18})$$

Où l'optimisation des fonctions objectif (B.12) - (B.13), qui minimisent le vecteur évalué $[\gamma, -\delta]$, vise à atteindre l'équité et la stabilité, respectivement. De plus, la contrainte (B.14) signifie que le coût total est réparti entre tous les DRA tandis que la variable auxiliaire δ dans (B.15) fournit la limite inférieure de l'économie de coûts de toutes les coalitions S sous la solution de répartition des coûts x . La satisfaction minimale, i.e., la pire des économies de coûts $\delta(\$)$ parmi toutes les coalitions S est maximisée dans (B.13). La contrainte (B.16) force l'allocation à être dans le noyau $x \in \mathcal{C}(v)$ tandis que la contrainte (B.17) fournit la limite inférieure $\underline{\Phi}$ et la limite supérieure $\overline{\Phi}$ pour le rapport entre le

coût alloué sous la grande coalition et le coût en raison du scénario non coopératif pour toutes les DRA k . L'écart maximal γ de l'économie de coût en pourcentage des DRA individuels, qui est la différence de $\underline{\Phi}$ et $\overline{\Phi}$ comme dans (B.18) est minimisé dans (B.12).

Pour obtenir les points optimaux de Pareto, on convertit le problème (P0) en un problème d'optimisation à un seul objectif (P3) en utilisant la méthode contrainte- ε [56] puisque le problème (P0) est linéaire. La fonction de stabilité objective (B.13) est choisie pour être optimisée tandis que (B.12) est converti en une contrainte. Soit $M + 1$ le nombre de points de réseau du front de Pareto et $m \in \{0, 1, \dots, M\}$. Deux points extrêmes, $m = 0$ et $m = M + 1$, sont déterminés en résolvant respectivement les deux problèmes d'optimisation suivants :

(P1)

$$\min_{\overline{\Phi}, \underline{\Phi}, \delta, x_k, \gamma} \gamma$$

s.c : contraintes (B.14) - (B.18).

(P2)

$$\max_{\delta, x_k} \delta$$

s.c : contraintes (B.14)- (B.15).

Ensuite, le point m^{th} sur le front de Pareto peut être obtenu en résolvant le problème d'optimisation à objectif unique suivant :

(P3)

$$\max_{\overline{\Phi}, \underline{\Phi}, \delta, x_k, \gamma} \delta$$

s.c : contraintes (B.14)-(B.15), (B.17)-(B.18)

$$\gamma \leq \gamma^m, \tag{B.19}$$

Où γ^m est un paramètre définissant le point m^{th} sur le front de Pareto. En particulier, γ^m est choisi comme $\gamma^{\min} \leq \gamma^m \leq \gamma^{\max}$. γ^{\min} et γ^{\max} peuvent être obtenus après avoir résolu (P1) et (P2), respectivement. Dans cette étude, le paramètre γ^m identifiant m^{th} est choisi comme suit :

$$\gamma^m = \gamma^{\min} + m \frac{\gamma^{\max} - \gamma^{\min}}{M}. \tag{B.20}$$

La construction du front de Pareto

On résout (P1), (P2) et (P3) pour avoir $M + 1$ points qui définissent le front de Pareto. Tous ces problèmes d'optimisation à grande échelle soumis à $2^{\text{NK}} - 2$ contraintes (B.15) avec seulement NK va-

riables d'optimisation x_k . Par conséquent, la génération de contraintes est une approche naturelle. En particulier, nous résolvons (P1) en résolvant itérativement le problème maître (MP1), qui est une version détendue de (P1) qui considère uniquement la condition (B.15) pour un sous-ensemble $\mathcal{O}(S) \in 2^{\text{NK}} - 2$, et le sous-problème (SP1) qui trouve la contrainte la plus violée avec x^* obtenu en résolvant (MP1). Le sous-problème (SP1) identifiant une coalition inexplorée S^* qui réalise la réduction la moins coûteuse est présenté comme suit :

(SP1)

$$\begin{aligned} \underline{\delta} = \min & \left[v(S) - \sum_{k=1}^{\text{NK}} e_k^S x_k^* v(\mathcal{K}) \right] = \min_{e_k^S, P_t^{\text{DA}}, P_t^{\text{RT}}, D_{k,t,s}^F, D_{k,b,t,s}^F, U_{k,t,s}, P_{k,t,s}^G, D_{k,t,s}^R, \xi, \eta_s} \\ & (1-\beta) \sum_{s=1}^{\text{NS}} \pi_s \sum_{t=1}^{\text{NT}} \left\{ \lambda_{t,s}^{\text{DA}} P_t^{\text{DA}} \Delta T + \lambda_{t,s}^{\text{RT}} (P_{t,s}^{\text{RT}} - P_t^{\text{DA}}) \Delta T \right. \\ & \left. + \lambda^p |P_{t,s}^{\text{RT}} - P_t^{\text{DA}}| \Delta T + \sum_{k=1}^{\text{NK}} \left(\lambda_k^r D_{k,t,s}^R \Delta T - U_{k,t,s} \right) \right\} \\ & + \beta \left(\xi + \frac{1}{1-\alpha} \sum_{s=1}^{\text{NS}} \pi_s \eta_s \right) - \sum_{k=1}^{\text{NK}} e_k^S x_k^* v(\mathcal{K}) \end{aligned} \quad (\text{B.21})$$

$$\text{s.c : } 1 \leq \sum_{k=1}^{\text{NK}} e_k^S \leq \text{NK} - 1, e_k^S \in \{0, 1\} \quad (\text{B.22})$$

$$\sum_{k \in S} (1 - e_k^S) + \sum_{k \notin S} e_k^S \geq 1, \forall S \in \mathcal{O}(S) \quad (\text{B.23})$$

$$\text{Contraintes (B.10) définissant } v(S). \quad (\text{B.24})$$

Le sous-problème (SP1) est un programme linéaire à variables mixtes (MILP) avec des variables binaires supplémentaires e_k^S agissant comme variables de premier niveau. La résolution (SP1) nous permet d'obtenir e^{S^*} , qui donnent S^* et $v(S^*)$ simultanément. La contrainte (B.22), c.-à-d., $S \in 2^{\text{NK}} \setminus \{\emptyset, \mathcal{K}, \mathcal{O}(S)\}$, et la contrainte B.23), c.-à-d., $S \notin \mathcal{O}(S)$, assurent que les coalitions inexplorées S sont considérées dans ce problème d'optimisation. Toutes les contraintes originales requises dans le calcul $v(S)$ sont données dans (B.24). Si nous résolvons (MP1) et (SP1) itérativement, on atteint finalement x^* tel que $\underline{\delta} \geq 0$ puisque le noyau est non vide. Alors, γ est minimisé et $x^* \in \mathcal{C}(v)$ est la solution finale d'allocation des coûts pour (P1). De même, nous pouvons résoudre (P2) et (P3) de façon optimale en utilisant l'approche de génération de contraintes en ligne car le nombre des contraintes est beaucoup plus grand que le nombre de variables d'optimisation. En résolvant (P1) (P2) et m (P3) avec différents γ^m , nous aurons $M + 1$ points de Pareto qui forment le front de Pareto.

Résultats numériques

Nous considérons un VPP qui coordonne la coopération de NK DRAs. L'horizon d'ordonnancement est d'un jour, divisé en $\text{NT} = 24$ créneaux horaires égaux, chacun représentant $\Delta T = 1$ heure. Nous supposons que dans chaque intervalle de temps t , chaque DRA k peut cumuler 10% de la charge non

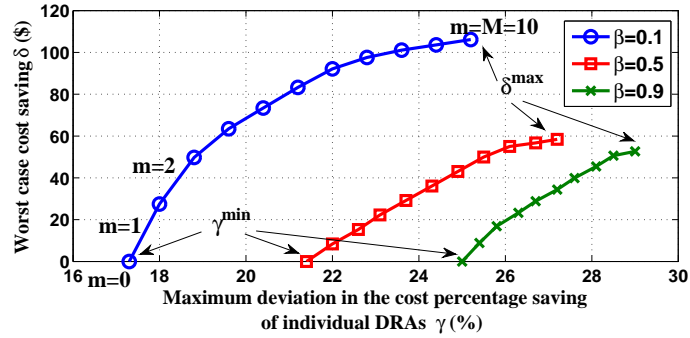
flexible totale, ce qui peut être réduit en utilisant les services de réduction de charge (LR) avec le prix $\lambda^r = 100\$/\text{MWh}$. La capacité de puissance transférée via le réseau principal est $P_k^{\max} = 15\text{MW}$. Enfin, $v(S)$ est supposé bien défini. D'autres données se trouvent au chapitre 5.

Figure B.11(a), B.11(b), B.11(c) montrent les fronts de Pareto pour le problème de répartition des coûts quand nous faisons varier le paramètre de risque β , l'échelle de charge flexible E_{scale}^F et le prix de pénalité λ^p , respectivement. Chaque front de Pareto obtenu décrit les compromis entre la stabilité représentée par la valeur d'épargne δ la plus défavorable et l'équité saisie par l'écart maximal du pourcentage d'économies γ . Pour tous les cas, lorsque $\gamma = \gamma^{\min}$ alors on a $\delta = 0$ ce qui signifie que nous atteignons la valeur minimale de δ tout en garantissant de fonctionner dans le noyau dont la définition est donnée dans (B.11). D'autre part, comme δ atteint sa valeur maximale δ^{\max} , ce qui correspond au nucléole comme écart minimum du pourcentage de réduction des coûts entre les joueurs, on atteint sa valeur maximale $\gamma = \gamma^{\max}$.

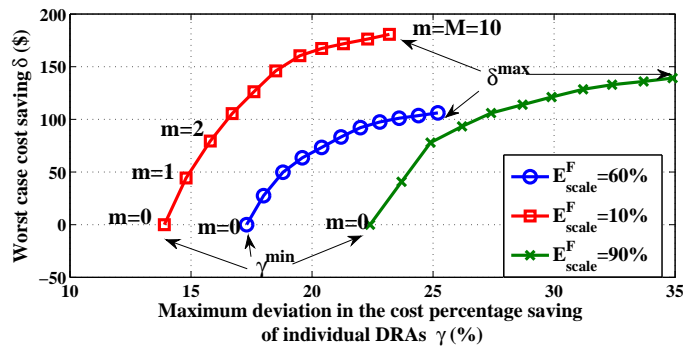
Ces deux points extrêmes dans le front de Pareto correspondent aux cas où la solution d'allocation de coûts x est soit au point noyau d'équité, γ^{\min} , soit au point optimal lexico-graphiquement, le nucléole δ^{\max} , dans le polyèdre $\mathcal{C}(v)$. Ces chiffres montrent que la conception proposée nous permet de déterminer plusieurs solutions efficaces Pareto différentes dans le noyau du jeu coopératif sous-jacent. De plus, on peut choisir un point d'opération sur le front de Pareto avec un compromis souhaitable de stabilité-équité. Plus précisément, pour une valeur d'écart maximal du pourcentage de coût épargnant γ , on peut déterminer le vecteur d'allocation de coûts correspondant à la valeur réalisable de la pire économie de coût δ maximisée. Cela démontre la souplesse et l'efficacité de notre conception de répartition des coûts proposée par rapport à d'autres conceptions existantes telles que la répartition des coûts basée sur le nucléole.

Conclusion

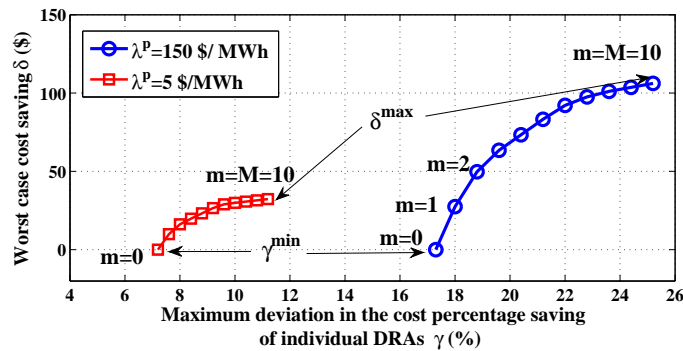
Cette étude présente une conception de répartition des coûts efficace du point de vue du calcul pour les DRA coopératives basées sur le concept de jeu coopératif. Nous avons proposé d'exploiter la propriété de noyau non vide du jeu équilibré sous-jacent et de développer un cadre d'optimisation bi-objectif qui établit l'équilibre entre la stabilité de l'allocation et l'équité. Nous avons utilisé les méthodes contrainte- ϵ et la génération des contraintes de ligne pour construire avec succès le front de Pareto des solutions d'allocation de coûts avec une complexité de calcul acceptable. La conception proposée peut allouer de manière efficace le pourcentage du coût total des soumissions aux DRA individuelles tout en garantissant un compromis souhaitable en matière de stabilité et d'équité.



(a) Pareto avant avec $\lambda^p = 150\$/MWh$, $E_{scale}^F = 60\%$, et variant β



(b) Pareto avant avec $\lambda^p = 150\$/MWh$, $\beta = 0.1$ et variant E_{scale}^F



(c) Pareto avant avec $E_{scale}^F = 60\%$, $\beta = 0.1$, et variant λ^p

FIGURE B.11 – Fronts de Pareto sous différents paramètres

Chapter 1

Introduction

1.1 Research Motivation

The electric industry has seen significant transformation from centralized power systems dominated by big utilities and highly dependent on fossil energy resources, to smart grids with high penetration of eco-friendly distributed renewable energy resources and active participation of energy consumers under market deregulation [2]. One important paradigm shift in this transformation is the widespread adoption of active demand side management in the smart grids [3]. In fact, it was defined in Title XIII of the Energy Independence and Security Act (EISA) in 2007 that the smart grid is an electrical grid which integrates a variety of operational and energy measures including smart meters, smart appliances, renewable energy resources, and energy efficient resources to support the active demand side management [3]. The framework for smart grid interoperability standards defined by the National Institute of Standards and Technology (NIST) is illustrated in Figure 1.1 [1].

Research and realization of various smart grid concepts and technologies have received tremendous investment from governments worldwide. In particular, advanced information and communication technology (ICT) infrastructure has been significantly upgraded in many countries [4–6] where a massive number of smart meters has been installed, e.g., over 45 million smart meters was deployed in 2013 with the Department of Energy (DoE) smart grid investment grant [7]. Moreover, the deployed communications networks and data management systems form the advanced metering infrastructure (AMI), which enables two-way communication between the utilities and customers [8]. The upgraded ICT infrastructure has paved the way for the realization of active demand side management [9–15]. Smart decision making taken by demand-side entities can receive benefits from the smart grid [2]. For example, home energy consumers can exploit dynamic pricing schemes to minimize their electricity consumption costs by smartly scheduling their energy consumption [16–23]. Here, the main decision making problem is to schedule energy consumption wisely to reduce the energy payment while still maintaining certain operations, user comfort, privacy requirements.

Thanks to the advanced grid's ICT infrastructure, home energy consumers and the grid operator are inter-connected and demand response (DR) services can be offered to the grid operator through changing the energy consumption [13, 14, 24–27], which can enable the grid to operate more efficiently. Hence, the grid operator may be interested in motivating their energy customers to actively participate

in its DR program by using for example a suitable pricing policy. A well-known approach to enable the grid operator to manage DR services from its customers is to deploy the so-called Load Serving Entity (LSE) model [28]. Finally, small-scale demand-side entities can cooperate to act as a single entity under the coordination of a demand-side resource aggregator [29, 30] or a virtual power plant [31], to purchase energy in the wholesale market since the wholesale energy prices tend to be cheaper than the retail prices [32]. In order to participate in the wholesale market, demand-side entities have to make several decisions such as coordination decisions to form a large cooperation coalition, energy bidding in the market, and sharing cooperation benefits with each other.

In general, design of smart decision making frameworks for demand-side entities in the smart grid environment with increasing penetration of renewable energy can be quite challenging [6, 33]. Although being friendly to environment, renewable energy resources such as solar and wind power can be quite unpredictable, which implies great difficulties to maintain efficient and reliable operations for the grid distribution network [2]. In particular, adoption of a poor energy management strategy can result in low utilization of renewable energy [19, 34]. In addition, inefficient pricing design cannot tackle the fluctuation of renewable energy sources, which eventually results in the instability of grid operations [35]. Finally, appropriate design of a bidding strategy can bring about positive impacts on the achieved profit/cost for demand-side entities participating in the electricity market. This is an important issue because market participants must be responsible for managing uncertainties of their renewable energy sources [29, 36].

In summary, successful exploitation of active demand-side resources requires to address several decision making problems for the involved smart grid entities in the distribution network. This dissertation aims to address some of these problems. In the following, we discuss research challenges related to these problems, describe the existing literature, and present the key contributions of this dissertation.

1.2 Challenges in Active Demand-Side Management

Figure 1.2 illustrates the demand-side domain in the NIST's smart grid model, which is a part of the energy consumer domain shown in Figure 1.1. As recommended by the Federal Energy Regulatory Commission (FERC), NIST has highlighted the importance of active demand-side management in the smart grid. In general, active participation of demand-side resources in the electricity market has been considered efficient and economic means to balance the supply and demand in smart grids with high renewable energy integration [10]. However, several challenges must be addressed to fully realize the benefits of active demand-side management. We discuss some of such challenges in the following.

1.2.1 Challenges in Smart Home Energy Management

One important topic within the active demand-side management domain concerns the demand response of residential customers [3, 16]. In fact, smart home energy management has received significant research interests in recent years [16, 17, 20, 23, 37, 57, 58]. In order to fully exploit the opportunities brought from the smart grid, various major challenges must be addressed and comprehensive decision making models for home energy management must be developed as discussed below.

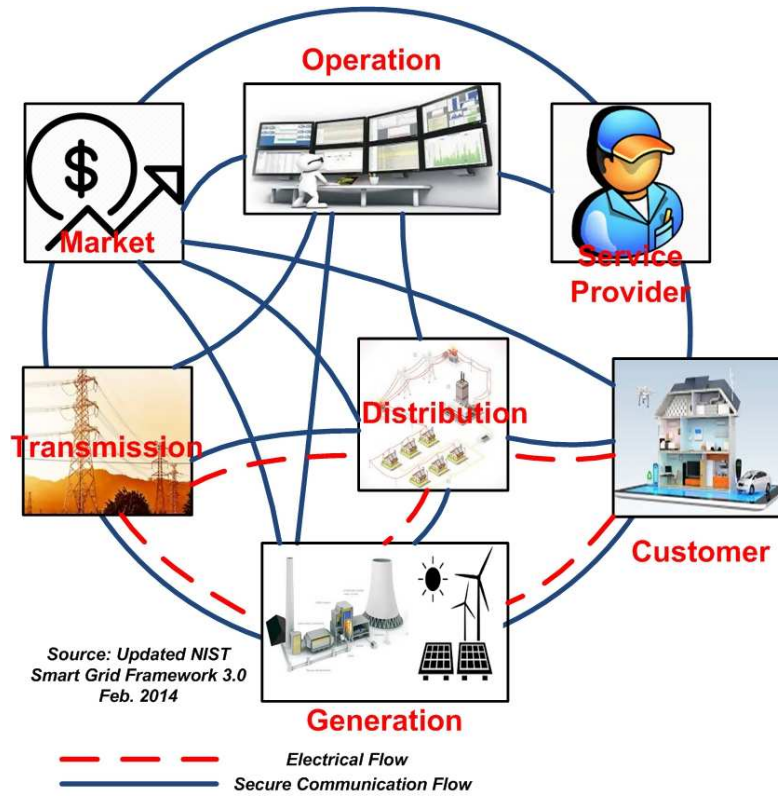


Figure 1.1 – NIST Smart grid conceptual model 3.0 [1]

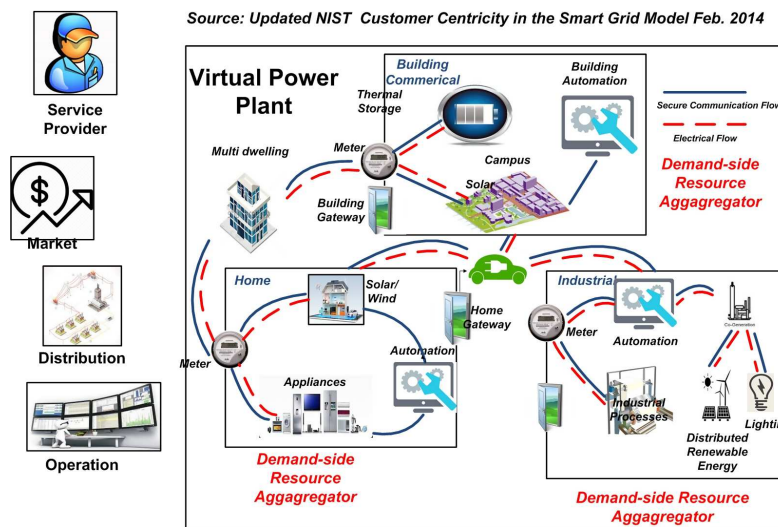


Figure 1.2 – Demand-side customer centrality in the smart grid [1]

The first challenge in smart home energy management is to appropriately model and exploit the time-varying electric pricing schemes. In particular, time-varying or dynamic pricing schemes such as Time of Use (ToU) or real time pricing (RTP) can be employed to replace the traditional flat rate scheme to better capture the actual price of energy production [16]. Moreover, the time-varying pricing scheme can be combined with an inclining block rate to improve the conservativeness of the electric price [17]. One major challenge in smart home energy management concerns how electric users can adaptively adjust their energy consumption in response to the time-varying pricing signals to save their electricity consumption cost [15, 20].

The second challenge concerns the heterogeneous characteristics of smart home appliances. In practice, home appliances can have very different energy consumption patterns and operation constraints [16]. In addition, some energy equipments such as electric vehicles [24, 59, 60], smart water buffers [61], battery storage [62–64], HVAC and water heating [25, 26] can support direct load controls and change their energy consumptions flexibly [16]. However, these appliances and equipment require corresponding models to capture their characteristics.

The third challenge concerns how to efficiently manage renewable energy sources integrated in smart homes. In particular, renewable energy sources such as rooftop solar bars, small wind turbines integrated in smart homes [33, 58, 65] produce the amount of energy, which is uncertain and difficult to predict [2]. Toward this end, modeling the renewable energy uncertainties is an important and challenging research topic [66]. Finally, guaranteeing user comfort [67] and protecting user privacy [57] must be considered in home energy management design. How to model and capture these modeling aspects and constraints in the home energy management design are challenging research issues.

1.2.2 Challenges in Demand Response Design for Distribution Networks

Intelligent demand response (DR) presents one of the most important characteristics of active demand-side management [28] which can lead to various DR benefits in electricity markets and power system operations [6, 68]. However, there are many technical and non-technical challenges related to the DR design in the distribution network from the grid operator's viewpoint [9].

The first challenge concerns the scalability of the DR design because coordination of DR services from many households and/or energy consumers is usually required as discussed in the previous section. In general, DR can be realized by either direct or indirect load control. Under the direct load control approach, the grid operator must send a large number of messages to individual loads such as EV charging systems [24], HVAC and water heating systems [25, 26]. Indirect load control is quite promising because the control can be implemented in a decentralized manner using the pricing signals [2]. However, determining the price is a complicated task [32, 53, 69–72] since it is desirable that the designed pricing scheme be compatible with the current market structure [2].

The second challenge is related to the development of efficient mechanisms to incentivize electric customers to participate and provide DR services [6]. In practice, it is not easy or even possible to obtain permissions from home users to access or control their appliances [24–26, 73] due to the privacy issue [57]. Another reason for which a dynamic pricing scheme might not be welcomed is that home owners' information can be revealed when it adjust its energy consumption in response to changes in the electricity price [57]. In addition, only certain electric users who have flexibility in changing their energy consumption can enjoy the DR benefits under current proposed pricing designs [16].

Last but not least, guaranteeing stability of the grid is vital for DR design in the distribution network since inefficient pricing design can lead to grid instability [35]. Moreover, the proposed DR should be compatible with the current market structure to motivate DR participation. There are some attempts to develop market based mechanisms for DR services such as a DR exchange market [13, 14, 46, 74], a regulation market [24], DR contracts [43], load reduction services [10]. However, these proposed frameworks require some modifications of the current market structure, which may not be desirable.

1.2.3 Challenges in Electricity Market's Decision Makings

Thanks to the market deregulation, smart grid's entities from the demand side such as smart homes, microgrids, and load aggregators, can be aggregated and/or coordinated to participate in the wholesale electricity market, i.e., the short-term electricity market [2, 24, 29, 75]. The work [32] shows that wholesale electricity prices are often much lower than the retail prices, which provides opportunities for demand-side entities to increase profits or reduce costs. However, design of decision making processes for demand-side entities to participate in the electricity market faces many challenges [2, 31].

The first challenge is related to the responsibility of demand-side entities to maintain the energy imbalance between their energy bidding scheduled in the day-ahead markets and their actual energy dispatch [2, 24, 29, 31, 36, 43, 75–77]. As uncertain renewable energy sources such as solar rooftop bars and small wind turbines are being integrated into the demand side at an increasing rate [29, 33], demand-side entities must usually rely on a balancing mechanism provided by expensive but controllable energy resources in the real-time balancing market to compensate for their inevitable imbalances [75, 77]. The prices in this balancing market are also uncertain [31]. Hence, their achieved profits/costs can be negatively affected if uncertainties are not appropriately addressed [77].

The second challenge concerns the modeling complexity of demand-side entities participating in the electricity market. These entities can be the aggregation of heterogeneous and different resources in the distribution network [29, 31, 32], which have different operation constraints [11, 29, 78], or the aggregation of a large number of similar loads [24, 27, 69], which must be appropriately modeled. In addition, demand-side entities can participate in several electricity markets such as short-term electricity markets including the day ahead (spot) market, real-time balancing market, adjustment market, and other market frameworks such as the reserve market [50], regulation market [24], and demand response exchange market [13, 46]. Co-optimization of demand-side entities in multiple markets is a challenging task in general. Balancing mechanisms can also vary in different markets, e.g., the single pricing scheme in the US market [29, 36] and the dual pricing scheme in the European markets [75, 77]. In addition, these entities can be further coordinated under emerging smart grid's cooperation concepts such as a virtual power plant (VPP) [31, 50], which can bring about more benefits but renders the modeling and coordination tasks more challenging.

The third challenge concerns how to choose appropriate solution approaches for underlying decision making problems. There are two main decisions to be made in the electricity markets, i.e., how to bid energy to optimize certain objectives such as maximization/minimization of profit/cost [29, 31] and how to share the profit/cost among cooperating members [32]. The first problem requires choosing an appropriate optimization model and a suitable solution approach while the other problem can be addressed with certain solution approaches such as cooperative game theory. These optimization/game theoretic models are usually complex as mentioned in the second challenge. In general, development of solution approaches to solve these problems accurately with manageable computation effort is quite challenging.

1.3 Literature Review

In this section, we present the literature survey on the decision making issues for active demand-side management, which is the focus of this PhD dissertation. In particular, we discuss recent research works in energy management issues for smart homes. Then, we discuss existing research on demand response integration in distribution network. Finally, we describe some recent literature related to the market participation of aggregated demand-side resources under the market liberalization.

1.3.1 Home Energy Management Under Smart Grid

Research in the smart home energy management topic generally focuses on designing residential demand response solutions through formulating and solving an optimization problem. As an example, such an optimization problem aims to minimize the energy payment while guaranteeing home appliances' operations and user comfort constraints.

Various optimization based decision making models for smart home energy management have been proposed in the literature where they are different in terms of considered electric pricing schemes and possible consideration of renewable energy integration. These existing optimization based frameworks can be classified into deterministic optimization and stochastic optimization models. Deterministic optimization models typically assume that the home controller has perfect information about the system and forecast data over the scheduling horizon [21, 37, 73, 79], e.g., perfect information about the electricity prices and renewable energy's generations. For example, the work [37] tackles the load power control problem under the flat-rate pricing model where the utility determines the thresholds of energy consumption at different time slots and broadcast these values to end users for load scheduling. The work [73] studies a deterministic residential microgrid scheduling problem exploiting the smart meter data and thermal load and evaluates the impacts of different forecast parameters such as electricity price, outdoor temperature, and demand on the achievable energy payment. In addition, dynamic programming and Markov Decision Process (MDP) theory have also been employed to develop an optimal control policy that allocates power consumption for each appliance in a deterministic manner [80, 81]. However, the deterministic optimization approach is only applicable to deterministic model, which might result in poor performance for smart homes experiencing uncertainties. The stochastic optimization approach, on the other hand, can effectively capture various system uncertainties [16, 17, 57, 82]. In [17], the model predictive control (MPC) based framework for scheduling home appliances is proposed to minimize the electricity cost. Moreover, residential DR algorithms are developed by using the rolling online stochastic programming approach in [16, 57].

Study of the heterogeneous smart home setting has also been conducted where various load models and load classifications have been proposed in the literature. In general, suitable mathematical models based on physical operations of home appliances must be developed and they are then integrated into underlying energy management optimization frameworks. In fact, conventional home appliances have been well modeled and they are generally classified based on their defferability and interruptibility characteristics [16, 17, 20, 23, 37, 57, 82]. Moreover, their operation constraints can be linear, mixed integer linear or mixed integer nonlinear constraints, which can be used to formulate classical optimiza-

tion frameworks for home energy management. In [83], the authors propose *weather dependent loads*, whose energy consumptions are assumed to be Markovian. This model then enables them to develop a MDP based energy management algorithm.

Integrating renewable energy as well as eco-friendly and energy efficient home appliances with automated capabilities into smart homes, especially thermal appliances such as HVAC and the water heating system, have received considerable attention. A good survey of uncertainty models for renewable energy sources can be found in [66]. There has been considerable research interest in combining thermal systems with the solar energy sources to enhance the coefficient of performance (COP) of a standalone HVAC system [39]. In particular, the design of a hybrid solar assisted HVAC and water heating system is motivated by the abundant presence, environmental sustainability, and quiet operation of solar energy and the maturity of thermal engineering research [38, 39, 64, 84–87]. Since, the contribution of HVAC and water heating to the electricity consumption of a typical household (e.g., over 50% of the total residential energy consumption [25]) is quite large, integrating the new generation of home appliances and renewable energy facility into unified energy management optimization frameworks is an important research topic.

Modeling user comfort and privacy in home energy management has also received a lot of attention. Specifically, different thermal user comfort models have been considered in home energy management including the simple temperature deviation [18, 19, 48, 58, 59, 65, 83, 88] and a more complicated Predicted Mean Vote (PMV) model [89, 90]. Various constraints on energy management scheduling are imposed in [57] where the authors observe that data mining methods can be employed to extract information regarding which appliances are equipped in the household based on the residential load adjustment in DR services. Hence, appropriate operation constraints could be added to prevent potential exploitation of the home's data from third parties [57].

1.3.2 Demand Response Designs in Distribution Network

Research related to DR integration in the distribution network has received much interests. However, it is not straightforward to develop an efficient DR strategy that is compatible with the current market structure, easy to implement, and receives acceptance from customers. Proposed DR frameworks in the distribution network can be classified as direct or indirect load control of flexible residential resources. Direct control of home appliances such as EV charging [24], water heater [25], and HVAC [26] has been addressed in the literature. However, this centralized approach might require heavy computation from the grid operator. To address this issue, some aggregation models are proposed [24–26], which trade computation complexity with the modeling accuracy. Moreover, direct load control also requires to know the operations of home appliances, which might not be desirable because of privacy issues [57]. The indirect load control, on the other hand, aims to motivate energy consumers to adjust the energy consumption by providing incentive through pricing signals. In fact, the indirect load control approach has received more attention in the decentralized market. However, determining the price, which often requires to solve a game [69, 88] or an optimization problem [53, 91], is not a straightforward task.

Several existing papers advocate the DR integration by showing its potential benefits and the positive impacts. Specifically, positive impacts of residential DR on reducing the electricity bill for house-

hold customers are reported in [16]. Different multi-objective optimization based energy management frameworks are introduced in [67, 92] to minimize the energy cost for a residential household considering customer thermal comfort preferences. The impact of DR integration on the market clearing price is investigated in [93]. In [94], the authors study the potential of DR resources for providing the frequency regulation service. In [15, 42, 44], different optimization models are proposed to maximize the benefits of large energy customers with DR capability. Furthermore, a novel load shaping strategy is presented in [95] exploiting the dynamic pricing and energy storage. These existing works mainly show that DR can be beneficial to both utilities and customers if it is implemented properly; however, it is not shown how to coordinate DR resources from several customers.

Pricing design based the indirect load control presented above is a very important research topic in DR for distribution networks. In general, the price signals can be sent from the grid utility to customers to motivate load adjustments (i.e., changing consumers' energy consumptions). Popular dynamic pricing designs such as time-of-use (TOU) and real-time pricing (RTP) for retail customers, however, may not be efficient since they may increase the energy cost for some customers with small flexible loads [16] or lead to the grid instability [35]. Moreover, complicated pricing designs would result in increasing complexity of the residential energy management [16, 17, 21, 37, 57, 73, 79–82] and might not receive widespread acceptance from home users.

Some recent papers propose DR contracts among customers, who are DR providers, and utilities or renewable energy producers, who are DR buyers [10, 13, 32, 43, 46, 96]. In addition, pricing designs based on game theory [69, 88] or agent based simulation [32] have also been conducted. However, these designs might be not compatible with the current market structure. Development of a pricing framework that can utilize flexible loads while maintaining efficient operations of the distribution network operator and ensuring cost saving for energy customers is a challenging problem. This problem is addressed in this dissertation.

1.3.3 Market Bidding and Cost Sharing Design

Demand-side decision making in the deregulated market has been an active research topic in recent years. There are two important problems to address: the first concerns how to optimize the total profit/cost of market participants and the second is to share the obtained profit/cost. Some aforementioned challenges must be considered in solving these decision making problems.

As demand-side entities with renewable energy must be responsible for the energy imbalance in the short-term electricity market, various optimization models and cooperation frameworks have been proposed to address this issue. In particular, the market bidding problem is often modeled as an optimization problem where each market participant aims to minimize the cost or maximize the profit [2]. Given various system uncertainties, stochastic programming [24, 29, 31, 43, 97] can be employed to find the optimal bidding quantities in the day ahead market such that the expected cost/profit are minimized/maximized considering the energy imbalance cost in the real-time balancing market [2]. Moreover, risk control [29, 31, 43] can be considered as design constraints to adjust the variation of achievable profit/cost after the operation day.

Many recent works focus on developing an appropriate bidding framework that can compromise the strengths and weaknesses of heterogeneous demand-side entities by allowing cooperation among them [31]. The work [10] presents the novel model for an aggregator that aggregates different DR services to sell in the DR exchange market. Modeling and bidding design for generic aggregated resources at the demand side, namely demand-side resource aggregator (DRA), is presented in [29]. The deployment of advanced communication and computation technologies in the smart grid enables coordination of multiple resources in the distribution network [31] through the so-called Virtual Power Plant (VPP) [31, 50, 97]. In fact, these papers have shown that cooperation among DRAs can lead to cost reduction or profit improvement by leveraging the strengths and weaknesses of individual members.

The potential of multiple market participation and different balancing mechanisms have also been well studied. Modeling and bidding strategy of the VPP in the conventional electricity market and reserve market is studied in [50]. A bidding strategy for a fleet of electric vehicles coordinated by an aggregator under both the short-term electricity market and the regulation market is presented in [24]. The authors also propose an aggregated battery model to capture the charging of a large number of electric vehicles. The work [43] studies how DR contracts help a microgrid improve its profit and manage risk due to profit variation when bidding in the short-term electricity market. The single pricing based balancing market model is considered in [24, 29, 30, 43] while the dual pricing based balancing market is studied in [31, 96]. In summary, modeling the joint participation in multiple electricity markets has been well addressed in the literature.

Although research on modeling and bidding under different demand-side cooperation models has been conducted by using stochastic programming, it is still unclear how to share the cost/profit among heterogeneous cooperative demand-side entities. Some recent papers consider pricing design by formulating and solving certain profit/cost allocation problems. In particular, the work [32] develops an electricity payment method to motivate the coordination between the EV aggregator and wind power producer. Moreover, the work [71] presents a ranking based pricing scheme to calculate the participants' cost saving/profit increment based on the submitted load profiles' flexibility. The work [72] proposes direct energy trading among producers and consumers where the internal price is determined by the Shapley value concept. However, all these proposed frameworks require market redesign; thus, they would not be applicable for current market practice.

In general, sharing profit or cost among cooperative entities can be theoretically addressed by using the cooperative game concept [54, 55, 98]. In fact, the cooperative game theory has been employed to address some profit/cost sharing problems in power systems such as energy producers' multilateral trading [99], energy management, and market design [70, 72, 100]. However, most papers only consider the profit/cost sharing for a small number of cooperative entities due to the high computational complexity of this approach [101–104]. Developing an efficient method to solve the profit/cost sharing problem for a large number of cooperative demand-side entities given the notorious computation burden of applying the cooperative game concepts is a challenging task, which is addressed in this dissertation.

1.4 Research Objectives and Contributions

This thesis aims to address three important challenges described above, whose contributions can be illustrated in Figure 1.3 and summarized as follows.

In Chapter 3, we study the home energy scheduling problem in the real-time pricing environment. Specifically, we propose a comprehensive model considering the integration of renewable energy in home energy system, i.e., the eco-friendly solar assisted HVAC-water heating system. Then, we propose a real-time Model Predictive Control (MPC) based design for a smart home equipped with solar assisted HVAC-water heating system and other controllable load in response to the real time pricing signal. We devise a rolling algorithm based on the two-stage stochastic programming for home energy management so that it can minimize the energy payment cost, guarantee system constraints while exploiting the energy coupling relation of the solar thermal storage and HVAC system to improve the system energy efficiency.

In Chapter 4, we consider the pricing design problem in the distribution network to motivate the demand response participation from energy consumers. In particular, we propose a dynamic pricing scheme implementable in the distribution network under the model of Load Serving Entity (LSE), which is easy to implement and compatible with the current market structure. Our design creates an incentive for flexible load to perform demand response that can help the LSE address the fluctuations of electricity prices, conventional nonflexible load, and distributed renewable energy. Specifically, we present the formulation of the proposed pricing design by using the bilevel programming framework. Given the lower-level sub-problem is linear, we employ the optimal KKT conditions to convert the bilevel problem into the single objective mathematical problem with equilibrium constraints (MPEC), which is then transformed into an equivalent single objective mixed integer linear program (MILP) by using the Fortuny-Amat formula and strong duality theorem of linear programming. The obtained MILP can be solved efficiently by using available commercial solvers. Numerical results are then presented to illustrate the effectiveness of our design in motivating demand response integration in the distribution network.

Chapter 5 studies how to share the cost for the cooperative Demand-Side Resource Aggregators (DRAs), which are based on generic models of active demand-side agents. Specifically, these DRAs are coordinated under the Virtual Power Plant framework to jointly bid in the electricity market and the corresponding attained cost must be split among members. Toward this end, we first present the comprehensive cost allocation model, which is applicable to the current market structure. Then, the cost allocation problem is modeled as the solution of a cooperative game where all DRAs act as players and the value function of coalitions of players are the outcomes of their optimal market bidding strategies which are obtained by solving the corresponding two-stage stochastic programs. We show that the core of the underlying game, which defines all budget-balanced and stable cost allocation vectors, is nonempty. Then, we propose to determine the cost allocation vector inside the core considering the trade-off between different criteria through solving a bi-objective optimization problem. This bi-objective optimization problem has an exponential number of constraints with implicit parameters which are the coalitions' function values. Since the number of cost shares are only equal to the number

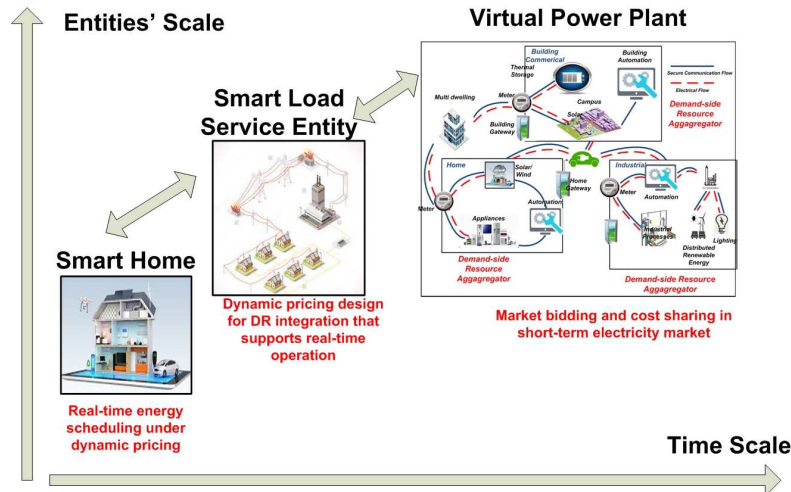


Figure 1.3 – Problems addressed in this thesis and their relations

of DRAs, which is much smaller than the number of constraints, we propose an algorithm based on the combination of ε -constraint and row constraint generation methods to construct the Pareto front with manageable computation effort.

1.5 Thesis Outline

The remaining of this thesis is structured as follows. Chapter 2 presents some technical background required to address the decision making problems addressed in this dissertation. Specifically, we will review fundamental optimization techniques including stochastic programming, bilevel programming, and multi-objective programming, and cooperative game theory. Chapter 3 discusses the proposed energy management for smart home equipped with solar assisted HVAC-water heating in the real-time pricing environment. Chapter 4 describes the dynamic pricing design for demand response integration in the distribution networks. Chapter 5 studies the cost allocation problem for multiple demand-side resource aggregators cooperating in the electricity market. Conclusion remarks are presented followed by some discussions of future research directions in Chapter 6.

Chapter 2

Mathematical Background

This chapter presents some fundamentals of important optimization and game theory methods, namely, stochastic programming, bilevel programming, multi-objective programming, and cooperative game theory. These mathematical tools are used to model and solve the decision-making problems in this thesis.

2.1 Mathematical Optimization

Many practical decision making problems can be modeled as optimization problems where optimal decisions must be made to optimize certain objective functions subject to a number of constraints [2].

2.1.1 Basic Concepts

The standard form of an optimization problem can be described as follows [105]:

$$\begin{aligned} \min_x f(x) & \tag{2.1} \\ \text{s.t. } g_i(x) \leq 0, i = 1, \dots, m \\ h_i x = 0, i = 1, \dots, p \end{aligned}$$

where $x \in R^n$ is a vector of optimization variables and $f(x) \in R$ is an objective function. The set of x that satisfies all m inequality and p equality constraints is the feasible set. If the feasible set is empty, the problem is infeasible. The optimal value of the problem is $f^*(x) = \inf\{f(x) \mid g_i(x) \leq 0, i = 1, \dots, m, h_i x = 0, i = 1, \dots, p\}$. If $f^*(x) = -\infty$, the problem is unbounded. If $f^*(x) = f(x^*) \in R$ then x^* is the optimal solution.

2.1.2 Linear Programming and Mixed Integer Linear Programming

If the objective function and constraints in (2.1) are linear, the problem (2.1) is a linear program which can be expressed in the following form [105]:

$$\min_x c^T x \quad (2.2)$$

$$\text{s.t. } Ax \leq b \quad (2.3)$$

$$Cx = d \quad (2.4)$$

where A, b, C, d are matrices with appropriate sizes. If some variables x_i are constrained to be integer, the problem becomes a mixed integer linear program (MILP). There are many methods to solve LP/MILP problems [2, 105]. In practice, the global optimal solution of LP/MILP can be found by using available commercial solvers such as CPLEX [106].

2.1.3 Stochastic Programming

If the input data and parameters of an optimization model are deterministic, we can find the optimal decision by solving a deterministic optimization problem. However, unknown input data are common in many smart grid's decision making problems where decisions must be determined even with the lack of perfect information [2]. Moreover, if the input data are unknown but bounded in certain ranges, robust optimization can be used. If the input data are unknown but can be described by some probability functions which can be approximated by a set of scenarios with associated probability of occurrence, the stochastic programming technique can be employed.

Uncertainty Characterization

In stochastic programming, uncertain parameters are considered as random variables represented by a finite set of scenarios [2]. For example, the future wind generation W at a given time slot can be described by a set of scenarios $W(s)$ with $s = 1, \dots, NS$, where s is the index of scenarios and NS is the total number of scenarios. Each scenario has a probability of occurrence $\pi(s) = P(s|W = W(s))$ where $\sum_{s=1}^{NS} \pi(s) = 1$. If the value of a random variable evolves over time, it is called a stochastic process. A stochastic process can be understood as a set of dependent random variables sequentially arranged in time, which can also be captured by scenarios. For example, the tomorrow wind generation W over 24 hour horizon can be captured by a set of NS scenarios, each is a 24×1 vector that represents one possible realization of wind generation with a probability of occurrence $\pi(s)$ and $\sum_{s=1}^{NS} \pi(s) = 1$.

Since uncertain parameters are described by scenarios, the resulting objective function is a random variable instead of a real-valued number. In a stochastic programming model, we often aim to optimize the expected value of the objective function. In addition, optimal decisions are often made over a decision horizon with a number of stages. Each stage represents a point in time where decisions are made or where uncertainty is partially or totally realized. Depending on the considered number of stages, we can have two-stage and multistage stochastic programming problems [2].

Scenario Generation/Reduction

A popular method that generates scenarios to capture uncertain parameters in stochastic programming models is Monte-Carlo simulation [107], which is employed in this thesis. In particular, the scenarios are generated by sampling from probability distribution functions of the uncertain parameters [107]. Popular sampling methods used in the literature include random sampling, Latin Hypercube sampling, and orthogonal sampling. These methods are slightly different in how to preserve the real variability. These probability distributions are often chosen and constructed from the historical data [2]. Their parameters can be calculated from historical data by curve fitting using the maximum likelihood method [66]. Generally, the chosen distributions are determined by studying the available data [2]. Some well known distributions in the literature to describe specific types of data include Weibull distribution for wind speeds [66], beta distribution for solar irradiance [66], Cauchy distribution for financial prices [63, 108, 109], normal or truncated normal distribution for forecast errors [43].

The number of scenarios should be chosen carefully considering the trade-off between the computational accuracy and computational burden of the scenario based optimization method. For a large-scale problem, scenario reduction methods can be employed to reduce the number of generated scenarios to reduce computational burden [24, 31, 65, 75, 107]. The principle of scenario reduction can be summarized as follows. Initially, the weights, i.e., the probabilities of occurrence of the generated scenarios, are adjusted to ensure that the statistical characteristics of the uncertain data are best represented. This step can be fulfilled by solving a large scale linear programming problem [107]. Then, the problem of scenario reduction can be understood as choosing and adjusting the weights of a subset of scenarios where the cardinality of the set is a predefined number. This step can be completed by solving a combinatorial optimization problem [107]. Popular methods for solving this problem in the literature are backward, forward, and fast forward, which are dynamic programming methods [107]. The problem of scenario generation/reduction can be solved by using available commercial software such as GAMS/SCENRED [40]. In this thesis, GAMS/SCENRED version 2.0 is used for scenario generation/reduction where the number of generated and reduced scenarios are chosen to guarantee the accuracy by tuning the parameters of the software.

Two-Stage Stochastic Programming

In a two-stage programming problem, decision variables include a set of first-stage (*here and now*) decisions and another set of second-stage (*wait and see*) decisions [2]. The first stage decision variables must be determined before the realizations of uncertain parameters at the second stage. Hence, the first-stage decisions do not depend on future observations. The second-stage decisions are made after the realization of uncertain parameters. If uncertainties are captured by scenarios, second-stage decisions are scenario dependent, i.e., they are defined for each scenario. In short, the solution of a two-stage program includes a single first-stage policy and a set of recourse decisions defining which second-stage action is made for each realized outcome. The general formulation of a two-stage stochastic linear programming problem is given as follows [2]:

$$\min_x c^T x + E [Q(x, s)] \quad (2.5)$$

$$\text{s.t. } Ax \leq b, x \in X \quad (2.6)$$

where x is a vector of first stage decision variables and matrices c, A, b represent the known input data. The term $Q(x, s)$ is the result of the following optimization problem:

$$Q(x, s) = \left\{ \min_{y(s)} q(s)^T y(s), \quad (2.7) \right.$$

$$\text{s.t. } T(s)x + W(s)y(s) = h(s), \quad (2.8)$$

$$\left. y(s) \in Y \right\} \quad (2.9)$$

where $y(s)$ is a vector of second-stage decision variables and matrices $T(s), W(s), h(s)$ represent uncertain input. We call (2.7)-(2.9) a recourse problem since its decision variables are made after uncertainties are realized, i.e., $T(s), W(s), h(s)$ are known. Under the some mild assumptions, problem (2.5)-(2.9) is equivalent to the following deterministic problem:

$$\min_{x, y(s)} c^T x + \sum_{s=1}^{NS} \pi(s) q(s)^T y(s) \quad (2.10)$$

$$\text{s.t. } Ax \leq b, \quad (2.11)$$

$$x \in X, \quad (2.12)$$

$$T(s)x + W(s)y(s) = h(s), \quad (2.13)$$

$$y(s) \in Y. \quad (2.14)$$

The bidding strategy of a market agent in the short-term two-settlement electricity market can be formulated as a two-stage program [24, 29, 31, 43, 48, 65, 77, 78, 102, 110–112]. The submitted bidding quantities are first-stage decisions, i.e., they are determined before the realization of day-ahead prices. The energy exchanges in the balancing market during the operation day are second-stage variables [24]. In many cases, the decision making consists of more than two stages, i.e., bidding in market with multiple trading floors [74, 75]. In this case, the decision making problem should be modeled as a multi-stage stochastic programming problem [2].

2.1.4 Bilevel Programming

In bilevel programming model, we are interested in solving the following optimization problem [113]:

$$\min_{x \in X, y} F(x, y) \quad (2.15)$$

$$\text{s.t. } G(x, y) \leq 0, \quad (2.16)$$

$$\min_{y \in Y} f(x, y) \quad (2.17)$$

$$\text{s.t. } g(x, y) \leq 0 \quad (2.18)$$

where problem (2.15)-(2.16) is called the upper-level problem and problem (2.17)-(2.18) is called the lower-level problem, $F(x, y) \in R$ and $f(x, y) \in R$ are upper-level and lower-level objective functions, $x \in R^d$ and $y \in R^q$ are upper-level and lower-level optimization variables, (2.15) and (2.18) are upper-level and lower-level constraints with $G(x, y) \in R^m$ and $g(x, y)^l$, respectively.

This bilevel optimization problem cannot be solved directly since it does not follow the standard form. It should be transformed to the solvable single objective optimization problem. Depending on the form of the studied problem, several methods are proposed in the literature such as the Karush-Kuhn-Tucker (KKT) equivalent conditions, complementary pivoting, and penalty function [113]. Generally, it is difficult to find the global optimal solution of the bilevel problem. However, in specific cases, we can transform it to an equivalent problem whose optimal solution can be found.

In particular, if the lower-level problem is a linear program, we can replace it by its KKT conditions. Hence, the original bilevel problem can be transformed into the following mathematical program with equilibrium constraints (MPEC) [113]

$$\min_{x \in X, y} F(x, y) \quad (2.19)$$

$$\text{s.t. } G(x, y) \leq 0, \quad (2.20)$$

$$\lambda_i \geq 0, \quad i = 1, \dots, l, \quad (2.21)$$

$$\lambda_i g_i(x, y) = 0, \quad i = 1, \dots, l \quad (2.22)$$

$$\nabla_y \mathcal{L}(x, y, \lambda) = 0. \quad (2.23)$$

where (2.21)-(2.23) represent the KKT optimal conditions of the lower-level problem (2.17)-(2.18). The MPEC has nonlinear sources including the complementary constraints (2.22) and the bilinear terms in the formula of (2.23). The complementary constraint (2.22) can be replaced by a set of mixed integer linear constraints by using the Fortuny-Amat formula [47]. The bilinear terms appeared in the formula of (2.23) can be eliminated by using the strong duality of the linear programming theory [113]. If the upper-level problem (2.15)-(2.16) is LP or MILP, the obtained equivalent problem is a MILP which can be solved efficiently by using the branch and cut algorithm employed in available solvers such as CPLEX [106].

Bilevel programming has been used to study different problems in power systems such as transmission and generation expansion planning [114, 115], generation maintenance [116], market equilibria

[117], and strategic bidding for power producers [118], retailers [91], and distribution companies [119]. In [120], a bilevel problem model is used to study the interaction between a large central production unit and an energy service provider (ESP) managing several microgrids (MGs). The central production unit computes and sends an optimal energy price signal to the ESP, then the ESP decides the optimal amount of energy purchased from the central generation unit as well as schedules its power generation and consumption accordingly. However, the formulated problem is a nonlinear mixed integer problem which requires nonlinear solvers. Stochastic bilevel formulation was also proposed in [121] to analyze the interaction between a distribution network operator (DNO) and networked MGs considering the renewable energy generation uncertainty where each entity aims at minimizing its individual operation cost. Our dissertation employs the bilevel programming to design a novel pricing signal for DR in the distribution network.

2.1.5 Multi-Objective Programming

Multi-objective programming or multi-objective optimization is an area of multiple criteria decision making where there are more than one objective function to be optimized simultaneously [122]. In general, we must find optimal decisions considering trade-offs between two or more conflicting objectives. Mathematically speaking, the multi-objective optimization can be formulated as [122]

$$\min_{x \in X} F(x) \quad (2.24)$$

where $F(x) = [f_1(x), \dots, f_m(x)]^T$, $F(x) \in R^m$, $m \geq 2$ is the vector valued objective function, x is a vector of decision variables, and X is the feasible region of x . Unfortunately, there are no single solution for this optimization problem since optimizing one objective can result in degradation of the others. In multi-objective programming, we are interested in Pareto optimal solutions where we cannot improve one objective function without degrading the others. A set of Pareto optimal solutions is called the Pareto front. There are many methods to construct the Pareto front for a general multi-objective optimization problem. This thesis considers the application of multi-objective linear programming [56]. There are two main classical optimization methods that construct the Pareto front for the linear case, namely the scalar (weighted) method and ε -constraint method [56].

In the ε -constraint method, one objective function is chosen to be optimized while the other is converted into a constraint [56]. For example, $f_1(x)$ is chosen to be optimized while other $f_i(x)$, $i = 2, \dots, m$ are converted to constraints with chosen parameters ε_i as follows:

$$\min_{x \in X} f_1(x) \quad (2.25)$$

$$\text{s.t. } f_i(x) \leq \varepsilon_i, \quad i = 2, \dots, m \quad (2.26)$$

In the scalar method, the multi-objectives are converted to the single objective problem by considering the weighted sum of all objective functions as follows:

$$\min_{x \in X} \sum_{i=1}^m w_i f_i(x) \quad (2.27)$$

where w_i , $i = 1, \dots, m$ represent the weights.

The ε -constraint method has several advantages over the scalar method for linear problems [56]. Specifically, the ε -constraint method alters the original feasible region to obtain non-extreme Pareto optimal solutions. On the other hand, the scalar method often results in a corner solution. Consequently, there can be many combinations of weights that result in the same Pareto optimal solution. Using the ε -constraint method, we can obtain a different Pareto optimal point by solving the corresponding ε -constraint based single objective problem, which improves the Pareto front's representation. In the ε -constraint method, it is easier to control the number of the generated Pareto optimal points by adjusting the number of grid points, which is not easy with the scalar method. Finally, the scalar method requires the objective functions to be scaled appropriately before forming the weighted sum, which is not necessary in the ε -constraint method [56, 122].

Many smart grid's decision making problems can be formulated as multi-objective programming problems. For example, for an optimal bidding strategy in the two-settlement electricity market, we usually aim to maximize the expected profit but limiting its variance. This problem can be formulated as a multi-objective optimization problem where we must determine the day-head bidding quantities such that the expected profit is maximized and the risk measure is minimized.

2.2 Cooperative Game Theory

In the decentralized market, several market agents can cooperate with each other to gain the benefit. One problem is how to share the benefit of cooperation among members. This decision-making problem can be addressed by using the cooperative game theory.

2.2.1 Basic Concepts

A cooperative game with transferable utility $\mathcal{G}(\mathcal{K}, v)$ is defined by an ordered pair (\mathcal{K}, v) . $\mathcal{K} = \{1, 2, \dots, NK\}$ is a finite and nonempty set of players which are decision makers. \mathcal{K} also denotes the grand coalition [98]. The transferable utility means the commodity, which can be cost or profit, can be transferred among the players without any third instance [54]. Every subset $S \in \mathcal{K}$ of cooperating players is called a coalition S represented by an indication vector $e^S = [e_1^S, e_2^S, \dots, e_{NK}^S]^T$ where $e_k^S = 1$ if $k \in S$ and $e_k^S = 0$, otherwise [98]. The notation v denotes the game characteristic function which maps each coalition S to a real number $v(S)$ [54, 55, 98] as follows:

$$v: 2^{NK} \rightarrow \mathcal{R}_+, v(\emptyset) = 0 \quad (2.28)$$

where v can be interpreted as profit or cost and $\mathcal{G}(\mathcal{K}, v)$ is called the cost game or profit game accordingly [54].

In a profit game, players prefer more allocated profit to less allocated profit. The profit game is *superadditive* if $v(S1 \cup S2) \geq v(S1) + v(S2)$ for any disjoint $S1$ and $S2$. In a cost game, players prefer less cost allocated to more cost allocated. The cost game is *subadditive* if $v(S1 \cup S2) \leq v(S1) + v(S2)$ for any disjoint $S1$ and $S2$. These conditions imply that the total profit/cost is maximized/minimized if all players join the grand coalition \mathcal{K} .

A *balanced map* $m : 2^{\text{NK}} \mapsto [0, 1]$ is a map that satisfies $\sum_{S \in 2^{\text{NK}}} m(S) e_k^S = 1, \forall k \in \mathcal{K}$ [55, 98].

A *balanced (cost) game* is a game that has $\sum_{S \in 2^{\text{NK}}} m(S) v(S) \geq v(\mathcal{K})$, for any balanced map m [55, 98].

A cooperative game $\mathcal{G}(\mathcal{K}, v)$ is called *totally balanced* if for each coalition S the sub-game $\mathcal{G}(S, v)$ is balanced [55, 98].

2.2.2 Solution Concepts and The Core

In general, we consider the case when the grand coalition is formed and we are interested in dividing the profit/cost to each member of the grand coalition. A payoff division or profit/cost allocation vector $x \in \mathcal{R}^{\text{NK}}$, where x_k is profit/cost allocated to player k , is considered as the cooperative game's solution concept. A comprehensive literature review of solution concepts for cooperative games with transferable utility can be found in [123]. One important solution concept of cooperative game is called the core.

The *core* $\mathcal{C}(v)$ is the set of payoff divisions such that no coalition can have better cost saving than the sum of the members' current allocated costs:

$$\mathcal{C}(v) = \left\{ x \in \mathcal{R}^{\text{NK}} : \sum_{k=1}^{\text{NK}} x_k = v(\mathcal{K}), \sum_{k \in S} x_k \leq v(S), \forall S \in 2^{\text{NK}} \setminus \{\emptyset\} \right\}. \quad (2.29)$$

A game solution x is called a *rational allocation* [54] if it lies in the core of the game $x \in \mathcal{C}(v)$. The core is nonempty if the game is *balanced* [98].

2.2.3 Linear Programming (LP) Game

In many practical smart grid models, the players can be interested in cooperation to maximize/minimize the total profit/cost and the characteristic function $v(S)$ can be modeled as an optimum (maximum/minimum) of an optimization problem corresponding to the coalition S [55]. In many cases, the optimization problem is modeled as a linear program.

Consider the following linear program:

(P)

$$v_P(A, H, b, d, c) = \min_z c^T z \text{ s.t.} \quad zA \leq b, \quad (2.30)$$

$$zH = d, \quad (2.30)$$

$$z \geq 0 \quad (2.31)$$

where $z \in \mathcal{R}^m$ denotes the optimization variables, $c \in \mathcal{R}^m, b \in \mathcal{R}^p, d \in \mathcal{R}^n$, A is a $m \times p$ matrix, H is an $m \times r$ matrix, and \hat{z} is the optimal solution, $c^T \hat{z}$ is the optimum of the linear program P, and $v_P(A, H, b, d, c) = c^T \hat{z}$.

The cooperative game $\mathcal{G}(\mathcal{K}, v)$ can be constructed from (P) by making all, or some of the right hand sides in the constraints, depend on the coalitions S [55]. This can be done in several ways. One way is to make the right hand side of constraints in (P) a linear combination of e_k^S . In addition, $v(S)$ is assumed to be well-defined, i.e., problem (P) with S is feasible and the value of $v(S)$ obtained from solving (P) is a real number [55].

Definition: A cooperative game $\mathcal{G}(\mathcal{K}, v)$ is called a LP game if there exists an $m \times p$ matrix A , an $m \times r$ matrix H , vectors $b(S) \in \mathcal{P}$, and $d(S) \in \mathcal{R}^r$ for all $S \in 2^{\text{NK}} \setminus \{\emptyset\}$ such that $v(S) = v_P(A, H, b(S), d(S), c)$ [55].

A LP-game is totally balanced (see Theorem 2.2.3 in [55]). That means the core of a LP game is nonempty. The proof can be found in [55] (page 24, Theorem 2.2.3).

2.3 Computation Setup and Numerical Study

All decision-making problems studied in this dissertation are modeled in the GAMS environment [40]. In the first part of this thesis, we model the home energy management problem with solar assisted thermal load under the real-time pricing scheme as a rolling two-stage stochastic program, which is converted into MILP by using the scenario based approach. In the second part, we model the pricing design problem of a Load Serving Entity (LSE) as a bilevel programming problem which is converted to a single-objective MILP. In the third part, we model the cost allocation problem of a virtual power plant consisting multiple demand-side resource aggregators as a cooperative LP game. To find the cost allocation vector inside the core, we consider a multi-objective programming problem. In addition, the scenario reduction is performed by using the GAMS/SCENRED package. All MILP/LP problems are solved by CPLEX [106] under GAMS [40] in a computer using Windows 8, Intel Core i5 3.3 GHz processor, and 8 GB RAM.

2.4 Summary

This chapter discussed several basic concepts of mathematical optimization methods and cooperative game theory. Firstly, basic concepts of mathematical optimization are introduced. In particular, we briefly discussed three classes of optimization problems, which are used to model the decision making problems studied in this thesis. They are stochastic programming, bilevel programming, and multi-objective programming. Finally, we presented the cooperative game with transferable utility which is used to model the profit/cost sharing problem. Specifically, we presented the concept of the core which defines how the benefit of cooperation should be divided and the form of linear programming game which can capture many cooperation models in smart grid. Finally, the computation setup for numerical studies in the thesis was presented.

Chapter 3

Energy Management of Smart Home with Solar Assisted Thermal Load Considering Price and Renewable Energy Uncertainties

This chapter studies DR from residential sector. In particular, we investigate how a single smart home equipped with renewable energy based appliances can respond to time-varying price signals in the best economic way. The content of this chapter was published in IEEE Transactions on Smart Grid in the following paper:

Hieu Trung Nguyen, Duong Tung Nguyen, and L. B. Le, “Energy Management for Households With Solar Assisted Thermal Load Considering Renewable Energy and Price Uncertainty,” *IEEE Transactions on Smart Grid*, vol. 6, no. 1, pp. 301-314, Jan. 2015. doi: 10.1109/TSG.2014.2350831

3.1 Abstract

This chapter investigates the energy scheduling problem for a household equipped with a solar assisted Heating, Ventilation, and Air Conditioning (HVAC) and water heating system in the real-time pricing (RTP) environment. Our objective is to minimize the electricity cost while maintaining users’ thermal comfort requirements. We consider different types of loads with different characteristics, detailed modeling of thermal dynamics, and uncertainty in electricity price and solar energy. The advantage of the proposed design lies in the exploitation of the solar assisted thermal system that can flexibly utilize the energy from the solar source or from the grid during low-price periods to support the home hot water demand, user thermal preference while reducing the electricity cost. Obtained numerical results are presented to illustrate the effectiveness of our proposed design. In particular, we show that the proposed design can achieve significant cost saving, allow flexible tradeoff between user comfort tolerance and electricity cost reduction, and efficiently adjust the electricity consumption load profile. The influence of solar assisted thermal system factors such as the water tank temperature limit, solar collector size, and weather condition on the achievable cost are also analyzed.

3.2 Introduction

Household appliance scheduling has been receiving significant research interest over the past few years [16–18, 23, 34, 37, 57]. Research works in this topic are very diverse in terms of mathematical models and solution approaches. In particular, some existing works determine residential demand response solutions by solving deterministic optimization problems assuming that the scheduler has perfect system and forecast information over the scheduling horizon [21, 37, 73, 79]. In [37], the authors tackle the load power control problem under the flat-rate pricing model where the utility is assumed to determine the thresholds of energy consumption at different time slots and broadcast these values to end users for load scheduling. Then, scheduling decisions are made by the end users to adapt to the utility control signal based on the predefined priority levels of different appliances. However, uncertainties in the real-time price, outdoor temperature, and load demand are not considered.

More recently, research on residential energy management has considered more complicated systems that integrate renewable energy resources, home energy automation system and smart appliances, novel electricity pricing schemes as well as smart grid communications. Facilitated by these technologies, residential energy users can actively participate in various demand response (DR) programs to minimize the electricity payment. The work [73] focuses on the scheduling of a residential micro-grid exploiting smart meter data and thermal load and it evaluates the sensitivity of different forecast parameters such as electricity price, outdoor temperature, and demand on the achievable energy cost. However, it does not consider the uncertainties of these parameters in the proposed optimization framework. In [79], the scheduling design for households with renewable energy under the Time of Use (TOU) pricing scheme is conducted assuming that pricing information is known for the whole scheduling horizon. This type of deterministic models may not result in good performance in practice since various forms of uncertainties are not captured.

There have been also some existing works showing that Real Time Pricing (RTP) can offer better economic and environmental advantages over flat-rate and time of use (TOU) pricing schemes [17]. In fact, RTP reflects the real-time and varying energy production cost of the power system [16], which would better guide the end users to schedule their energy consumption [17]. However, RTP may lead to certain grid stability issues [35] since many users may shift their loads to low-price period simultaneously. It has been shown that employment of “inclining block rate” (IBR) [17, 82] or optimal real-time pricing design under suitable criteria considering demand response activities [124] can help maintain the grid stability.

Engineering of home energy management algorithms under RTP is an important and hot research topic [17],[16],[57],[80]. In [17], an optimization framework for scheduling home appliances is proposed to minimize the electricity cost. In addition, the works [80], [81] propose to employ dynamic programming in conjunction with Markov Decision Process (MDP) theory to determine an optimal control policy that allocates power consumption for each appliance. In [16, 57], the authors develop Demand Response (DR) algorithms for a household with various types of residential appliances and price uncertainty by using the rolling online stochastic programming approach. The authors of [82] model the scheduling delay as a penalty term in the objective function of the scheduling problem,

which is solved by using genetic algorithms. All these works, however, focus on conventional types of home appliances, model the uncertainty of only real-time pricing where integration of renewable energy is not considered.

In general, thermal loads such as HVAC and the water heating system make considerable contribution to the electricity consumption of a typical household (e.g., over 50% of the total residential energy consumption [25]). Research on optimal scheduling for thermal loads and exploiting them for various smart-grid services are also very active research areas. The works [16, 57] consider HVAC and the water heating system in their scheduling problem formulations, which, however, rely on very simple thermal dynamic models. The authors of [25–27] study the possibility of employing the water heater and HVAC for load regulation services; however, energy management for other loads is not considered. In addition, exploiting building thermal mass [18, 48, 59] or water heating buffer [61] as energy storage for DR are also studied. The works [58, 65] suggest that proper cooperation of various electricity, renewable energy resources, and energy storage facilities can improve the building energy efficiency and DR ability. These papers, however, consider a large building application with a Combined Cooling Heat and Power (CCHP) system, which may not be applicable for small household scenarios. Overall, these existing works consider the HVAC and water heating system in separation where the potential benefit of the combined hybrid HVAC and water heating system is not studied.

Recently, design of the HVAC and water heating system for better energy efficiency has attracted a lot of attention. In particular, there is considerable interest in combining the thermal system with the solar energy source. In fact, the coefficient of performance (COP) of a standalone HVAC system, which is about 2–3, can be improved significantly when being combined with solar energy sources [39]. The development of the hybrid solar assisted HVAC and water heating system is motivated by the abundant presence, environmental sustainability, and quiet operation of solar energy [38, 39, 64, 84–87]. The key component of this hybrid system is the solar hot water tank, which stores the energy from solar collector for supporting both HVAC and hot water demand [84].

In the hybrid solar assisted HVAC and water heating system, heat from the solar water tank can be used to increase the enthalpy for refrigerant after condenser process, thus reducing the working cycle and energy usage of the HVAC compressor [39]. For the design in [38], a solar cooling system is connected to the conventional air conditioner to reduce the condensing temperature, which improves the COP of the hybrid system. In [87], it is proposed that water from the solar tank is delivered to support the water heating demand and for the heat-pump to support HVAC. The work [86] investigates the system coefficient of operation and empirical modeling for hybrid solar HVAC and water heating system. In [64, 86], optimal control algorithms, empirical modeling, and system identification of hybrid solar HVAC and water heating system are investigated. The papers [84, 85] review various mathematical models of solar assisted thermal loads. The work [61] focuses on modeling and designing the control interface for the water storage tank.

None of the previous works have considered exploiting the benefits of the hybrid solar assisted HVAC-water heating system in home energy management. In this study, we investigate the home energy scheduling considering solar assisted HVAC and water heating system and other types of household appliances. We propose to exploit the thermal solar water tank as a dynamic storage facility to

support thermal demand of water heating and the HVAC system. The main contributions of this study can be summarized as follows:

1. We propose a comprehensive model for home energy management including hybrid solar assisted thermal loads and various types of controllable appliances, which aims to minimize the electricity cost and maintain user comfort. Our model accounts for detailed modeling of the hybrid solar assisted HVAC and water heating system, characteristics of other loads, users' comfort preference, and thermal dynamics. We also consider the uncertainty of solar energy and electricity price.
2. We describe how to solve the underlying energy scheduling problem by using rolling stochastic optimization approach. We investigate the potential economic benefits achieved by smartly scheduling the solar assisted HVAC and water heating system and other household loads. In particular, we show that the solar assisted thermal system can help reduce the energy cost significantly.
3. We study the impacts of different parameters on the total energy cost including solar collector size, tank temperature level, thermal comfort tolerance, and weather condition.

The remaining of this chapter is organized as follows. The notations used in this study are presented in Section 3.3. The system model is presented in Section 3.4. The proposed energy management design is presented in Section 3.5. Section 3.6 presents numerical results and Section 3.7 concludes this study.

3.3 Notations

Notation	Explanation
Sets and Indices	
t, j	Time slot index, $t = 1, 2, \dots, N$
s	scenarios, $s = 1, 2, \dots, NS$
A	Set of loads
i	Load index
Parameters	
a_1	1.505 (W/m^2K) APSE-10 solar collector parameter
a_2	0.0111 (W/m^2K^2) APSE-10 solar collector parameter
G	800(W/m^2) APSE-10 Solar collector parameter
$p_{i,t}^s$	Power consumption at t for load i scenario s (kW)
$\eta_{sl,t}^s$	Solar collector energy conversion efficiency at t scenario s
N	Number of time slots
NS	Number of scenarios
a_I, b_I	Beta distribution parameters
ΔT	Room (indoor) thermal comfort tolerance ($^{\circ}C$)
a_{λ}, b_{λ}	Cauchy distribution parameters
$T_{o,t}^s$	Ambient (outdoor) temperature at t scenario s ($^{\circ}C$)

σ	Heating (1) or cooling mode (-1)
R_a	Room equivalent thermal resistance($^{\circ}C/kW$)
c_t^s	Electricity price at t scenario s ($\$/kWh$)
τ	Duration of time slots (hours)
A_{sl}	Solar collector size (m^2)
COP_a	HVAC coefficient of performance at stand alone mode
COP_c	HVAC coefficient of performance at combination with renewable energy mode
C_r	Room thermal capacity ($kWh/^{\circ}C$)
$T_{r,t}^s$	Room (indoor) temperature at t , scenario s
A_w	Room effective window (m^2)
I_t^s	Solar irradiance at t , scenario s (kW/m^2)
ρ^s	Probability of scenario s
C_{wt}	Thermal capacity of water tank storage ($kWh/^{\circ}C$)
A_{wt}	Surrounding area associated with tank heat loss (m^2)
U_{wt}	Tank heat loss factor due to radiation
Variables	
$p_{sh,t}^s$	Heat support HVAC from water tank storage at t scenario s (kW)
$p_{sl,t}^s$	Power captured from solar collector at t scenario s (kW)
$p_{wd,t}^s$	Water demand at t scenario s (kW)
$p_{u,t}^s$	Heat transfer at t scenario s (kW)
$p_{hvac,t}^s$	Power consumption of HVAC at t scenario s
$p_{hvac,t}^{s,a}$	Power consumption of HVAC in standalone mode at t scenario s (kW)
$p_{hvac,t}^{s,c}$	Power consumption of HVAC in combination mode at t scenario s (kW)
$p_{h,t}^{s,c}$	Power consumption of back up auxiliary heater at t scenario s (kW)
$T_{wt,t}^s$	Tank temperature at t scenario s ($^{\circ}C$)
$u_{i,t}^s$	binary operation status at t for load i scenario s (0-off, 1-on)
$y_{i,t}^s$	“Turn-on” status at t for load i , scenario s
$z_{i,t}^s$	“Shut-down” status at t for load i , scenario s

3.4 System Model

We consider a typical household in the RTP environment where energy scheduling is performed for the 24-hour scheduling period. The household is equipped with a solar assisted HVAC-water heating system and other loads of different types such as electric vehicle (EV), washing machine, washing dryer, television, and water supply pump. The household loads excluding the joint HVAC-water heating system is classified into controllable and non-controllable types [37]. Non-controllable loads are those whose operations are dependent on the will of users such as computer, lighting, and television. The operations of non-controllable loads are not considered in our optimization. In contrast, the operation schedule of controllable loads can be optimized without disturbing the user life style. We divide the

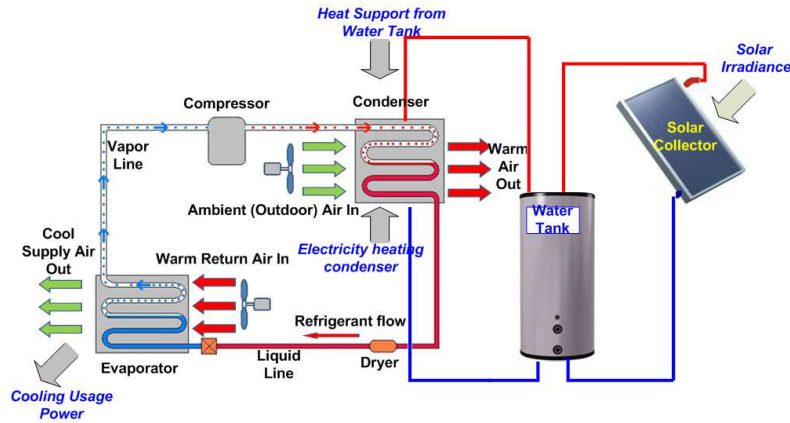


Figure 3.1 – Solar assisted HVAC-water heating system

considered scheduling period into N scheduling time slots of equal length τ where the electricity price in each time slot is assumed to be constant.

Denote A as the set of all controllable appliances and A_1 represents the HVAC, A_2 for interruptible and deferrable loads, A_3 for noninterruptible and deferrable loads, and A_4 for noninterruptible and nondeferrable loads. Then, we have $A = A_1 \cup A_2 \cup A_3 \cup A_4$.

The solar assisted HVAC-water heating system represents an important load of the household, which is described in the following. The typical components and design of this system is illustrated in Figure 3.1 [38]. It consists of a solar collector, a water storage tank, and the HVAC system. Solar energy is collected and transformed into thermal energy which is stored in the water tank by the solar collector. Hot water from the tank then supports the domestic hot water demand and heating/cooling demand of the HVAC system. The operation of HVAC is based on the principle that energy which is used to move heat around is often smaller than the energy used to generate heat. Hence, extra heat from the water tank can be used to support the necessary energy which is used to control the heat cycle in heating/cooling mode of HVAC. To cover the remaining heat demand for the cloudy day or during night time, the water tank is also equipped with an auxiliary heater. In this chapter, we use t and s to denote time slot and scenario indices, respectively.

3.5 Energy Management Design

3.5.1 Design Objective and Solution Approach

In this study, we explicitly consider the uncertainties in the electricity price and renewable energy in our energy management problem. Our design objective is to minimize the electricity cost (i.e., payment of the home owner). In fact, there is quite rich literature on home energy management considering various system uncertainties and using different solution techniques. In [80], [81], the scheduling problem is modeled as a Markov Decision Process (MDP), which is solved by using the dynamic programming approach. In general, if the system uncertainties do not depend on the taken decisions at each time interval, which is the case for our model, then the MDP would not be a useful approach [125]. In [82], the energy management problem is solved by using genetic algorithms. However, genetic

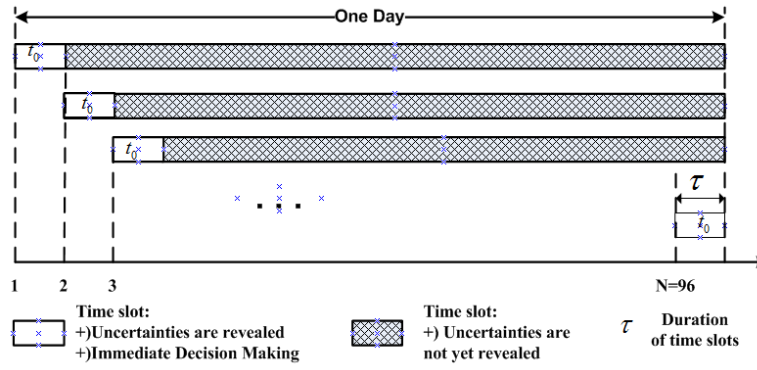


Figure 3.2 – Rolling stochastic scheduling for Home Energy Management system

algorithms may not scale well with the system size, which implies that only suboptimal solutions can be obtained in practice. Rolling online stochastic programming is another efficient tool to deal with uncertainties, which has been employed in several existing works [16],[57],[125]. It is indeed suitable for our problem formulation since the system uncertainties are exogenous and do not depend on the taken decisions [57],[125]. In addition, this method enables us to determine an optimal immediate decision given the revealed information of uncertainties at the beginning of each time slot.

In this study, we employ the two-stage stochastic programming to formulate the scheduling problem where the Monte Carlo simulation technique is used to generate random scenarios. In addition, the formulated problem is solved by using the rolling procedure [16]. Toward this end, we repeatedly solve the underlying stochastic optimization problem in each time slot given the realization of the random variables (i.e., electricity price and renewable energy) in the current time slot t_0 . In particular, we minimize the sum of the electricity cost due to energy consumption at the current time t_0 (as electricity price, solar irradiance, and outdoor temperature at the current time slot are known) and the expected electricity cost from time slot $t_0 + 1$ to the last time slot N . Known information about system uncertainties such as price, solar irradiance, outdoor temperature, non-controllable load power consumption are updated during this rolling process. Therefore, we consider the following optimization objective at each time t_0

$$\min_{P_{i,t}} \sum_{i \in A} \left\{ p_{i,t_0} c_{t_0} \tau + \sum_{s=1}^{NS} \rho^s \sum_{t=t_0+1}^N p_{i,t}^s c_t^s \tau \right\} \quad (3.1)$$

where ρ^s denotes the probability of scenario s , which is used to calculate the expected cost toward the end of the scheduling period.

This rolling two-stage stochastic programming technique for home energy management follows the tree reduction method where multiple scenarios are generated to capture the uncertainty in electricity price and weather factors [16]. The underlying optimization in each time slot can be solved by using the GAMS/CPLEX solver. This optimization problem is subject to various constraints, which are described in the following.

3.5.2 Solar Assisted HVAC and Water Heating System

In the solar assisted HVAC and water heating system, solar energy is collected and transformed into thermal energy which is stored in the water tank by solar collector. In addition, HVAC transfers heat by circulating a refrigerant through a cycle of evaporation and condensation. The refrigerant is pumped between two heat exchanger coils named evaporator and condenser by the compressor pump. In the evaporator coil, the refrigerant is evaporated at the low pressure and absorbs heat from its surroundings. The refrigerant is compressed at high pressure and then transferred to the condenser coil where it is condensed at the high pressure and releases the heat it absorbed earlier in the evaporator. The cycle is fully reversible; hence, the HVAC can provide cooling and heating mode. For cooling, the heat is extracted from home and released to outside area. For heating, the heat extracted from outside is used to heat the indoor area.

Energy consumption of HVAC lies mostly in the compressor pump and condenser, especially to maintain temperature at the condenser [39]. By adding support heat to the condenser, less energy consumption is needed for the HVAC to operate the heat cycle, hence the coefficient of operation (COP) is increased. For solar assisted HVAC, the heat captured in the water tank is used to support heat for the HVAC. For modeling, we impose the following constraints for the solar assisted HVAC and water heating system.

Solar Collector

The solar energy collected by the solar collector is transformed into thermal energy of the water tank. This solar energy can be calculated as

$$p_{sl,t}^s = \eta_{sl}^s A_{sl} I_t^s \quad (3.2)$$

where the conversion efficiency η_{sl} is generally not a fixed value but it depends on the outdoor temperature and solar parameters as

$$\eta_{sl} = \eta_{sl}^0 - \frac{a_1}{G} (T_{sl,t}^s - T_{o,t}^s) - \frac{a_2}{G} (T_{sl,t}^s - T_{o,t}^s)^2. \quad (3.3)$$

The curve representing the relationship between η_{sl} and related parameters a_1, a_2, G is often provided in the product manual. This second-order curve can be approximated in the linearized form as

$$\eta_{sl}^s = \eta_{sl}^0 - \bar{a} (T_{sl,t}^s - T_{o,t}^s). \quad (3.4)$$

Since we typically have $a_2 \ll a_1$, we can approximate $\bar{a} \approx \frac{a_1}{G}$.

Water Storage

Since the thermal stratification technology is usually used in the storage tank to improve its thermal capacity, the tank can be modeled to consist of a number of mixed water layers [61, 64, 85]. This model, however, is complicated and may not be valid for the long time scale of minutes. Instead, the first-order and one layered model is sufficient for describing the heat dynamics of the tank [126]. This is indeed based on the energy balance equation where the tank can receive energy from the solar collector, back-up auxiliary heater and dispatch energy to support hot water demand and HVAC.

$$C_{wt} \frac{dT_{wt}}{dt} = p_h + p_{sl} - U_{wt} A_{wt} (T_{wt} - T_r) - p_{sh} - p_{wd}. \quad (3.5)$$

This equation can be converted into the discrete form over discrete intervals of τ as

$$\begin{aligned} T_{wt,t+1}^s &= \left(1 - \frac{\tau U_{wt} A_{wt}}{C_{wt}} \right) T_{wt,t}^s + \frac{U_{wt} A_{wt} \tau}{C_{wt}} T_{r,t}^s + \\ &\frac{\tau}{C_{wt}} \left(p_{h,t} + p_{sl,t}^s - p_{wd,t}^s - p_{sh,t}^s \right). \end{aligned} \quad (3.6)$$

To counteract the randomness in the output solar energy, the water tank employs an electric auxiliary heater as a backup heat source. The power consumption constraint of this auxiliary heater can be written as

$$p_h^{\min} u_{h,t}^s \leq p_{h,t}^s \leq p_h^{\max} u_{h,t}^s. \quad (3.7)$$

Finally, we need to impose the following constraint on the water temperature

$$T_{wt}^{\min} \leq T_{wt,t}^s \leq T_{wt}^{\max}. \quad (3.8)$$

HVAC Load

The energy scheduling for the HVAC system must be performed in such a way that the indoor temperature is maintained in a predetermined range $[T_r^{\min}, T_r^{\max}]$ during the scheduling time window $[\alpha_{HVAC}, \beta_{HVAC}]$ when the household is occupied, i.e.,

$$T_r^{\min} \leq T_{r,t}^s \leq T_r^{\max}, t \in [\alpha_{hvac}, \beta_{hvac}]. \quad (3.9)$$

There is an inherent relationship between indoor temperature T_r in consecutive time slots that depends on the energy supplied to the HVAC, outdoor temperature T_o , solar irradiance I , and other building parameters. This relationship is captured in a thermal dynamics model expressed as follows [59, 127]:

$$C_r \frac{dT_r}{dt} = \frac{T_o - T_r}{R_a} + \eta_w A_w I + \sigma_h p_u. \quad (3.10)$$

where p_u denotes the heat that the HVAC transfers. This thermal dynamics can be transformed into the discrete form for scenario s as

$$T_{r,t+1}^s = \left(1 - \frac{\tau}{R_a C_r}\right) T_{r,t}^s + \frac{\tau}{R_a C_r} T_{o,t}^s + \frac{\eta_w A_w \tau}{C_r} I_t^s + \sigma \frac{p_{u,t}^s \tau}{C_r} \quad (3.11)$$

In order to transfer $p_{u,t}$, the HVAC needs to consume the power of p_{hvac} . The ratio between the amount of heat transfer $p_{u,t}$ and the amount of electricity consumption represents the COP of the HVAC, i.e., $COP = p_{u,t}/p_{\text{hvac}}$.

By using the thermal storage to support the HVAC, the system COP can be improved significantly [86]. Denote COP_a and COP_c as the COP of the system as it operates in the standalone mode and as it is supported by thermal storage, respectively. When the HVAC works at standalone mode, we have $p_u = COP_a p_{\text{hvac}}$. When the HVAC operates in the combined mode, a portion of its required energy is provided by the water thermal storage, which can be written as

$$p_u = COP_a (p_{\text{hvac}} + p_{\text{sh}}) = COP_c p_{\text{hvac}}. \quad (3.12)$$

Hence, we have the following constraints for the HVAC system

$$p_{u,t}^s = COP_a p_{\text{hvac},t}^{s,a} + COP_c p_{\text{hvac},t}^{s,c} \quad (3.13)$$

$$u_{\text{hvac},t}^{s,a} + u_{\text{hvac},t}^{s,c} \leq 1 \quad (3.14)$$

$$u_{\text{hvac},t}^{s,a} p_{\text{hvac}}^{\min} \leq p_{\text{hvac},t}^{s,a} \leq u_{\text{hvac},t}^{s,a} p_{\text{hvac}}^{\max} \quad (3.15)$$

$$u_{\text{hvac},t}^{s,c} p_{\text{hvac}}^{\min} \leq p_{\text{hvac},t}^{s,c} \leq u_{\text{hvac},t}^{s,c} p_{\text{hvac}}^{\max}. \quad (3.16)$$

Here, the constraints (3.13), (3.14) capture the fact that the HVAC can operate in the standalone or cooperated mode with extra heat support (its control variables are $u_{\text{hvac},t}^{s,a}$ and $u_{\text{hvac},t}^{s,c}$, respectively); however, only one mode can be chosen at any time interval. Also, the constraints (3.15), (3.16) represent the max and min power limits of the HVAC.

Also, the electricity consumption of HVAC system can be expressed as

$$p_{\text{hvac},t}^s = p_{\text{hvac},t}^{s,a} + p_{\text{hvac},t}^{s,c}. \quad (3.17)$$

And the support power from thermal storage is

$$p_{\text{sh},t}^s = \frac{COP_c - COP_a}{COP_a} p_{\text{hvac},t}^{s,c}. \quad (3.18)$$

Finally, the total electricity consumption of solar assisted HVAC and water heating in one time slot is due to the total electricity consumption of back-up heater of the water tank and the HVAC, i.e., $p_{A_1,t} = p_{\text{sh},t}^s + p_{\text{hvac},t}^s$.

Thermal Load With Non-continuously Modulated Power Consumption

In the previous presented formulation, the power consumptions of HVAC and auxiliary heater are assumed to be continuously modulated. That means their power consumption can be adjusted in a continuous range $[P^{\min}, P^{\max}]$ when these systems are turned on. This assumption for HVAC and water heating system would only be valid when these systems are equipped with variable frequency drives (VFD). This may not be the case in reality where control actions can be simply ON-OFF. In this case the power consumption constrains of water auxiliary heater and HVAC (3.7), (3.15), (3.16) can be replaced by (3.19), (3.20), and (3.21) respectively as follows:

$$P_{h,t}^s = p_h^{\text{Rated}} u_{h,t}^s \quad (3.19)$$

$$P_{\text{hvac},t}^{s,a} = p_{\text{hvac}}^{\text{Rated}} u_{\text{hvac},t}^{s,a} \quad (3.20)$$

$$P_{\text{hvac},t}^{s,c} = p_{\text{hvac}}^{\text{Rated}} u_{\text{hvac},t}^{s,c} \quad (3.21)$$

Therefore, the scheduling solution can be obtained accordingly in the case considering these new constraints.

3.5.3 System Constraints

In general, total power consumption of all controllable loads is limited due to the power limit that can be transferred from the distribution grid to the home grid point of common coupling [23]. Suppose that power consumption of other non-controllable loads can be extracted from historical data then we have to impose the following constraint

$$\sum_{i \in A} p_{i,t}^s + P_{\text{NCL},t}^s \leq P_{\text{grid}}^{\max} \quad (3.22)$$

where $P_{\text{NCL},t}^s$ is total power consumption of non-controllable load.

We further impose energy consumption limits E_{δ}^{\max} (kWh) for each hour δ [17]. This means the total energy consumption during all time slots of one particular hour must be upper bounded by the corresponding limit. This is required to avoid being over-charged by the utility. We can write this constraint as follows:

$$\sum_{i \in A} \sum_{t=K(\delta-1)+1}^{K\delta} p_{i,t}^s \tau \leq E_{\delta}^{\max}, \delta = 1, 2, \dots, 24 \quad (3.23)$$

where K denotes the number of scheduling slots per hour.

3.5.4 Constraints for Different Controllable Loads

Suppose each controllable load i is required to operate in the time window $[\alpha_i, \beta_i]$ then we need to impose the following constraint

$$p_{i,t} = 0, t \notin [\alpha_i, \beta_i]. \quad (3.24)$$

Constraints of Deferrable Load

For a deferrable load i with the maximum tolerable delay of D_i time slots, we have the following constraint

$$\sum_{t=\alpha_i}^{\alpha_i+D_i-1} u_{i,t}^s \geq 1. \quad (3.25)$$

If load i is nondeferrable then we can simply set $D_i = 0$.

We may also want to impose additional constraints on the number of times that a particular load can be turned on and shut down in the scheduling interval. This is typically required to maintain desirable lifetime of the underlying appliances. These constraints can be written as

$$u_{i,t}^s - u_{i,t-1}^s - y_{i,t} + z_{i,t} = 0 \quad (3.26)$$

$$y_{i,t} + z_{i,t} \leq 1 \quad (3.27)$$

$$\sum_{t=\alpha_i}^{\beta_i} y_{i,t} + z_{i,t} \leq L_i \quad (3.28)$$

where L_i denotes the maximum number of times that load i can change its state.

Constraints of Interruptible and Deferrable Loads (Type I)

We will consider electric vehicle (EV) as an example of this load in the study. For this load, we have the following constraints

$$E_{i,\beta_i} \geq E_{id} \quad (3.29)$$

$$E_{i,t+1}^s = E_{i,t}^s + \eta_{ev_i} p_{i,t}^s \tau \quad (3.30)$$

$$E_i^{\min} \leq E_{i,t}^s \leq E_i^{\max} \quad (3.31)$$

where η_{ev_i} represents the charging efficiency coefficient, E_{i,β_i} is the energy stored in the EV at β_i , $E_i^{\min(\max)}$ is the EV minimum (maximum) levels of energy (kWh), $E_{i,t}^s$ is energy stored in EV (kWh) at time t , scenario s , and E_{id} describes the charging demand. In reality, some EV batteries can perform both charging and discharging operations. Other EVs can only draw energy from the grid in one direction without being able to send energy back to the grid. In this study, since our objective is to focus on the control of the solar assisted HVAC and water heating system, we only consider EV as a conventional energy consumption appliance whose charging task can be deferrable and interruptible [16].

Constraints of Noninterruptible and Deferrable Loads (Type II)

This load requires the following constraint:

$$\sum_{\hat{t}=t+1}^{t+H_i} u_{i,\hat{t}}^s \geq H_i (u_{i,t+1}^s - u_{i,t}^s), \quad t \in [\alpha_i, \beta_i] \quad (3.32)$$

where D_i denotes the delay tolerance and H_i represents the number of operation time slots required by the load.

Constraints of Noninterruptible and Nondeferrable Loads (Type III)

For this type of load, we only need to impose the operation time constraint as¹

$$\sum_{t=\alpha_i}^{\alpha_i+H_i-1} u_{i,t}^s = H_i. \quad (3.33)$$

3.5.5 Uncertainty Modeling

We consider the uncertainty in the RTP where the price at t can be modeled as

$$c_t = \bar{c}_t + \lambda_{c_t} \quad (3.34)$$

where \bar{c}_t denotes the value of DAP or estimated price, which is assumed to be provided by aggregator or obtained by certain price estimation algorithm embedded in the home energy management system. Also, λ_{c_t} represents the price forecast error with known probability density function. In this study, we assume the price forecast error follows the Cauchy distribution [109] whose the probability density function (pdf) is

$$f_{\Lambda_{c_t}}(\lambda_{c_t}) = \frac{b_\lambda}{\pi \left[(\lambda_{c_t} - a_\lambda)^2 + b_\lambda^2 \right]}. \quad (3.35)$$

The parameters a_λ and b_λ in this pdf can be obtained from historical data by curve fitting using the maximum likelihood method. Note that the Cauchy distribution has been also used to represent electricity price uncertainty in the literature [108], [109], [63]. The solar irradiance is also subject to uncertainty, which depends on the weather condition. Its uncertainty is assumed to follow the beta distribution as follows:

$$f_{I_t}(I_t) = \frac{\Gamma(a_I + b_I)}{\Gamma(a_I)\Gamma(b_I)} \left(\frac{I_t}{I_0}\right)^{a_I-1} \left(1 - \frac{I_t}{I_0}\right)^{b_I-1} \quad (3.36)$$

¹This type of loads does not allow flexible scheduling control. We simply need to maintain their operation constraints.

where the values of a_I and b_I can be calculated from historical data by curve fitting using the maximum likelihood method [66]. Outdoor temperature can be modeled as

$$T_{o,t}^s = \bar{T}_{o,t} + \lambda_{T_{o,t}} \quad (3.37)$$

where $\bar{T}_{o,t}$ denotes forecast outdoor temperature and $\lambda_{T_{o,t}}$ denotes the outdoor temperature uncertainty factor which is assumed to follow Gaussian distribution.

3.5.6 Energy Scheduling Optimization Problem

In summary, the energy scheduling optimization problem can be applied for a household with any combination of the considered load types. Considering the RTP scheme with uncertainty, we propose to repeatedly solve the following rolling optimization problems for each time slot t_0 in the scheduling interval

$$\min \sum_{i \in A} \left\{ p_{i,t_0} c_{t_0} \tau + \sum_{s=1}^{NS} \rho^s \sum_{t=t_0+1}^N p_{i,t}^s c_t^s \tau \right\} \quad (3.38)$$

- s. t. Solar HVAC-water heating constraints (3.2), (3.4),
 (3.6) – (3.9), (3.11), (3.13) – (3.18)
 System constraints (3.22)-(3.23)
 Remaining load constraints (3.24)-(3.33).

This problem is a MILP, which is solved by using the CPLEX solver under GAMS. We assume that this problem is feasible, which is the case if the exchanged power and energy limits with the grid (i.e., P_{grid}^{\max} and E_{δ}^{\max}) are sufficiently large. In addition, CPLEX can typically find the optimal solution of this problem within affordable time. We will illustrate typical computation time of this problem in Section IV.

We employ the Monte Carlo simulation method to generate scenarios to represent various uncertain factors including price forecast error, solar irradiance, outdoor temperature, and power consumption of non-controllable load. In general, the number of generated scenarios needs to be sufficiently large to guarantee the energy scheduling efficiency. However, a large number of scenarios may lead to large computation complexity. For a large-scale problem, a scenario reduction method can be used to eliminate the scenario with very low probability, aggregate scenarios of close distances based on certain probability metric, reduce the number of scenarios, and consequently relax the computation burden. We use GAMS/SCENRED software [40] to generate/reduce the set of scenarios in this study.

3.5.7 Grid Stability under RTP

In this study, we consider the energy scheduling problem of a single house and assume that its impact on the grid is negligible. In reality, the large number of users participating in DR activities under real-time pricing could cause volatility to the grid [35]. The utility can employ the “*conservation rate model with inclining block rate (IBR)*” to discourage many users to draw energy from the grid during

low-price periods, which, therefore, helps maintain the grid stability [17]. In general, the design of pricing schemes that can exploit the DR benefits while maintaining the grid stability is an important research area, which is beyond the scope of the current study. We would like to address these research issues in our future works.

3.6 Numerical Results

3.6.1 Simulation Data

We consider a typical household with solar assisted HVAC-water heating and 3 different controllable loads whose parameters are given in Table 3.2. The power limit of all controllable loads is assumed 20 KW for simplicity and the threshold for energy consumption in one hour is 15 KWh. Water demand data is taken from [25]. The parameters for solar assisted HVAC and water heating system are described as follows. The solar collector has aperture area about $5 m^2$, the peak power of auxiliary heater is 5 KW, and the initial energy conversion efficiency $\eta_{sl}^0 = 0.7$. The solar efficiency curve is shown in Fig 3.4(e). The thermal storage tank has volume of 84 gal, which is equivalent to $0.32 m^3$. The tank can receive energy from the heater and solar collector. *COP* of hybrid and stand alone system are 5 and 3, respectively [39]. Other parameters of the solar system are taken from [41]. Tank temperature is required to be in the range of $[40^\circ C, 70^\circ C]^2$. The temperature comfort range is chosen as $[20 - \Delta T, 20 + \Delta T]$ where ΔT represents the thermal tolerance, which is set equal 1 unless stated otherwise. Details on the parameter setting for the base case are given in Table 3.3 and Table 3.4.

We divide one hour into $K = 4$ equal scheduling time slots, each of which is 15 mins. The outdoor temperature, solar irradiation, and electricity price data are taken from National Oceanic and Atmospheric Administration (NOAA) and ISO New England (ISO-NE) websites on July 17th, 2012, which are shown in Figure 3.4. We employ the neural network technique for electricity price estimation in RTP [128]. The uncertainty factors for electricity price and solar irradiation are obtained from the historical data by curve fitting using the maximum likelihood method [66], [109]. The number of scenarios generated is 1000 and the number of reduced scenarios is 10 to solve the underlying stochastic optimization problem. The average computation time in each time slot is about 150s as shown in Figure 3.3, which suggests that real-time implementation can be realized since the length of one time slot is 15 mins.

3.6.2 Energy Management Performance

We consider two case studies, namely using solar assisted thermal load (case 1) and conventional thermal load (case 2), respectively. Figures 3.5 and 3.6 show the energy consumption of different loads in the two cases. Figure 3.5(a) illustrates the thermal energy stored in the water tank. It is obvious that more energy is charged to the tank in the thermal form during the low-price period and/or when the solar energy is abundant (from 6am to 19pm). When the solar energy is abundant, the auxiliary heater

²The water is typically required to be stored at sufficiently high temperature to eliminate Legionella (most active at 30-35°C) and is used at lower temperature to prevent skin burn. Various daily activities can require quite different temperature levels. Also, anti-scald mixing valves installed at each point of use can automatically adjust the output temperature by mixing hot and cold water with a suitable ratio for the different purposes.

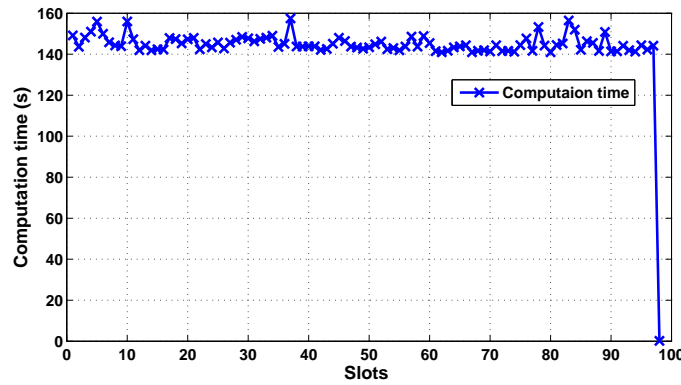


Figure 3.3 – Computation time of proposed scheduling algorithm

Table 3.2 – Parameters for Different Loads

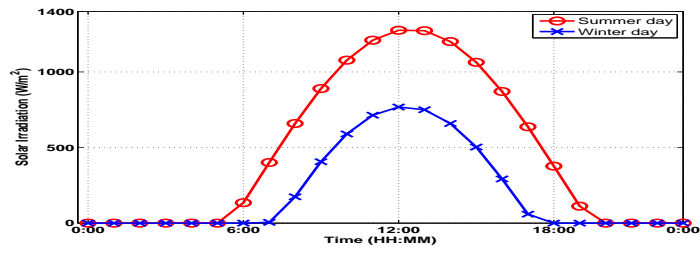
Loads	EV	Washing Machine	Clothes Dryer
Type	I	II	III
Power (kW)	3.3	0.5	2.5
Starting Time	17:00	11:30	17:00
Ending Time	8:00	17:30	18:00
Required Slots	N/A	10	4

remains off since solar energy is utilized to charge the water tank, which is shown in Figure 3.5(d). In the conventional system (case 2), the auxiliary heater is the only energy source, hence it must operate through out the day, which increases the electricity consumption as shown in Figure 3.6(d). In addition, due to the limit power of the heater, the maximum tank temperature in the conventional system (case 2) is smaller than that in the new system (case 1) where both electricity and solar energy are used. This implies the better utilization of water tank thermal capacity. The new system also has shorter HVAC working cycle compared with the conventional HVAC system, which is confirmed by Figures 3.5(c) and 3.6(c). Furthermore, Figures 3.5(b) and 3.6(b) show that the indoor temperature falls in the range of interest $[19, 21]^{\circ}C$.

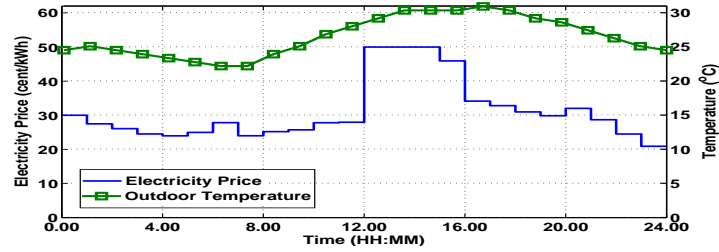
Figure 3.7 shows the water tank temperature when solar energy is used for water heating only. Due to the page constraint, we do not show the detailed power consumption of other loads since they are quite similar to the conventional HVAC and water heating case. It is interesting to notice that the maximum temperature in this figure is higher than those in the two cases above. This is due to the fact that tank thermal energy only supports water demand without considering HVAC consumption. In fact, the temperature evolution shows that, due to the heat loss, solar energy stored in the tank can be wasted if it is not utilized during the day. Figure 3.8 presents the energy consumption of other controllable loads, which are the same for the three considered cases. In addition, Figure 3.9 shows total energy

Table 3.3 – Solar assisted HVAC-water heating for based case

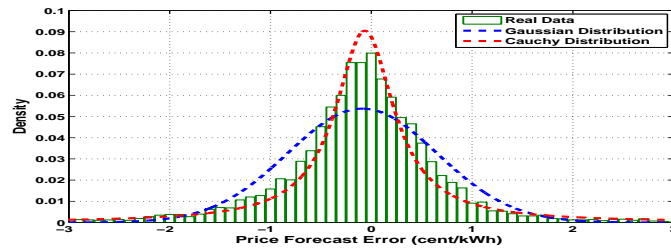
η_{sl}^0	a_1 (W/m^2K)	a_2 (W/m^2K^2)	A_{sl} (m^2)	G (W/m^2)	P_h^{max} (kW)
0.7	1.505	0.0111	5	800	5
C_{wt} ($kWh/^{\circ}C$)	A_{wt} (m^2)	U_{wt}	P_{hvac}^{max} (kW)	COP_a	COP_c
1.77	3.62	0.1	4	3	5



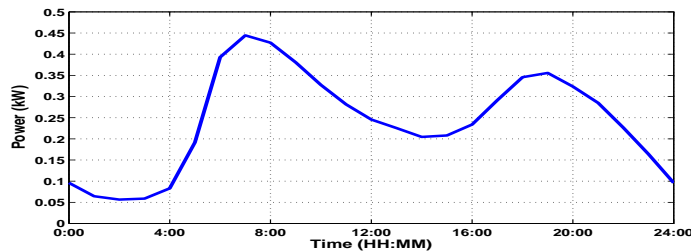
(a) Winter and summer solar irradiance



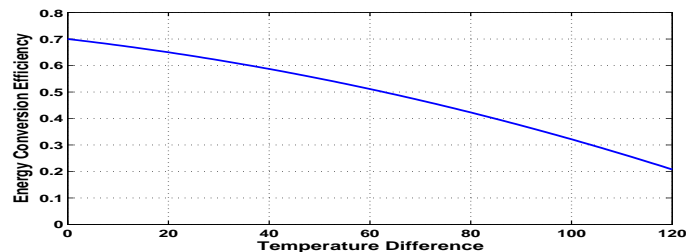
(b) Electricity and outdoor temperature for summer case



(c) Electricity price forecast error distribution



(d) Water demand



(e) Energy conversion efficiency of solar collector

Figure 3.4 – Simulation data for numerical results

consumption of all scheduled loads, which illustrates the significant energy consumption reduction for the household using the solar assisted HVAC and water heating system.

Table 3.4 – House Thermal Parameters

C_r ($kWh/^\circ C$)	A_w (m^2)	R_a ($^\circ C/kW$)
8.188	20.203	47.984

Figure 3.10 and 3.11 illustrate the electricity consumption and system dynamics for the solar assisted HVAC-water heating and conventional HVAC-water heating when the power consumption is non-continuously modulated (i.e., the control action at each time slot is On-Off only). In general, the results are quite similar to the case where power consumption of thermal system is continuously modulated. The exploitation of solar energy and the joint coordination of HVAC and water heating can help reduce the working cycle of HVAC and the auxiliary heater of the water tank significantly. Similar to Figure 3.5(a) and 3.6(a), water temperature in the solar assisted system is also higher than conventional system, which is demonstrated in Figure 3.10(a) and 3.11(a). This is because the water tank in the solar assisted case can exploit both solar energy and electricity of auxiliary heater, while electricity is the only energy source in the conventional system. This implies that the solar assisted thermal system can achieve better energy and cost saving than the conventional one.

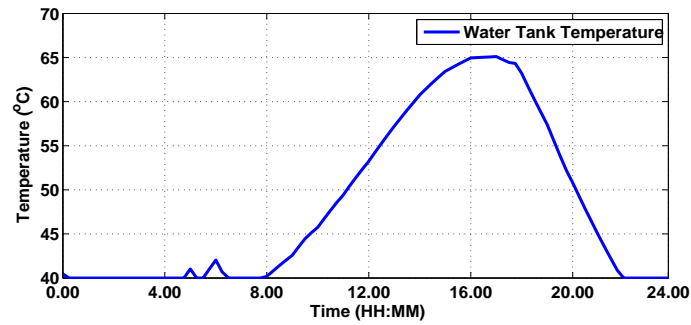
It is worth to mention that, due to the only On-Off operation, the room temperature and water temperature are not as smooth as in the continuously modulated power case. However, the temperature still falls in the requirement range even through it fluctuates more over time. Figure 3.12 presents the energy cost comparison for continuously and non-continuously modulated power based thermal system. The figure shows that system with only On-Off control action achieves slightly higher cost than that with continuously modulated power consumption. Note, however, the later may require higher investment cost, which should be considered in practical system design.

3.6.3 Parameter Sensitivities Analysis

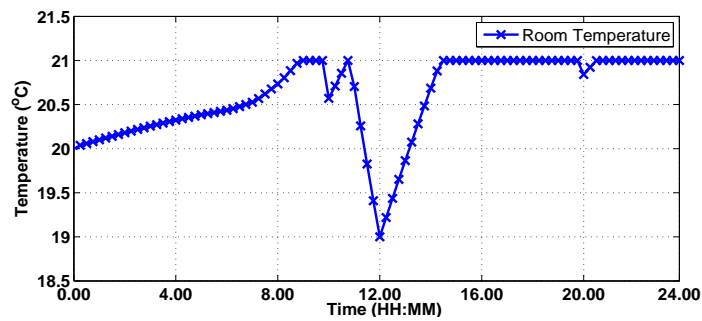
The operations and corresponding costs of the household are influenced by different system parameters including the thermal comfort tolerance, water tank temperature constraint, and solar collector size. We study the variations of energy cost for three different cases, namely conventional HVAC-water heating, conventional HVAC-solar water heating, and solar assisted HVAC-water heating. First, the effect of room temperature tolerance on the energy cost is shown in Figure 3.13(a). This figure shows that increasing the room temperature tolerance result in reduction of electricity cost as expected.

Figure 3.13(b) illustrates the influence of maximum water tank temperature on energy cost. By increasing the maximum temperature of water tank, more energy can be stored, which allow more flexibility in scheduling energy consumption to reduce the electricity cost. It is interesting to notice that the electricity cost decreases before saturating at the minimum value. This implies that for a given solar collector size and auxiliary heater, the amount of captured solar energy and the heater power are limited; hence, the energy stored in tank is also limited. Note also that increasing the maximum water tank temperature can result in better cost-saving, which, however, may affect the equipment life time.

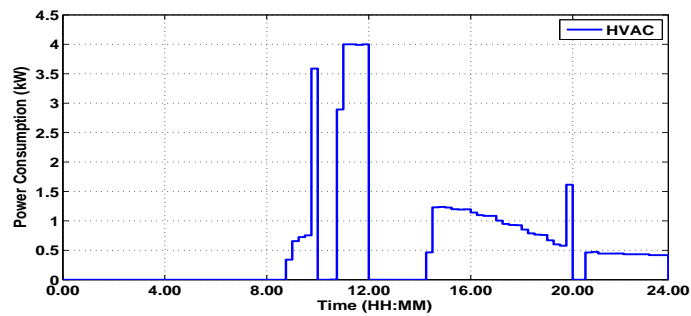
Figure 3.13(c) describes the variation of electricity cost with the solar collector size. For the conventional HVAC and water heating system, solar energy is not utilized so the electricity cost remained unchanged. For systems integrating solar energy, as we increase the solar collector size, which means more solar energy can be captured, the electricity cost reduces before setting down at the minimum value. The minimum value corresponds to the thermal capacity limit of the water tank. From the results in Figures 3.13(a), 3.13(b), and 3.13(c), it can be seen that the solar assisted HVAC-water heating achieves the largest cost saving. This is indeed thanks to the utilization of solar energy and the flexible



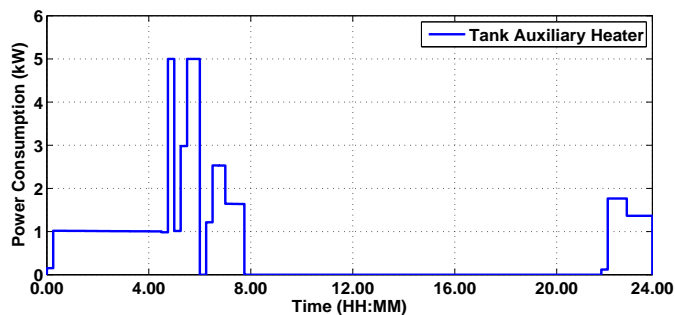
(a) Water tank temperature



(b) Room temperature



(c) Electricity consumption of HVAC

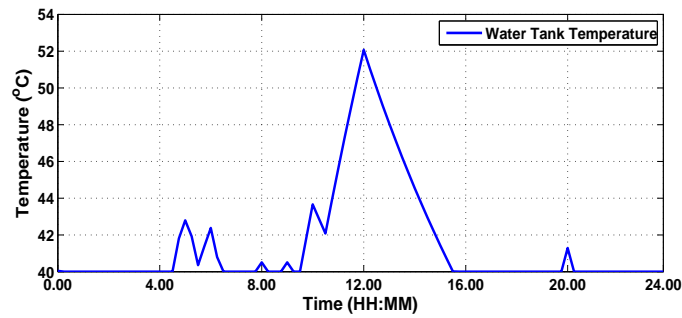


(d) Electricity consumption of auxiliary heater

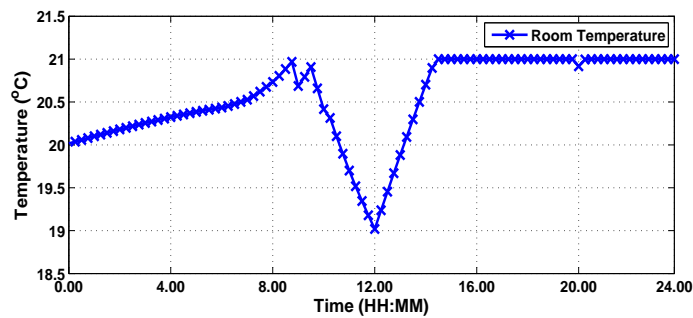
Figure 3.5 – Energy management with solar assisted HVAC-water heating

operation of the water tank, which serves as energy storage facility to support both HVAC and water heating loads.

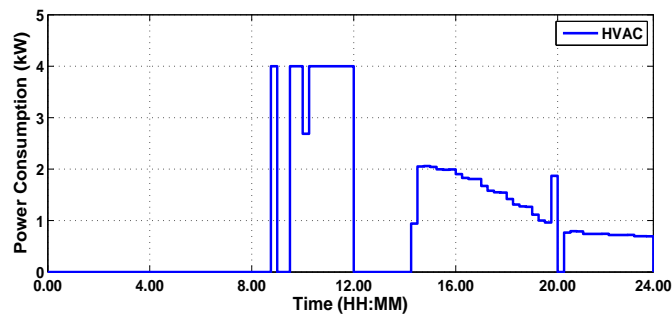
Figures 3.14(a) and 3.14(b) illustrate the impacts of the solar collector size and maximum water tank temperature allowance, which is proportional to the tank thermal capacity, on the energy cost. These figures show that increasing the maximum water tank temperature allowance, which would



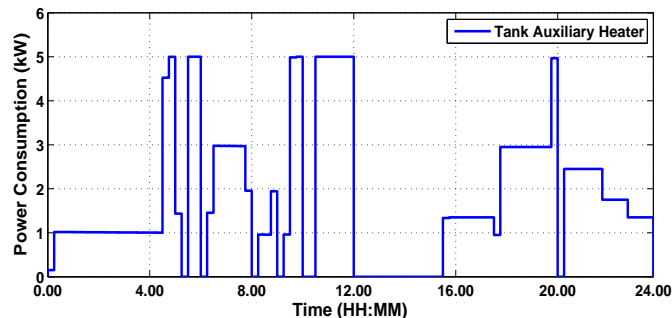
(a) Water tank temperature



(b) Room Temperature



(c) Electricity consumption of HVAC



(d) Electricity consumption of auxiliary heater

Figure 3.6 – Energy management with conventional HVAC and water heating

reduce the life time of the water tank, and increasing solar collector size result in the reduction of energy cost. However, the energy cost converges asymptotically to its minimum values. Thus, above a certain value of solar collector size and maximum temperature allowance, the working cycle of the auxiliary heater reaches its minimum to maintain the water tank temperature when the solar is not available. This minimum value corresponds to the water tank capacity (m^3) and the heat loss. When

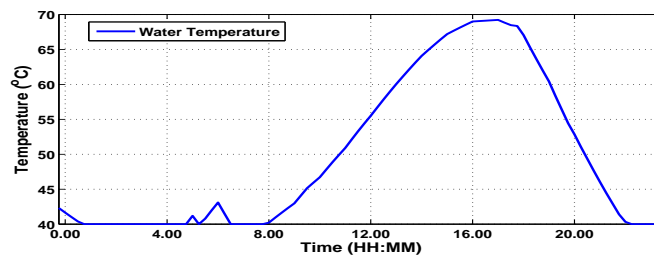
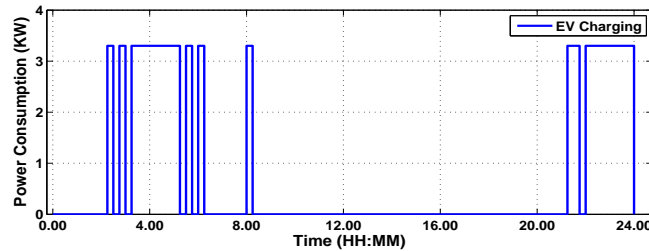
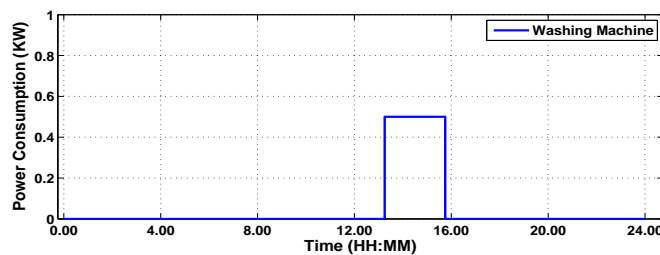


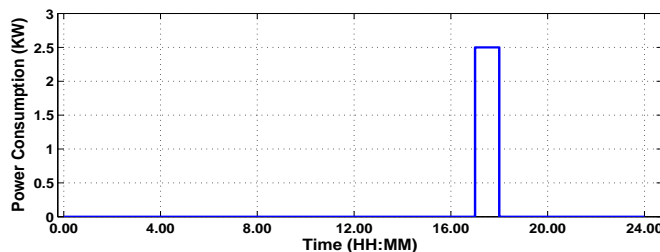
Figure 3.7 – Water tank temperature in conventional HVAC and solar water heating system



(a) Electric vehicle (EV)



(b) Washing machine

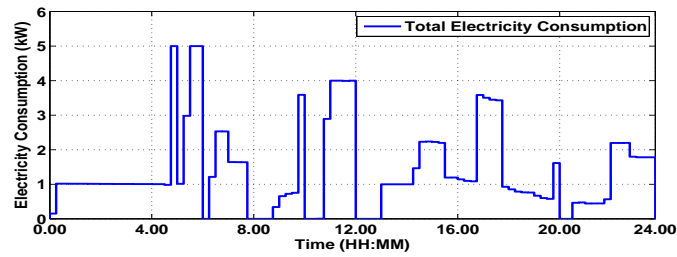


(c) Clothes dryer

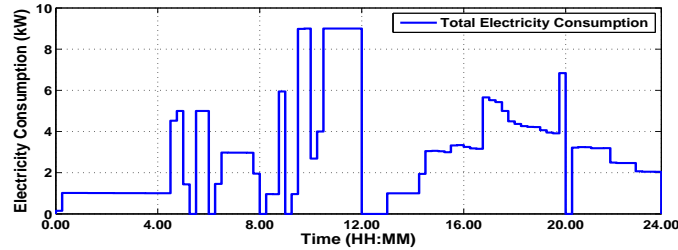
Figure 3.8 – Energy consumptions of other controllable loads

the solar collector size is small, apparently the cost is not effected by the auxiliary heater. This is because the captured solar energy is insufficient to support the heat loss and the thermal load. Hence, the tank operates mainly by relying on its auxiliary heater. The impact of the maximum water tank temperature limit is only significant when the solar collector size is large enough (above $3m^2$) when the amount of solar energy captured is considerable.

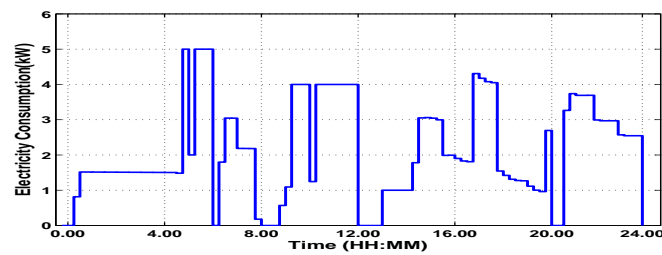
Similarly, Figures 3.15(a) and 3.15(b) show the impacts of other parameters on the energy cost. The presented results demonstrate that relaxing room and water tank temperature constraints as well as increasing solar collector size can reduce the energy cost. Specifically, increasing the room temperature tolerance can reduce the cost significantly but this cost saving would compromise the user comfort. In these figures, we consider the maximum room temperature deviation of $3^{\circ}C$, which corresponds to the worst case of building class C with over 30% level of dissatisfaction according to the ISO 7730 : 2005



(a) Solar assisted HVAC and water heating



(b) Conventional HVAC and water heating



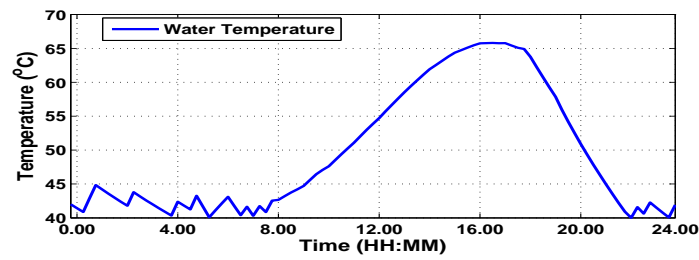
(c) Conventional HVAC and solar water heating

Figure 3.9 – Total energy consumption of scheduled loads.

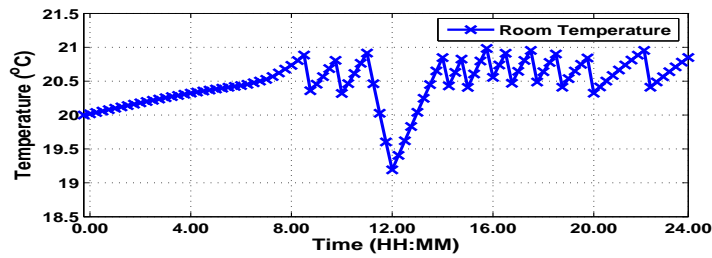
standard. Water temperature also affects user comfort since various daily activities may need different water temperature. However, this requirement can be achieved easily since the water temperature at end-user points can be adjusted automatically by using household water mixing valves. Hence, the water tank temperature can vary in a large range, for example $43 - 70^{\circ}\text{C}$, $43 - 65^{\circ}\text{C}$ [61], due to its high thermal insulation³. However, increasing the water temperature limits as well as solar collector size only helps reduce the cost up to a certain value due to the tank thermal capacity limit.

In general, the amount of solar energy varies over different seasons, which is typically high in the summer and low in the winter. Figure 3.4(a) illustrates the differences in the solar energy between summer and winter seasons. In addition, energy consumption to support heating or cooling demands also depends on the seasons. We compare the electricity costs in different months corresponding to the four seasons, i.e., spring, summer, autumn, and winter in Figure 3.16. In the summer, the strong solar intensity can provide more energy to the system but it may also require large cooling demand. In the winter, the solar irradiance is low while the outdoor temperature can fall below zero, which is also far from the preferred indoor temperature. This implies that the larger HVAC load demand is required to meet users' comfort requirement. Another factor contributing to the larger electricity cost in the winter is the low energy efficiency of the solar system as can be seen in Figure 3.4(e). It can be seen that the

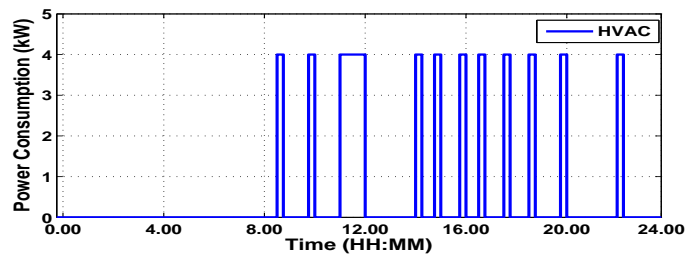
³According to the Apricus solar hot water system owner manual, the large-size Caleffi solar storage tank can reach the maximum temperature 180°C under high pressure. Hot water is mixed with cold water for domestic usage by anti-scald mixing valves.



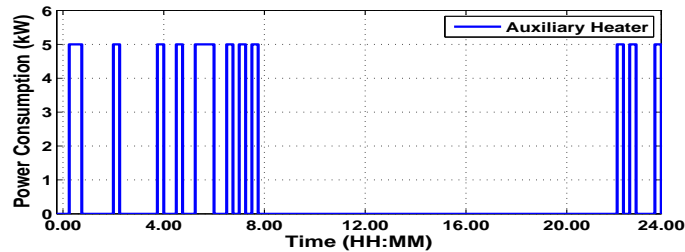
(a) Water tank temperature



(b) Room temperature



(c) Electricity consumption of HVAC



(d) Electricity consumption of auxiliary heater

Figure 3.10 – Energy management with solar assisted HVAC-water heating (Noncontinously Modulated Power)

system with solar assisted thermal load achieve the lowest cost in comparison with the two remaining systems, which confirms the advantages of our proposed design.

The results in Figure 3.16 can be used to calculate the cost saving per year, which can then be used to calculate the Return of Investment on the capital cost and economics of the solar assisted thermal load system for the given investment cost (of solar collector and thermal storage).

3.7 Conclusion and Future Works

We have proposed unified HEM design to minimize the electricity cost that considers users' comfort preference and solar assisted thermal load. The developed mathematical model captures the joint operation of the solar assisted HVAC and hot water system accounting for detailed operations of various

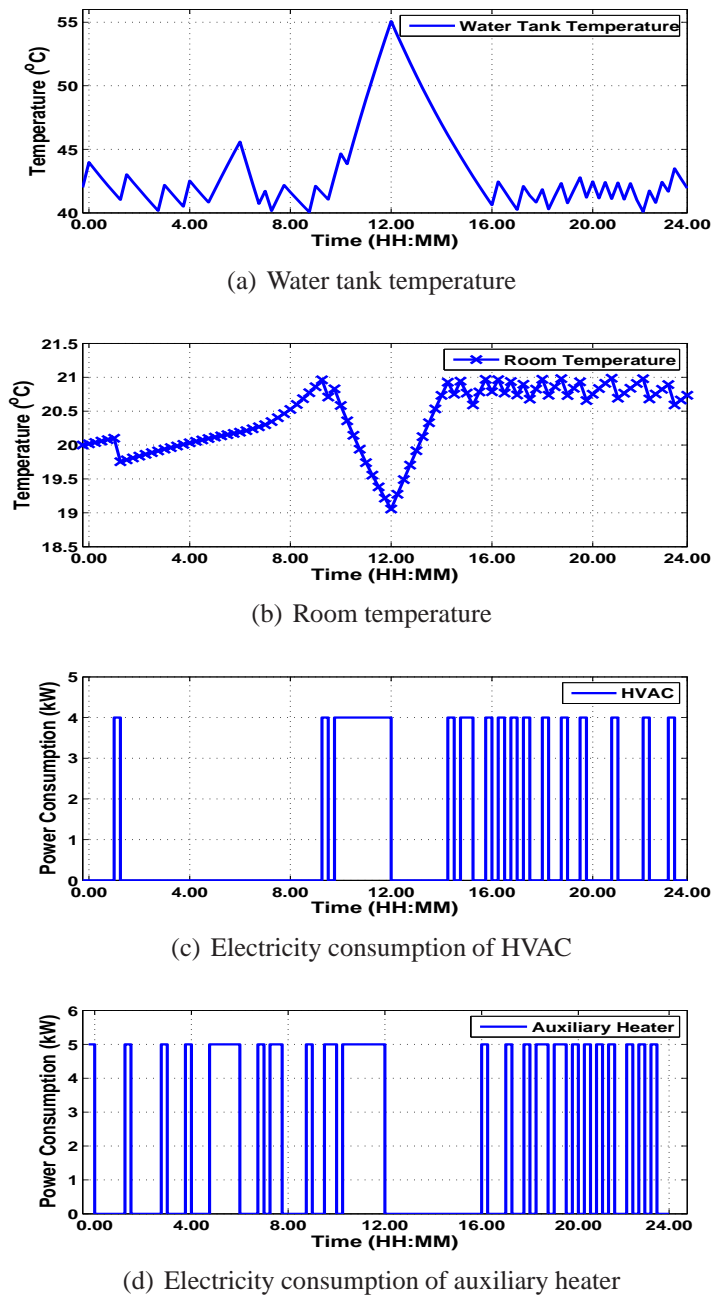


Figure 3.11 – Energy management conventional HVAC and water heating (Noncontinously Modulated Power)

types of home appliances and the uncertainty in the solar energy and electricity price. We have proposed to solve the energy problem by using the rolling two-stage stochastic optimization approach. Finally, numerical results have been presented to show the significant energy saving for the system with solar assisted thermal load in comparison with other conventional systems.

It is worth to mention that the solar thermal tank is an example of short-term solar storage facility since the energy cannot be stored for a long time due to heat loss. Household energy management using long-term solar storage facility such as seasonal thermal storage, which can capture and store solar energy for several months, is an interesting direction for further research. In general, solar energy technologies have been under rapid development and there is a rich area of research, which explores how various solar storage technologies can be exploited for active DR and energy management. This indeed offers many open research problems for our future studies.

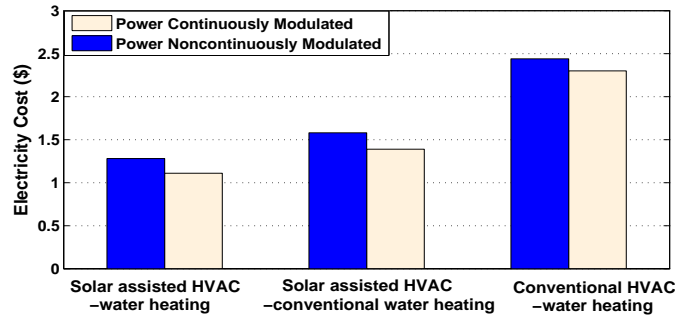
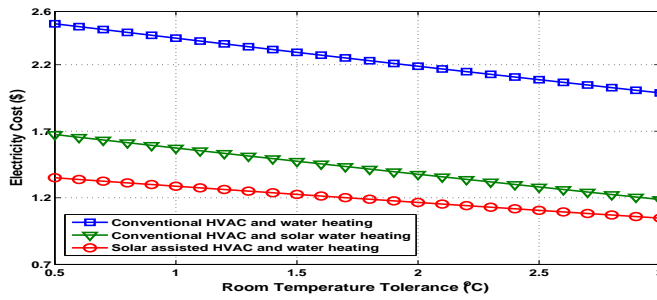
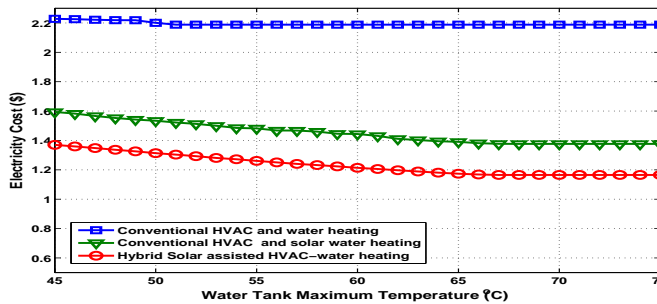


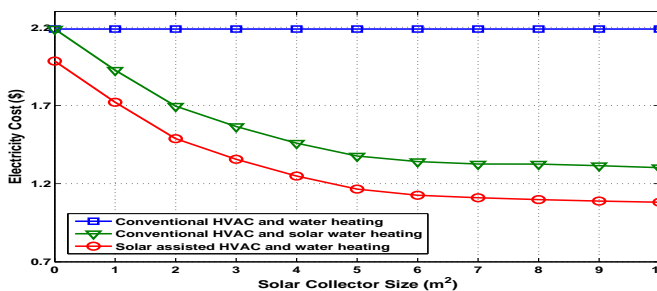
Figure 3.12 – Energy cost comparison between power continuously and noncontinuously modulated thermal system



(a) Effect of room temperature tolerance

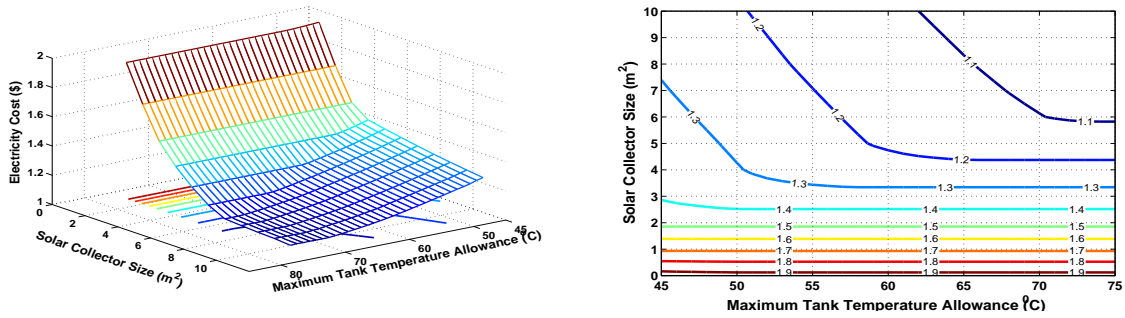


(b) Effect of water tank temperature limit



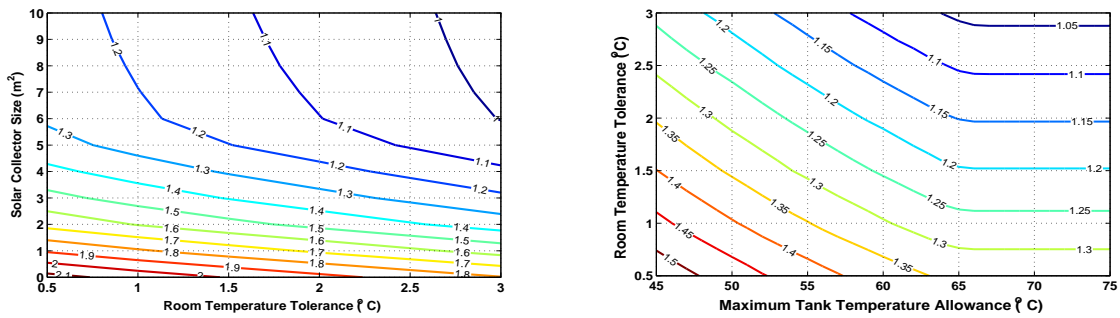
(c) Effect of solar collector size

Figure 3.13 – Effects of system parameters on electricity cost



(a) Electricity cost as a function of solar collector size and tank temperature limit (b) Pareto-optimal constant-cost curves for solar collector size and tank temperature limit

Figure 3.14 – Energy cost versus solar collector size and tank temperature limit



(a) Pareto-optimal constant-cost curves vs solar collector size and room temperature tolerance (b) Pareto-optimal constant-cost curves vs Solar collector size and tank temperature limit

Figure 3.15 – Pareto-optimal constant-cost curves vs solar collector size, room temperature tolerance, tank temperature limit

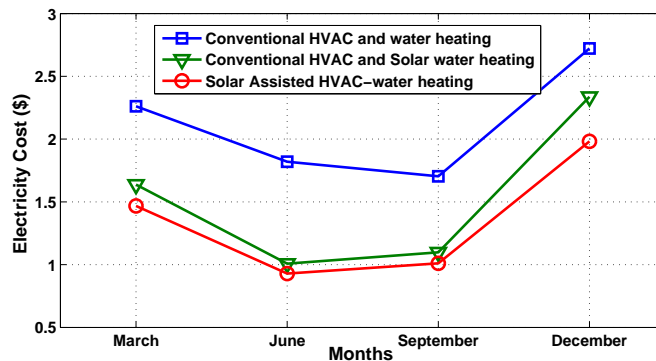


Figure 3.16 – Energy costs in different months

Chapter 4

Dynamic Pricing Design for Demand Response Integration in Distribution Networks

In this chapter, we discuss how to design that price signal to motivate the customers to adjust their energy consumption such that the total system's economics are improved. The content of this chapter was published in IEEE Transactions on Power Systems in the following paper:

Duong Tung Nguyen, Hieu Trung Nguyen, and L. B. Le, "Dynamic Pricing Design for Demand Response Integration in Power Distribution Networks," *IEEE Transactions on Power Systems*, vol. 31, no. 5, pp. 3457-3472, Sept. 2016. doi: 10.1109/TPWRS.2015.2510612

4.1 Abstract

This chapter presents optimal pricing design for demand response (DR) integration in the distribution network. In particular, we study the energy scheduling problem for a load serving entity (LSE) that serves two types of loads, namely inflexible and flexible loads. Inflexible loads are charged under a regular pricing tariff while flexible loads enjoy a dynamic pricing tariff that ensures cost saving for them. Moreover, flexible loads are assumed to be aggregated by several DR aggregators. The interaction between the LSE and its customers is formulated as a bilevel optimization problem where the LSE is the leader and DR aggregators are the followers. The optimal solution of this problem corresponds to the optimal pricing tariff for flexible loads. The key advantage of the proposed model is that it can be readily implemented thanks to its compatibility with existing pricing structures in the retail market. Extensive numerical results show that the proposed approach provides a win-win solution for both the LSE and its customers.

4.2 Introduction

Demand response have been studied at higher system levels such as stochastic security constrained unit commitment of system operators [129], DR aggregator in DR exchange market [10], market clearing optimization [93], ancillary services [24, 27, 94], large energy customers with DR capabilities [15, 42, 44], and DR exchange market operator [13]. In previous chapter, we also discussed a rich literature review on demand response of residential sectors [16–19, 67, 82, 92, 95]. A question arises: how entities at system levels can aggregate or motivate smaller entities at lower levels, i.e., smart homes,

provide demand response services? This question can be addressed by efficient pricing designs, which is the main concentration of this chapter.

This chapter presents a novel pricing design for DR in the distribution network by using the bilevel programming approach. In fact, bilevel programming has been used to study different problems in power systems such as transmission and generation expansion planning [114, 115], generation maintenance [31], market equilibria [117], and strategic bidding for power producers [118], retailers [91], and distribution companies [119]. Recently, there have been some research works on the energy management design for smart grids using bilevel programming. In particular, Asimakopoulou *et al.* [120] formulated a bilevel problem to study the interaction between a large central production unit and an energy service provider (ESP) managing several microgrids (MGs). The central production unit computes and sends an optimal energy price signal to the ESP, then the ESP decides the optimal amount of energy purchased from the central generation unit as well as schedules its power generation and consumption accordingly. However, renewable energy sources (RESs) and the interaction with the main grid (utility grid) were not considered in this chapter. Moreover, the formulated problem in [120] is a nonlinear mixed integer problem which requires nonlinear solvers.

Stochastic bilevel formulation was also proposed in [121] to analyze the interaction between a distribution network operator (DNO) and networked MGs considering the renewable energy generation uncertainty where each entity aims at minimizing its individual operation cost. The information exchanged between the DNO and MGs includes the generation and demand of MGs while the price of energy exchange between the DNO and MGs is fixed. In both [120, 121], the authors studied single-period optimization problems. In contrast, we consider a multi-period optimization problem which is able to capture time-coupling constraints such as raming limit of dispatchable DGs, charging/discharging constraints of batteries, especially the price arbitrage potential in electricity markets.

In this work, the retail price that the LSE charges flexible loads is set dynamically, which depends on actual operation conditions of the system (e.g., renewable energy generation, grid electricity price, status of batteries and DGs). The key optimization variable in this design is the DR price which is defined as the retail price that the LSE charges flexible load customers. Hence, it is expected that the DR capability of flexible loads can be exploited more efficiently to maximize the benefits of both the LSE and energy customers. Table 4.1 describes a few state-of-the-art designs related to DR research, which help demonstrate the novelty of our proposed design compared to the existing literature. In particular, our proposed system is suitable for exploiting DR capabilities of small and medium-sized customers in the distribution network while it does not require significant changes to the existing market structure. Furthermore, the proposed pricing design considers the time-varying nature of the operation conditions of system components under the control of the LSE and the willingness of changing loads from customers so that the optimal DR price will maximize the benefits of both the LSE and its customers. Finally, our pricing design takes some practical aspects of economic design in the distribution network to attract flexible load customers to participate in our scheme, as will be explained in the following.

Different from prevailing time-varying pricing schemes such as time-of-use (TOU) and real-time pricing (RTP) for retail customers [16], which may increase the energy cost for some customers with small flexible loads, the proposed scheme does not have negative impacts on inflexible customers. Our proposed model aims at exploiting flexible loads to achieve efficient operations of a LSE via a smart pricing scheme which ensures cost saving for energy customers of the LSE. Indeed, there can be various uncertainty factors in the system such as renewable energy generation and grid electricity price. However, uncertainty modeling is not considered in this study since our main design objective is to demonstrate the benefits of smart pricing for facilitating DR integration into the distribution network. It is possible to extend our model to integrate system uncertainties, for example, by using stochastic optimization frameworks as considered in [19, 43, 48] and other popular optimization techniques such as robust optimization [15]. Our main contributions can be summarized as follows.

Table 4.1 – Summary of discussed DR methodologies

Paper	Solution approach	Pros	Cons
[43]	Stochastic programming	-Optimal day-ahead bidding design -Risk measure is considered -Economic contracts between MG aggregator vs DR resources	-DR prices are fixed and do not depend on the actual system operation conditions
[10]	MILP	-DR services from small/medium-sized customers including load curtailment, load shifting, utilizing on-site generation, and utilizing energy storage	-DR aggregators interact directly with the wholesale market. -Requires significant changes in the wholesale market
[15]	Rolling robust optimization	-Maximize energy customers' utility (households/small businesses) considering price uncertainty	-Customers are passive, i.e., receiving prices from system operators -Pricing design is not addressed
[42]	Rolling robust optimization	-Maximize energy customers' utilizes considering price and renewable energy uncertainties	-Customers are passive entities [15] -Pricing design between system controller and flexible loads is not considered
[44]	Stochastic bilevel programming	-Optimize the bidding curve of a large customer in the pool market considering uncertainties	-The model targets large customers in pool market -Does not consider DR integration in the distribution networks
[16]	Rolling stochastic programming and robust optimization	-Motivates residential load shifting by real time pricing signal -Detailed modeling of home appliances	-Pricing signal design is not mentioned -Negative impact on less flexible customers -Applicable for small scale residential load
[67, 92]	Multi-objective optimization	-Comfort and lifestyle are addressed	-Pricing signal design is not mentioned
[95]	Distributed optimization	-Maximize customer's utility -Minimize grid fluctuation -Dynamic pricing design for households	-Applicable for small scale residential load
[120]	Bilevel programming	-Pricing design between microgrids and a LSE	-The final problem is a MINLP - Single period optimization -Does not consider renewable energy and main grid
[121]	Stochastic p bilevel programming	-Uncertainties are captured -minimize MG's cost -Applicable for networked MGs	-Pricing design among MGs is not considered
Our study	Bilevel programming	-A novel and practical pricing scheme between a LSE and energy customers -Compatible with existing retail market structures	-Uncertainties are not considered and will be the subject of our future work

- We present a comprehensive decision-making framework for short-term operation of a LSE in the future smart grids where distributed energy resources (DERs), renewable energy, DR, and other important system parameters are considered. We introduce a novel and practical pricing model for DR loads in the distribution network. The proposed model can be readily implemented since it does not require any significant changes to the existing retail market structure.
- We model the interaction between the LSE and its customers as a bilevel programming problem where the LSE is the leader and each DR aggregator is a follower. The nonlinear bilevel mixed-integer program is transformed into a single mixed integer linear program (MILP) using some transformation techniques such as the Karush-Kuhn-Tucker (KKT) optimality conditions and strong duality theorem. The outcome of this problem contains the optimal hourly retail prices for flexible (DR) loads. Extensive numerical results show that the proposed scheme provides a win-win solution for both the LSE and its customers. In particular, it can help improve the optimal profit for the LSE, increase the payoffs for DR aggregators, and decrease the amount of potential involuntary load curtailment as well as renewable energy curtailment.

The remaining of this chapter is organized as follows. In Section 4.3, we present the notations used in this study. In Section 4.4, we describe the proposed system model. Section 4.5 formulates the problem and Section 4.6 presents the solution approach. Numerical results are shown in Section 4.7 followed by conclusion in Section 4.8.

4.3 Notations

Notation	Explanation
Abbreviations	
<i>RES</i>	Renewable energy source
<i>DER</i>	Distributed energy resource
<i>DR</i>	Demand response
<i>DG</i>	Dispatchable distributed generator
<i>LSE</i>	Load serving entity
<i>PCC</i>	Point of common coupling
<i>ILC</i>	Involuntary load curtailment
<i>RESSF</i>	RES scaling factor
Indices	
<i>i</i>	Index of DGs
<i>k</i>	Index of batteries
<i>t</i>	Index of time slots
Parameters	
<i>NT</i>	Number of time slots
<i>NG, NB</i>	Number of DGs/batteries
<i>ND</i>	Number of DR aggregators
<i>d</i>	Index of DR aggregators
<i>m</i>	Index of demand blocks of DR aggregators
<i>NM_d</i>	Number of demand blocks of DR aggregator <i>d</i>
<i>u_{d,m,t}</i>	Marginal utility of demand block <i>m</i> of DR aggregator <i>d</i> at time <i>t</i> (\$/MWh)
<i>U_{d,t}(.)</i>	Utility function of DR aggregator <i>d</i> at time <i>t</i>
<i>E_d</i>	Minimum total energy consumption of DR aggregator <i>d</i> over the scheduling horizon (MWh)

R_d^D	Ramping down limit of DR aggregator d (MW)
R_d^U	Ramping up limit of DR aggregator d (MW)
$P_{d,t}$	Scheduled load for DR aggregator d (MW)
$P_{d,t}^{\min}$	Minimum power consumption of DR aggregator d at time t (MW)
$P_{d,m,t}^{\max}$	Maximum load of demand block m of DR aggregator d at time t (MW)
$P_t^{\text{RES},a}$	Available renewable generation at time t (MW)
$P_t^{\text{g},\max}$	Power limit at point of common coupling (MW)
ΔT	Length of time slot
η_k^c, η_k^d	Charging/discharging efficiency of battery k
P_k^c	Maximum charging power of battery k (MW)
P_k^d	Maximum discharging power of battery k (MW)
E_k	Capacity of battery k (MWh)
D_t	Inflexible load at time t (MW)
c_t^R	Regular retail price at time t (\$/MWh)
c_t^g	Grid electricity price (\$/MWh)
c_t^{RES}	Renewable energy cost at time t (\$/MWh)
c^{LC}	Cost of involuntary load curtailment (\$/MWh)
P_i^{\min}, P_i^{\max}	Minimum/maximum power generation of DG i (MW)
$CU_{i,t}$	Start-up offer cost of DG i (\$)
DT_i, UT_i	Minimum down/up time of DG i (h)
DR_i, UR_i	Ramping-down/up rate limit of DG i (MW)
Variables	
$P_{d,m,t}$	Scheduled load for demand block m of DR aggregator d (MW)
P_t^{RES}	Scheduled renewable generation at time t (MW)
P_t^g	Power exchange with the main grid at time t (MW)
c_t^{DR}	Retail price for DR aggregators (\$/MWh)
D_t^{LC}	Involuntary load curtailment at time t (MW)
$P_{k,t}^c$	Charging power of battery k at time t (MW)
$P_{k,t}^d$	Discharging power of battery k at time t (MW)
$b_{k,t}^c, b_{k,t}^d$	Binary variable, “1” if charging/discharging
$\text{SOC}_{k,t}$	State of charge of battery k
$I_{i,t}$	Commitment status of DG i at time t {0, 1}
$C_i(\cdot)$	Production cost of DG i (\$)
$SU_{i,t}$	Start-up cost of DG i (\$)
$y_{i,t}, z_{i,t}$	Start-up and shutdown indicators {0, 1}
$P_{i,t}$	Power generation of DG i at time t (MW)

4.4 System Model

The energy scheduling problem is considered in a one-day period which is divided into 24 equal time slots. We consider a LSE which can procure energy from various sources including the main grid, DR resources, batteries, and local DERs including RESs (e.g., wind and solar energy) and dispatchable DGs (e.g., diesel generators, microturbines, and fuel cells) to serve its customers. Figure 4.1 illustrates the considered system model.

The LSE itself may possess some DERs and it can also buy energy from privately owned DERs (e.g., from third party companies, households). If the LSE purchases electricity from third party companies or households, it must pay these entities for the procured energy. The price paid to each privately

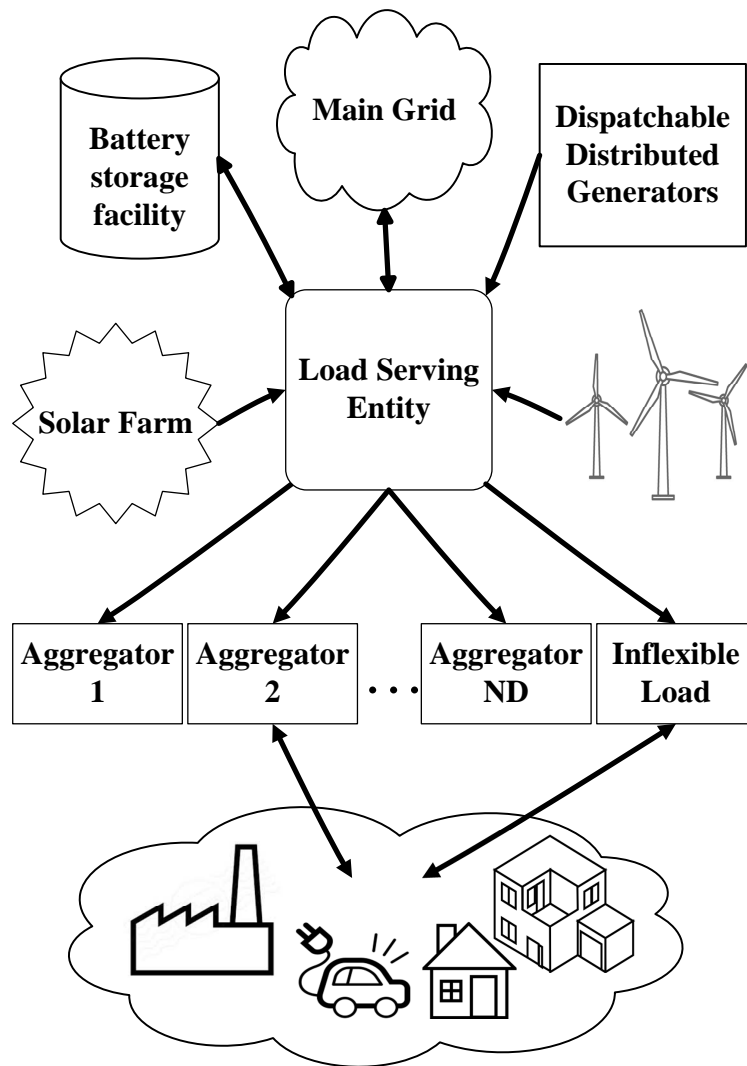


Figure 4.1 – System Model

owned DER can be different, which depends on specific agreements or contracts between the LSE and those sources. If a third party company or a household owns some DERs, the company or the household is responsible for the operation cost of those energy generating sources; however, it can receive the revenue from selling energy to the LSE. On the other hand, if the LSE operates some DERs by itself, the operation cost of those DERs is imposed directly on the LSE.

For simplicity, we assume that the LSE possesses several conventional DGs such as diesel generators and fuel cells, and it does not buy energy from privately owned conventional DGs. Additionally, the LSE does not own any renewable energy sources. We assume that the LSE has *take-or-pay* contracts [42], which are also called Power Purchase Agreements (PPA) in some markets [42, 43], with local wind farms and/or solar farms to buy renewable energy from them. In the *take-or-pay* contracts, the LSE buys all available renewable energy generated from these wind/solar farms at a fixed price which is typically lower than the average price from the main grid [42]. Without loss of generality, we assume that the prices paid to all renewable energy sources are the same (c_t^{RES})¹. Finally, the LSE may own some battery storage units.

¹The LSE must pay for all available renewable energy $P_t^{\text{RES},a}$ (i.e., it does not just pay for the amount of scheduled renewable energy P_t^{RES}).

System loads are assumed to belong to one of the two categories, namely flexible and inflexible loads. Inflexible loads or critical loads are those that the LSE has to serve. If the LSE cannot fully serve the inflexible loads, a portion of the inflexible loads has to be shed, which is called involuntary load curtailment (ILC). A very high penalty cost (c^{LC}) is imposed on the LSE for ILC since the main goal of the LSE is to guarantee electricity supply to its customers [43]. Inflexible loads are charged under the regular retail price (c_t^{R}). In contrast, flexible loads are assumed to be aggregated by one or several DR aggregators which enjoy a dynamic pricing tariff that should be designed to bring advantages to the DR aggregators. One practical strategy to encourage DR aggregators participating in our proposed operation model is to ensure cost saving for them.

In practice, a flexible load customer might be hesitant to participate in a real-time pricing scheme since electricity prices in this scheme may be greater than the regular retail price for several hours of a day. The loads of a flexible load customer include critical load which should not be shed or shifted and flexible load that can be shed or shifted. Therefore, if the flexible load customer has a large portion of critical load during high price hours, we might not be able to guarantee cost saving for the customer compared to the case where the customer is charged at the fixed retail price. Hence, one of the most practical approaches that the LSE may use to attract flexible load customers to participate in the proposed pricing model is to offer DR price (i.e., the retail price that the LSE charges flexible loads or DR aggregators), which is always lower or equal to the retail price in each hour. In the worst case when the DR price is equal to the regular retail price, the cost imposed on participating entities is the same with the one when they are charged under the regular retail price.

The proposed system model can be applied to the practical setting where a LSE provides energy services to a certain geographical area. In particular, there can be several DR aggregators in the area which aggregate flexible loads from energy users and each DR aggregator serves a given set of flexible loads. A DR aggregator can be a company which is interested in the DR market (e.g., EnerNOC).² This design allows us to prevent individual small flexible energy customers from interacting directly with the wholesale market, which would complicate the operation of the wholesale market. Moreover, our design ensures that the number of participating parties in our model as well as the number of variables in our formulated optimization problem be reduced significantly. In addition, we assume that DR aggregators have DR contracts with flexible load customers so that these customers can declare the characteristics of their loads (e.g., utility function [14, 42, 44–46] or discomfort function in the case of load reduction or load shifting [10, 43, 44]) to the DR aggregators. Based on the load information provided by their customers, each DR aggregator can construct a suitable aggregated utility function, as described in Section 4.5.9, which is then sent to the LSE. Detailed study on how DR aggregators interact with their customers and construct their aggregated utility function is out of scope of this study.

The underlying optimization problem is formulated as a bilevel program where the LSE is the leader and each DR aggregator is a follower. The outcome of this problem contains optimal dynamic DR price series (c_t^{DR}) over the scheduling horizon. Additionally, the outputs of the proposed problem include the hourly energy trading between the LSE and the main grid (P_t^{g}), the scheduled generation of local RESs (P_t^{RES}) and local DGs ($P_{i,t}$), charging/discharging power of batteries ($P_{k,t}^{\text{c}}, P_{k,t}^{\text{d}}$), amount of ILC (D_t^{LC}), and hourly energy consumption of DR aggregators ($P_{d,t}$).

² <http://www.enernoc.com/>

4.5 Problem Formulation

4.5.1 Objective Function of the LSE

We are interested in maximizing the profit of the LSE which is given as follows:

$$Profit = Rev - Cost \quad (4.1)$$

where Rev is the retail revenue obtained by serving inflexible loads (at price c_t^R) and flexible loads (at price c_t^{DR}), i.e.,

$$Rev = \sum_{t=1}^{NT} \Delta T \left[c_t^R (D_t - D_t^{LC}) + \sum_{d=1}^{ND} c_t^{DR} P_{d,t} \right] \quad (4.2)$$

where $D_t - D_t^{LC}$ is the amount of inflexible load that the LSE serves at time t .

The operating cost of the LSE includes the cost of buying/selling electricity from/to the main grid $c_t^g P_t^g$, renewable energy procurement cost $c_t^{RES} P_t^{RES,a}$, operation costs of DGs including start-up cost and dispatch cost $\sum_{i=1}^{NG} (SU_{i,t} + C_i(P_{i,t}))$ [43], and the penalty cost for involuntary load curtailment $c^{LC} D_t^{LC}$. For simplicity, the battery operation cost is not considered in this study. Hence, we have

$$Cost = \sum_{t=1}^{NT} \Delta T \left[c_t^g P_t^g + c_t^{RES} P_t^{RES,a} + \sum_{i=1}^{NG} (SU_{i,t} + C_i(P_{i,t})) + c^{LC} D_t^{LC} \right]. \quad (4.3)$$

From these expressions, the design objective becomes

$$\begin{aligned} & \max_{c_t^{DR}, P_t^g, P_{i,t}, P_t^{RES}, D_t^{LC}, P_{k,t}^c, P_{k,t}^d, P_{d,t}} \sum_{t=1}^{NT} \Delta T \left[c_t^R (D_t - D_t^{LC}) + \sum_{d=1}^{ND} c_t^{DR} P_{d,t} \right] \\ & - \sum_{t=1}^{NT} \Delta T \left[P_t^g c_t^g + c_t^{RES} P_t^{RES,a} + \sum_{i=1}^{NG} (SU_{i,t} + C_i(P_{i,t})) + c^{LC} D_t^{LC} \right] \end{aligned} \quad (4.4)$$

subject to the following constraints.

4.5.2 Power Balance Constraints

At any time slot t , the total power generation including power exchanged with the main grid P_t^g , power generated by DGs $\sum_{i=1}^{NG} P_{i,t}$, power generated by renewable energy resources P_t^{RES} , power dispatched of batteries $\sum_{k=1}^{NB} (P_{k,t}^d - P_{k,t}^c)$, and load curtailment D_t^{LC} must be equal to the total power consumption of nonflexible load D_t and flexible load $\sum_{d=1}^{ND} P_{d,t}$. This condition is described by the following constraint:

$$P_t^g + \sum_{i=1}^{NG} P_{i,t} + P_t^{RES} + \sum_{k=1}^{NB} (P_{k,t}^d - P_{k,t}^c) + D_t^{LC} = D_t + \sum_{d=1}^{ND} P_{d,t}, \quad \forall t. \quad (4.5)$$

4.5.3 Power Trading with Main Grid

The power exchanged with the main grid is constrained by $P_t^{\text{g,max}}$, which is described as follows:

$$-P_t^{\text{g,max}} \leq P_t^{\text{g}} \leq P_t^{\text{g,max}}, \quad \forall t. \quad (4.6)$$

4.5.4 Renewable Energy Constraints

The scheduled renewable energy generation must be smaller or equal to the available renewable energy generation. Hence,

$$0 \leq P_t^{\text{RES}} \leq P_t^{\text{RES,a}}, \quad \forall t. \quad (4.7)$$

4.5.5 Involuntary Load Curtailment

The amount of involuntary load curtailment is always smaller or equal to the total inflexible load, i.e., we have

$$0 \leq D_t^{\text{LC}} \leq D_t, \quad \forall t. \quad (4.8)$$

4.5.6 DR Price

As explained in Section 4.4, the DR price is set to be smaller or equal to the regular retail price at every time slot t to attract the participation of DR aggregators in the proposed DR pricing scheme, i.e., we have

$$c_t^{\text{DR}} \leq c_t^{\text{R}}, \quad \forall t. \quad (4.9)$$

4.5.7 Operation Constraints of DGs

In this study, a widely used piecewise linear cost function [31, 43, 130] is employed to model approximately the production cost $C_i(\cdot)$ of DG i where n and N_i are the segment indices and number of segments in the cost function of DG i , respectively. Parameter $\lambda_{i,n}$ (\$/MWh) denotes the marginal cost associated with segment n in the cost function of DG i . The cost of operating DG i at its minimum power generation [130] is a_i . Finally, we define $P_{i,n}$ (MW) as the upper limit of power generation from the n -th segment in the cost function of DG i and $P_{i,n,t}$ is scheduled power generation of DG i from the n -th segment at time t . We have [31, 43, 130]

$$C_i(P_{i,t}) = a_i I_{i,t} + \Delta T \sum_{n=1}^{N_i} \lambda_{i,n} P_{i,n,t} \quad (4.10)$$

$$0 \leq P_{i,n,t} \leq P_{i,n}; \quad P_{i,t} = P_i^{\text{min}} I_{i,t} + \sum_{n=1}^{N_i} P_{i,n,t} \quad (4.11)$$

where constraints (4.10)–(4.11) describe the generation cost and power output of DG i . Additionally, the following constraints are imposed on the operation of DG i [31]:

$$P_i^{\min} I_{i,t} \leq P_{i,t} \leq P_i^{\max} I_{i,t}; \quad SU_{i,t} = CU_i y_{i,t} \quad (4.12)$$

$$P_{i,t} - P_{i,t-1} \leq UR_i \quad (4.13)$$

$$P_{i,t-1} - P_{i,t} \leq DR_i \quad (4.14)$$

$$\sum_{h=t}^{t+UT_i-1} I_{i,h} \geq UT_i y_{i,t} \quad (4.15)$$

$$\sum_{h=t}^{t+DT_i-1} (1 - I_{i,h}) \geq DT_i z_{i,t} \quad (4.16)$$

$$y_{i,t} - z_{i,t} = I_{i,t} - I_{i,t-1}; \quad y_{i,t} + z_{i,t} \leq 1. \quad (4.17)$$

Power generation limits and start-up cost are described in (4.12). The remaining constraints capture ramping up/down limits, limits on minimum ON/OFF duration, and relationship between binary variables [31, 43, 130].

4.5.8 Battery Constraints

The following constraints are imposed on the operation of battery k for $\forall t$ [131]:

$$0 \leq P_{k,t}^c \leq b_{k,t}^c P_k^c; \quad 0 \leq P_{k,t}^d \leq b_{k,t}^d P_k^d \quad (4.18)$$

$$SOC_k^{\min} \leq SOC_{k,t} \leq SOC_k^{\max} \quad (4.19)$$

$$SOC_{k,t+1} = SOC_{k,t} + \Delta T \left(\frac{\eta_k^c P_{k,t}^c}{E_k} - \frac{P_{k,t}^d}{\eta_k^d E_k} \right) \quad (4.20)$$

$$b_{k,t}^c + b_{k,t}^d \leq 1; \quad b_{k,t}^c, b_{k,t}^d \in \{0, 1\}. \quad (4.21)$$

Limits on the charging and discharging power of battery k are presented in (4.18). Constraint (4.19) imposes limits on State of Charge (SOC) of battery k . Note that SOC_k^{\max} and SOC_k^{\min} are the maximum SOC and minimum SOC of battery k , respectively. Battery energy dynamics model is given in (4.20). Finally, conditions on binary variables representing battery charging/discharging status are captured in (4.21) so that battery k cannot be charged and discharged simultaneously.

4.5.9 Follower Problems

In addition to the above operation constraints, the optimization of the leader problem is subject to ND follower problems each of which corresponds to an optimization problem of DR aggregator d . The lower-level problem for DR aggregator d is presented in the following. First, we define the payoff function for each DR aggregator as the utility (benefit) minus the cost due to energy consumption over the scheduling horizon. We assume that each DR aggregator wishes to maximize its payoff function as follows:

$$\max_{P_{d,t}} \sum_{t=1}^{NT} \left[U_{d,t}(P_{d,t}) - \Delta T c_t^{\text{DR}} P_{d,t} \right]. \quad (4.22)$$

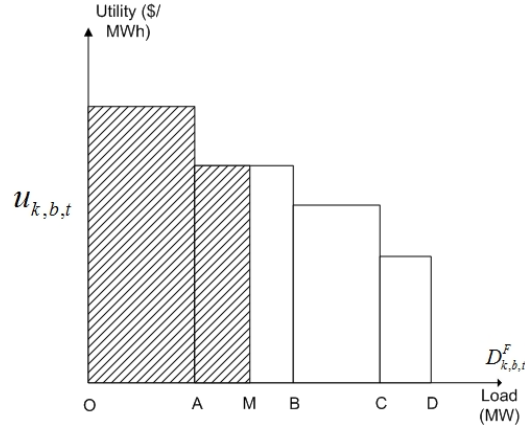


Figure 4.2 – DR utility function

In this study, the utility functions of DR aggregators are modeled by multi-block utility functions³, which are commonly used in the literature [42, 44–46]. The marginal utility of a demand block decreases as the index of demand blocks increases. Figure 4.2 shows the utility function of DR aggregator d at time t . As we can observe, this function has four demand blocks (i.e., $NM_d = 4$). The values at point A, C, D, E are $P_{d,1,t}^{\max}$, $P_{d,1,t}^{\max} + P_{d,2,t}^{\max}$, $P_{d,1,t}^{\max} + P_{d,2,t}^{\max} + P_{d,3,t}^{\max}$, and $P_{d,1,t}^{\max} + P_{d,2,t}^{\max} + P_{d,3,t}^{\max} + P_{d,4,t}^{\max}$, respectively. If the scheduled demand of DR aggregator d at time t is OB (i.e., $P_{d,t} = OB$), then the utility value for load consumption of aggregator d at time t is equal to the shaded area. Generally, we have

$$U_{d,t}(P_{d,t}) = \Delta T \sum_{m=1}^{NM_d} u_{d,m,t} P_{d,m,t} \quad (4.23)$$

$$P_{d,t} = \sum_{m=1}^{NM_d} P_{d,m,t}. \quad (4.24)$$

Therefore, the follower (lower) optimization problem of DR aggregator d can be written as follows:

$$\min_{P_{d,t}, P_{d,t,m}} \Delta T \sum_{t=1}^{NT} [c_t^{\text{DR}} P_{d,t} - \sum_{m=1}^{NM_d} u_{d,m,t} P_{d,m,t}] \quad (4.25)$$

³In the literature, there exist other models for flexible loads. For example, price elasticity of the load model is considered in [51–53]. However, we choose the multi-block utility function model since it is suitable for the proposed solution approach and current practice in the electricity market.

subject to

$$P_{d,t} = \sum_{m=1}^{NM_d} P_{d,m,t}, \quad \forall t \quad (\lambda_{d,t}) \quad (4.26)$$

$$P_{d,m,t} \leq P_{d,m,t}^{\max}, \quad \forall m, t \quad (\mu_{d,m,t}^1) \quad (4.27)$$

$$P_{d,m,t} \geq 0, \quad \forall m, t \quad (\mu_{d,m,t}^2) \quad (4.28)$$

$$\Delta T \sum_{t=1}^{NT} P_{d,t} \geq E_d, \quad (\mu_d^3) \quad (4.29)$$

$$P_{d,t} \geq P_{d,t}^{\min}, \quad \forall t \quad (\mu_{d,t}^4) \quad (4.30)$$

$$P_{d,t} - P_{d,t-1} \leq R_d^U, \quad \forall t \quad (\mu_{d,t}^5) \quad (4.31)$$

$$P_{d,t-1} - P_{d,t} \leq R_d^D, \quad \forall t \quad (\mu_{d,t}^6). \quad (4.32)$$

The power constraints for each demand block m for the flexible load of DR aggregator d are captured in (4.27)-(4.28). Constraint (4.29) describes the minimum energy consumption for the load of DR aggregator d over the scheduling horizon. The constraint on the minimum power consumption for DR aggregator d at each time slot t is expressed in (4.30) while maximum power consumption constraints for DR aggregator d are described in (4.26)-(4.27). Finally, (4.31)-(4.32) impose the ramping up and ramping down constraints for the load of DR aggregator d where $P_{d,0}$ is the initial load of DR aggregator d . In addition, $\lambda_{d,t}$, $\mu_{d,m,t}^1$, $\mu_{d,m,t}^2$, μ_d^3 , $\mu_{d,t}^4$, $\mu_{d,t}^5$, and $\mu_{d,t}^6$ are the Lagrange multipliers which associated with these constraints.

4.5.10 Extension with Power Flow Constraints

For ease of exposition, in the problem formulation described above, we have implicitly assumed that all entities are located at one bus, which is valid for a small-scale system (e.g., a LSE manages loads in a small town or a village). However, a general distribution network model can also be integrated into our optimization framework. The power flow constraints are described as follows. We define p, q as the indices of two buses, $B_{p,q}$ is the susceptance of line p - q , $F_{p,q}^{\max}$ is the transmission capacity of line p - q , and $\theta_{p,t}$ is the voltage angle of bus p at time t . Additionally, we define A_p as the set of buses connected to bus p , B_p as the set of batteries located at bus p , C_p is the set of DGs located at bus p , and D_p as the set of DR aggregators located at bus p . Moreover, $D_{p,t}$ is the total inflexible load at bus p and time t while $D_{p,t}^{\text{LC}}$ is the amount of involuntary load curtailment at bus p and time t ($D_{p,t}^{\text{LC}} \leq D_{p,t}, \forall p, t$). In addition, $P_{p,t}^{\text{RES}}$ is the amount of scheduled renewable energy generation at bus p and time t ; and $P_{p,t}^{\text{g}}$ is the amount of energy exchange with the main grid at bus p and time t . Note that $P_{p,t}^{\text{g}} = 0, \forall t$ if bus p is not connected to the main grid.

For simplicity, reactive power is not considered in this study and the lossless DC power flow model is used to model the distribution network [78], which imposes the following constraints:

$$P_{p,t}^{\text{g}} + \sum_{i \in C_p} P_{i,t} + P_t^{\text{RES}} + \sum_{k \in B_p} (P_{k,t}^{\text{d}} - P_{k,t}^{\text{c}}) + D_{p,t}^{\text{LC}} - D_{p,t} + \sum_{d \in D_p} P_{d,t} = \sum_{q \in A_p} B_{p,q} (\theta_{p,t} - \theta_{q,t}), \quad \forall p, t. \quad (4.33)$$

$$-F_{p,q}^{\max} \leq B_{p,q} (\theta_{p,t} - \theta_{q,t}) \leq F_{p,q}^{\max}, \quad \forall t, p, q \quad (4.34)$$

where constraint (4.33) enforces the power balance at each bus in the system while constraint (4.34) presents power flow limits of each line. All operation constraints of the LSE as well as the follower

problem remain the same as in Section 4.5. However, the power balance constraint (4.5) is replaced by the set of power flow constraints presented above.

We are aware of the fact that the lossless DC power flow model may not be the most suitable for the distribution network. Integration of a full power flow model and reactive power management into the proposed optimization framework is a subject of our future work. In particular, the adoption of DC power flow model enables the tractability of solving the underlying bilevel optimization problem. This approach is also used in [78] where the DC power flow is used in the distribution company's optimization model. To accurately capture reactive power flows and voltage stability's constraints, a full model of AC power flow can be adopted, which results in a MINLP. In this case, various heuristic evolutionary algorithms such as genetic algorithm or particle swarm can be used, which is the subject of our future work. A recent linearized power flow model for distribution network is proposed in [11] where the accuracy of the approximation model is well justified. Consideration of this linearized model, which results in the MILP, will also be the subject of our future research.

4.6 Solution Approach

We propose to convert the optimization problem of the LSE into an equivalent MILP problem. Note that optimization variables in each follower problem include $P_{d,m,t}$ and $P_{d,t}$. Moreover, the variable c_t^{DR} in the upper-level (leader) problem is a parameter in each lower-level (follower) problem. Also, for a given vector c_t^{DR} , each follower problem is simply a linear program. Therefore, we can replace each follower problem with its corresponding KKT optimality conditions [91]. Toward this end, the Lagrangian of each lower-level problem (4.25)-(4.32) for DR aggregator d can be expressed as

$$\begin{aligned}
L_d = & \Delta T \sum_{t=1}^{NT} [c_t^{\text{DR}} P_{d,t} - \sum_{m=1}^{NM_d} u_{d,m,t} P_{d,m,t}] + \sum_{t=1}^{NT} \lambda_{d,t} (P_{d,t} - \sum_{m=1}^{NM_d} P_{d,m,t}) \\
& + \sum_{t=1}^{NT} \sum_{m=1}^{NM_d} \mu_{d,m,t}^1 (P_{d,m,t} - P_{d,m,t}^{\max}) - \sum_{t=1}^{NT} \sum_{m=1}^{NM_d} \mu_{d,m,t}^2 P_{d,m,t} - \mu_d^3 (\Delta T \sum_{t=1}^{NT} P_{d,t} - E_d) \\
& - \sum_{t=1}^{NT} \mu_{d,t}^4 (P_{d,t} - P_{d,t}^{\min}) + \sum_{t=1}^{NT} \mu_{d,t}^5 (P_{d,t} - P_{d,t-1} - R_d^{\text{U}}) + \sum_{t=1}^{NT} \mu_{d,t}^6 (P_{d,t-1} - P_{d,t} - R_d^{\text{D}}) \quad (4.35)
\end{aligned}$$

where $\lambda_{d,t}$, $\mu_{d,m,t}^1$, $\mu_{d,m,t}^2$, μ_d^3 , $\mu_{d,t}^4$, $\mu_{d,t}^5$, and $\mu_{d,t}^6$ denote the Lagrange multipliers associated with the constraints in the corresponding follower problem. The KKT necessary optimality conditions of the lower-level problem of DR aggregator d include the primal feasibility constraint (4.26) and the following

constraints

$$\begin{aligned} \frac{\delta L_d}{P_{d,t}} &= \Delta T c_t^{\text{DR}} + \lambda_{d,t} - \Delta T \mu_d^3 - \mu_{d,t}^4 + \mu_{d,t}^5 - \mu_{d,t+1}^5 \\ &+ \mu_{d,t+1}^6 - \mu_{d,t}^6 = 0, \quad \forall t < NT \end{aligned} \quad (4.36)$$

$$\begin{aligned} \frac{\delta L_d}{P_{d,t}} &= \Delta T c_t^{\text{DR}} + \lambda_{d,t} - \Delta T \mu_d^3 - \mu_{d,t}^4 + \mu_{d,t}^5 \\ &- \mu_{d,t}^6 = 0, \quad \text{if } t = NT \end{aligned} \quad (4.37)$$

$$\begin{aligned} \frac{\delta L_d}{P_{d,m,t}} &= -\Delta T u_{d,m,t} - \lambda_{d,t} + \mu_{d,m,t}^1 - \mu_{d,m,t}^2 = 0 \\ &, \forall m, t \end{aligned} \quad (4.38)$$

$$0 \leq \mu_{d,m,t}^1 \perp P_{d,m,t}^{\max} - P_{d,m,t} \geq 0, \quad \forall m, t \quad (4.39)$$

$$0 \leq \mu_{d,m,t}^2 \perp P_{d,m,t} \geq 0, \quad \forall m, t \quad (4.40)$$

$$0 \leq \mu_d^3 \perp \Delta T \sum_{t=1}^{NT} P_{d,t} - E_d \geq 0, \quad (4.41)$$

$$0 \leq \mu_{d,t}^4 \perp P_{d,t} - P_{d,t}^{\min} \geq 0, \quad \forall t \quad (4.42)$$

$$0 \leq \mu_{d,t}^5 \perp R_d^{\text{U}} - P_{d,t} + P_{d,t-1} \geq 0, \quad \forall t \quad (4.43)$$

$$0 \leq \mu_{d,t}^6 \perp R_d^{\text{D}} - P_{d,t-1} + P_{d,t} \geq 0, \quad \forall t. \quad (4.44)$$

Complementarity conditions associated with the inequality constraints (4.27)-(4.32) are given in (4.39)-(4.44). Note that a complementarity condition $0 \leq \mu \perp P \geq 0$ (i.e., $P \geq 0$; $\mu^T P = 0$; $\mu \geq 0$) can be transformed into the following set of mixed-integer constraints based on the Fortuny-Amat transformation [44, 47, 115]:

$$\mu \geq 0; P \geq 0 \quad (4.45)$$

$$\mu \leq (1 - u)M \quad (4.46)$$

$$P \leq uM \quad (4.47)$$

$$u \in \{0, 1\} \quad (4.48)$$

where M is a sufficiently large constant. Note that the value of M will affect the effectiveness of the proposed solution. In particular, we should select M appropriately to avoid numerical ill-conditioning [132]. Several guideline on how to select a suitable value of M can be found in [47, 132, 133]. We need to select a sufficiently large value of M so as not to make the optimal solution outside the feasible space of (4.46) [132]. On the other hand, a too large value of M may result in computational inefficiencies for the solution of the resulting mixed-integer optimization problems [132]. A general principle to find a reasonable constant M is based on the *trial and error* approach [133]. However, in some cases, a suitable value of M can be found based on specific characteristics of the studied problems [133].

Therefore, the set of constraints (4.39)-(4.44) can be rewritten as follows:

$$\mu_{d,m,t}^1 \geq 0; \quad P_{d,m,t}^{\max} - P_{d,m,t} \geq 0 \quad (4.49)$$

$$\mu_{d,m,t}^1 \leq (1 - v_{d,m,t}^1)M^1; \quad P_{d,m,t}^{\max} - P_{d,m,t} \leq v_{d,m,t}^1 M^1 \quad (4.50)$$

$$\mu_{d,m,t}^2 \geq 0; \quad P_{d,m,t} \geq 0 \quad (4.51)$$

$$\mu_{d,m,t}^2 \leq (1 - v_{d,m,t}^2)M^2; \quad P_{d,m,t} \leq v_{d,m,t}^2 M^2 \quad (4.52)$$

$$\mu_d^3 \geq 0; \quad \sum_{t=1}^{NT} P_{d,t} - E_d \geq 0 \quad (4.53)$$

$$\mu_d^3 \leq (1 - v_d^3)M^3; \quad \Delta T \sum_{t=1}^{NT} P_{d,t} - E_d \leq v_d^3 M^3 \quad (4.54)$$

$$\mu_{d,t}^4 \geq 0; \quad P_{d,t} - P_{d,t}^{\min} \geq 0 \quad (4.55)$$

$$\mu_{d,t}^4 \leq (1 - v_{d,t}^4)M^4; \quad P_{d,t} - P_{d,t}^{\min} \leq v_{d,t}^4 M^4 \quad (4.56)$$

$$\mu_{d,t}^5 \geq 0; \quad R_d^U - P_{d,t} + P_{d,t-1} \geq 0 \quad (4.57)$$

$$\mu_{d,t}^5 \leq (1 - v_{d,t}^5)M^5; \quad R_d^U - P_{d,t} + P_{d,t-1} \leq v_{d,t}^5 M^5 \quad (4.58)$$

$$\mu_{d,t}^6 \geq 0; \quad R_d^U - P_{d,t} + P_{d,t-1} \geq 0 \quad (4.59)$$

$$\mu_{d,t}^6 \leq (1 - v_{d,t}^6)M^6; \quad R_d^D - P_{d,t-1} + P_{d,t} \leq v_{d,t}^6 M^6 \quad (4.60)$$

$$v_{d,m,t}^1, v_{d,m,t}^2, v_d^3, v_{d,t}^4, v_{d,t}^5, v_{d,t}^6 \in \{0, 1\} \quad (4.61)$$

where M^1, M^2, M^3, M^4, M^5 , and M^6 are sufficiently large numbers. After the follower problems are replaced by the sets of mixed-integer linear constraints as presented above, the upper-level optimization problem is still a mixed-integer nonlinear (MINLP) problem since the term $\Delta T \sum_{t=1}^{NT} \sum_{d=1}^{ND} c_t^{\text{DR}} P_{d,t}$ in the objective function (4.4), which is the sum of several bilinear product of variables $c_t^{\text{DR}} P_{d,t}$, is nonlinear. However, each term $\Delta T \sum_{t=1}^{NT} c_t^{\text{DR}} P_{d,t}$ of the sum can be equivalently replaced by linear expressions by using the strong duality theorem [44, 91]. Please refer [134] for more details. The strong duality theorem renders

$$\begin{aligned} \Delta T \sum_{t=1}^{NT} c_t^{\text{DR}} P_{d,t} &= \Delta T \sum_{t=1}^{NT} \sum_{m=1}^{NM_d} u_{d,m,t} P_{d,m,t} \\ &+ \sum_{t=1}^{NT} \sum_{m=1}^{NM_d} [-\mu_{d,m,t}^1 P_{d,m,t}^{\max} + \mu_{d,t}^4 P_{d,t}^{\min}] + \mu_d^3 E_d \\ &- \sum_{t=1}^{NT} \mu_{d,t}^5 R_d^U - \sum_{t=1}^{NT} \mu_{d,t}^6 R_d^D. \end{aligned} \quad (4.62)$$

Substitute the results in (4.62) into the objective function in (4.4), we arrive at

$$\begin{aligned}
Profit &= \sum_{d=1}^{ND} \Delta T \sum_{t=1}^{NT} \sum_{m=1}^{NM_d} u_{d,m,t} P_{d,m,t} \\
&+ \sum_{t=1}^{NT} \left[- \sum_{m=1}^{NM_d} \mu_{d,m,t}^1 P_{d,m,t}^{\max} + \mu_{d,t}^4 P_{d,t}^{\min} \right] + \mu_d^3 E_d \\
&- \sum_{t=1}^{NT} \mu_{d,t}^5 R_d^U - \sum_{t=1}^{NT} \mu_{d,t}^6 R_d^D + \sum_{t=1}^{NT} \Delta T c_t^R (D_t - D_t^{\text{LC}}) \\
&- \sum_{t=1}^{NT} \Delta T \left[P_t^g c_t^g + c_t^{\text{RES}} P_t^{\text{RES,a}} \right. \\
&\left. + \sum_{i=1}^{NG} (S U_{i,t} + C_i(P_{i,t})) + c^{\text{LC}} D_t^{\text{LC}} \right]. \tag{4.63}
\end{aligned}$$

Finally, the original nonlinear bilevel optimization problem can be recast by the following MILP

$$\min_{P_{d,t}, P_{d,t,m}, c_t^{\text{DR}}, P_t^g, P_t^{\text{RES}}, D_t^{\text{LC}}, P_{k,t}^c, P_{k,t}^{\text{pd}}} Profit \tag{4.64}$$

subject to

$$(4.5) - (4.9), (4.26), (4.36) - (4.38), (4.49) - (4.61), (4.62), (4.63).$$

Figure 4.3 summarizes the proposed solution technique. The proposed optimization model is indeed a bilevel optimization problem, which is transformed to a single level optimization problem by replacing the lower problem with its equilibrium KKT conditions since the lower problem is linear and convex. The obtained mathematical problem with equilibrium constraints (MPEC) is, however, still difficult to solve, due to the bi-linear term and complementary constraints. Hence, strong duality theorem and big M approximation are utilized to transform the given MPEC to an equilibrium mixed integer linear programming (MILP), which can be solved efficiently by branch and bound algorithm implemented in commercial software such as CPLEX [106].

In practice, the proposed system can be implemented as follows. First, each DR aggregator collects load preference information from flexible load customers and constructs aggregated utility functions for each hour in the operating day. Then, DR aggregators send these constructed utility functions to the LSE. Based on data supplied by the forecasting entities, data related to specifications and status of batteries, DGs, and operation constraints (e.g., maximum power exchange with the main grid), and flexible load data, the LSE solves the optimization problem (59). The outcome of this problem is the optimal DR price and scheduled decisions of flexible loads. These results are sent back to the DR aggregators to implement corresponding load scheduling actions and to be utilized for quantification of cost and revenue.

4.7 Numerical Results

4.7.1 Simulation Data

Simulation data in the base case is given in Table 4.3. Specifically, the penalty cost for involuntary load curtailment is set equal to 1000 \$/MWh [48]. The renewable energy price that the LSE pays

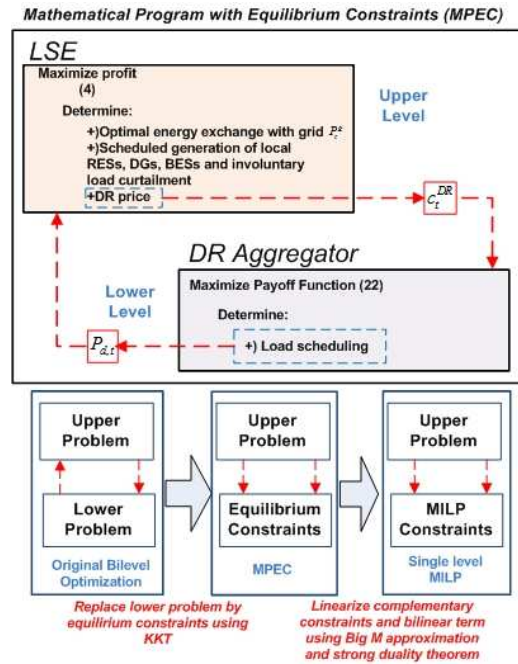


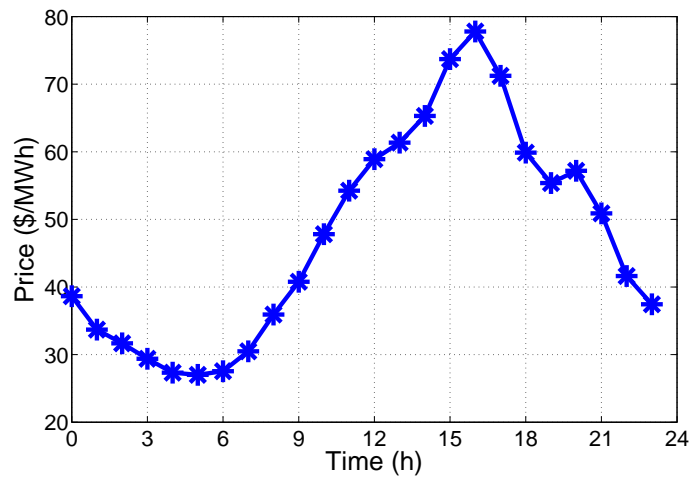
Figure 4.3 – Summary of the proposed solution algorithm

for local wind/solar farms is assumed to be 40 \$/MWh. For simplicity, we assume that $P_t^{g,\max} = P^{g,\text{grid}}$ and $c_t^R = c^R, \forall t$. The regular retail price in the base case is \$60/MWh and we assume the LSE does not possess any battery storage unit in the base case. Dispatchable DG data is taken from [48]. Moreover, we assume that the LSE can predict electricity price, inflexible load, and renewable energy generation with high accuracy. For simplicity, we use historical data of the corresponding system parameters as their forecast values. Electricity price data is taken from PJM website [48]. Hourly inflexible load data is retrieved from [135]. Renewable energy generation data is constructed from data in [48]. Figs. 4.4(a), 4.4(b) shows forecast data of electricity price, inflexible load, and renewable energy generation.

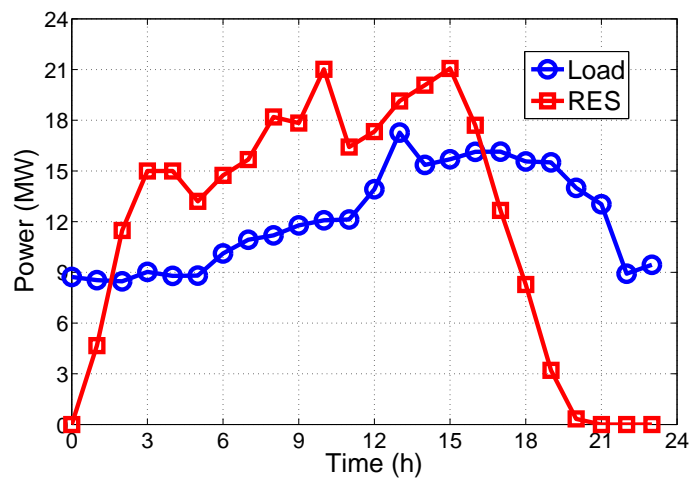
Table 4.3 – System Parameters in Base Case

c^{LC} (\$/MWh)	c_t^{RES} (\$/MWh)	p^{grid} (MW)	c^R (\$/MWh)	Battery	DG
1000	40	40	60	No	No

We assume that flexible loads are aggregated by three DR aggregators. The modeling method in [42, 44] is employed to construct flexible load data. The data of the *base-case multi-block utility functions* for DR aggregators is given in Table 4.4. To obtain the utility functions for DR aggregators over the scheduling horizon, we multiply the base-case utility by 0.8, 1.0, and 1.2 in periods (1-8), (9-16), and (17-24), respectively [42]. For simplicity, the amount of flexible load (i.e., demand blocks) is assumed to be the same for all time slots. The minimum energy consumption (E_d) of each DR aggregator d over the considering day is set equal to 60% of its maximum energy consumption level (e.g., $E_3 = 0.6 \times (1+1+2+2) \times 24 = 86.4$ MWh). For simplicity, the minimum hourly power consumption



(a) Price forecasts



(b) Load and generation forecasts

Figure 4.4 – Forecast data

of every DR aggregator is set to be zero (i.e., $P_{d,t}^{\min} = 0, \forall d, t$). Without loss of generality, limits on load ramping up and ramping down are assumed to be sufficiently large.

Table 4.4 – Data for DR aggregators

d	Load blocks (MW)	Marginal utility (\$/MWh)	E_d (MWh)
1	1, 1, 1, 1	56, 52, 51, 46	57.6
2	1, 1, 1, 1	61, 56, 52, 46	57.6
3	1, 1, 2, 2	59, 56, 52, 47	86.4

4.7.2 Sensitivity Analysis

We consider the two following schemes.

- **Scheme 1 (S1):** The LSE solves the proposed optimization model. The DR aggregators enjoy a dynamic retail price tariff.
- **Scheme 2 (S2):** The LSE solves the same optimization problem. However, the regular retail price is applied to DR aggregators (i.e., $c_t^{\text{DR}} = c_t^{\text{R}}, \forall t$). In this scheme, DR aggregators have no incentives to modify their loads.

Table 4.5 – Comparison between Scheme 1 and Scheme 2

c_t^{R} \$/MWh	Payoff 1 \$	Payoff 2 \$	Profit 1 \$	Profit 2 \$	DR1 MWh	DR 2 MWh
47	2607.2	2403.2	695.7	146.8	272.0	213.6
50	2061.2	1786.6	2103.9	1476.9	270.0	201.6
55	1250.2	778.6	4599.9	3942.8	240.0	201.6
60	251.0	-229.4	7191.3	6408.7	201.6	201.6
65	-756.9	-1237.4	9657.2	8874.6	201.6	201.6

Table 4.5 presents the performance comparison between Scheme 1 and Scheme 2 for different values of the regular retail price. Payoff 1, Payoff 2 represent total payoffs of DR aggregators; Profit 1, Profit 2 indicate the optimal profit values of the LSE; and DR1 and DR2 represent the total energy consumption of DR aggregators over the scheduling horizon for Scheme 1 and Scheme 2, respectively. We can see from Table 4.5 that the minimum energy consumption level of all DR aggregators is 201.6 MWh. Table 4.5 also shows that the total payoff of DR aggregators as well as the optimal profit of the LSE in Scheme 1 are significantly larger than those in Scheme 2. Therefore, we can conclude that Scheme 1 outperforms Scheme 2 in terms of DR aggregators' payoffs and LSE's profit.

Furthermore, we can observe that the total energy consumption of DR aggregators over the scheduling horizon in Scheme 1 is greater than the minimum energy consumption requirement (i.e., 60% of the total flexible loads or 201.6 MWh) for regular retail prices of 47 \$/MWh, 50 \$/MWh, and 55 \$/MWh, and is equal to the minimum level for regular retail prices of 60 \$/MWh and 65 \$/MWh. Similar observation can be drawn for Scheme 2. Additionally, for the same value of regular retail price, DR1 is greater than DR2 since DR prices in Scheme 1 are always smaller or equal to the regular retail price while DR prices in Scheme 2 are equal to the regular retail price.

Figure 4.5 shows the optimal hourly DR prices over the scheduling horizon for different values of c^{R} and P^{grid} . We can observe that DR price is very low during time slots 1-8, quite low for some period during time slots 9-16, and very high during time slots 17-24. Intuitively, the LSE would set a low DR price during some time slots to encourage DR aggregators to consume more energy. In addition, it can set a high DR price (i.e., close or equal to the regular retail price) to discourage DR aggregators from consuming energy.

There are several reasons for the LSE to set low DR price. First, when the *grid price* is low, the LSE would be interested in buying more energy from the main grid to serve its customers at a DR price between the grid price and the regular retail price. Second, the grid price can vary significantly over the scheduling horizon, which offers opportunities for the LSE to arbitrate between low and high

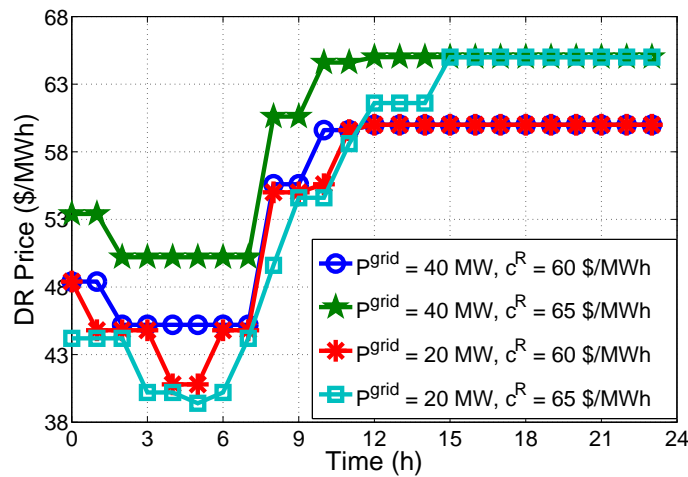


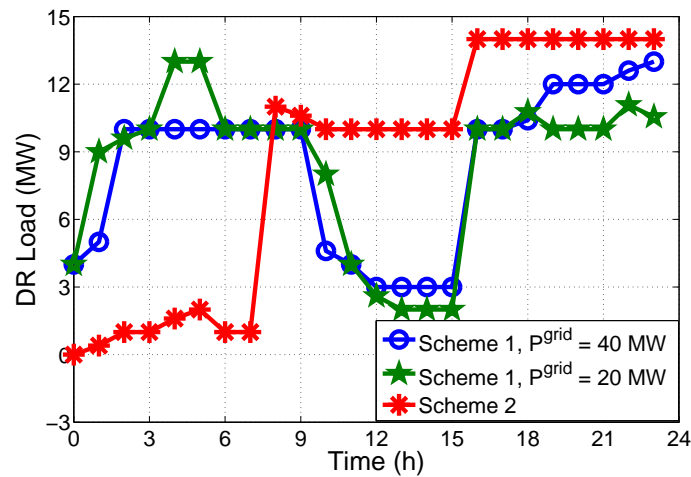
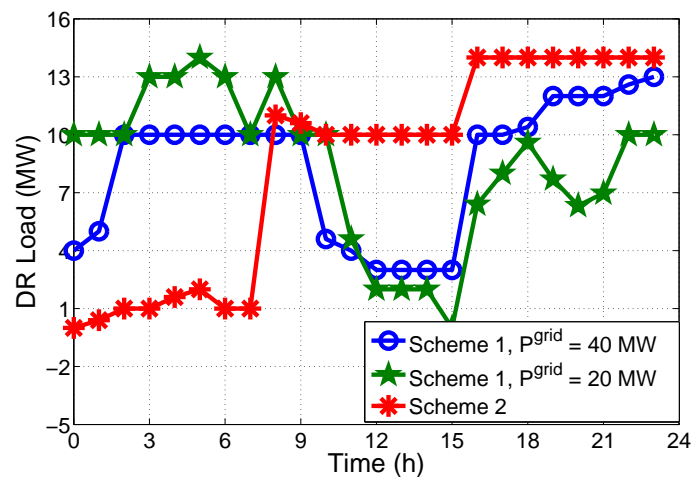
Figure 4.5 – DR price

price periods. Therefore, the LSE sets low DR prices at some time slots and high at some other time slots to encourage load shifting from DR aggregators in order to reduce the importing cost of energy from the main grid. Also, DR aggregators can reduce their bills by shifting their loads to low DR price hours. Finally, if renewable energy generation is high, the LSE faces the power limit at the PCC (i.e., P^{grid}); hence, it would sell as much energy as possible to its customers at low DR prices rather than curtailing the renewable energy surplus.

During hours 1-8, the marginal utility (benefit) of consuming load for DR aggregators is relatively low (i.e., 0.8 times the base-case marginal utility in Table 4.4), and the grid price is low. Therefore, the optimal DR price is low during this period to encourage DR aggregators to consume more energy and to shift load to this period. During hours 9-16, although the marginal utility is the same as the base-case marginal utility, the grid price is high; therefore, only for some first hours in this period, DR prices are lower than the regular retail prices. During hours 17-24, the grid prices include both high price hours and low price hours; however, the marginal utilities of consuming energy achieved by DR aggregators are high, which are equal to 1.2 times the base-case utilities. DR prices are high during this period even during low price hours. This is because the benefits of consuming energy for DR aggregators outweigh the energy costs. Furthermore, we can observe that when P^{grid} is 20 MW, DR prices during hours 1-8 tend to be lower than DR prices when P^{grid} is 40 MW. As will be illustrated in Figs. 4.6(a), 4.6(b), 4.7, and 4.8, involuntary load curtailment occurs for some hours in time slots 17-24 when P^{grid} is 20 MW. This explains why the DR prices are lower during hours 1-8 so as to encourage DR aggregators to shift their load to this period.

Figs. 4.6(a) and 4.6(b) present the total hourly load of DR aggregators over the scheduling horizon with the regular retail prices of 60 \$/MWh and 65 \$/MWh, respectively. For Scheme 2⁴, the total DR load is low during hours 1-8, higher during hours 9-16, and highest during hours 17-24. This is because the marginal utility prices of DR aggregators are lowest during hours 1-8, and highest during hours 17-24. Furthermore, the DR price in Scheme 2 is equal to the regular retail price (i.e., fixed); hence, DR aggregators have no incentive to shift their loads. On the other hand, DR load in Scheme 1 is significantly higher than that in Scheme 2 during hours 1-8, and DR load in Scheme 1 is generally lower than DR load in Scheme 2 during time slots 9-24. This demonstrates the effectiveness of the proposed scheme in shifting load in favor of the LSE. Moreover, we can observe that more load shifting occurs when P^{grid} is 20 MW than when P^{grid} is 40 MW. This is to reduce load curtailment when P^{grid} is 20 MW since renewable energy generation during time slots 19-24 is low. When the regular retail price

⁴Note that results for Scheme 2 are independent of the grid limit P^{grid} .

(a) $c^R = 60$ \$/MWh(b) $c^R = 65$ \$/MWh**Figure 4.6** – DR load

is 60 \$/MWh, utility due to energy consumption tends to outweigh the energy cost; therefore, even if the LSE sets lower DR price during hours 1-8, DR aggregators still consume a significant amount of energy during hours 17-24. On the other hand, when the regular retail price is 65 \$/MWh, DR aggregators have more incentive to shift their loads to low DR price hours.

The results in Figure 4.7 can be explained by the results in Figs. 4.6(a) and 4.6(b). Renewable energy generation is generally low during hours 18-24 and the total load of DR aggregators is very high during hours 17-24. For Scheme 1, more load shifting occurs when the regular retail price is 65 \$/MWh than that when the regular retail price is 60 \$/MWh. As a result, Scheme 1 outperforms Scheme 2 in terms of involuntary load curtailment. The hourly power trading between the LSE and main grid is shown in Figure 4.8. As we can observe, in Scheme 2, the LSE has to sell electricity to the main grid during hours 1-8 when the grid prices are low, and it has to import a large amount of energy during high price hours to serve load. However, in Scheme 1, the LSE imports electricity during low price hours 1-8; hence, it can reduce the amount of imported electricity during high price hours.

Figs. 4.9(a), 4.9(b) illustrate the impact of the minimum energy consumption requirement of DR aggregators on the optimal solution. Parameter $minDR$ is the ratio between the minimum energy consumption E_d and the maximum total load of each DR aggregator d . As we can observe, the optimal

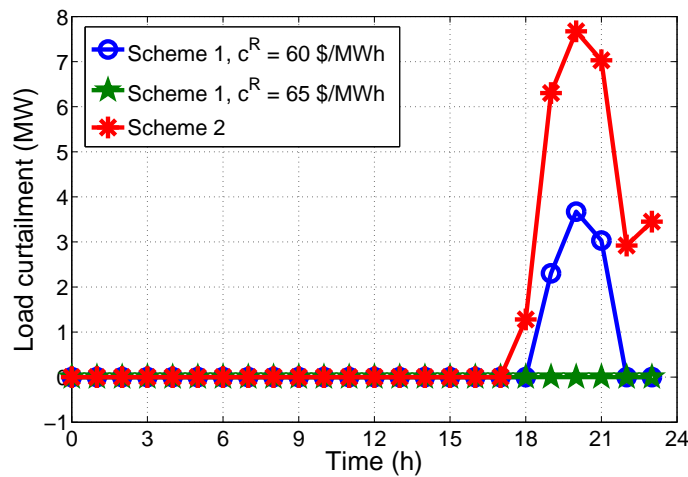


Figure 4.7 – Involuntary load curtailment

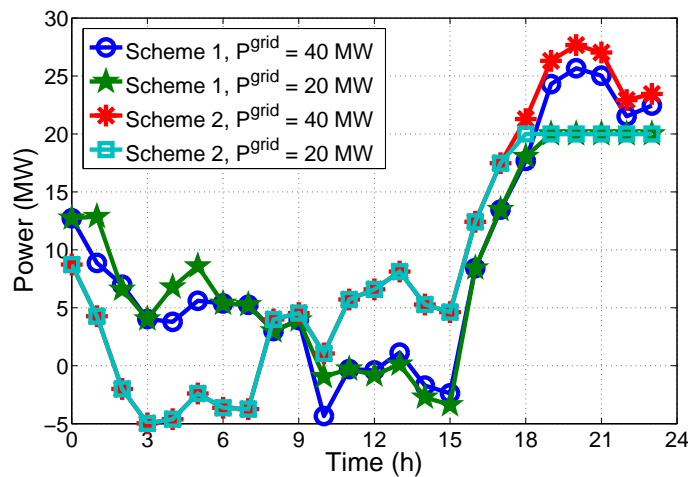


Figure 4.8 – Power exchange with the main grid ($c_t^R = 60$ \$/MWh)

profit of the LSE tends to increase as $minDR$ increases. This is because DR aggregators are forced to consume more energy as $minDR$ increases. Furthermore, the total payoff of DR aggregators tends to decrease as $minDR$ increases. When $minDR$ is equal to 100%, the loads of DR aggregators become inflexible since DR aggregators have to consume the maximum energy level. Also, when $minDR$ is smaller than 100%, Scheme 1 outperforms Scheme 2 in terms of optimal LSE profit as well as total payoff of DR aggregators.

In Figs. 4.10(a), 4.10(b), 4.11, and 4.12, we show the impact of renewable energy generation on the optimal solution where P^{grid} is 20 MW. Parameter $RESSF$ (Renewable Energy Source Scaling Factor) is a scaling factor to scale the base-case renewable energy generation profile in Figure 4.4(b). As we can observe in Figs. 4.10(a), 4.10(b), Scheme 1 outperforms Scheme 2 in reducing renewable energy curtailment. The results in Figure 4.10(a) can be explained by those in Figure 4.11. Compared to Scheme 2, DR aggregators consume a significantly larger amount of energy in Scheme 1 during hours with high renewable energy generation and lower during hours with low renewable energy generation. Furthermore, DR aggregators consume much more energy as $RESSF$ is 3 than when $RESSF$ is 2.5. This is because DR prices are very low as $RESSF$ is 3, and DR aggregators consume more energy to increase their utilities. Utility due to energy consumption outweighs the energy cost in this case. Hourly DR prices are shown in Figure 4.12.

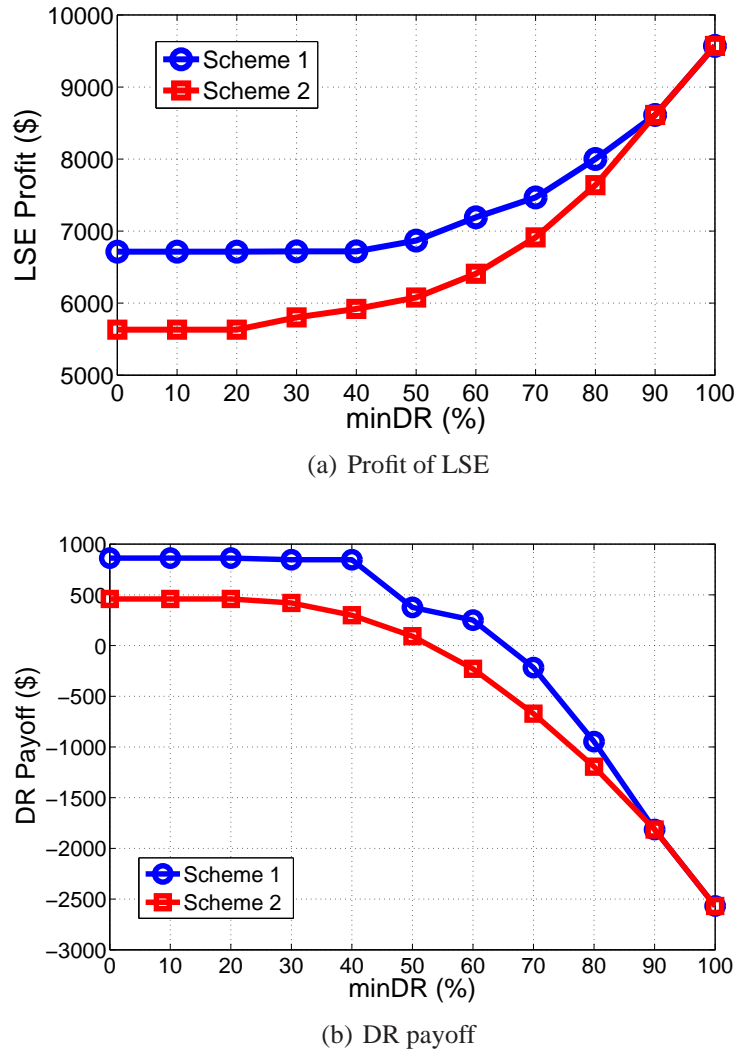
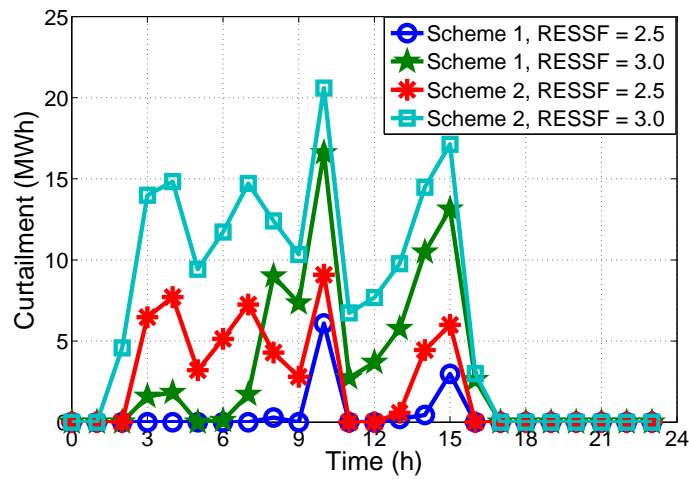


Figure 4.9 – Impact of min DR on the optimal revenue

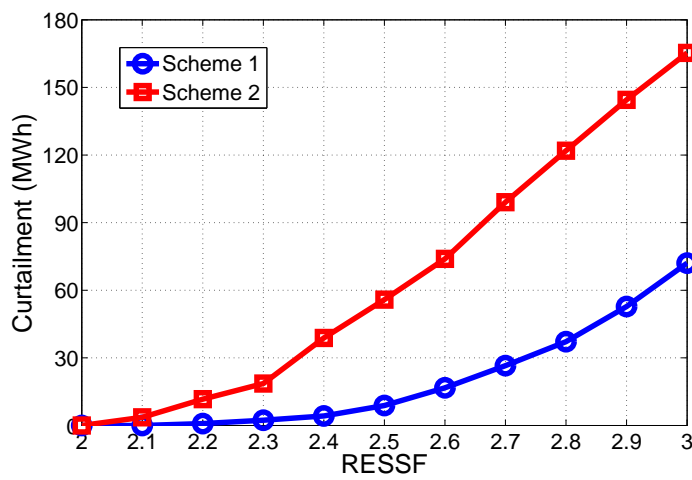
Finally, in Figure 4.13, we consider the case where P^{grid} is equal to 20 MW and there is no renewable energy (i.e., $P_t^{\text{RES},a} = 0, \forall t$). Hourly power trading between the LSE and the main grid (P_t^{g}), total hourly DR load of DR aggregators, and total hourly involuntary load curtailment in Scheme 1 and Scheme 2 are presented in Figure 4.13. Due to load shifting from DR aggregators in Scheme 1, we can observe that the power exchange with the main grid in Scheme 1 is higher than that in Scheme 2 during low grid price hours 1-8, and it tends to be lower than that in Scheme 2 during high grid price hours 9-17. Furthermore, involuntary load curtailment in Scheme 1 is significantly lower than that in Scheme 2.

4.7.3 Complexity of Proposed Approach

In this study, the proposed pricing model is formulated as a bilevel program which can be recast as a single level MILP by using appropriate approximation methods. The global optimal solution of MILP can be obtained efficiently by using branch and cut algorithms embedded in available commercial solvers [31]. The optimization problem (4.64) is solved by CPLEX 12.4 [106] under GAMS [40] on a laptop with 3.5 GHz Intel Core i7-3370 CPU and 8 GB RAM. The optimal solution is obtained with an optimality gap of 0.1%. The computation time with respect to number of DR aggregators



(a) Hourly RES curtailment



(b) Total RES curtailment

Figure 4.10 – Renewable energy curtailment

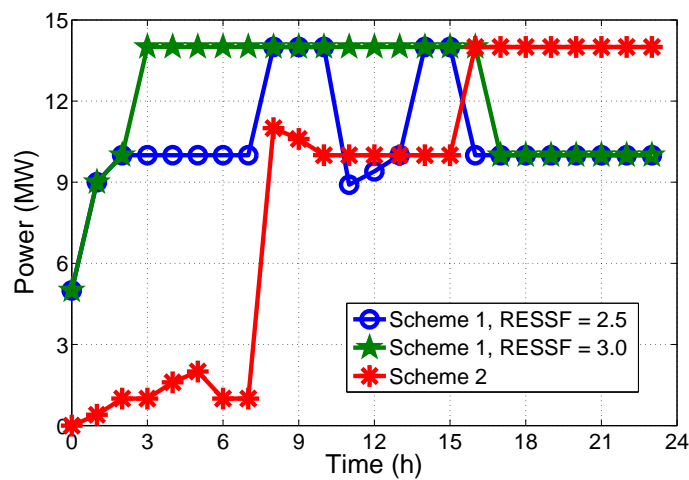


Figure 4.11 – DR load

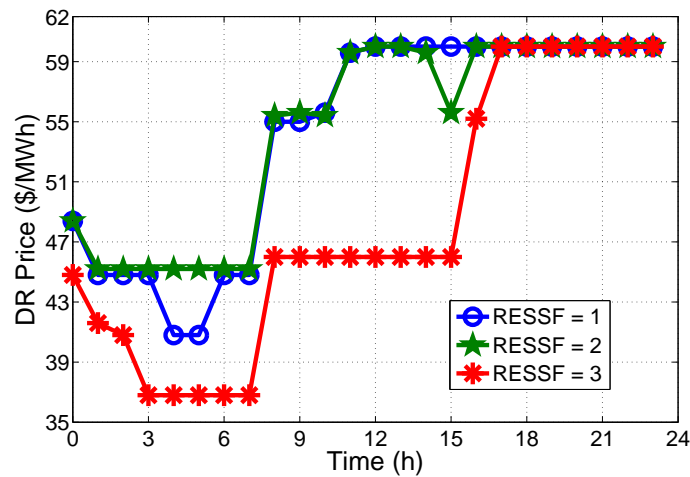


Figure 4.12 – DR price

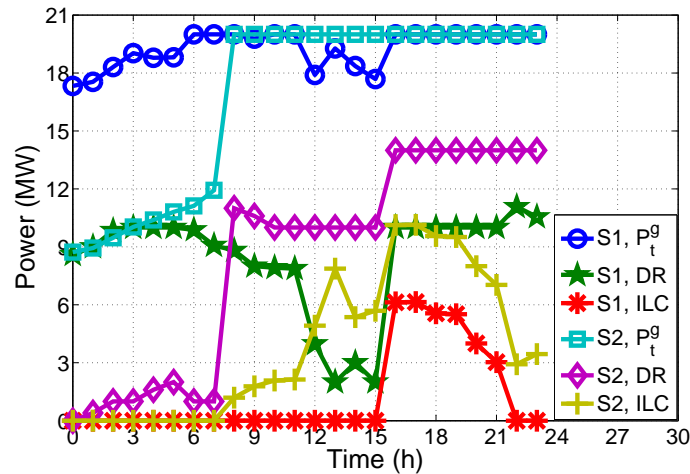


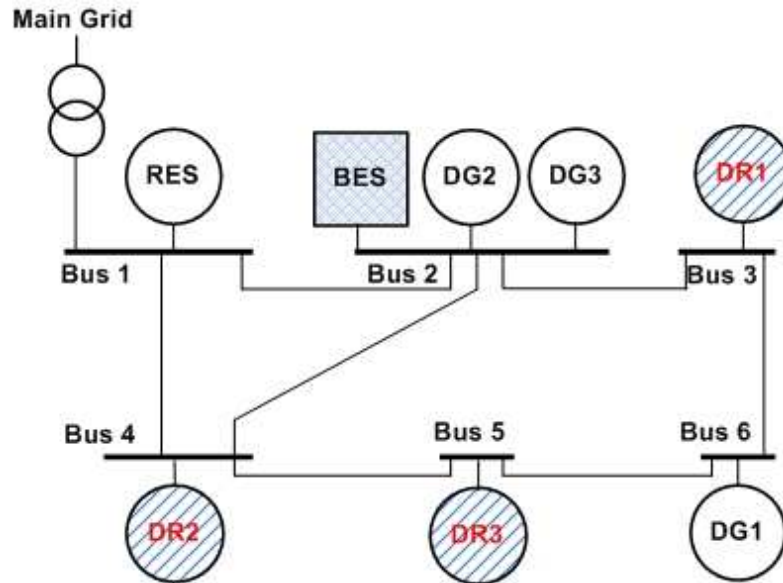
Figure 4.13 – Comparison between Scheme 1 (S1) and Scheme 2 (S2)

is summarized in Table 4.6. For fairness, the power limit at PCC ($P_t^{g,max}$) is set to be 500 MW to ensure that the LSE’s load can be served when the number of DR aggregators increases. Obviously, as the number of aggregators increases, the number of binary variables, and number of columns and rows in the reduced MILP obtained by GAMS/CPLEX increases, which results in the increase in the computation time. However, the computation time with 7 DR aggregators is only about 28s, which is acceptable.

The computation burden of the MILP, however, depends on several factors, especially the number of binary variables and constraints. The computation time of our model depends on many factors such as number of DGs, number of batteries, and the number of DG aggregators since these elements determine the number of binary variables and constraints. For example, operational constraints of conventional DGs such as ramping rate, minimum ON/OFF time duration increase the number of binaries and constraints, which consequently increase the computation burden. However, in this chapter, we focus on a small-scale LSE that provides electricity to a community or a small network located at one single node or at a few nodes. The number of generators and the number of DR aggregators are, therefore, expected to be small. Hence, the underlying MILP can be solved efficiently using GAMS/CPLEX within reasonable computation time.

Table 4.6 – Impact of number of DR aggregators on computation time

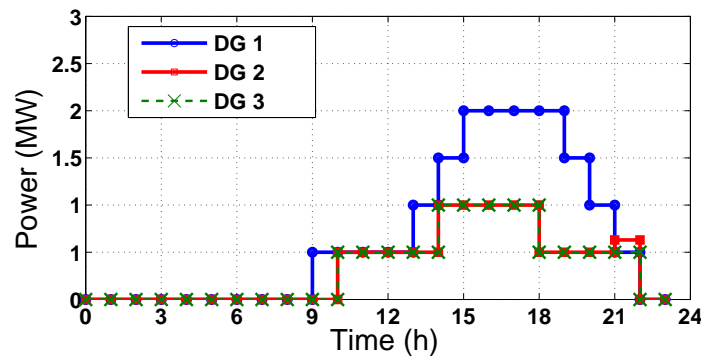
Number DR aggregators	Binaries	Columns	Rows	Computation Time
3	499	1293	1283	12.387s
4	676	1736	1739	19.773s
5	837	2141	2148	21.126s
6	998	2564	2570	25.237s
7	1159	2964	2981	28.453s

**Figure 4.14** – IEEE 6-bus system

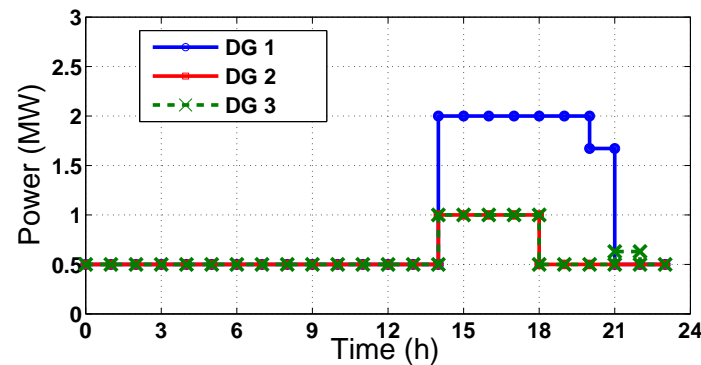
For a larger-scale application (e.g., a LSE serving a large distribution network with a significant number of generators and loads), it can be very challenging to solve the resulted large scale MILP. In this case, state-of-the-art decomposition techniques for a large scale MILP or the application of evolutionary algorithms such as particle swarm optimization (PSO) can be employed to reduce the computational time. However, these issues will be the subject of our future work.

4.7.4 Constraints of Distribution Network, Batteries, and DGs

For the simulation, the network of LSE is modeled using a widely used IEEE 6-bus system as in [12]. For simplicity, the network flow limits at each line are set sufficiently large (i.e. 15 MW) to avoid congestion. Furthermore, we assume that the LSE owns three DGs and one battery. The data of these components are available in [48]. The minimum power outputs of DGs are $P_i^{\min} = 0.5$ MW, both ramping up and ramping down are set to 0.5 MW, minimum ON/OFF duration is 2 h. DR aggregators 1, 2, and 3 are located at bus 3, 4, and 5, respectively. DG 1 with generation capacity of 2 MW is located at bus 6. The 1 MWh battery ($SOC^{\min} = 0.2$, $SOC^{\max} = 0.9$, $SOC_0 = 0.5$, $P^c = P^d = 0.1$ MW) and two DGs 2 and 3 each of which has generation capacity of 1 MW, are located at bus 2. Other system data is the same as in the base case. The inflexible load in Figure 4.4(b) is allocated evenly to buses 3, 4, and 5. The network's line susceptance data is taken from MatPower software [136]. The considered system topology is presented in Figure 4.14.



(a) With ramp rate and minimum ON/OFF duration constraints



(b) Without ramp rate and minimum ON/OFF duration constraints

Figure 4.15 – Dispatch of DGs

Figure 4.15(a) presents the outputs of DGs, which increases significantly in the period between time slots 14 and 21, which is associated with high grid electricity price and peak load period. In particular, during on-peak time with high grid price the LSE tends to increase its energy generated from DGs to reduce the energy drawn from the grid and to compensate for the increase of customers' demand and the deficit of renewable energy generation.

The difference of power dispatch schedules of DGs in the two cases with and without consideration of ramp rate and minimum ON/OFF time constraints are shown in Figure 4.15(a) and Figure 4.15(b), respectively. It is revealed that without these technical constraints, the LSE has more flexibilities to adjust its on-site DGs' power generation. When ramp rate and minimum ON/OFF time constraints are more relaxed, the outputs of DGs exhibit larger variation. The LSE tends to turn on all units all the time (the minimum power of each unit is $P_i^{\min} = 0.5$ MW) to reduce the energy drawn from the grid. Consequently, the profit of LSE is slightly better, e.g., it is equal to 10216\$ with ramp rate and minimum ON/OFF duration constraints and equal to 10518\$ when these inter-temporal constraints are ignored. Batteries and DGs add additional flexibility to the operation of the LSE. The increasing LSE's generation's flexibility enables the LSE to exploit the advantages of time-varying grid electricity price, which is illustrated in Figure 4.16. For example, it can buy less energy from the grid or sell more energy to the main grid during periods with high grid price to improve its profit.

The computation time of the optimization problem considering distribution network constraints (IEEE 6-bus system), batteries, and ramp rate and minimum ON/OFF time constraints of DGs is 18.627s, which is slightly higher than the computation time reported in Table 4.6 (with 3 DR aggregators). This is due to the additional constraints including the network flow constraints and operation constraints of batteries and DGs, which increase the computation burden of the problem.

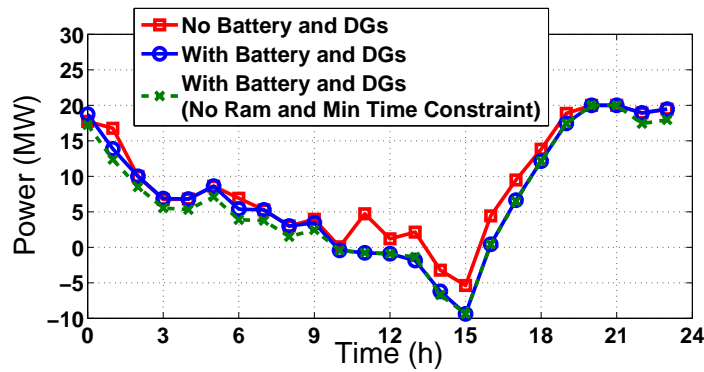


Figure 4.16 – Power exchange with the main grid

Our design in this chapter aims at developing an efficient DR pricing scheme which is suitable for a LSE deployed over a small area. Hence, the number of nodes in the LSE's network is assumed to be small, and in many cases, all entities in the system can be located at just one node (e.g., a LSE supplies electricity to a small town or a village). In fact, the computation burden of the proposed LSE optimization model depends mainly on the number of DR aggregators, DGs, and batteries since these added elements introduce more binary variables. The proposed optimization can be extended to a stochastic bilevel programming problem, which can be tackled by using the scenario-based optimization approach. Due to the space constraint, study of the stochastic problem is reserved for our future works. In the stochastic case, the computation burden of the stochastic mathematical programs with equilibrium constraints (MPECs) depends highly on the number of scenarios. However, the complexity of the stochastic MPEC problem can be reduced by using a novel coordinate decent algorithm [44] to decompose the stochastic problem by scenario, or by using Bender decomposition as suggested in [110], or heuristic evolutionary algorithms [137].

4.8 Conclusion and Future Directions

In this chapter, we have proposed a novel operation framework for a LSE, which serves both flexible and inflexible loads. The proposed pricing scheme can be readily implemented since it is compatible with the existing pricing structure in the retail market. Extensive numerical results have shown that the proposed scheme helps increase the profit of the LSE, increase payoff for DR aggregators, reduce involuntary load curtailment, and renewable energy curtailment.

There are several directions that the proposed optimization framework can be further extended.

- First, there are various uncertain system parameters in the considered model such as renewable energy generation and grid electricity price. Addressing this uncertainty issue by using popular optimization techniques such as robust optimization [15], stochastic optimization [16], and model predictive control [138] is an interesting research topic for further works. The MPC-based design, however, must consider the feasibility and stability of the closed loop system.
- Reactive power management is an important technical issue in the distribution network. Our future work will consider how the reactive power management can be integrated into the proposed optimization framework.
- The complexity of the proposed model increases as the number of DR aggregators increases. Additionally, the computational burden of the model increases significantly if we consider a scenario-based stochastic model to tackle the system uncertainties. The proposed model is computationally tractable when the number of DR aggregators and/or the number of scenarios is

moderate, which is a reasonable assumption for the setting where the LSE serves a small area. It is interesting to study how one can reduce the computational time of the proposed model.

- There could be several LSEs operating in one (large) geographical area, and DR aggregators can choose the best LSE based on the offered DR prices. Therefore, LSEs need to determine an optimal DR pricing offer to attract more DR loads while maximizing their profits. The problem then becomes a multi-leader multi-follower game, which will be considered in the future.

Chapter 5

Cost Allocation for Cooperative Demand-Side Resource Aggregators

Previous chapters discussed the decision making problems of demand-side entities in real-time operation [2], i.e., how smart homes respond to time-varying price signals and how Load Serving Entities (LSE) determine the price signals. In smart grid, demand-side resources can be aggregated to participate in the electricity market [24, 29, 30], which can be considered as a short-term time scale decision making problem [2]. We will investigate how the aggregate demand-side resources bid energy in the market and allocate the cost to each member. The content of this chapter was published in IEEE Transactions on Smart Grid in the following paper:

Hieu Trung Nguyen and Long Bao Le, “Bi-Objective Based Cost Allocation for Cooperative Demand-Side Resource Aggregators,” *IEEE Transactions on Smart Grid*, vol.PP, no.99, pp.1-1, doi: 10.1109/TSG.2017.2653060

5.1 Abstract

This chapter presents a cooperative game theoretic approach to tackle the cost allocation problem for a virtual power plant (VPP) which consists of multiple demand-side resource aggregators (DRAs) participating in the short-term two settlement electricity market. Given the considered game is balanced, we propose to employ the cooperative game theory’s core cost allocation concept to efficiently allocate the bidding cost to the DRAs. Since the non-empty core contains many potential solutions, a bi-objective optimization framework is used to determine the core cost allocation solution that can achieve efficient tradeoff between stability and fairness. To solve this problem, we jointly employ the ϵ -constraint and row constraint generation methods to construct the Pareto front, based on which we can specify a desired operation point with reasonable computation effort. Numerical studies show that our proposed design can efficiently exploit the non-empty core to find a cost allocation for the participants, achieve the desirable tradeoff between stability and fairness, and can address the practical DRAs’ large-scale cooperation design.

5.2 Introduction

5.2.1 Background and Motivation

Active participation of demand-side resources in the electricity market has been considered efficient and economic means to balance the supply and demand in smart grids with high renewable energy

integration [10]. Demand-side resource aggregators (DRA), which can coordinate various demand-side resources and bid in the Day-ahead (DA) and real-time (RT) electricity market with certain objectives (e.g., minimization of energy payment cost, maximization the total utilities) will play an important role in the electricity market [24, 29]. However, participation in the electricity market can be challenging for DRAs due to the uncertainty of renewable energy resources, nonflexible load consumption, and market price volatility [31].

Cooperation among different market participants has been considered as an efficient approach to address the uncertainties and reduce the bidding risk in the electricity market [24, 29–32, 43, 50, 71, 72, 97, 100, 102, 139]. Thanks to the reconstruction of the electricity market, multiple DRAs [30] can be coordinated under an emerging smart grid cooperation entity, namely virtual power plant (VPP), to further exploit the aforementioned resources [31, 50]. Although cooperation among different DRAs which might belong to different stakeholders [32] can result in benefits such as total cost reduction or profit improvement, how to efficiently share the cooperation benefits, e.g., determine the cost shares, among participants is an important and open research issue.

5.2.2 Aims and Approach

This chapter aims at developing an efficient cost allocation scheme for a VPP consisting of multiple DRAs [29, 30] that participate in the two settlement short-term electricity market [24, 29, 30]. We consider a generic DRA model which includes distributed renewable energy resources, aggregated flexible load, aggregated nonflexible load, and reducible load [29]. We assume that a large number of DRAs can be coordinated and jointly bids in the electricity market through *a commercial VPP* [50]. The bidding strategy is modeled as a risk averse two-stage stochastic optimization problem [24, 31, 43]. Given the uncertainties of renewable energy generations, load demands, and market prices, the VPP cannot allocate a fixed cost to each participant. Instead, the VPP can allocate a percentage quota of expected total bidding cost to each DRA, which must be determined before the planning horizon.

The cost allocation problem is modeled as a cooperative game where each DRA acts as a player and the value of the cost function is the outcome of the market bidding optimization. Given the considered cooperative game is a linear programming game [55], which is totally balanced, we propose a cost allocation scheme based on the game core concept [54, 98]. Because a nonempty core can contain many allocation vectors, choosing an arbitrary cost allocation in the core can lead to very small cost reduction for certain coalitions of DRAs making the cooperation *less stable*, or high deviation in percentage cost reduction among DRAs making the cooperation *unfair* [54] (i.e., some DRAs may have significantly smaller percentage cost reduction than others). To address these issues, we formulate the cost allocation problem as a bi-objective optimization problem which aims at determining an efficient solution in the core of the game with desirable tradeoff between stability and fairness.

5.2.3 Literature Review, Contributions, and Chapter Organization

Modeling and bidding of DRA in the electricity market are active research topics. In particular, modeling and bidding design for a single aggregator is presented in [10, 24, 29, 43] while coordination of multiple DRAs in a VPP framework is studied in [31, 50, 97]. These papers show that cooperation among DRAs can lead to cost reduction or profit improvement by leveraging the strengths and weaknesses of individual aggregators. However, they do not address how to share the cooperation gain among the participants. The work [32] develops an electricity payment method to motivate the coordination between the EV aggregator and wind power producer. The work [71] presents a ranking based pricing scheme to calculate participants' cost saving/profit increment based on submitted load profiles' flexibility. The work [72] proposes direct energy trading among producers and consumers where the

internal price is determined by the Shapley value concept. However, all these proposed frameworks require market redesign; thus, they would not be applicable for current market practice.

Cooperative game theory has been employed to address various design problems in power systems such as energy producers' multilateral trading [99], energy management, and market design [70, 72, 100]. It is also used to study the cooperation's profit sharing under current market practice [112] where the nucleolus based allocation is used to split profit of multiple renewable energy producers which jointly bid in the forward market. Although the nucleolus is unique and lies in the core, other core cost allocation vectors, which can have advantages over the nucleolus, are ignored. Moreover, none of aforementioned papers considers the cooperation among heterogeneous participants.¹ More importantly, none of them explores the core, which contains a large number of potential allocation solutions, for flexible and efficient cost allocation design. Our current study addresses these major issues where we make the following contributions.

1. We present a cooperative game model for the cost allocation problem for a VPP that consists of multiple DRAs participating in the two settlement short-term electricity market. The framework can be applied to the current market structure considering heterogeneous characteristics of the participants.
2. We study a bi-objective optimization based core cost allocation design that can achieve efficient tradeoff between stability, i.e., the minimal cost saving among all coalitions, and fairness, i.e., the deviation of percentage cost saving among individual DRAs.
3. We develop a computationally efficient procedure to compute a desirable Pareto optimal cost allocation vector and construct the Pareto front, which can be applied to practical large-scale settings.
4. Extensive numerical results are presented. We demonstrate the advantages and efficacy of the proposed design framework where a desirable cost allocation solution on the Pareto front can be achieved and we also study the computation complexity of our proposed design.

The remainder of this chapter is organized as follows. Section 5.3 explains the notations used in this study. Section 5.4 presents the system model and assumptions of the cost allocation problem for cooperative DRAs. Section 5.5 presents the cooperative game formulation of the cost allocation problem. The proposed bi-objective core cost allocation design are described in Section 5.6. The proposed solution approach is presented in Section 5.7. Section 5.8 presents numerical results, Section 5.9 discusses extensions and future work, and Section 5.10 concludes the chapter.

5.3 Notations

Notation	Explanation
Sets and Indices	
t, s	Time intervals, scenarios
k	Demand-side resource aggregators (DRA), $k = 1, 2, \dots, NK$
b	Block b in multi-utility block function of DRA k 's flexible load model, $b \in \mathcal{B}_k$
m	Pareto front's point, $m = 0, 1 \dots, M$
i_1, i_2, i_3	Iterations in Pareto front's construction
S, e^S	Coalition S and its indicate vector e^S
\mathcal{H}	Grand coalitions of DRAs

¹Heterogeneous participants are those having various types of resources with different operation constraints.

$v(\cdot)$	Cost function of the game $\mathcal{G}(\mathcal{K}, v)$
$\mathcal{C}(v)$	Core set of the game $\mathcal{G}(\mathcal{K}, v)$
Parameters	
NI	Total number of iterations in Pareto front's construction
NK	Number of demand side resource aggregators (DRAs)
NS	Number of scenarios
NT	Number of time slots (24)
ΔT	Length of one time slot, $1h$
π_s	Probability of scenario s
$\lambda_{t,s}^{\text{DA}}, \lambda_{t,s}^{\text{RT}}$	Day ahead (DA)/Real-time (RT) electricity price (\$/MWh)
λ^{P}	Penalty cost of energy mismatch between DA and RT (\$/MWh)
λ_k^{r}	Load reduction (LR) cost of DRA k (\$/MWh)
$E_{k,t,s}^{\text{R}}$	Load reduction capacity of DRA k , (MWh)
E_k^{F}	Flexible load minimum requirement of DRA k , (MWh)
$u_{k,b,t}$	Marginal utility of demand block b of DRA k , (\$/MWh)
$D_{k,b,t}^{\text{F,max}}$	Maximum load of demand block b of DRA k , (MW)
$R_k^{\text{U}}, R_k^{\text{D}}$	Ramping Up/Down limits of flexible load of DRA k , (MW)
$D_{k,t,s}^{\text{I}}$	Inflexible load of aggregator k , (MW)
$P_{k,t,s}^{\text{G,max}}$	Maximum aggregated renewable DG power of DRA k , (MW)
P_k^{max}	Maximum power bidding of DRA k , (15MW)
Variables	
P_t^{DA}	DA power bidding, (MW)
$P_{t,s}^{\text{RT}}$	RT power dispatch, (MW)
$D_{k,t,s}^{\text{F}}$	Flexible load power consumption of DRA k , (MW)
$D_{k,b,t,s}^{\text{F}}$	Flexible load power consumption at block b of DRA k , (MW)
$U_{k,t,s}$	Utility of flexible load of DRA k , (\$)
$P_{k,t,s}^{\text{G}}$	Renewable DG power of DRA k , (MW)
$D_{k,t,s}^{\text{R}}$	Reducible load of DRA k , (MW)
ξ, η_s	Auxiliary variables used to calculate CVaR

5.4 System Model

5.4.1 Cooperative Demand-Side Resource Aggregator under Virtual Power Plant

We consider a set of cooperative DRAs [29] coordinated by a commercial *virtual power plant* (VPP) [31] as shown in Figure 5.1. The commercial VPP [50] manages the output of on-site distributed renewable energy generators, energy consumption of flexible loads, deploys load reduction services, and satisfies nonflexible load demands of multiple cooperative DRAs [29]. Each DRA can be considered as a cluster of several types of load, namely nonflexible load, flexible load, reducible load, and distributed renewable energy sources such as rooftop solar panels and wind turbines [29]. Nonflexible load is the one whose energy consumption cannot be deferred [16, 29]. The flexible load is modeled by a multi-block utility function widely adopted in the literature [14, 28, 42, 44–46]². The DRA can employ various load reduction services including load curtailment, back-up generator, and battery which are captured via “reducible load” [10]. Detailed load reduction modeling is not considered for simplicity [10].

²Other flexible load models such as energy aggregation [29], EV aggregator [24], HVAC aggregator [16], load elastic model [51–53] and their uncertainties can be integrated into the model, which will be considered in our future work.

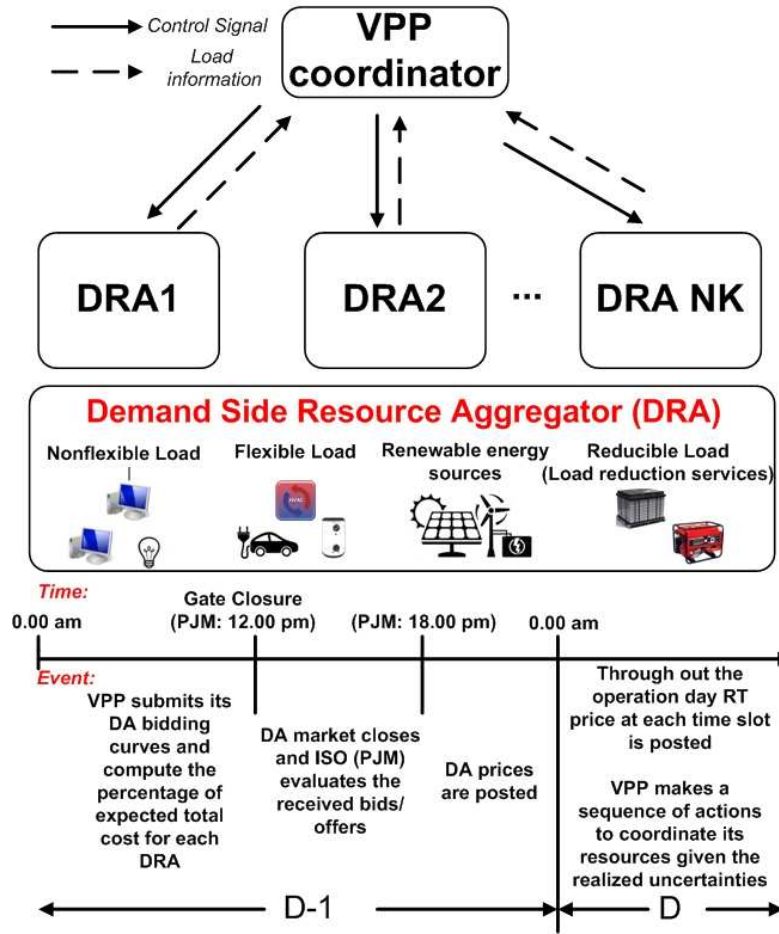


Figure 5.1 – Schematic of cooperative DRAs under the VPP’s coordination

5.4.2 Market Framework

All DRAs are coordinated via a commercial VPP [50], which participates in the short-term two-settlement electricity market including the wholesale day-ahead (DA) and the real-time (RT) markets [24, 29] as a single entity [31]. The VPP is assumed to act as a price taker [31] and the bids do not affect the DA/RT clearing prices [24, 29, 31]. Unidirectional interaction with the grid is adopted [24], i.e., we can bid to purchase but cannot sell surplus energy to the grid [24, 29, 30]. The uniform pricing rule and two-settlement system are used to model the financial settlement of DA and RT energy deliveries [24]. In particular, the market participant pays [24, 29]:

$$\Delta T \lambda_{t,s}^{\text{DA}} P_t^{\text{DA}} + \Delta T \lambda_{t,s}^{\text{RT}} (P_{t,s}^{\text{RT}} - P_t^{\text{DA}}),$$

where $\Delta T (P_{t,s}^{\text{RT}} - P_t^{\text{DA}})$ represents the energy deviation between DA bidding and RT dispatch. In addition, the total cost of VPP or coalitions of DRAs must include the penalty cost of energy bidding deviation [24], the load reduction services’ cost [10], and the flexible load utility [42], which will be presented in Section IV. Detailed description of the considered market framework is presented in [24].

5.4.3 Cost Allocation Procedure

Previous days’ data including market prices and each DRA’s nonflexible energy consumption, renewable energy are available. Each DRA also needs to aggregate and submit its load reduction services’

capacity and price, and flexible load parameters to the VPP [30, 42]. The VPP makes decisions on the joint bidding strategy, i.e., the DA bidding decisions before the stochastic scenario materializes [29, 31]³, and determines the cost share of each DRA.

In this study, the bidding strategy is modeled as risk averse two-stage stochastic program widely used in electricity market bidding strategy [2]:

$$v(\mathcal{K}) = \min (1 - \beta) \mathbf{E}(\text{Cost}) + \beta \text{CVaR}_\alpha(\text{Cost}),$$

where $\mathbf{E}(\text{Cost})$ is the expected cost and $\text{CVaR}_\alpha(\text{Cost})$ is its Conditional Value at Risk (CVaR) at α confidence level, α often takes value from 0.9 to 0.99 [76]. CVaR is employed as a risk measure since it has been widely used in the literature [2, 29, 43, 75, 76] to control the tradeoff between the expected cost and the cost variation given its advantages over other risk measures (e.g., variance, shortfall probability, expected shortage, value-at-risk) [2]. When uncertainties are captured by scenarios, CVaR_α is defined approximately as the expected cost over the $(1 - \alpha) \times 100\%$ worst scenarios [2]. The weight β represents the tradeoff between the expected cost and CVaR.

The resulting bidding cost $v(\mathcal{K})$ must be split among the participants, i.e., the VPP needs to allocate each DRA's percentage quota $x_k(\%)$ of total expected bidding cost $v(\mathcal{K})$ before the planning horizon begins:

$$\sum_{k=1}^{\text{NK}} x_k = 1 \text{ (100\%)}, x_k \geq 0.$$

Hence, the expected cost that is allocated to each DRA is equal to $x_k v(\mathcal{K})$. The cost allocation problem, i.e., the determination of x_k , is addressed by using the cooperative game theory [54].

5.4.4 Uncertainties Modeling

Uncertainties of renewable energy, nonflexible load, and electricity prices are captured via scenarios, which are generated by using the Monte Carlo simulation approach [107]. The VPP employs appropriate forecasting tools to forecast renewable energy, nonflexible load, and market prices based on available historical datasets with high accuracy. This task can be achieved by employing certain forecasting methods such as time series prediction, artificial neural networks, and support vector machines [2], whose detailed design is outside the scope of this thesis. Since any forecasting technique can suffer from inevitable forecasting errors [2], an efficient model for forecasting errors should be based on the studied datasets. We assume that the VPP can achieve a reliable modeling of uncertainties by fitting the forecasting error data into appropriate distributions or time series based on the historical data and forecast data over a sufficiently long period [2, 43].

Modeling forecasting errors, which is an important research topic [2], is not the focus of this study. In this study, for simplicity, the forecast errors of DA, RT prices, renewable energy, and nonflexible load are assumed to follow zero-mean normal distributions whose standard deviations are 10%, 10%, 15%, and 10% of the forecast values, respectively [43]. Note that the assumption that forecasting errors of system load [65, 140], renewable energy [65, 139–142], and electricity prices [140, 142] follow normal distributions is widely adopted in the literature. We further assume the system uncertainties are independent [139, 142]. This assumption is also adopted in [142] where the authors conduct their study on the same dataset [143] used in this chapter. Note, however, that considerations of other distributions (e.g., Weibull distribution for wind speed) or the correlation among different uncertainties [66]

³PJM time line: <http://pjm.com//media/training/nerc-certifications/EM3-twosettlement.ashx>

can be easily integrated into our proposed cost allocation framework by applying a suitable sampling technique in the scenario generation procedure [2, 141].

5.5 Problem Formulation

In this study, we model the cost allocation for a VPP that consists of NK DRAs as a cooperative game with transferable utility $\mathcal{G}(\mathcal{K}, v)$. The cost function v is modeled as the optimal cost value achieved by a risk averse bidding optimization in the electricity market and the percentage quota $x_k(\%)$ of the total VPP's bidding cost $v(\mathcal{K})$ is considered as the solution of the studied cooperative game.

5.5.1 Cost Function

The cost function $v(S)$ of a coalition S of DRAs can be defined as follows:

$$v(S) = v(e^S) = \min_{P_t^{\text{DA}}, P_{t,s}^{\text{RT}}, D_{k,t,s}^F, D_{k,b,t,s}^F, U_{k,t,s}, P_{k,t,s}^G, D_{k,t,s}^R, \xi, \eta_s} (1-\beta) \sum_{s=1}^{\text{NS}} \pi_s \sum_{t=1}^{\text{NT}} \left\{ \lambda_{t,s}^{\text{DA}} P_t^{\text{DA}} \Delta T + \lambda_{t,s}^{\text{RT}} (P_{t,s}^{\text{RT}} - P_t^{\text{DA}}) \Delta T + \lambda^p |P_{t,s}^{\text{RT}} - P_t^{\text{DA}}| \Delta T + \sum_{k=1}^{\text{NK}} (\lambda_k^r D_{k,t,s}^R \Delta T - U_{k,t,s}) \right\} + \beta \left(\xi + \frac{1}{1-\alpha} \sum_{s=1}^{\text{NS}} \pi_s \eta_s \right). \quad (5.1)$$

The cost function value obtained from (5.1) results from the risk averse expected cost minimization of a coalition S consisting of individual DRAs $k \in S$ participating in the two-settlement electricity market. It is the weighted sum of the expected cost of market bidding and the CVaR (the last term) which are multiplied with coefficients $1 - \beta$ and β , respectively. The expected market bidding's cost includes the energy trading costs in DA market $\lambda_{t,s}^{\text{DA}} P_t^{\text{DA}} \Delta T$, RT market $\lambda_{t,s}^{\text{RT}} (P_{t,s}^{\text{RT}} - P_t^{\text{DA}}) \Delta T$, plus penalty cost due to mismatch between DA bidding and RT dispatch $\lambda^p |P_{t,s}^{\text{RT}} - P_t^{\text{DA}}| \Delta T$ [24, 29], plus the cost of using load reduction minus flexible load's utility $\sum_{k=1}^{\text{NK}} (\lambda_k^r D_{k,t,s}^R \Delta T - U_{k,t,s})$ [10, 42]. These cost components are calculated over NT time slots and NS generated scenarios where π_s is the probability of scenario s . Note that although this formulation can be applied to a coalition S with up NK aggregators, only the values of individual DRAs $k \in S$ are activated based on the values of e_k^S , i.e., $e_k^S = 0$ if $k \notin S$, as will be explained later. This optimization is subject to the following constraints.

Constraints of Flexible Load

Each DRA k can aggregate various flexible load, which can be modeled by the multi-block utility function [14, 28, 42, 44–46], as follows:

$$U_{k,t,s} = \Delta T \sum_{b=1}^{\text{NB}_k} u_{k,b,t} D_{k,b,t,s}^F, \quad (5.2)$$

$$D_{k,t,s}^F = \sum_{b=1}^{\text{NB}_k} D_{k,b,t,s}^F, \quad 0 \leq D_{k,b,t,s}^F \leq D_{k,b,t}^{\text{max}} e_k^S, \quad (5.3)$$

$$D_{k,t,s}^F - D_{k,t-1,s}^F \leq R_k^U, \quad D_{k,t-1,s}^F - D_{k,t,s}^F \leq R_k^D e_k^S, \quad (5.4)$$

$$\Delta T \sum_{t=1}^{\text{NT}} D_{k,t,s}^F \geq E_k^F e_k^S. \quad (5.5)$$

Constraint (5.2) calculates the flexible load's utility of DRA k at each time slot t and scenario s . The constraint corresponding to each demand block b is given in (5.3). Ramping up and down constraints are captured in (5.4). The temporal constraint (5.5) means that the energy consumption of the total flexible load over the scheduling horizon must be greater than a predefined minimum value E_k^F . Detailed description and how to construct the considered flexible load model can be found in [42].

Note that for any DRA $k \notin S$, we have $e_k^S = 0$, then the condition $0 \leq D_{k,b,t,s}^F \leq D_{k,b,t}^{F,\max} e_k^S$ in (5.3) is satisfied because $D_{k,b,t,s}^F = 0$, which results in $D_{k,t,s}^F = \sum_{b=1}^{NB_k} D_{k,b,t,s}^F = 0$. Consequently, we have $U_{k,t,s} = 0$ according to (5.2), which means its value is not counted in the objective function (5.1). Moreover, constraints (5.4) and (5.5) for $k \notin S$ are always satisfied and they will not affect the feasible region of the underlying optimization problem. In other words, the DRA k 's flexible load constraints (5.2)-(5.5) for $k \notin S$ are not activated since they do not affect the objective function (5.1) and the power balance constraint (5.8) given later. That means we exclude the flexible load constraints (5.2)-(5.5) for DRAs $k \notin S$ and only consider the constraints of $k \in S$ in computing $v(S)$.

Constraint of Reducible Load

Each DRA can utilize several load reduction services which can be considered as a negative load behind the meters [10]. We assume that in each time slot, the amount of energy consumption reduction of DRA k can be upper-bounded by a certain aggregated load reduction value $E_{k,t,s}^R$, which is charged at the price λ_k^r . In particular, we have

$$0 \leq D_{k,t,s}^R \Delta T \leq E_{k,t,s}^R e_k^S. \quad (5.6)$$

Similarly, for DRA $k \notin S$, $e_k^S = 0$ then $D_{k,t,s}^R = 0$ and it does not affect the power balance constraint (5.8). It can be interpreted that only constraint (5.6) for DRA $k \in S$ is considered for the computation of $v(S)$ while constraint (5.6) for DRA $k \notin S$ is not activated.

Constraint of DGs

Renewable energy resources can be aggregated by the DRAs [29]. Similar to the reducible load, aggregated renewable DGs can be considered as a negative load behind the meters. We assume that renewable energy is free of charge (the price of renewable energy is 0). Moreover, the time-varying maximum generation profile of DRA's total renewable energy, which can be forecast and captured by scenarios, is denoted as $P_{k,t,s}^{G,\max}$. Then, the actual output of distributed generators in scenario s can be controlled by the DRA ranging from 0 to $P_{k,t,s}^{G,\max}$ as follows [29]:

$$0 \leq P_{k,t,s}^G \leq P_{k,t,s}^{G,\max} e_k^S. \quad (5.7)$$

Again, for DRA $k \notin S$, $e_k^S = 0$ then $P_{k,t,s}^G = 0$ and it does not affect power balance constraint (5.8). It can be interpreted equivalently as DRA k 's constraint (5.7) is not activated, i.e., $P_{k,t,s}^G$ is not considered in the computation of $v(S)$.

Power Balance Constraints

These constraints can be expressed as

$$P_{t,s}^{\text{RT}} = \sum_{k=1}^{\text{NK}} \left(D_{k,t,s}^I e_k^S + D_{k,t,s}^F - D_{k,t,s}^R - P_{k,t,s}^G \right) \quad (5.8)$$

$$0 \leq P_t^{\text{DA}}, P_{t,s}^{\text{RT}} \leq \sum_{k=1}^{\text{NK}} P_k^{\text{max}} e_k^S. \quad (5.9)$$

Constraint (5.8) describes the power balance constraint in real time dispatch while constraint (5.9) represents the unidirectional power constraint on P_t^{DA} and $P_{t,s}^{\text{RT}}$ [24, 29]. Similarly, constraint (5.8) only considers $k \in S$ since $e_k^S = 0$ for $k \notin S$.

CVaR Constraints

The CVaR constraints can be written according to the Rockafellar and Uryasev formula as follows [2, 29, 43]:

$$\eta_s \geq \Delta T \sum_{t=1}^{\text{NT}} \left\{ \lambda_{t,s}^{\text{DA}} P_t^{\text{DA}} + \lambda_{t,s}^{\text{RT}} \left(P_{t,s}^{\text{RT}} - P_t^{\text{DA}} \right) + \lambda^p \left| P_{t,s}^{\text{RT}} - P_t^{\text{DA}} \right| + \sum_{k=1}^{\text{NK}} \left(\lambda_k^r D_{k,t,s}^R - U_{k,t,s} \right) \right\} - \xi \quad (5.10)$$

$$\eta_s \geq 0. \quad (5.11)$$

5.5.2 Bi-objective Optimization Based Core Cost Allocation

In this study, the form of the cost functions $v(S) = v(e^S)$ is defined as the optimum of a linear program where the entire right-hand-side vector due to all constraints is a linear transformation of coalition indication vector e^S [112]. This is a LP game, which is totally balanced and has a nonempty core [55]. The nonempty core by definition (2.29) is a polyhedron with $\text{NK}-1$ dimensions, which can contain many potential cost allocation vectors x . In particular, different allocation vectors x might result in different allocation performance with respect to some allocation metrics [54]. An arbitrary allocation x in the core can correspond to a *weak stable* solution since some coalitions attain very small or zero cost saving value and they might not receive significant benefits to stay in the cooperation [54]. It might also be *unfair* since some DRAs have larger percentage cost reduction than others [54].

Therefore, an efficient design must address two main issues mentioned above, namely stability and fairness. In particular, the stability and fairness metrics employed to design an efficient cost allocation strategy are described as follows:

- *Stability metric*: captures the minimal satisfaction, i.e., the worst-case cost saving $\delta(\$)$ among all coalitions S . Although a cost allocation vector x in the core $\mathcal{C}(v)$ guarantees non-negative cost saving among S , i.e., $v(S) - \sum_{k \in S} x(s) v(\mathcal{K}) \geq 0$, some coalitions S have less cost saving than others and the worst coalition will have very small cost saving, which is denoted as $\delta(\$)$. In particular, different values of x result in different values of δ , which implies different levels of stability [54]
- *Fairness metric*: captures the maximum deviation of the percentage cost saving among individual DRAs which is the difference in percentage cost saving $\gamma(\%)$ between the DRA that achieves the highest percentage cost saving and the DRA that achieves smallest percentage cost saving for a given allocation vector $x \in \mathcal{C}(v)$ [54]. Obviously, different x result in different values of γ , which implies different levels of fairness [54]

In summary, to achieve good *stability*, the worst-case cost saving δ among all coalitions S should be maximized and to achieve good *fairness* for the cost allocation, the maximum deviation for the percentage cost saving of individual DRAs γ should be minimized simultaneously. Moreover, the cost allocation solution must lie in the core of the game. The core cost allocation design aims to find a cost allocation vector $x \in \mathcal{C}(v)$ that achieves efficient tradeoff between the fairness and stability metrics, which can be modeled as a bi-objective optimization problem as follows:

(P0)

$$\min_{\overline{\Phi}, \underline{\Phi}, \delta, x_k, \gamma} \gamma \quad (5.12)$$

$$\min_{\delta, x_k} -\delta \quad (5.13)$$

$$\text{s.t: } \sum_{k=1}^{\text{NK}} x_k = 1, x_k \geq 0, \quad (5.14)$$

$$\delta \leq v(S) - \sum_{k \in S} x_k v(\mathcal{K}), \forall S \in 2^{\text{NK}} \setminus \{\emptyset, \mathcal{K}\} \quad (5.15)$$

$$\delta \geq 0 \quad (5.16)$$

$$\underline{\Phi} \leq x_k \frac{v(\mathcal{K})}{v(\{k\})} \leq \overline{\Phi}, \forall k \in \mathcal{K} \quad (5.17)$$

$$\gamma = \overline{\Phi} - \underline{\Phi}, \quad (5.18)$$

where the optimization of the objective functions (5.12)-(5.13), which minimizes the valued vector $[\gamma, -\delta]$, aims to achieve the fairness and stability, respectively. Moreover, constraint (5.14) means that the total cost (in fraction) is distributed among all DRAs while the auxiliary variable δ in (5.15) provides the lower bound of the cost saving of all coalitions S under cost allocation solution x . The minimal satisfaction, i.e., the worst-case cost saving δ (\$) among all coalitions S is maximized in (5.13). The constraint (5.16) forces the allocation to be in the core $x \in \mathcal{C}(v)$ while constraint (5.17) provides the lower bound $\underline{\Phi}$ and upper bound $\overline{\Phi}$ for the ratio between allocated cost under grand coalition and cost due to the non-cooperative scenario for all DRAs k (i.e., the cost percentage saving). The maximum deviation γ of the percentage cost saving of individual DRAs, which is the difference of $\underline{\Phi}$ and $\overline{\Phi}$ as in (5.18), is minimized in (5.12).

Fairness Core Allocation

We define problem (P1) as the one with objective (5.12) and the core constraints (5.14)-(5.18). It is indeed the percentage fairness core allocation problem [54]. Without constraints (5.15)-(5.16), the fairness core allocation becomes the *proportional allocation* [54] where the optimum $\gamma^* = 0$, i.e., each DRA k is allocated $x_k = v(\{k\}) / \sum_{k'=1}^{\text{NK}} v(\{k'\})$ fraction of $v(\mathcal{K})$, and the cost saving in percentage is distributed equally to each DRA. In contrast, simply maintaining the core characteristics (2.29) can cause some deviation in percentage cost saving among DRAs, i.e., $\gamma > 0$. In short, the problem (P1) is defined as follows:

(P1)

$$\min_{\bar{\Phi}, \Phi, \delta, x_k, \gamma} \gamma$$

s.t: constraints (5.14) - (5.18).

Nucleolus Allocation

We denote problem (P2) as the one with objective (5.13) and constraints (5.14)-(5.15). It is indeed the nucleolus allocation problem which aims at maximizing the cooperation's stability by maximizing the minimal satisfaction, i.e., the worst case cost saving δ among all coalitions [54, 98]. Constraint (5.16) is unnecessary since the non-empty core contains the nucleolus [54]. The problem (P2) can be defined as follows:

(P2)

$$\max_{\delta, x_k} \delta$$

s.t: constraints (5.14)- (5.15).

It is worth to mention that stability and fairness cannot be achieved at the same time, which motivates the bi-objective optimization framework in this thesis. The nucleolus aims to maximize the worst case cost saving $\delta(S^*)$ among all coalitions S by reducing the cost allocated to members belong to S^* . This results in the increase of cost saving in percentage for DRA $k \in S^*$, which results in the deterioration of fairness, i.e., the increase of γ . On the other hand, improving fairness, i.e., minimizing γ , only requires the positive value of δ as shown in constraint (5.16). This results in a very small positive value of δ in the fairness core allocation. Mathematically speaking, the fairness core and the nucleolus are different points located in the core $\mathcal{C}(v)$. In general, solving the cost allocation problems with different designed objectives will result in different allocation vectors since the core is a polyhedron with dimension $NK - 1$.

5.6 Solution Approach

5.6.1 The ε -Constraint Approach

The core cost allocation problem (P0), which is a bi-objective linear program, has no single optimal solution optimizing both objective functions (5.12) and (5.13) simultaneously. Intuitively, to maximize the worst case cost saving δ (minimize $-\delta$) as in (5.13), we need to allocate less cost share to the DRAs belonging to the coalition S that has the least cost saving, which results in higher deviation among the percentage cost saving of individual DRAs. Mathematically speaking, the allocation vector that maximizes the stability metric (the nucleolus) and the allocation vector that has the best fairness performance are two different points in the polyhedron $\mathcal{C}(v)$. Hence, it is desirable to determine Pareto optimal solutions where for each of such solutions one cannot improve the value of one objective function without deteriorating the value of the other objective function [56].

To obtain Pareto optimal points, we propose to convert problem (P0) into a single-objective optimization problem (P3) using the ε -constraint method [56] since problem (P0) is linear. In particular, there are two main methods to solve the multi-objective linear optimization, namely, the ε -constraint

and scalar (weighted) methods. The ε -constraint method has several advantages over the scalar method for linear problems [122]. Hence, the ε -constraint method is adopted.

In the ε -constraint method, one objective function is chosen to be optimized while the other is converted into a constraint [56]. It can be observed that γ involves only NK fairness constraints (5.17) where $v(\{k\})$ and $v(\mathcal{K})$ can be pre-computed easily. On the other hand, δ involves $2^{\text{NK}} - 2$ values of $v(S)$ in (5.15). Hence, the stability objective function (5.13) is chosen to be optimized while the fairness objective (5.12) is converted into a constraint. Let $M + 1$ be the number of grid points of the Pareto front and $m \in \{0, 1, \dots, M\}$. Then, the m^{th} point on the Pareto front can be obtained by solving the following single-objective optimization problem:

(P3)

$$\begin{aligned} & \max_{\Phi, \underline{\Phi}, \delta, x_k, \gamma} \delta \\ \text{s.t:} & \text{ constraints (5.14)-(5.15), (5.17)-(5.18)} \\ & \gamma \leq \gamma^m, \end{aligned} \quad (5.19)$$

where γ^m is a parameter defining the m^{th} point on the Pareto front. In particular, γ^m is chosen as $\gamma^{\min} \leq \gamma^m \leq \gamma^{\max}$. γ^{\min} and γ^{\max} can be obtained from the payoff table when we solve (P1), which minimizes the maximum deviation of the percentage cost saving γ^{\min} , and (P2), which finds the nucleolus allocation solution with δ^{\max} , respectively. The payoff table contains the 0^{th} point, $(\gamma^{\min}, \delta^{\min})$, and the M^{th} point, $(\gamma^{\max}, \delta^{\max})$. In this study, the parameter γ^m identifying m^{th} is chosen as follows:

$$\gamma^m = \gamma^{\min} + m \frac{\gamma^{\max} - \gamma^{\min}}{M}. \quad (5.20)$$

Note that constraint (5.16) is unnecessary and ignored in (P3) since constraint (5.20) implies the intersection of its feasible region and the core is non-empty.

5.6.2 The Row Constraint Generation Approach

In order to construct the Pareto front, we need to solve (P1) and (P2) to obtain the payoff table first, which indicates the 0^{th} and M^{th} points. Then, we solve problem (P3) multiple times, each corresponding to one value of m to obtain the remaining $M - 1$ points (i.e., points $(\gamma(m), \delta(m))$, $m = 1, 2, \dots, M - 1$). All three problems (P1), (P2), and P(3) are *large-scale LPs* subject to stability constraints (5.15). The full set of stability constraints (5.15) requires the pre-calculation of $2^{\text{NK}} - 2$ values of $v(S)$ for all coalitions S which are results of the corresponding stochastic programs. Many constraints in (5.15) are indeed unnecessary, i.e., we do not need all these $2^{\text{NK}} - 2$ constraints to determine only NK variables x_k .

To reduce the complexity, we employ the row constraint generation method to solve problems (P1), (P2), and (P3) without imposing all aforementioned $2^{\text{NK}} - 2$ constraints in (5.15). This is realized by decomposing each problem into a master problem, which is solved to find the allocation vector x^* , and a sub-problem, which is solved to find the coalition S^* that can violate the stability constraint with the obtained x^* the most. Then, the stability constraint corresponding to S^* is added to the master problem. The problem is solved iteratively until no coalition's stability constraint is found to be violated.

Solving Problem (P1)

The master problem (MP1) is a relaxed version of the original problem (P1). Let $\mathcal{O}(S)$ be the set of coalitions considered in the current iteration and their values $v(S)$ are already known (in the first iteration, we initialize $\mathcal{O}(S) = \{\{1\}, \{2\}, \dots, \{NK\}\}$), problem (MP1) can be cast as the following LP:

(MP1)

$$\min_{\bar{\Phi}, \underline{\Phi}, \delta, x_k, \gamma} \gamma$$

s.t: constraints (5.14), (5.16), (5.17), (5.18):

$$\text{relaxed (5.15): } \delta \leq v(S) - \sum_{k \in S} x_k v(\mathcal{K}), \forall S \in \mathcal{O}(S). \quad (5.21)$$

Constraint (5.15) is replaced by its relaxed version (5.21), which only considers $S \in \mathcal{O}(S)$ instead of $\forall S$ in the set of all $2^{\text{NK}} - 2$ coalitions. Hence, for a given x^* obtained from solving (MP1), there are many coalitions S that can violate the stability constraint (5.15) of problem (P1). In addition, $v(S)$ is implicit since it is the optimal value of the objective function of the stochastic program (5.1), which has not been solved yet. We need to design sub-problems, which identify a unique S^* and its corresponding value $v(S^*)$ [144]. We define a sub-problem (SP1) identifying a unexplored coalition S^* that achieves the least cost reduction as follows:

(SP1)

$$\begin{aligned} \underline{\delta} = \min & \left[v(S) - \sum_{k=1}^{\text{NK}} e_k^S x_k^* v(\mathcal{K}) \right] = \min_{e_k^S, P_t^{\text{DA}}, P_t^{\text{RT}}, D_{k,t,s}^{\text{F}}, D_{k,b,t,s}^{\text{F}}, U_{k,t,s}, P_{k,t,s}^{\text{G}}, D_{k,t,s}^{\text{R}}, \xi, \eta_s} \\ & (1-\beta) \sum_{s=1}^{\text{NS}} \pi_s \sum_{t=1}^{\text{NT}} \left\{ \lambda_{t,s}^{\text{DA}} P_t^{\text{DA}} \Delta T + \lambda_{t,s}^{\text{RT}} (P_{t,s}^{\text{RT}} - P_t^{\text{DA}}) \Delta T + \lambda^p |P_{t,s}^{\text{RT}} - P_t^{\text{DA}}| \Delta T + \sum_{k=1}^{\text{NK}} (\lambda_k^{\text{R}} D_{k,t,s}^{\text{R}} \Delta T - U_{k,t,s}) \right\} \\ & + \beta \left(\xi + \frac{1}{1-\alpha} \sum_{s=1}^{\text{NS}} \pi_s \eta_s \right) - \sum_{k=1}^{\text{NK}} e_k^S x_k^* v(\mathcal{K}) \end{aligned} \quad (5.22)$$

$$\text{s.t: } 1 \leq \sum_{k=1}^{\text{NK}} e_k^S \leq \text{NK} - 1, e_k^S \in \{0, 1\} \quad (5.23)$$

$$\sum_{k \in S} (1 - e_k^S) + \sum_{k \notin S} (e_k^S) \geq 1, \forall S \in \mathcal{O}(S) \quad (5.24)$$

$$\text{constraints (5.2)-(5.11).} \quad (5.25)$$

The sub-problem (SP1) is a mixed integer linear program (MILP) with extra binary variables e_k^S acting as first-stage variables. Solving (SP1) enables us to obtain e^{S^*} , which give S^* and $v(S^*)$ simultaneously.

The purpose of solving problem (SP1) is to *identify the unexplored $S^* \notin \mathcal{O}(S)$ that can potentially violate the core stability constraint the most for a given cost allocation vector x^* (i.e., S^* has least cost reduction)*. Constraint (5.23), which means $S \in 2^{\text{NK}} \setminus \{\emptyset, \text{NK}, \mathcal{O}(S)\}$, and constraint (5.24), which means $S \notin \mathcal{O}(S)$, ensures only unexplored coalitions S are considered in this optimization problem. All original constraints required in computing $v(S)$ are given in (5.25).

If we solve (MP1) and (SP1) iteratively as summarized in Algorithm 1, we finally reach x^* such that $\underline{\delta} \geq 0$ since the core is nonempty. Then, γ is minimized and the obtained $x^* \in \mathcal{C}(v)$ is the final cost allocation solution for (P1). We provide the proof of convergence for Algorithm 1 in the following.

Proof. The proof is based on the result in [144], which is summarized as follows. As (MP1) is the relaxed version of (P1), its obtained solution x^* can be infeasible for (P1). However, if x^* is feasible for (P1), it will be the optimal solution of (P1).

Algorithm 1 SOLVING PROBLEM P1

-
- 1: Initialization: iteration $i_1 = 0$, compute $v(\mathcal{H})$ and $v(\{k\})$, $\mathcal{O}(S) = \cup_{k=1}^{NK} \{k\}$
 - 2: **while** $\underline{\delta} < 0$ **do**
 - 3: Solve (MP1) to obtain x^* to feed it to (SP1)
 - 4: Solve (SP1) to obtain S^* , $v(S^*)$,
 - 5: Update $\mathcal{O}(S) := \mathcal{O}(S) \cup S^*$, $i_1 = i_1 + 1$
 - 6: **end while**
-

Suppose at iteration i_1 , we have $\mathcal{O}(S)$ and obtain x^* after solving (MP1). Let S^* denote the optimal solution of (SP1). If we have

$$\underline{\delta} = v(S^*) - \sum_{k \in S^*} x_k^* v(\mathcal{H}) < 0, \quad (5.26)$$

then the following condition of (P1) is not satisfied by x^* :

$$0 \leq \delta \leq v(S^*) - \sum_{k \in S^*} x_k^* v(\mathcal{H}),$$

which means the obtained solution is not in the core, i.e., $x^* \notin \mathcal{C}(v)$. To move the obtained allocation solution x^* towards the feasible region of (P1) in future iterations, a new constraint corresponding to S^* is added to constraint (5.21) of (MP1), i.e., S^* is added to $\mathcal{O}(S)$ as follows:

$$\delta \leq v(S^*) - \sum_{k \in S^*} x_k v(\mathcal{H}). \quad (5.27)$$

In the next iteration, solving (MP1) will generate a new x^* and solving (SP1) will generate a new S^* . Since the size of $\mathcal{O}(S)$ increases, the number of coalitions $S \notin \mathcal{O}(S)$ considered by (SP1) is reduced after each iteration. Hence, the maximum number of iterations is bounded by $2^{NK} - 2 - NK$. Since the core is nonempty, we can ultimately find x^* that satisfies constraint (5.15) and constraint (5.16) of (P1) for $\forall S$. Hence, Algorithm 1 converges. \square

Solving Problem (P2)

Similarly, the master problem (MP2) which is a relaxed version of the original problem (P2) can be defined as the following LP:

(MP2)

$$\max_{x_k, \delta} \delta$$

s.t: constraints (5.14) and (5.21).

We define a new sub-problem (SP2) identifying a coalition S^* that achieves the least cost reduction as follows:

Algorithm 2 SOLVING PROBLEM P2/P3

-
- 1: Initialization: iteration $i_2 = 0/i_3 = 0$, initialize $\mathcal{O}(S)$ (and γ^m for P3)
 - 2: **while** $|\delta^* - \underline{\delta}| \leq \varepsilon_\delta$ **do**
 - 3: Solve (MP2)/(MP3) to obtain x^* and δ^* , feed x^* to (SP2)
 - 4: Solve (SP2)/(SP3) to obtain S^* , $v(S^*)$, and $\underline{\delta}$
 - 5: Update $\mathcal{O}(S) := \mathcal{O}(S) \cup S^*$, $i_2 = i_2 + 1$ / $i_3 = i_3 + 1$
 - 6: **end while**
-

(SP2-3)

$$\underline{\delta} = \min \left[v(S) - \sum_{k=1}^{NK} e_k^S x_k^* v(\mathcal{K}) \right]$$

$$\text{s.t: } 1 \leq \sum_{k=1}^{NK} e_k^S \leq NK - 1, e_k^S \in \{0, 1\}$$

constraints (5.2)-(5.11). (5.28)

Sub-problem (SP2) is the same with sub-problem (SP1) except that the constraint (5.24) has been removed. Problem (SP2) is solved to *find* S^* that can potentially violate the core stability constraint the most for a given cost allocation vector x^* (S^* has the least cost reduction $\underline{\delta}$) over the set $2^{NK} \setminus \{\emptyset, NK\}$. Problem (P2) is solved by Algorithm 2. Due to numerical precision of commercial solvers, the stopping conditions are relaxed as $|\delta^* - \underline{\delta}| \leq \varepsilon_\delta$ where ε_δ is a tolerance threshold and the obtained cost allocation vector x^* is the final cost allocation solution of (P2), i.e., the nucleolus x^M .

The convergence proof for this algorithm is also based on the result in [144], which is similar to the proof of Algorithm 1 presented above. In particular, the difference between (SP1) and (SP2) is due to the removal of (5.24). However, it is easy to show that the (SP2) never regenerates explored $S \in \mathcal{O}(S)$ except at convergence, which means the maximum number of iterations is also bounded and Algorithm 2 must converge. Detailed convergence proof of Algorithm 2 is omitted due to page limitation.

Solving Problem (P3)

Similarly, the master problem (MP3) which is a relaxed version of the original problem (P3) can be defined as the following LP:

(MP3)

$$\max_{x_k, \delta, \gamma, \Phi, \underline{\Phi}} \delta$$

$$\text{s.t: } \text{constraints (5.14), (5.17), and (5.18)}$$

$$\text{constraint (5.19) of } m^{\text{th}} \text{ grid point,}$$

$$\text{constraint (5.21).}$$

Constraint (5.15) is replaced by (5.21), which is updated by adding S^* obtained by solving the sub-problem (SP3) to the set of explored coalitions $\mathcal{O}(S)$ in each iteration. (SP3) is the same with (SP2). Similarly, if we solve (MP3) and (SP3) iteratively as shown in Algorithm 2, we finally reach

Algorithm 3 PARETO-FRONT CONSTRUCTION

-
- 1: Run scenario generation/reduction algorithms to obtain the NS scenarios s , Compute $v(\mathcal{K})$ and $v(\{k\})$, $\mathcal{O}(S) = \cup_{k=1}^{\text{NK}} \{k\}$
 - 2: Solve P1 using Algorithm 1 to obtain γ^{\min} , $\delta(0) := \underline{\delta}$, $x(0) := x^*$. The 0th point is then determined. Keep $\mathcal{O}(S)$
 - 3: Solve P2 using Algorithm 2 to obtain δ^M , $\delta(0) := \underline{\delta}$, $x(0) := x^*$. The M^{th} point is then determined. Keep $\mathcal{O}(S)$
 - 4: **for** $m = 1, 2, \dots, M - 1$ **do**
 - 5: Solve P3 using Algorithm 2 with γ^m defined in (5.20) to obtain x^* , δ^* . Keep $\mathcal{O}(S)$
 - 6: Update $x^m := x^*$, $\delta^m := \delta^*$, and m^{th} point is defined.
 - 7: $\text{NI} = \text{Card}(\mathcal{O}(S)) - \text{NK}$
 - 8: **end for**
 - 9: Construct the Pareto-front from the obtained $M + 1$ points.
-

$|\delta^* - \underline{\delta}| \leq \varepsilon_\delta$ and the obtained cost allocation vector x^* is the final cost allocation solution of (P3) corresponding to γ^m .

The sub-problems (SP1), (SP2), (SP3) are *stochastic programs where the uncertainties are captured via scenarios*. To manage the computation complexity, the scenario reduction method can be employed [107]. Discussion on scenario based stochastic optimization can be found in [31, 43]. The resulting MILP with a reduced number of scenarios can be solved efficiently by using available MILP solvers such as CPLEX.

Pareto Front Construction

The complete procedure to construct the Pareto front of the core cost allocation problem (P0) is summarized in Algorithm 3. Specifically, we first calculate the VPP's bidding cost $v(\mathcal{K})$ and initialize $\mathcal{O}(S) = \cup_{k=1}^{\text{NK}} \{k\}$, i.e., compute NK individual bidding cost $v(k)$, NI. The fairness core cost allocation problem (P1) is solved by iteratively solving (MP1) and (SP1) as shown in Algorithm 1. Then the nucleolus allocation problem (P2) is solved by solving (MP2) and (SP2-3) iteratively as shown in Algorithm 2. Then, the payoff table with the 0th and M^{th} points is obtained. We then compute $M - 1$ remaining points on the Pareto front by solving problem (P3) for the corresponding values of $m \in \{1, 2, \dots, M - 1\}$. Each corresponding problem (P3) is solved by iteratively solving (MP3) and (SP2-3). Finally, we count the total number of iterations NI, which is equal to the number of new explored coalitions added to $\mathcal{O}(S)$. We use NI for analyzing the computation performance.

5.7 Numerical Results

5.7.1 Simulation Data

We consider a VPP that coordinates the cooperation of NK DRAs. The scheduling horizon is one day, which is divided into $\text{NT} = 24$ equal time slots, each lasting $\Delta T = 1$ hour. The electricity prices are taken from the PJM market [43]. The penalty price λ^p varies from $\lambda^p = 5\$/\text{MWh}$ (PJM market) to $\lambda^p = 150\$/\text{MWh}$ (Greek market) [24]. Moreover, 20 profiles of hourly inflexible loads, which are scaled to the range of 0 – 10 MW, and the aggregated renewable DG, which is scaled into the range of 0 – 8 MW, are taken from [145] and [143], respectively. Figure 5.2 presents simulation data for the electricity pricing and the first 10 DRA load/renewable energy profiles. We assume that in each time slot t , each DRA k can aggregate 10% of total nonflexible load, which can be reduced by using the load reduction (LR) services with price $\lambda^r = 100\$/\text{MWh}$. The power capacity transferred via main grid is $P_k^{\max} = 15\text{MW}$. Finally, $v(S)$ is assumed to be well-defined, i.e., the market bidding optimization problem due to coalition S is feasible.

Table 5.2 – Flexible Load Data

Load blocks (MW)	Marginal utility (\$/MWh)	E_k^F (MWh)
1, 1, 2, 2	20, 18, 13, 11	86.4

The parameters of the multi-block utility function for DRAs are given in Table 5.2. We employ the modeling method in [42, 44] to construct flexible load data. In particular, we multiply the base utility by 0.8, 1.0, and 1.2 in time periods [1-8], [9-16], and [17-24], respectively [42], to obtain the utility functions for DRAs' flexible loads over the scheduling horizon. The amount of flexible load (i.e., demand blocks) is assumed to be the same for all time slots, the minimum hourly power consumption is set to be zero, and the limits on load ramping up/down are assumed to be sufficiently large. The minimum energy consumption (E_k^F) of each DRA k over the scheduling horizon is set equal to $E_{\text{scale}}^F = 60\%$ of its maximum energy consumption level (e.g. $E_k^F = 0.6 \times (1 + 1 + 2 + 2) \times 24 = 86.4$ MWh) [42].

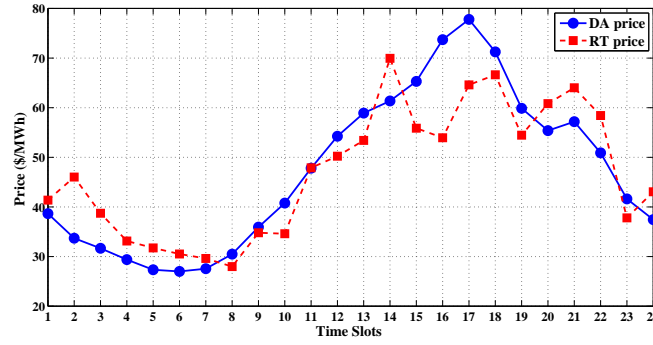
We employ the GAMS/SCENRED to reduce scenarios by using the *backward* method [107]. Considering the tradeoff between computation demand and modeling accuracy, we choose 30 from 2000 generated scenarios, which results in sufficiently small variation of the objective function $v(\mathcal{K})$. This is done by conducting some sensitivity analysis which are not presented in this study due to the space constraint. All the MILPs are solved by using the GAMS/CPLEX in a computer using Windows 8, Intel Core i5 3.3 GHz Processor, and 8 GB RAM. For the base case, we set $NK = 10$, the risk parameters β and α are set equal to 0.1 and 0.9, respectively.

5.7.2 Numerical Performance Analysis

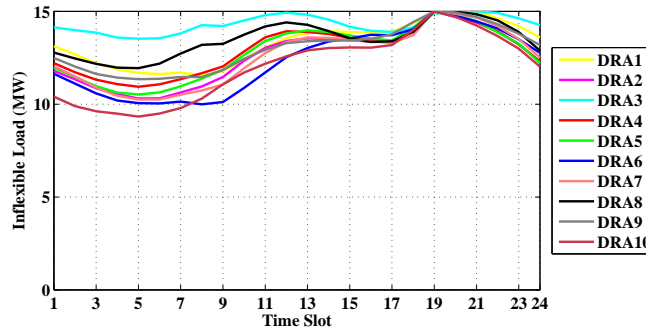
Figs. 5.3(a), 5.3(b), 5.3(c) show the Pareto fronts for the cost allocation problem when we vary the risk parameter β , flexible load scale E_{scale}^F , and penalty price λ^p , respectively. Each obtained Pareto front describes the tradeoffs between the stability represented by the worst-case cost saving value δ and the fairness captured by the maximum deviation of the percentage cost saving γ . For all cases, when $\gamma = \gamma^{\min}$ then we have $\delta = 0$ meaning that we reach the minimum value of δ while still guaranteeing to operate in the core whose definition is given in (2.29). On the other hand, as δ reaches its maximum value δ^{\max} , which corresponds to the nucleolus as the minimum deviation of the percentage cost saving among players, we achieves its maximum value $\gamma = \gamma^{\max}$.

These two extreme points in the Pareto front correspond to the cases where the cost allocation solution x is either at the fairness core point, γ^{\min} , or the lexicographically optimal point, the nucleolus δ^{\max} , in the polyhedron $\mathcal{C}(v)$. These figures show that the proposed design enables us to determine multiple different Pareto-efficient solutions in the core of the underlying cooperative game. Moreover, one can choose an operation point on the Pareto front with desirable stability-fairness tradeoff. Specifically, for a certain desired value of the maximum deviation of the cost percentage saving γ , one can determine the corresponding cost allocation vector with the achievable value of the worst-case cost saving δ being maximized. This demonstrates the flexibility and efficiency of our proposed cost allocation design compared to other existing designs such as the nucleolus-based cost allocation.

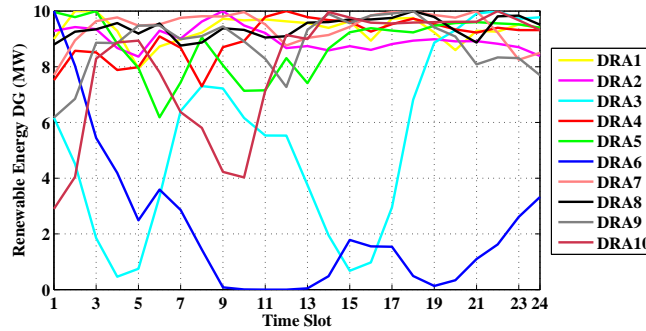
Figure 5.4 illustrates the difference of the obtained allocation vectors in the two extreme points. Figure 5.4(a) shows the performance of two allocation schemes in terms of the cost saving $\text{cost}_{\text{saving}}(k)$



(a) Electricity prices



(b) Forecast inflexible load



(c) Forecast renewable energy

Figure 5.2 – Simulation data

for the base case, which is calculated as follows:

$$\text{cost}_{\text{saving}}(k) = 100\% - \frac{x_k v(\mathcal{K})}{v(k)}, \quad (5.29)$$

where $x_k v(\mathcal{K})$ is the expected cost that the DRA k receives in grand cooperation and $v(k)$ is its individual bidding cost. Figure 5.4(a) shows that the gap between the maximum and minimum cost saving in percentage among DRAs is minimized by the fairness core cost allocation vector while it is not optimized in the nucleolus cost allocation. Although both allocation schemes lie in the core $\mathcal{C}(v)$ (both have $\delta \geq 0$), they achieve different performances in terms of fairness and stability metrics. In particular, the nucleolus allocation ($m = M$) aims to maximize the worst case cost saving among all coalitions (the minimal satisfaction) δ^M by allocating less cost shares among DRAs in the worst-case coalition,

which results in high deviation of cost saving in percentage among DRAs γ^M . On the other hand, the fairness core allocation ($m = 0$) aims to minimize the gap between the maximum and minimum cost saving in percentage among DRAs while ensuring the core condition is just satisfied, i.e., it requires the minimum satisfaction $\delta \geq 0$. This results in the minimized gap γ^{\min} with the low value of δ , i.e., $\delta = 0$, which is just enough to satisfy the core condition.

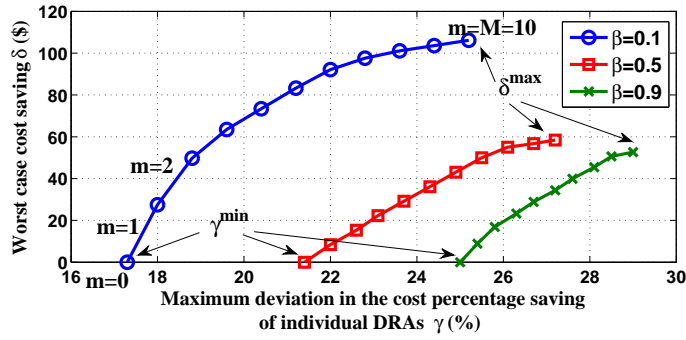
Figure 5.4(b) presents the cost shares among DRAs, i.e., the cost allocation vector x . It can be observed that a small change in x_k can result in a significant change in $\text{cost}_{\text{saving}}(k)$ shown in Figure 5.4(a) since $v(\mathcal{K}) \gg v(k)$ and equation (5.29) implies $\frac{d\text{cost}_{\text{saving}}(k)}{dx_k} = -\frac{v(\mathcal{K})}{v(k)}$. It also explains another observation that for similar change in the cost shares x_k , the DRA k with smaller $v(k)$ has higher change in the obtained cost saving. Figure 5.4(c) shows the individual bidding costs of DRAs, i.e., $v(k)$. There are correlations between the evolutions of x_k in both fairness core scheme and nucleolus scheme shown in Figure 5.4(b) and the individual bidding cost of each DRA $v(k)$ shown in Figure 5.4(c). In particular, the DRA which has higher individual bidding cost $v(k)$ tends to get more allocated cost value x_k .

We now discuss the impacts of different parameters on two extreme points on the Pareto front, namely the fairness cost allocation point (the 0th point) achieving γ^{\min} and the nucleolus cost allocation point (the Mth point) achieving δ^{\max} . It can be observed that as any parameters β , E_{scale}^F , or λ^P increases, γ^{\min} becomes larger, which shifts the Pareto front to the right. The achieved δ^{\max} corresponding to nucleolus cost allocation solution, however, varies differently as we vary these parameters. Specifically, as β , E_{scale}^F , and λ^P increase, the decision making problems faced by the VPP in both bidding and cost allocation become more difficult. In particular, with increasing β the bidding becomes more risk conservative in utilizing available resources to counter uncertainties. Moreover, increasing E_{scale}^F tightens constraint (5.5) which reduces the flexibility of flexible load and increases the amount of load required to serve while increasing λ^P will stress the VPP's bidding deviation between DA and RT market.

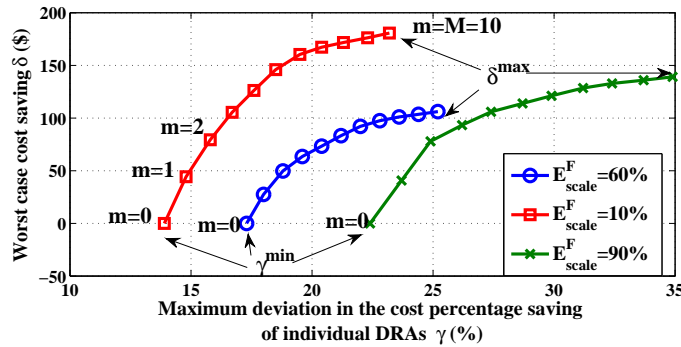
In general, the shape and size of the core $\mathcal{C}(v)$ as well as the values of γ^{\min} and δ^{\max} are complicated functions of different system and design parameters. Moreover, different coalitions S , depending on their available resources, can have different levels of impacts on the cost saving achieved via cooperation. When the cooperation plays a significant role, it could be harder to distribute the cost saving fairly for the DRAs while satisfying the core constraint. Harder bidding environment can also affect the cooperation's stability, which is captured by δ^{\max} where the larger value of δ^{\max} implies greater cooperation benefits for the DRAs.

Figure 5.5 compares the costs under cooperation and noncooperation scenarios for the DRAs as we vary different parameters β , E_{scale}^F , λ^P , and P_k^{\max} . In all cases, the cooperative bidding strategy of DRAs results in smaller total cost than that due to the noncooperative bidding strategy taken by each DRA. This cost reduction due to cooperation can be explained by the *subadditive* property of the underlying cooperative cost game [54]. By cooperation, DRAs can utilize available resources more efficiently to counter the uncertainties in electricity price and renewable energy, and to reduce energy imbalance between DA and RT dispatch, which leads to cost reduction.

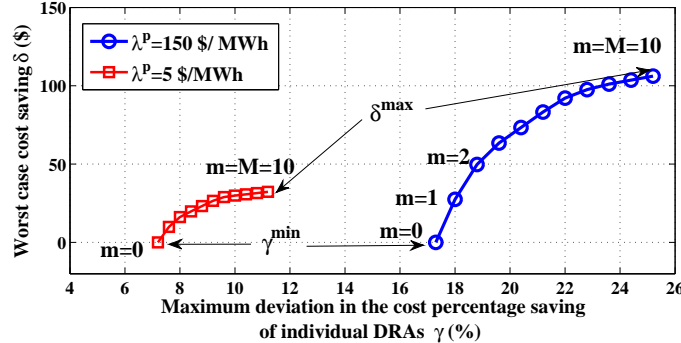
Adding new DRAs to an existing group of cooperative DRAs can also affect the cooperation gain significantly, which is illustrated in Figure 5.6. Since newly added DRAs may have different profiles of resources, they can have positive or negative impacts on the stability and fairness of the existing cooperative DRAs, e.g., decreasing or increasing γ^{\min} and δ^{\max} . Mathematically speaking, adding a new DRA will double the number of stability constraints that define the core $\mathcal{C}(v)$. It also illustrates the main characteristic of the LP game, i.e., totally balanced, which means the core is always nonempty when adding or removing DRAs to/from the VPP. Since the proposed framework enables us to completely characterize the Pareto fronts under different sizes of DRAs coordinated by the same VPP, admission control decisions for DRAs, which are interested in joining an existing group of cooperative DRAs, can be made to achieve the best desirable performance. In particular, if one wishes to operate



(a) Pareto front with $\lambda^p = 150\$/\text{MWh}$, $E_{\text{scale}}^F = 60\%$, and varying β



(b) Pareto front with $\lambda^p = 150\$/\text{MWh}$, $\beta = 0.1$ and varying E_{scale}^F



(c) Pareto front with $E_{\text{scale}}^F = 60\%$, $\beta = 0.1$, and varying λ^p

Figure 5.3 – Pareto fronts under different parameter settings

the VPP at a specific value of γ then the achievable values of δ on the Pareto fronts corresponding different values of NK can be determined. This can be used to optimize the number of cooperative DRAs to achieve the maximum value of δ .

The market model considered in this study is unidirectional [24, 29]. However, some markets allow bidirectional power constraint, which grant DRAs the opportunities to sell their surplus energy to further reduce the costs. To study the impact of bidirectional constraints on power exchange, we relax the flexible load constraint (5.5) by reducing E_{scale}^f from 60% to 0%, which reduces the total load demands of each DRA, and multiply the forecast values in the base case with $\text{RES}_{\text{scale}}$ by 1.1 and 1.4 respectively, which increases the generated renewable energy of all DRAs. This results in increasing the chance that DRAs have surplus energy at some time t in scenarios s to sell back to the

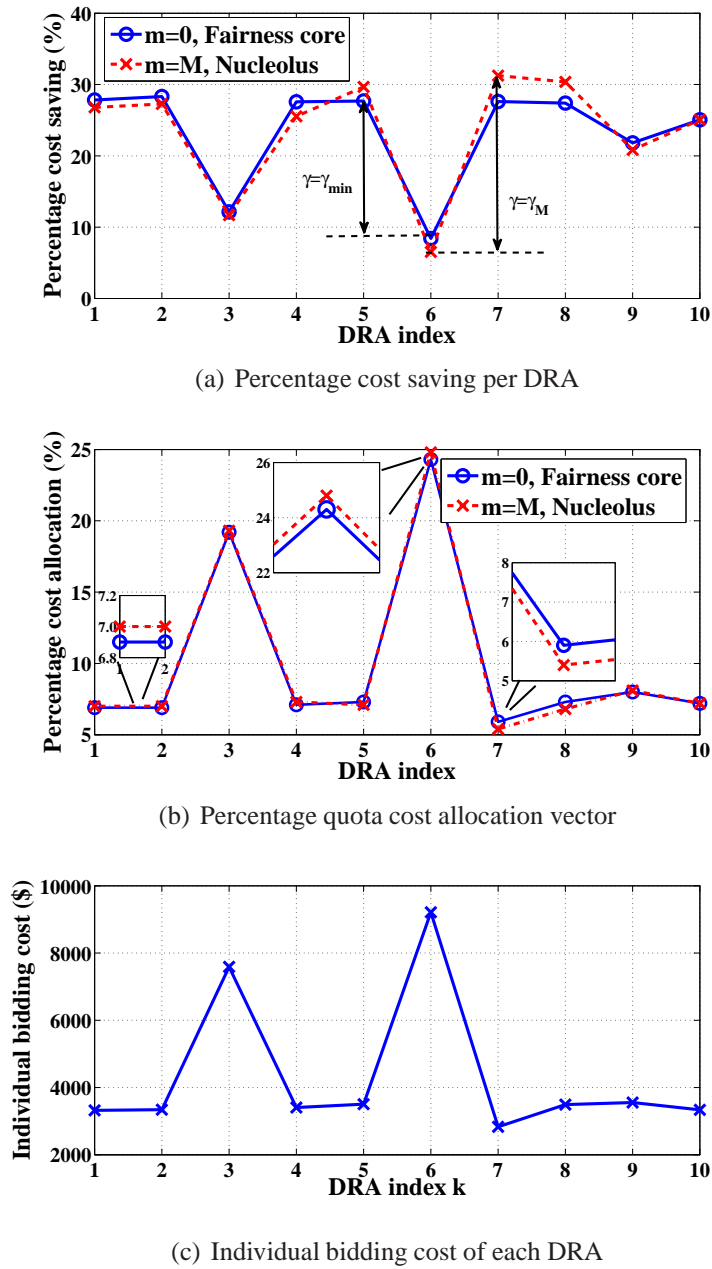


Figure 5.4 – Illustration of Fairness core and Nucleolus allocation

market. Three case studies are conducted, i.e., case 1 with $E_{scale}^f = 60\%$, $RES_{scale} = 1.1$, case 2 with $E_{scale}^f = 0\%$, $RES_{scale} = 1.1$, and case 3 with $E_{scale}^f = 0\%$, $RES_{scale} = 1.4$. Figure 5.7 shows the gap between the bidirectional and unidirectional market based individual bidding cost of DRAs and Figure 5.8 shows the obtained Pareto fronts in three case studies. The gap of two Pareto fronts is larger when there are more chances of surplus energy scenarios. In case 1, bidirectional power constraint has no impact there is no energy surplus scenarios, the gap shown in Figure 5.7 is 0 and both Pareto fronts in Figure 5.8(a) overlap. In case 2, participating in the bidirectional market has a little positive impact on cost reduction as shown in Figure 5.7, which results in slight difference between two Pareto fronts shown in Figure 5.8(b). In case 3, the benefit of participating in the bidirectional market is significant as shown in Figure 5.7, which results in the bigger gap between two Pareto fronts shown in Figure 5.8(c).

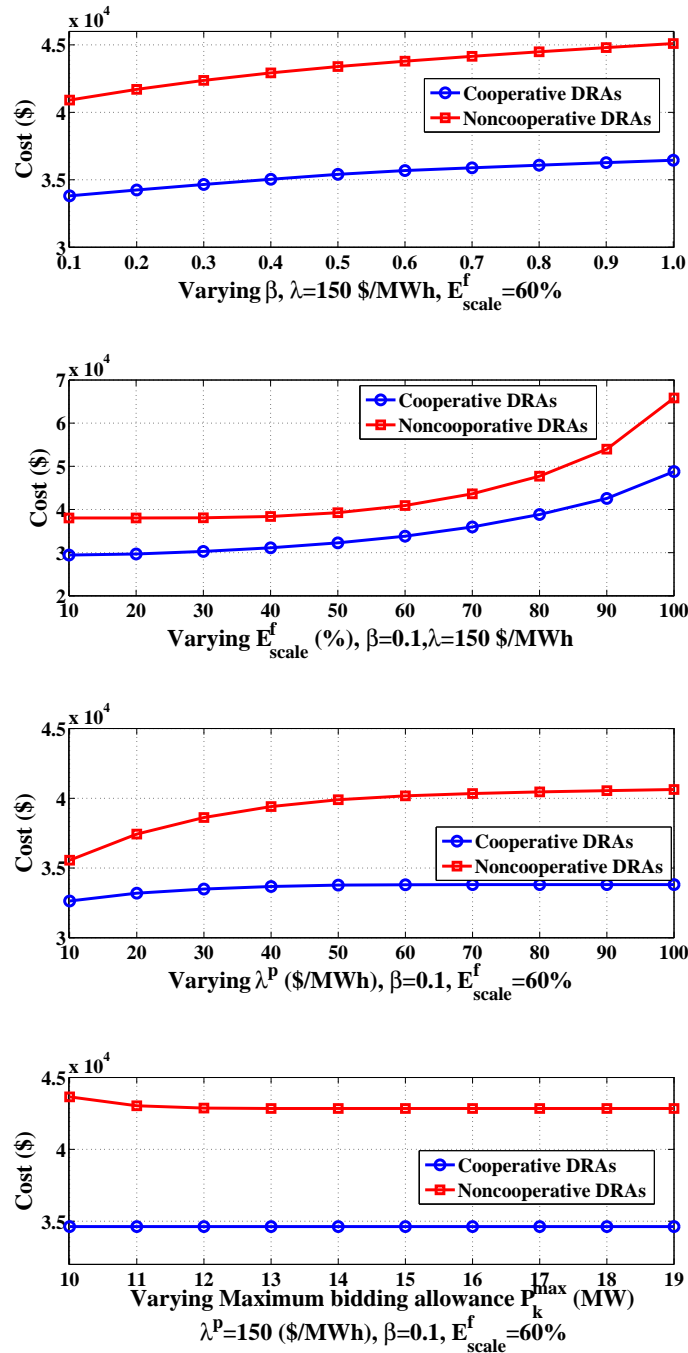


Figure 5.5 – Cost saving due to cooperation

5.7.3 Computation Analysis

We study the impact of several modeling aspects on the computation performance such as the number of scenarios (NS), the number of DRAs (NK), the number of Pareto points ($M + 1$), and the complexity of DRA’s model.

Table 5.3 illustrates the impacts of number of scenarios NS and number of DRAs NK on the computation time. Part A shows that as the number of scenarios increases, the computation time increases significantly due to the increasing size of the MILP based sub-problem while the number of iterations remains stable. In fact, since uncertainties can be captured well with NS=30 scenarios, computation

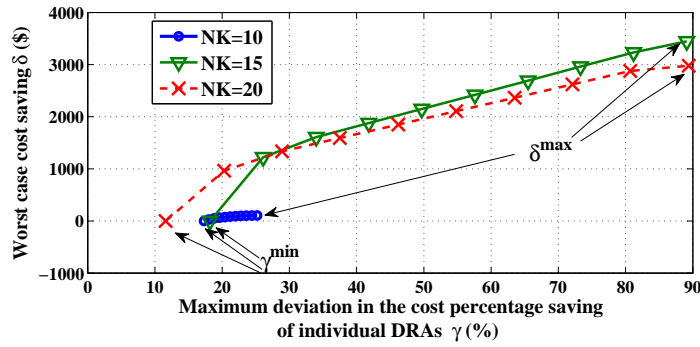


Figure 5.6 – Pareto front with $\lambda^P = 150\$/MWh$, $\beta = 0.1$ and varying NK

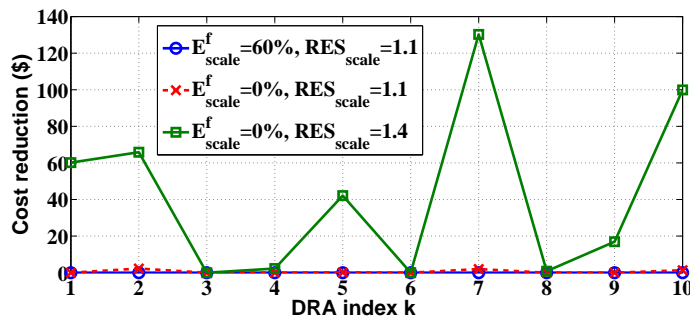


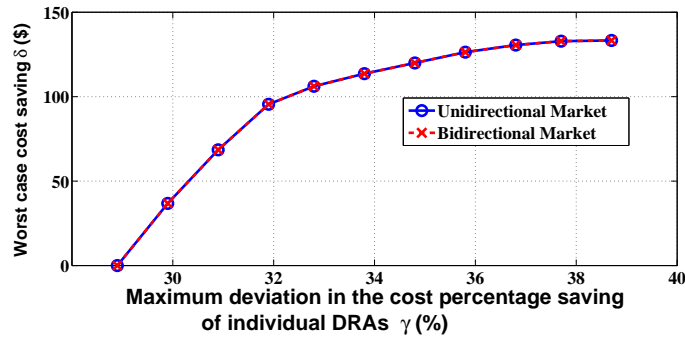
Figure 5.7 – The gap of individual bidding cost between bidirectional and unidirectional market

accuracy of sub-problem can be guaranteed while we can maintain the reasonable computational complexity with the relatively small size of the MILP. Part B demonstrates that as the number of DRAs NK increases, the number of iterations and computation time increase significantly. This is because of the increasing size of the underlying MILP sub-problem and the increasing number of binary variables e_k^S . We also present the number of iterations required by our design and the original number of stability constraints $2^{NK}-2$ (without using the row constraint method), which demonstrates the huge computation reduction. In particular, we calculate the ratio between the number of iterations, which equals the number of coalitions S to be explored (the number of sub-problems (SP1, SP2, and SP3) to be solved) over the original number of stability constraints $2^{NK}-2$ as follows:

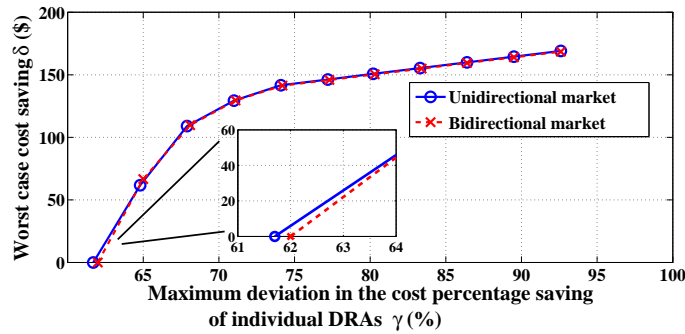
$$\text{ratio} = \frac{NI}{2^{NK}-2}. \quad (5.30)$$

It can be observed that this ratio can be reduced significantly (from 0.044 to 1.29×10^{-4} for the studied cases). This confirms computation efficiency of the proposed design in dealing with larger-scale VPP settings in term of *computation reduction*, i.e., the number of MILP sub-problems we need to solve will not increase as exponentially as the original number of stability constraints $2^{NK}-2$.

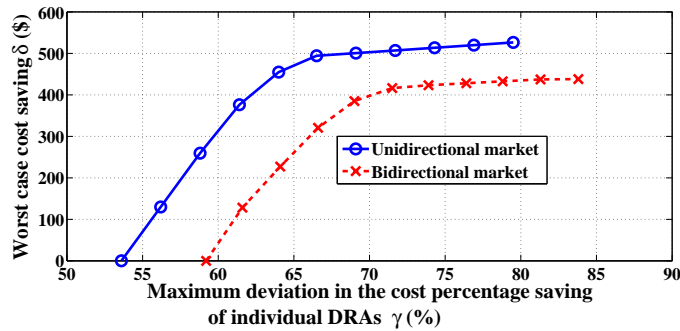
Beside the increasing number of binary variables e_k^S , there are two other factors significantly affecting the computation time in the larger-scale VPP setting, i.e., the chosen number of Pareto points and the DRA's model. Table 5.4 shows that when we relax these settings, the computation time can be reduced. In practice, we only need to determine a single operating point on the Pareto front so we only need to find three cost allocation solutions (i.e., the fairness core, the nucleolus, and the desired allocation solutions). In particular, after solving problems (P1) and (P2), the VPP can obtain γ_{\min} , γ_{\max} ,



(a) Case 1: $E_{scale}^f = 60\%$, $RES_{scale} = 1.1$



(b) Case 2: $E_{scale}^f = 0\%$, $RES_{scale} = 1.1$



(c) Case 3: $E_{scale}^f = 0\%$, $RES_{scale} = 1.4$

Figure 5.8 – The difference of Pareto fronts obtained in two markets

and δ_{max} . The VPP can then choose an appropriate value of γ^m in (5.20), which specifies the problem (P3) to be solved to determine the final cost allocation solution.

As mentioned above, when NK increases, the dimension of $\mathcal{C}(v)$ increases, and the number of core stability constraints (5.15) increases exponentially. This results in larger number of iterations, i.e., more MILP based sub-problems to be computed. Moreover, solving the MILP sub-problem at each iteration takes longer time for larger value of NK. Hence, it is more time consuming to compute a large number of points on the Pareto front when NK is large. Note, however, that we have computed many points on the Pareto front (e.g., $M+1=11$ points) to illustrate the stability-fairness tradeoff. For most practical applications, we might not need to obtain too many Pareto points to make a final decision on the desirable operating point.

Table 5.3 – Computation Report

Part A: Impact of number of scenarios NS (NK = 10)			
NS	30	50	100
Iterations $2^{NK} - 2$	41 10^3	42 10^3	41 10^3
Total computation time (s)	665	10759	47628
Average computation time per point (s)	60 (0.017h)	266 (0.063h)	4330 (1.2h)
Part B: Impact of number of DRAs NK (NS = 30)			
NK	10	15	20
Iterations $2^{NK} - 2$	41 10^3	74 3.27×10^4	136 10^6
Total computation time (s)	665	32135	54346
Average computation time per point (s)	60 (0.017h)	2921 (0.81h)	4941 (1.37h)
Iteration reduction ratio	0.044	0.0038	1.29×10^{-4}

Table 5.4 – Impact of number of Pareto points and complexity of $v(S)$

Cases	Number of iterations	Computation time (s)
Smaller number (3) of Pareto points	57	7327
Remove flexible load constraints	82	1077

The computation time of the sub-problem also depends on the market bidding problem that defines $v(S)$, which in turns depends on the complexity of the DRA's model. In particular, the modeling and consideration of each DRA's component will affect the number of constraints and variables considered in the MILP-based sub-problem (5.25). In this study, to illustrate the applicability of the proposed cost allocation in several potential applications, we have considered the heterogeneous setting where individual DRAs can have different models of nonflexible load, flexible load, renewable energy, and load reduction. This results in increasing complexity for the formulation of $v(S)$ and the MILP based sub-problems. The proposed algorithm can be applied for the simpler setting when some of these components are excluded, e.g., profit sharing for renewable energy portfolio [75], cost allocation for load aggregators such as EV clusters in an EV aggregator [24], or considering a simplified energy aggregation model to reduce complexity [29]. In particular, Table 5.4 shows that the computation time with $NK = 20$ and $M = 10$ can be reduced significantly when the constraints of flexible load are removed.

5.8 Extensions and Future Work

5.8.1 Verifying The Existence of The Core

There are several smart grid applications to be considered in our future work, which can be modeled as a LP-game such as cooperation of wind power producers [75, 112], the aggregation of several EV clusters that form an EV aggregator [24]. For these applications, the market bidding optimization

problems are also modeled as two-stage stochastic linear programming problems [24, 75]. In these cases, the state of the art modeling of uncertainties (uncertainties of wind generation, arrival time of EV) or new market frameworks (multiple trading floors [75], regulation market integration [24]) can be incorporated into these designs. In some applications, $v(S)$ can be modeled by a nonlinear program (NLP). Extension of LP-games considering some nonlinear constraints and objective functions, which is still balanced, is reported by P. Dubey and L.S. Shapley in [146]. In addition, $v(S)$ can be modeled by an MILP. For example, the consideration of demand response contracts [43], thermal generators [31, 43], battery energy storage [31], detailed demand response strategies [10], can introduce binary variables, which turns the formulation of $v(S)$ into an MILP. For design scenarios where we cannot conclude the balance of the underlying game based on the form of $v(S)$ [55], we can verify the existence of the core by simply solving the following LP [54]:

(P4)

$$\min_{\omega, x_k} \omega \quad (5.31)$$

$$\text{s.t: } \sum_{k \in S} x_k v(\mathcal{K}) \leq v(S) + \omega, \forall S \quad (5.32)$$

$$\sum_{k=1}^{NK} x_k = 1, x_k \geq 0, \omega \geq 0. \quad (5.33)$$

If we have $\omega^* = 0$ after solving (P4), $\mathcal{C}(v)$ is nonempty. Otherwise ($\omega^* > 0$), the condition $\sum_{k \in S} x_k v(\mathcal{K}) \leq v(S)$ cannot be satisfied $\forall S$ and $\mathcal{C}(v) = \emptyset$ [54]. Problem (P4) can be solved by using a similar iterative computation procedure based on the row constraint generation approach. Detailed discussions on how to solve (P4) and to verify the core's existence can be found in [54].

If the core is nonempty, we can apply the proposed cost allocation directly. If the core is empty, we can use the relaxed versions of the core such as ε -core and minmax core concepts [54, 98]. The new solution concepts still define polyhedron of payoff vector x which implies certain tradeoff in the cost allocation design proposed in this study is still important. Another potential approach is to stabilize the game via taxation as players or subset of players are taxed (cooperation fee), which has been investigated in the literature [55, 147, 148]. As mentioned above, since $v(S)$ can be modeled as MILP or mixed integer nonlinear program (MINLP) and the game can be unbalanced, designing an efficient taxing scheme to ensure the existence of the core is challenging and it will be studied in our future work.

5.8.2 Computation Improvement

The sub-problems studied in this study aim to identify the coalition S^* that potentially violates the core condition the most. However solving these MILP based sub-problems (SP1-3) can be time consuming. The sub-problems can also be MINLP depending on specific modeling and application requirements. One approach to reduce the computation burden is to solve these sub-problems by using evolutionary algorithms such as particle swarm optimization with fast computation time. Another approach is to find the suboptimal S' instead of optimal S^* . Intuitively, because the set of coalitions is limited, we might just need to find a *violated coalition* S' to move the allocation vector x^* towards the feasible region of the original problems instead of identifying *the most violated one*. This approach may require a larger number of iterations but the computation time for each iteration is reduced, which can significantly reduce the total computation time [149]. We would like to consider these research directions in the future work.

5.9 Conclusion

In this study, we have presented a computationally efficient cost allocation design for cooperative DRAs based on the cooperative game core concept. We have proposed to exploit the nonempty core property of the underlying balanced game and develop a bi-objective optimization framework that strikes the balance between the allocation stability and fairness. We have employed the ε -constraint and row constraint generation methods to successfully construct the Pareto front of the cost allocation solutions with manageable computation complexity. The proposed design can efficiently allocate percentage quota of total bidding cost to individual DRAs while achieving desirable stability-fairness trade-off.

Chapter 6

Conclusions and Future Works

Active demand-side management is an important research topic in the smart grid domain which can help improve operation efficiency and to enable increasing integration of renewable energy in the power grid. Our research in this dissertation aims at tackling some major challenges related to the demand-side management where we focus on the design, analysis, and development of concrete solution frameworks to solve decision making problems concerning several demand-side smart grid entities ranging from the small-scale residential level to the large-scale aggregator level. This chapter summarizes our key research contributions and draws some potential future research directions.

6.1 Major Contributions

In this dissertation, we have studied three important decision making problems in smart grid's demand-side management. Our research has resulted in three journal publications [19, 28, 49] and several corresponding conference papers [18, 34, 96, 150–152].

In the first research problem, we address the energy management of a small-scale smart grid's entity, namely, the smart home [19]. Specifically, the energy scheduling design of the smart home equipped with solar assisted thermal load is conducted considering the real-time pricing scheme. Toward this end, the energy scheduling problem is formulated as a rolling two-stage stochastic programming problem where the optimal control actions at each time slot are implemented in the rolling manner. The proposed framework can minimize the energy payment cost, guarantee system constraints while exploiting the positive gain of the energy coupling of the solar thermal storage and HVAC system to improve the system energy efficiency considering the uncertainties of renewable energy and electricity price. Numerical studies show that a significant energy cost gain of more than 100% can be achieved by the proposed design compared to the conventional water heating and HVAC system.

In the second research problem, we study the pricing design in the distribution network which motivates demand-side entities such as smart homes to participate in the demand response program under the Load Serving Entity (LSE) model [28]. In particular, we formulate the proposed pricing design problem as a bilevel program where the LSE determines the price and the demand response aggregators respond to that price signal. Given the lower-level problem is linear, we propose to transform the underlying bilevel optimization problem into an equivalent single-objective mixed integer linear program (MILP) by using the optimal KKT conditions, the Fortuny-Amat formula, and the strong duality theorem of linear programming. The obtained MILP can be solved efficiently by using available commercial solvers. Numerical studies show that our proposed design can provide a win-win solution for both LSE and flexible load aggregators.

In the last research problem, we study the cost sharing problem for cooperative demand-side resource aggregators (DRAs), each of which aggregates multiple resources including distributed renew-

able energy, demand responses services, non-flexible load, and flexible load [49]. Specifically, these DRAs are coordinated by a Virtual Power Plant (VPP) to jointly bid in the short-term two settlement electricity market where the problem is addressed by using the core concept in the cooperative game theory. Since the core can contain many cost sharing solutions, we need to choose an appropriate solution inside the core that balances between stability and fairness. Solving the underlying bi-objective optimization problem is highly complex because of the exponential number of implicit constraints related to the core definition. We develop a computation-efficient algorithm based on the combination of ϵ -constraint and row constraint generation methods to construct the Pareto front without calculating all coalitions' function values. Numerical studies confirm the significant reduction of computation time compared to direct computation approach and a great cost gain with respect to the conventional system with non-cooperative DRAs due to the proposed design.

6.2 Future Research Directions

6.2.1 Multi-Agent System Approach for Smart Grid Energy Management

One potential direction is related to efficient cooperation designs for emerging smart grid entities in the deregulated electricity market. This potential research will aim to answer some importation questions: how to ensure that different smart grid entities cooperate efficiently, what should be the good mechanism design for their coordination, how to divide the achieved payoff, how each entity can learn to coordinate efficiently in a decentralized manner. These challenging research issues can be addressed by employing the Multi-Agent Systems (MAS) approach. In fact, MAS in conjunction with machine learning (ML) techniques provide efficient approaches to understand various interesting and complex interactions in the smart grid under the deregulated and decentralized electricity market.

There are several sub-topics and possible research issues to be further considered in this direction. In the short term, I will complete my ongoing work on the profit/cost allocation in power systems where the notorious complexity of the cooperative game's solution concepts (the core, nucleolus, Shapley values) will be addressed. In the longer term, I would like to investigate how efficient coalitions among cooperative entities should be formed in the general cooperation game model where the super-additive property may not hold, e.g., there is the non-negligible computation and communication cost for forming a large coalition. Dynamic programming, reinforcement learning, mechanism design, and other methods will be explored to address these research issues. Furthermore, decentralized coordination design of multiple smart grid entities will be investigated by employing the agent based simulation and Bayesian game theory.

6.2.2 Machine Learning for Decision Making Problems in Smart Grids

In the past research, we have employed the optimization and cooperative game theory to solve decision making problems for various smart grid entities. However, consideration of different system uncertainties such as renewable energy generation and electric pricing plays an important role in efficient smart grid's decision making. Here, employment of machine learning techniques to process certain input data of decision making problems is a good research direction. Moreover, machine learning can be employed to address the power system security assessment issue. Toward this end, complex network and physical models of the power system dynamics should be considered in the design of the machine learning based security assessment instead of using machine learning in a black box approach.

Using ML for reducing computational complexity can be considered in my future research. For example, the game theory or bilevel optimization method is often used to model the cyber-physical attack in the smart grid. As discussed in chapter 4, the bilevel optimization can be used for dynamic

pricing design even though design of fast algorithms to solve underlying bilevel optimization problems can be challenging. Toward this end, the neurodynamic optimization approach can be employed to transform the game or optimization theoretic model of the cyber-physical attack and pricing design problems into the dynamics of neural networks, which can potentially tackle these underlying problems with manageable computation complexity. Development of ensemble learning methods for smart grid decision making problems is another interesting research issue for which we have obtained some initial results [151].

6.3 Publications

Journals

- [J1] Hieu Trung Nguyen and Long Bao Le, “Bi-objective cost allocation for cooperative demand-side resource aggregators,” *IEEE Trans. Smart Grid*, (to appear).
- [J2] Duong Tung Nguyen, Hieu Trung Nguyen, and Long Bao Le, “Dynamic pricing design for demand response integration in power distribution networks,” *IEEE Trans. Power Syst.*, vol. 31, no. 5, pp. 3457 – 3472, Jan. 2016.
- [J3] Hieu Trung Nguyen, Duong Tung Nguyen, and Long Bao Le, “Energy Management for Households With Solar Assisted Thermal Load Considering Renewable Energy and Price Uncertainty,” *IEEE Transactions on Smart Grid*, vol. 6, no. 1, pp. 301–314, Jan. 2015.

Conferences

- [C1] Hieu Trung Nguyen and Long Bao Le, “Bidding Strategy for Virtual Power Plant With Intraday Demand Response Exchange Market Using Stochastic Programming,” in *Proc. IEEE ICSET 2016*, Hanoi, Vietnam, Nov. 2016 (**Best Paper Award**).
- [C2] Hieu Trung Nguyen and Long Bao Le, “Minmax profit sharing scheme for cooperative wind power producers,” in *Proc. IEEE ICSET 2016*, Hanoi, Vietnam, Nov. 2016 (**Invited paper**).
- [C3] Hieu Trung Nguyen and Long Bao Le, “Online ensemble learning for security assessment in PMU-based power systems,” in *Proc. IEEE ICSET 2016*, Hanoi, Vietnam, Nov. 2016 (**Invited paper**).
- [C4] Hieu Trung Nguyen and Long Bao Le, “Optimal energy management for building micro-grid with constrained renewable energy utilization,” in *Proc. IEEE SmartGridComm’14*, Venice, Italy, Nov. 2014.
- [C5] Duong Tung Nguyen, Hieu Trung Nguyen, and Long Bao Le, “Coordinated dispatch of renewable energy sources and HVAC load using stochastic programming,” in *Proc. IEEE SmartGridComm’14*, Venice, Italy, Nov. 2014.
- [C6] Hieu Trung Nguyen, Duong Tung Nguyen, and Long Bao Le, “Home energy management with generic thermal dynamics and user temperature preference,” in *Proc. IEEE SmartGridComm’13*, Vancouver, BC, Canada, Oct. 2013.

References

- [1] NIST Office of the National Coordinator for Smart Grid Interoperability (2013). **NIST Framework and Roadmap for Smart Grid Interoperability Standards, Release 3.0**. <http://www.nist.gov/smartgrid/upload/Draft-NIST-SG-Framework-3.pdf>, 2013. [Online; accessed 02-March-2013].
- [2] A. J. CONEJO, M. CARRIÓN, MIGUEL AND J. M. MORALES. *Decision making under uncertainty in electricity markets*, volume 1. Springer, 2010.
- [3] US Congress. **Title XIII of the Energy Independence and Security Act of 2007**. <https://www.ferc.gov/industries/electric/indus-act/smart-grid/eisa.pdf>, 2007. [Online; accessed 10-February-2017].
- [4] V. GUNGOR, D. SAHIN, DILAN, T. KOCAK, S. ERGUT, SALIH. C. BUCCELLA, C. CECATI, CARLO. AND G. HANCKE. **Smart grid technologies: Communication technologies and standards**. *IEEE Trans. Indus. Inform.*, 7(4):529–539, 2011.
- [5] E. HOSSAIN, Z. HAN, AND H. V. POOR. *Smart grid communications and networking*. Cambridge University Press, 2012.
- [6] Independent Electricity System Operator. **Opportunities for demand side management in Ontario**. http://www.ieso.ca/Documents/smart_grid/materials/20120912/SGF-20120912-CPC-DSM_Paper.pdf, 2012. [Online; accessed 10-February-2017].
- [7] Federal Energy Regulatory Commission . **Assessment of Demand Response and Advanced Metering Staff Report**. <https://www.ferc.gov/industries/electric/indus-act/smart-grid/eisa.pdf>, 2014. [Online; accessed 10-February-2017].
- [8] US Department of Energy. **Advanced Metering Infrastructure**. https://www.smartgrid.gov/recovery_act/deployment_status/sdgp_ami_systems.html, 2015. [Online; accessed 10-February-2017].
- [9] A. YASSINE. **Implementation challenges of automatic demand response for households in smart grids**. In *2016 3rd International Conference on Renewable Energies for Developing Countries (REDEC)*, pages 1–6, July 2016.
- [10] M. PARVANIA, M. FOTUHI-FIRUZABAD, AND M. SHAHIDEHPUR. **Optimal demand response aggregation in wholesale electricity markets**. *IEEE Trans. Smart Grid*, 4(4):1957–1965, December 2013.
- [11] A. SAFDARIAN, M. FOTUHI-FIRUZABAD, AND M. LEHTONEN. **Integration of price-based demand response in DisCos’ short-term decision model**. *IEEE Trans. Smart Grid*, 5(5):2235–2245, September 2014.
- [12] M. PARVANIA, M. F. FIRUZABAD, AND M. SHAHIDEHPUR. **ISO’s optimal strategies for scheduling the hourly demand response in day-ahead markets**. *IEEE Trans. Power Syst.*, 29(6):2636–2645, November 2014.

- [13] D. T. Nguyen, M. Negnevitsky, and M. de Groot. **Pool-based demand response exchange market concept and modeling.** *IEEE Trans. Power Syst.*, 26(3):1677–1685, August 2011.
- [14] D. T. NGUYEN, M. NEGNEVITSKY AND M. DE GROOT. **Modeling load recovery impact for demand response applications.** *IEEE Trans. Power Syst.*, 28(2):1216–1225, May 2013.
- [15] A. J. CONEJO, J. M. MORALES, AND L. BARINGO. **Real-time demand response model.** *IEEE Trans. Smart Grid*, 1(3):236–242, December 2010.
- [16] Z. CHEN, L. WU AND Y. FU. **Real-time price-based demand response management for residential appliances via stochastic optimization and robust optimization.** *IEEE Trans. Smart Grid*, 3(4):1822–1831, December 2012.
- [17] MOHSENIAN-RAD AND A. LEON-GARCIA. **Optimal residential load control with price prediction in real-time electricity pricing environments.** *IEEE Trans. Smart Grid*, 1(2):120–133, September 2010.
- [18] H. T. NGUYEN, D. T. NGUYEN, AND L. B. LE. **Home energy management with generic thermal dynamics and user temperature preference.** In *Proc. IEEE SmartGridComm 13*, pages 552–557, October 2013.
- [19] H. T. NGUYEN, D. T. NGUYEN, AND L. B. LE. **Energy management for households with solar assisted thermal load considering renewable energy and price uncertainty.** *IEEE Trans. Smart Grid*, 6(1):301–314, January 2015.
- [20] P. SCOTT, S. THIBAUX, M. V. D. BRIEL, P. V. HENTENRYCK. **Residential Demand Response under Uncertainty.** *Principles and Practice of Constraint Programming*, 8124:645–660, January 2013.
- [21] N. GATSIS AND G. B. GIANNAKIS. **Residential load control: Distributed scheduling and convergence with lost ami messages.** *IEEE Trans. Smart Grid*, 3(2):770–786, June 2012.
- [22] Z. WU, W. GU, R. WANG, X. YUAN, AND W. LIU. **Economic optimal schedule of CHP microgrid system using chance constrained programming and particle swarm optimization.** In *Proc. IEEE-PES General Meeting*, , CA, July 2011.
- [23] T. HUBERT AND S. GRIJALVA. **Modeling for residential electricity optimization in dynamic pricing environment.** *IEEE Trans. Smart Grids*, 3(4):2224–2231, December 2012.
- [24] S. I. VAGROPOULOS AND A. G. BAKIRTZIS. **Optimal bidding strategy for electric vehicle aggregators in electricity markets.** *IEEE Trans. Power Syst.*, 28(4), November 2013.
- [25] J. KONDOH, N. LU, AND D. J. HAMMERSTROM. **An evaluation of the water heater load potential for providing regulation service.** *IEEE Trans. Smart Grid*, 26(3):1309–1316, February 2012.
- [26] N. LU. **An evaluation of the HVAC load potential for providing load balancing service.** *IEEE Trans. Smart Grid*, 3(3):1263–1270, September 2012.
- [27] H. HAO, B. M. SANANDAJI, K. POOLLA, AND T. L. VINCENT. **A generalized battery model of a collection of thermostatically controlled loads for providing ancillary service.** In *Proc. 51st Annual Allerton Conference on Communication Control and Computing*, 2013.
- [28] D. T. NGUYEN, H. T. NGUYEN, AND L. B. LE. **Dynamic pricing design for demand response integration in power distribution networks.** *IEEE Trans. Power Syst.*, 31(5):3457–3472, September 2016.

- [29] Z. XU, Z. HU, Y. SONG, AND J. WANG. **Risk averse optimal bidding strategy for demand side resource aggregators in day ahead electricity markets under uncertainty.** *IEEE Trans. Smart Grid*, PP(PP), November 2015.
- [30] Z. XU, Z. HU, Y. SONG AND J. WANG. **Data-driven pricing strategy for demand-side resource aggregators.** *IEEE Trans. Smart Grid*, PP(PP), August 2016.
- [31] H. PANDZIC, J. M. MORALES, A. J. CONEJO, AND I. KUZLE. **Offering model for a virtual power plant based on stochastic programming.** *Appl. Energy*, 105:282–292, May 2013.
- [32] M. VASIRANI, R. KOTA, R. CAVALCANTE, S. OSSOWSKI, AND N. JENNINGS. **An agent-based approach to virtual power plants of wind power generators and electric vehicles.** *IEEE Trans. Smart Grid*, 4(3):1314–1322, September 2013.
- [33] E. D. ANESE, S. V. DHOPLE, AND B. GIANNAKIS. **Optimal dispatch of photovoltaic inverters in residential distribution systems.** *IEEE Trans. Sustain. Energy*, 5(2):487–497, April 2014.
- [34] H. T. NGUYEN AND L. B. LE. **Optimal energy management for building microgrid with constrained renewable energy utilization.** In *Proc. IEEE SmartGridComm'2014*, pages 133–138, November 2014.
- [35] M. ROOZBEHANI, M. A. DAHLEH, AND S. K. MITTER. **Volatility of power grids under real-time pricing.** *IEEE Trans. Power Syst*, 27(4):1926–1940, November 2012.
- [36] L. BARINGO AND A. J. CONEJO. **Strategic Offering for a Wind Power Producer.** *IEEE Trans. Power Syst*, 28(4):4644–4654, November 2013.
- [37] M. PIPATTANASOMPORN, M. KUZLU AND S. RAHMAN. **An algorithm for intelligent home energy management and demand response analysis.** *IEEE Trans. Smart Grid*, 3(4):2166–2173, December 2012.
- [38] B. J. HUANG, J. H. WU, H. Y. HSU, AND J. H. WANG. **Development of hybrid solar assisted cooling/heating system.** *Energy Conversion and Management*, 51:1643–1650, 2010.
- [39] V. VAKILOROAYAA, Q. P. HA AND M. SKIBNIEWSKIB. **Modeling and experimental validation of a solar-assisted direct expansion air conditioning system.** *Energy and Building*, 66:524–526, February 2013.
- [40] R. E. ROSENTHAL. **GAMS, A. User's Guide.** *Washington, DC, USA, GAMS Development Corp*, 2012.
- [41] Apricus. **Solar System Manual.** <http://www.apricus.com>, 2013. [Online; accessed 23-December-2013].
- [42] M. RAHIMIYAN AND L. BARINGO AND A. J. CONEJO. **Energy management of a cluster of interconnected price-responsive demands.** *IEEE Trans. Power Syst*, 29(2):645–655, March 2014.
- [43] D. T. NGUYEN AND L. B. LE. **Risk-constrained profit maximization for microgrid aggregators with demand response.** *IEEE Trans. Smart Grid*, 6(1):135–146, January 2015.
- [44] S. KAZEMPOUR AND A. CONEJO AND C. RUIZ. **Strategic bidding for a large consumer.** *IEEE Trans. Power Syst*, 30(2):848–856, March 2015.
- [45] A. KHODAEI, M. SHAHIDEHPOUR, AND S. BAHRAMIRAD. **SCUC with hourly demand response considering intertemporal load characteristics.** *IEEE Trans. Smart Grid*, 2(3):564–571, September 2011.

- [46] H. WU, M. SHAHIDEHPOUR, AND M. E. KHODAYAR. **Hourly demand response in day-ahead scheduling considering generating unit ramping cost.** *IEEE Trans. Power Syst.*, 28(3):2446–2454, August 2013.
- [47] J. FORTUNY-AMAT AND B. MCCARL. **A representation and economic interpretation of a two-level programming problem.** *Journal of the operational Research Society*, 32(9):783–792, 1981.
- [48] D. T. NGUYEN AND L. B. LE. **Optimal bidding strategy for microgrids considering renewable energy and building thermal dynamics.** *IEEE Trans. Smart Grid*, 5(4):1608–1620, July 2014.
- [49] H. T. NGUYEN AND L. B. LE. **Bi-Objective Based Cost Allocation for Cooperative Demand-Side Resource Aggregators.** *IEEE Trans. Smart Grid*, PP(99), January 2017.
- [50] E. MASHHOUR AND S. TAFRESHI. **Bidding strategy of virtual power plant for participating in energy and spinning reserve markets Part I: problem formulation.** *IEEE Trans. Power Syst.*, 26(2):949–956, May 2011.
- [51] D. KIRSCHEN, G. STRBAC, P. CUMPERAYOT, AND D. DE PAVIA MENDES. **Factoring the elasticity of demand in electricity prices.** *IEEE Trans. Power Syst.*, 15(2):612–617, May 2000.
- [52] D. KIRSCHEN AND G. STRBAC. *Fundamentals of power systems economics.* Wiley, West Sussex, U.K., 2004.
- [53] R. GARCIA-BERTRAND. **Sale prices setting tool for retailers.** *IEEE Trans. Smart Grid*, 4(4):2028–2035, December 2013.
- [54] J. DRESHEL. *Cooperative Lot Sizing Games in Supply Chains.* Springer, 2010.
- [55] I. CURIEL. *Cooperative Game Theories and Applications: Cooperative Games Arising from Combinatorial Optimization Problems.* Springer, 1997.
- [56] N. AMJADI, J. AGHAEI, AND H. SHAYANFAR. **Stochastic multiobjective market clearing of joint energy and reserves auctions ensuring power system security.** *IEEE Trans. Power Syst.*, 24(4):1841–1854, November 2009.
- [57] Z. CHEN AND L. WU. **Residential appliance DR energy management with electric privacy protection by online stochastic optimization.** *IEEE Trans. Smart Grid*, 4(4):1861–1869, December 2013.
- [58] Z. XU, X. GUAN, Q. S. JIA, J. WU, D. WANG, AND S. CHEN. **Performance analysis and comparison on energy storage devices for smart building energy management.** *IEEE Trans. Smart Grid*, 3(4):2136–2147, December 2012.
- [59] D. T. NGUYEN AND L. B. LE. **Joint optimization of electric vehicle and home energy scheduling considering user comfort preference.** *IEEE Trans. Smart Grid*, 5(1):188–199, January 2014.
- [60] S. HAN AND K. SEZAKI. **Estimation of achievable power capacity from plug-in electric vehicles for V2G frequency regulation: case studies for market participation.** *IEEE Trans. Smart Grid*, 2(4):632–641, December 2011.
- [61] K. VANTHOURNOUT, R. D’HULST, D. GEYSEN, AND G. JACOBS. **A smart domestic hot water buffer.** *IEEE Trans. Smart Grid*, 3(4):2121–2127, December 2012.

- [62] G. PAPAETHYMIU, B. HASCHE, AND C. NABE. **Potential of heat pumps for demand side management and wind power integration in the German electricity market.** *IEEE Trans. Sustain. Energy*, 3(4):636–642, October 2012.
- [63] A. A. THATTE, L. XIE, D. E. VIASSOLO, AND S. SINGH. **Risk measure based robust bidding strategy for arbitrage using a wind farm and energy storage.** *IEEE Trans. Smart Grid*, 4(4):2191–2199, December 2013.
- [64] M. ORTIZ, H. BARSUN, H. HE, AND P. VOROBIEFF. **Modeling of a solar-assisted HVAC system with thermal storage.** *Energy and Buildings*, 42:500–509, April 2010.
- [65] X. GUAN, Z. XU, AND Q. S. JIA. **Energy-efficient buildings facilitated by microgrid.** *IEEE Trans. Smart Grid*, 1(3):243–252, December 2010.
- [66] A. ARABALI, M. GHOFRANI, M. ETEZADI-AMOLI, M. S. FADALI, AND Y. BAGHZOUZ. **Genetic algorithm based optimization approach for energy management.** *IEEE Trans. Power Del.*, 28(1):162–170, January 2013.
- [67] A. A. MOGHADDAM, H. MONSEF, AND A. R. KIAN. **Optimal smart home energy management considering energy saving and a comfortable lifestyle.** *IEEE Trans. Smart Grid*, 6(1):324–332, January 2015.
- [68] F. RAHIMI AND A. IPAKCHI. **Demand response as a market resource under the smart grid paradigm.** *IEEE Trans. Smart Grid*, 1(1):82–88, June 2010.
- [69] R. COUILLET, S. M. PERLAZA, H. TEMBINE AND M. DEBBAH. **Electrical vehicles in the smartgrid: A mean field game analysis.** *IEEE J. Sel. Areas Commun.*, 30:6, July 2012.
- [70] P. H. NGUYEN, W. L. KLING, AND P. F. RIBEIRO. **A game theory strategy to integrate distributed agent-based functions in smart grids.** *IEEE Trans. Smart Grid*, 4(1):568–576, March 2013.
- [71] A. MNATSAKAYAN AND S. W. KENEDY. **A novel demand response model with an application for a virtual power plant.** *IEEE Trans. Sustain. Energy*, 3(4):636–642, October 2012.
- [72] W. LEE, L. XIANG, R. SCHOBBER, AND V. W. S. WONG. **Direct electricity trading in smart-grid: A coalitional game analysis.** *IEEE JSAC*, 32(7):1398–1411, July 2014.
- [73] M. TASDIGHI, H. GHASEMI, AND A. RAHIMI-KIAN. **Residential microgrid scheduling based on smart meters data and temperature dependent thermal load modeling.** *IEEE Trans. Smart Grid*, 5(1):349–357, January 2014.
- [74] E. HEYDARIAN-FORUSHANI, M. P. MOGHADDAM, M. K. SHEIK-EL-ESLAMI, M. SHAFIE-KHAH, AND J. P. S. CATALAO. **Risk constrained offering strategy of wind power producers considering intraday demand response exchange.** *IEEE Trans. Substain. Energy*, 5(1):1036–1047, October 2014.
- [75] J. M. MORALES AND A. J. CONEJO AND J. PEREZ-RUIZ. **Short-term trading for a wind power producer.** *IEEE Trans. Power Syst*, 25(1):554–564, February 2010.
- [76] J. P. S. CATALAO AND H. M. I. POUSINHO AND V. M. F. MENDES. **Optimal offering strategies for wind power producers considering uncertainty and risk.** *IEEE Syst. J*, 6(2):270–277, June 2012.
- [77] V. G. MESTRE, A. A. SANCHEZ DE LA NIETA, J. CONTRERAS, AND J. P. S. CATALAOS. **Optimal bidding of a group of wind farms in day-ahead markets through an external agent.** *IEEE Trans. Power Syst.*, 31(4):2688–2700, July 2016.

- [78] A. SAFDARIAN, M. FOTUHI-FIRUZABAD AND M. LEHTONEN. **A stochastic framework for short-term operation of a distribution company.** *IEEE Trans. Power Syst*, 28(4):4712–4721, November 2013.
- [79] M. A. A. PEDRASA, T. D. SPOONER AND I. F. MACGILL. **Coordinated scheduling of residential distributed energy resources to optimize smart home energy services.** *IEEE Trans. Smart Grid*, 1(2):134–143, September 2010.
- [80] T. T. KIM AND H. V. POOR. **Scheduling power consumption with price uncertainty.** *IEEE Trans. Smart Grid*, 2(3):519–527, August 2011.
- [81] H. TISCHER AND G. VERBIC. **Towards a smart home energy management system: A dynamic programming approach.** In Australia . Perth, editor, *Proc. 2011 Innovative Smart Grid Technologies Asia (ISGT)*, pages 1–7, November 2011.
- [82] Z. ZHAO, W. C. LEE, Y. SHIN, AND K. B. SONG. **An optimal power scheduling method for demand response in home energy management system.** *IEEE Trans. Smart Grid*, 4(3):1391–1400, September 2013.
- [83] M. NISTOR AND C. ANTUNES. **Integrated Management of Energy Resources in Residential Buildings-a Markovian Approach.** *IEEE Trans. Smart Grid*, PP(99), April 2016.
- [84] I. SARBU AND C. SEBARCHIEVICI. **Review of solar refrigeration and cooling systems.** *Energy and Buildings*, 67:286–297, December 2013.
- [85] H. M. HENNING. **Solar assisted air conditioning of buildings: An overview.** *Applied Thermal Engineering*, 27(10):1734–1749, July 2007.
- [86] A. MAMMOLIA, P. VOROBIEFF, H. BARSUNA, R. BURNETT, AND D. FISHERA. **Energetic, economic and environmental performance of a solar-thermal-assisted HVAC system.** *Energy and Buildings*, 42(9):1524–1535, September 2010.
- [87] T. FERHATBEGOVIC, P. PALENSKY, G. FONTANELLA, AND D. BASCIOTTI. **Modelling and design of a linear predictive controller for a solar powered HVAC system.** In China . Hangzhou, editor, *Proc. IEEE International Symposium on Industrial Electronics (ISIE)*, pages 869–874, May 2012.
- [88] S. MHANNA, AND A. C. CHAPMAN, AND G. VERBIC. **A fast distributed algorithm for large-scale demand response aggregation.** *IEEE Trans. Smart Grid*, 7(4):2094–2107, 2016.
- [89] A. KUMAR AND G. P. HANCKE. **An energy-efficient smart comfort sensing system based on the IEEE 1451 standard for green buildings.** *IEEE Sensors Journal*, 14(12):4245–4252, 2014.
- [90] C. CHEN, J. WANG, Y. HEO, AND S. KISHORE. **MPC-Based Appliance Scheduling for Residential Building Energy Management Controller.** *IEEE Trans. on Smart Grid*, 4(3):1401–1410, September 2013.
- [91] M. CARRION, J. M. ARROYO AND A. J. CONEJO. **A bilevel stochastic programming approach for retailer futures market trading.** *IEEE Trans. Power Syst*, 24(3):1446–1456, August 2009.
- [92] F. BRAHMAN, M. HONARMAND, AND S. JADID. **Optimal electrical and thermal energy management of a residential energy hub, integrating demand response and energy storage system.** *Energy and Build*, 90:65–75, March 2015.
- [93] Z. ZHAO, L. WU, AND G. SONG. **Convergence of volatile power markets with price-based demand response.** *IEEE Trans. Power Syst*, 29(5):2107–2118, September 2014.

- [94] S. A. POURMOUSAVI AND M. H. NEHRIR. **Real-time central demand response for primary frequency regulation in microgrids.** *IEEE Trans. Smart Grid*, 3(4):1988–1996, December 2012.
- [95] T. JIANG, Y. CAO, L. YU, AND Z. WANG. **Load shaping strategy based on energy storage and dynamic pricing in smart grid.** *IEEE Trans. Smart Grid*, 5(6):2868–2876, November 2014.
- [96] H. T. NGUYEN AND L. B. LE. **Bidding strategy for virtual power plant with intraday demand response exchange market using stochastic programming** (best paper award). In *2016 IEEE International Conference on Sustainable Energy Technologies (ICSET)*, pages 96–101, November 2016.
- [97] E. G. KARDAKOS, C. K. SIMOGLU, AND A. G. BAJIRTZIS. **Optimal offering strategy of a virtual power plant: a stochastic bi-level approach.** *IEEE Trans. Smart Grid*, PP(PP), 2015.
- [98] R. BRANZEI, D. DIMITROV AND S. TIJS. *Models in Cooperative Game Theory*. Springer, second edition, 2008.
- [99] C. YEUNG, A. POON AND F. WU. **Game theoretical multi-agent modeling of coalition formation for multilateral trade.** *IEEE Trans. Power Syst*, 14(3):929–934, July 1999.
- [100] W. SAAD, Z. HAN, AND H. V. POOR. **Coalitional game theory for cooperative microgrid distribution networks.** In Japan . Kyoto, editor, *Proc. IEEE Int. Conf. Communications, Workshop on Smart Grid Communications*, pages 1–5, May 2011.
- [101] E. KARANGELOS AND F. BOUFFARD. **A cooperative game theory approach to wind power generation imblance cost allocation.** In *Proc. Workshop Power System Computation Conf.*, August 2011.
- [102] M. BOCKARJOVA, J. MATEVOSYAN, M. ZIMA, AND L. SODER. **Sharing profit from coordinated operation planning and bidding of hydro and wind power.** *IEEE Trans. Power Syst*, 25(3):1663–1673, August 2010.
- [103] S.R. DABBAGH AND M.K. SHEIKH-EL-ESLAM. **Risk based profit allocation to DERs integrated with a virtual power plant using cooperative game theory.** *Electr. Power Syst. Res.*, 121:368–378, April 2015.
- [104] G. O’BRIEN, E. G. ABASS, AND R. RAJAGOPAL. **Shapley value estimation for compensation of participants in demand response programs.** *IEEE Trans. Smart Grid*, 6(6):2837–2844, November 2015.
- [105] E. K. CHONG AND S. H. ZAK. *An introduction to optimization*, volume 76. John Wiley & Sons, 2013.
- [106] IBM. **Ilog CPLEX Optimizer.** <https://www-01.ibm.com/software/commerce/optimization/cplex-optimizer/>, 2008. [Online; accessed 10-February-2017].
- [107] N. GROWE-KUSKA, H. HEISCH, AND W. ROMISCH. **Scenario reduction and scenario tree construction for power management problem.** In Italy Bologna, editor, *Proc. 2003 IEEE Power Tech. Ann.*, June 2003.
- [108] A. A. Thatte and L. Xie. **Towards a unified operational value index of energy storage in smartgrid environment.** *IEEE Trans. Smart Grid*, 3(3):1418–1426, September 2012.
- [109] W. K. Gatterbauer. **Inter-dependencies of electricity market characteristics and bidding strategies of power producers.** Master’s thesis, Massachusetts Institute of Technology, 2002.

- [110] L. BARINGO AND A. J. CONEJO. **Offering Strategy of Wind-Power Producer: A Multi-Stage Risk-Constrained Approach.** *IEEE Trans. Power Syst.*, 31(2):1420–1429, March 2016.
- [111] J. G. GONZALEZ AND R. M. R. MUELA AND L. M. SANTOS AND A. M. GONZALEZ. **Stochastic joint optimization of wind generation and pumped storage units in an electricity market.** *IEEE Trans. Power Syst*, 23(2):460–468, May 2008.
- [112] L. FERIRE, A. STREET, AND D. LIMA AND L. BARROSO. **A hybrid MILP and Benders decomposition approach to find the Nucleolus quota allocation for a renewable energy portfolio.** *IEEE Trans. Power Syst*, 30(6):3265–3276, November 2015.
- [113] S. GABRIEL, A. J. CONEJO, J. D. FULLER, B. F. HOBBS, AND C. RUIZ. *Complementarity modeling in energy markets*, volume 180. Springer Science & Business Media, 2012.
- [114] L. P. GARCIA, A. J. CONEJO, R. G. BERTRAND, AND R. ROMERO. **A bilevel approach to transmission expansion planning within a market environment.** *IEEE Trans. Power Syst*, 24(3):1513–1522, August 2009.
- [115] S. J. KAZEMPOUR, A. J. CONEJO, AND C. RUIZ. **Strategic generation investment using a complementarity approach.** *IEEE Trans. Power Syst*, 26(2):940–948, May 2011.
- [116] H. PANDZIC, A. J. CONEJO, AND I. KUZLE. **An EPEC approach to the yearly maintenance scheduling of generating units.** *IEEE Trans. Power Syst*, 28(2):922–930, May 2013.
- [117] C. RUIZ, A. J. CONEJO, AND Y. SMEERS. **Equilibria in an oligopolistic electricity pool with stepwise offer curves.** *IEEE Trans. Power Syst*, 27(2):752–761, May 2012.
- [118] C. RUIZ AND A. J. CONEJO. **Pool strategy of a producer with endogenous formation of locational marginal prices.** *IEEE Trans. Power Syst*, 24(4):1855–1866, November 2009.
- [119] H. HAGHIGHAT AND S. W. KENNEDY. **A bilevel approach to operational decision making of a distribution company in competitive environments.** *IEEE Trans. Power Syst*, 27(4):1797–1807, November 2012.
- [120] G. E. ASIMAKOPOULOU, A. L. DIMEAS, AND N. D. HATZIARGYRIOU. **Leader-follower strategies for energy management of multi-microgrids.** *IEEE Trans. Smart Grid*, 4(4):1909–1916, December 2013.
- [121] Z. WANG, B. CHEN, J. WANG, M. M. BEGOVIC, AND C. CHEN. **Coordinated energy management of networked microgrids in distribution systems.** *IEEE Trans. Smart Grid*, 6(1):45–53, January 2015.
- [122] G. MAVROTAS. **Effective implementation of the ϵ -constraint method in multi-objective mathematical programming problems.** *Applied mathematics and computation*, 213(2):455–465, July 2009.
- [123] M. MASCHLER. **The bargaining set, kernel, and nucleolus.** *Handbook of Game Theory with Economic Applications*, 1:591–667, 1992.
- [124] P. SAMADI, H. MOHSENIAN-RAD, V. W. S. WONG, AND R. SCHOBBER. **Real time pricing for demand response based on stochastic approximation.** *IEEE Trans. Smart Grid*, 5(2):789–798, March 2014.
- [125] P. V. HENTENRYCK AND R. BENT. *Online stochastic combinatorial optimization.* MIT Press, 2006.

- [126] R. HALVGAARD, P. BACHER, B. PETERS, E. ANDERSEN, S. FURBO, J. B. JORGENSEN, N. K. POULSEN, AND H. MADSEN. **Model predictive control for a smart solar tank based on weather and consumption forecasts.** In *Proc. SHC 2012*, 2012.
- [127] A. THAVLOV. **Dynamic optimization of power consumption.** Master's thesis, Technical University of Denmark, DTU, DK-2800 Kgs. Lyngby, Denmark, 2008.
- [128] Mathworks. **Electricity load and price forecasting with Matlab.** <http://www.mathworks.com/videos/electricity-load-and-price-forecasting-with-matlab-81765.html>, 2013. [Online; accessed 23-December-2013].
- [129] M. PARVANIA AND M. FOTUHI-FIRUZABAD. **Demand response scheduling by stochastic SCUC.** *IEEE Trans. Smart Grid*, 1(1):89–98, June 2010.
- [130] M. CARRION AND J. M. ARROYO. **A computationally efficient mixed-integer linear formulation for the thermal unit commitment problem.** *IEEE Trans. Power Syst*, 21(3):1371–1378, August 2006.
- [131] D. E. OLIVARES AND C. A. CANIZARES AND M. KAZERANI. **A centralized energy management system for isolated microgrids.** *IEEE Trans. Smart Grid*, 5(4):1864–1875, July 2014.
- [132] J. M. MORALES, A. J. CONEJO, H. MADSEN, P. PINSON, AND M. ZUGNO. *Integrating renewables in electricity markets.* International Series in Operations Research & Management Science, Springer, 2014.
- [133] S. A. GABRIEL AND F. U. LEUTHOLD. **Solving discretely-constrained MPEC problems with applications in electric power markets.** *Energy Economics*, 32(1):3–14, January 2010.
- [134] **Strong duality theorem of linear programming problem.** <http://www.princeton.edu/>. [Online; accessed 20-April-2015].
- [135] A. KHODAEI. **Microgrid optimal scheduling with multi-period islanding constraints.** *IEEE Trans. Power Syst*, 29(3):1383–1392, May 2014.
- [136] R. D. ZIMMERMAN, C. E. MURILLO-SANCHEZ, AND R. J. THOMAS. **Matpower: Steady state operations, planning and analysis tools for power systems research and education.** *IEEE Trans. Power Syst*, 26:1, February 2011.
- [137] G. ZHANG, G. ZHANG, Y. GAO, AND J. LU. **Competitive strategic bidding optimization in electricity markets using bilevel programming and swarm technique.** *IEEE Trans. Ind. Electron*, 58(6):2138–2145, June 2011.
- [138] A. PARISIO, E. RIKOS, AND L. GLIELMO. **A model predictive control approach to microgrid operation optimization.** *IEEE Trans. Control Syst. Technol*, 22(5):1813–1827, September 2014.
- [139] C. SAHIN, M. SHAHIDEHPOUR, AND I. ERKMEN. **Allocation of hourly reserve versus demand response for security-constrained scheduling of stochastic wind energy.** *IEEE Trans. Sustain. Energy*, 4(1):219–228, January 2013.
- [140] B. ZHAO, Y. SHI, X. DONG, W. LUAN, AND J. BORNEMANN. **Short-term operation scheduling in renewable-powered microgrids: a duality-based approach.** *IEEE Trans. Sustain. Energy*, 5(1):209–217, January 2014.
- [141] Q. WANG, J. WANG, AND Y. GUAN. **Price-based unit commitment with wind power utilization constraints.** *IEEE Trans. Power Syst*, 28(3):2718–2726, August 2013.

- [142] Y. ZHAO, J. QIN, R. RAJAGOPAL, A. GOLDSMITH, AND H. V. POOR. **Wind Aggregation Via Risky Power Markets**. *IEEE Trans. on Power Syst*, 30(3):1571–1581, May 2015.
- [143] NATIONAL RENEWABLE ENERGY LABORATORY. *Eastern wind integration and transmission study*. Tech. Rep, 2010.
- [144] A. HALLEFJORD, R. HELMING AND K. JORNSTEN. *Computing the nucleolus when the characteristic function is given implicitly: A constraint generation approach*. *International Journal of Game Theory*, 1995.
- [145] Ercot. **Load data**, 2014. [Online; accessed 05-April-2014].
- [146] P. DUBEY AND L. S. SHAPLEY. **Totally balanced games arising from convex program**. *The Institute for Advanced Studies, The Hebrew University, Jerusalem, Israel, Report No 15/80*, 1984.
- [147] C. BEJAN AND J. GOMEZ. **A market interpretation of the proportional extended core**. *Economics Letters*, 117(3):636–638, December 2012.
- [148] C. BEJAN AND J. GOMEZ. **Core extensions for non-balanced TU-games**. *International Journal of Game Theory*, 38:3–16, 2009.
- [149] J. F. BONNANS AND M. ANDRE. **Fast computation of the leastcore and prenucleolus of cooperative games**. *RAIRO-Oper. Res*, 42(3):299–314, September 2008.
- [150] H. T. NGUYEN AND L. B. LE. **Minmax profit sharing scheme for cooperative wind power producers**. In *2016 IEEE International Conference on Sustainable Energy Technologies (ICSET)*, pages 390–395, November 2016.
- [151] H. T. NGUYEN AND L. B. LE. **Online ensemble learning for security assessment in PMU based power system**. In *2016 IEEE International Conference on Sustainable Energy Technologies (ICSET)*, pages 384–389, 2016.
- [152] D. T. NGUYEN, H. T. NGUYEN, AND L. B. LE. **Coordinated dispatch of renewable energy sources and HVAC load using stochastic programming**. In *Proc. IEEE SmartGrid-Comm'2014*, pages 139–144. IEEE, 2014.